Adhesive Bonding in Composite Structures for Aerospace Applications

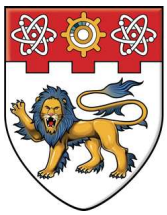

NANYANG TECHNOLOGICAL UNIVERSITY

SHASHI BHUSHAN KUMAR

SCHOOL OF MECHANICAL AND AEROSPACE ENGINEERING
NANYANG TECHNOLOGICAL UNIVERSITY

2006

Adhesive Bonding in Composite Structures for Aerospace Applications

Shashi Bhushan Kumar

School of Mechanical and Aerospace Engineering

A thesis submitted to the Nanyang Technological University
in fulfillment of the requirement for the Degree of
Doctor of Philosophy

2006

Acknowledgements

I would like to express my utmost gratitude and appreciation to my supervisors, Dr. Sridhar Idapalapati and Dr. Sathiamoorthy Sivashanker for their invaluable advice, guidance and encouragement throughout the progress of my studies. My thanks also goes to Dr. S.O. Osiyemi for his invaluable advice in overcoming the experimental hitches during my study. I am very grateful to Dr. Subodh G Mhaisalkar for allowing me to use his laboratory facilities.

Apart from above, I would like to thank all the staffs of Center for Advanced Numerical Engineering Simulations (CANES), Materials Laboratory A and B, Strength of Materials Laboratory, and Ceramics and Polymer Laboratory of Materials Science and Engineering for providing cheerful working environment during progress of my research work.

I also like to express my gratitude to my parents and relatives. Finally, I would like to thank my wife, children and friends for their love and support. Nonetheless, I heartily address the existence of God, and fully accept that without his mercy nothing would have been possible.

Contents

Abstract

In the defense and several other high performance industries, advanced composite materials are continuously used in large volumes to build relatively light and strong structures such as bullet proof vests, lightweight ammunitions, aircraft, spacecrafts, ships and offshore platforms, armored automobiles and bridges etc. An important requirement for the complete design of these practical structures is, design and development of attachment/joining methods as joint designs are very challenging and complex in composites structures. Currently, the three most commonly employed methods of joining are mechanical fastening (those using bolts, nut, staplers, rivets etc), welding and adhesive bonding. Of these three methods, adhesive bonding is the most versatile and is finding wide acceptance in the industrial arena as many dissimilar materials can be joined, problems associated with high stress concentrations around holes in bolted joints can be greatly eliminated, and good sealing can be achieved.

In the present research work, the mechanical behavior of adhesively bonded scarf and lap joints comprising carbon fiber reinforced polymer (CFRP) composites and epoxy based adhesives under quasi-static tensile and/or compressive loadings were studied experimentally. A limited amount of numerical verification was carried out as needed. The research project was executed in four phases.

In the first phase, test geometries were developed to study the knock-down in the joint strength of adhesively bonded scarf joints (those required for high performance applications) with scarf angle, under both uniaxial compressive and tensile loading conditions. Compressive and tensile specimens were carefully prepared and quasi-static tests were performed to study the joints' behavior. The test results were simulated numerically using ABAQUS finite element program. The failure modes (adhesive, cohesive and/or adherend failure) in the bonded region were also studied and summarized in the report.

In the second phase of the study, a simple modification was made to the single lap joint (SLJ) specimen for accurate experimental measurement of mechanical properties in bonded joints. The test geometry, named as modified single lap joint (MSLJ), was made by implanting end pre-cracks (starter pre-crack) at the end of the overlap in the adhesive layer in the middle of the bond line in a conventional SLJ. The purpose of this modification was to ensure that during testing, the crack propagated from the sharp crack tip of the starter pre-crack from both ends of the overlap, and reduces the effect of spew fillets and hence the scatter in experimental data. The adhesive fracture energy, G_a, or toughness of adhesively bonded joints comprising carbon fiber reinforced polymer composite substrates and three different types of adhesives was measured using this modified single lap joint (MSLJ). The MSLJ specimens were tested to failure and the adhesive fracture energy was calculated using the Kinloch-Osiyemi (KO) model. The values of the adhesive fracture energy obtained from the MSLJ tests were compared with those from SLJ and the Double Cantilever Beam (DCB) test geometries. Numerical simulation was also performed for bonded MSLJ made from Redux 322 adhesive to show the state of stress near the pre-crack tip.

In the third phase, the MSLJ test geometry was used to study the effect of exposure (moisture absorption) on mode I adhesive fracture energy, G_a. The mechanical test specimens were aged in distilled water for varying periods and taken out at intervals of 28 days till 186 days (period of study) and static tests were performed at laboratory conditions (23 ± 2^0 and $50 \pm 5\%$ relative humidity). To study the moisture absorption behaviour in the bulk adhesive, bonded adhesive and composite laminate, five test specimens from each group were also aged under the same environment and taken out at intervals of one week. The test results were compared with DCB specimens exposed and tested in an identical environment. The results of MSLJ correlated well with DCB tests.

Finally, a fatigue life prediction was investigated experimentally and analytically with MSLJ, SLJ and DCB test geometries. Some MSLJ and SLJ test specimens were tested under sinusoidal cyclic loading at the different load levels and the maximum applied load

per unit width, T_{max}, vs. the number of cycles to failure,N_f, was plotted. DCB test specimens were tested to obtain fracture mechanics parameters of the predictive model, and the fatigue life of MSLJ specimens was calculated analytically. The application of the new test geometry produced higher accuracy in experimental measurements of fatigue life and fitted better with the analytical solution.

List of Figures

List of Tables

List of Abbreviations and Symbols

ASTM	American Society for Testing of Materials
BSI	British Standards Institution
CFRP	Carbon Fibre Reinforced Polymer
DCB	Double Cantilever Beam
DT	Double Torsion
ES	European Standards
FRC	Fibre Reinforced Composites
FEA	Finite Element Analysis
IITRI	Illinois Institute of Technology Research Institute
ISO	International Organization for Standardization
KO	Kinloch-Osiyemi
LEFM	Linear Elastic Fracture Mechanics
MSLJ	Modified Single Lap Joint
SEM	Scanning Electron Microscopy
SLJ	Single Lap Joint
SSJ	Single Scarf Joint
A_c, B_c	Failure modes of scarf joints under compression
A_t, B_t	Failure modes of scarf joints under tension
a	Crack length
a_0	Initial flaw size
a_f	Crack length before fast fracture
B	Width of the specimen
c	Half of overlap length
d	Fibre diameter
D	Paris law contant
$\frac{da}{dN}$	Crack growth rate

E	Young's modulus
E_a	Young's modulus of bulk adhesive
E_s	Longitudinal tensile Young's modulus of substrate/adherend
E_{11}^c	Longitudinal compressive elastic modulus
E_{22}^c and E_{33}^c	Transverse compressive elastic modulus
E_{11}^t	Longitudinal tensile elastic modulus
E_{22}^t and E_{33}^t	Transverse tensile elastic modulus
e	Eccentricity
f	Frequency of cyclic loading
G	Shear modulus of adhesive
G_{12}	In-plane shear modulus
G_{13} and G_{23}	Out-of-plane shear modulus
G_a	Mode-I adhesive fracture energy
G_I	Mode-I energy release rate
G_{IC}	Mode-I toughness
G_{IIC}	Mode II toughness
G_{IIIC}	Mode III toughness
G_c	Critical strain energy release rate
G_{max}	Maximum energy release rate
G_{th}	Strain energy release rate at threshold
h	Thickness of the substrate
K	Bending moment factor
l	Free length of substrate
L	Length dimension
M_0	Bending moment
M_e	Bending moment per unit width
N_f	Number of cycles to failure
n	Paris law exponent
n_1	Fatigue curve-fitting constant in threshold region
n_2	Fatigue curve-fitting constant in fast fracture region
P	Failure load

S	Bending stiffness per unit width
T	Applied load per unit width
T_f	Applied fracture load per unit width
T_{max}, T_{min}	Maximum, and minimum applied load per unit width under fatigue
t	Substrate/adherend thickness
t_a	Adhesive layer thickness
Φ	Average fiber rotation angle
β	Kink-band angle
γ_{lv}, γ_{sv}, γ_{sl}	Surface tension between liquid-vapour, solid-vapour and solid-liquid
δ_{max}, δ_{min}	Maximum, and minimum amplitude
$\Delta\sigma$	Stress range
δ_R	Displacement ratio
ϵ	Strain
ϵ_{max}, ϵ_{min}	Maximum, and minimum strain in a fatigue cycle
ϵ_{amp}	Strain amplitude
θ	Scarf angle
σ_{amp}	Stress amplitude
σ_m	Mean stress
σ_{max}, σ_{min}	Maximum, and minimum stress in a fatigue cycle
σ_u	Ultimate tensile strength
σ_y	Yield strength
σ^c_{11}, σ^c_{22}	Longitudinal, and transverse compressive strength
σ_{22},	Peel stress at the crack-tip in the adhesive layer
σ^t_{11}, σ^t_{22}	Longitudinal, and transverse tensile strength
τ_u	Ultimate shear strength
τ_{13}	Interlaminar shear strength
ε_{11}	Longitudinal tensile strain
η	Stress concentration factor
ν	Poisson's ratio
ν_{12}, ν_{13} and ν_{23}	Major Poisson's ratio of substrate

Chapter 1

Introduction

In this Chapter, a general introduction to joining methods is covered. The importance of composite materials and adhesive bonding in reference to aircraft structures is discussed. The advantages and disadvantages of adhesive bonding are highlighted. Also the objectives, scope of the work and thesis layout are presented.

1.1 Background

For many structures, an ideal design would seemingly be one containing no joints, since joints are normally a possible source of weakness or excess weight, or both. However, in practice, there are actually many reasons why structures might need to contain joints, sometimes by necessity and sometimes by preference. Joining can be made possible by following three fundamental methods or processes, namely, (1) mechanical joining, (2) welding and (3) adhesive bonding. Mechanical joints are made by using bolts, nuts, rivets or pins. Joining by welding is accomplished by atomic forces. In adhesive bonding, materials and the structures they comprise are joined one to the other with the aid of a substance capable of holding those materials together by surface attraction forces arising principally from chemical origins. Usually a polymeric substance capable of holding at least two surfaces together in a strong and permanent manner is called an adhesive. Adhesives function primarily by the property of adhesion. Adhesion is the attraction of two different substances resulting from intermolecular forces between the substances. This is all together different from cohesion, which involves only the intermolecular attractive

forces within a single substance. They are generally materials having high shear and tensile strength.

Most adhesives evolved from vegetable, animal, or mineral substances. In the early 1900s, synthetic polymeric adhesives began to displace many naturally occurring materials owing to their stronger adhesion, greater formulation possibilities, and superior resistance to operating environments. At the same time the development of modern polymeric adhesives also began. In 1910 phenol formaldehyde adhesives for the ply wood industry were developed. Later on, between 1940 - 1950 significant growth occurred with the development of structural adhesives (those having shear strength greater than 7 MPa) for the military aircraft industry. The durability of adhesive joints was a problem in aircraft service until the advanced adhesive system was developed, introduced and verified in the late 1970s. With successful experiences in these industries, it was soon realized that the adhesive could be used to economically replace welding, brazing, bolting, and riveting in joint fabrication. The science of adhesion is well accepted, and the basic rules and methods for achieving high performance joints have been well established by now. However, it is cautioned that each joining method should be considered with regard to its special/critical requirements. There are cases when adhesives are the worst possible option for joining two substrates, and there are cases when adhesives may be the best or only alternative. For example the joining of ceramics or elastomeric materials, the joining of very thin substrate, the joining of surface skin to honeycomb, and several others which can not be done without adhesives. The advantages and disadvantages of adhesive bonding are summarized in Table 1.1 [6].

Any rational design of a structural bonded joint must be based on adequate knowledge of the stresses in the joint and the strength of the joint. To determine the stresses in a structural bonded joint and further to predict its strength and service life, it is necessary to know the material properties of adhesive and adherend. For prediction of the static strength of a bonded joints, material properties such as Young's modulus and Poisson's ratio (in case of elastic materials) or stress-strain curves, material yielding strength and hardening rules

Table 1.1: Advantages and Disadvantages of Adhesive Bonding

Advantages	Disadvantages
1. High load-carrying capacity possible due to large surface (area) bonding	1. Sensitive to peel or cleavage versus pure tension or shear
2. Minimal stress concentration due to load spreading over bond area	2. Complicated stress analysis required for critical applications
3. Suitability to very thin as well as thick adherends	3. Requires careful joint (adherends) surface preparation
4. Causes little or no change to the chemistry or structure of adherends	4. Requires rigid process control
5. Suitability for joining similar or dissimilar materials	5. Sometimes limited working times
6. Seals against many environments	6. Curing times can be long
7. Insulates against electricity or heat	7. Direct inspection is not possible; NDE method is needed
8. Minimizes or prevents galvanic corrosion between dissimilar materials	8. Repair of defective joints is virtually impossible
9. Damps vibrations and shock loads	9. Upper service temperature is very limited; especially for organic types
10. Resists fatigue and imparts damage tolerance	10. Life of joints is sensitive to environmental condition
11. Provides attractive strength-to-weight ratio	
12. Facilitate smooth contours	
13. Can be faster and cheaper than mechanical fastening	

(in case of non-linear materials) are needed for both adherend and adhesives materials. To determine service life of a bonded structure, critical adhesive fracture energy, and an accurate and repeatable fatigue testing method must be available and should be able to capture the effect of various service conditions. The material properties can only be calculated by using some experimental techniques and one must resort to testing. A variety of standard test methods have been developed by government, industrial societies, and university researchers to characterize adhesives when sandwiched between different adherend materials. A brief search of database of major standards bodies such as American Society for Testing and Materials (ASTM) [7] , British Standards Institute (BSI) [8], European Standards (ES) [9] and International standards Organizations (ISO) [10] revealed that several hundred test methods exist and continually updated and revised. A review of existing test methods can be found in literature published in the form of books [11–14].

Lap joint test methods are widely used in a variety of forms and are the most popular in the adhesives industry and research because they are simple to construct and represent a close resemblance to geometry and service conditions for many bonded structural members. The single lap joint (SLJ) test specimens prepared in accordance with the procedure mentioned in ASTM D1002 [15] is commonly employed for several purposes such as to calculate apparent tensile shear strength, compare and select the adhesives/adherends systems or bonding processes, in quality control of production of adhesive, in the evaluation of surface pretreatment, adhesive environmental durability, etc. Kinloch and Osiyemi [16] have performed experimental and analytical work on this type of bonded geometry and calculated fatigue life. Their experimental results were in good agreement with analytical solutions. Recently, several researchers [5, 17–19] have employed this type of test coupon to predict the fatigue life of SLJ and bonded structures. In contrast, some of the researchers have reported only a moderate agreement of experimental result with analytical and finite element analysis (FEA) solutions.

Many scientists [20, 21] have reported that testing of adhesives by mechanical test methods is a complex issue due to the state in which the adhesives are tested. An adhesive

test actually tests the total bonded assembly, i.e., the substrates, the joint geometry, the interface, the primer coat, the surface preparation, the curing cycle, and the adhesive itself. The geometry of an adhesively bonded joint involve the shape of the adherend and a geometrical description of the adhesive layer or bondline. The geometry of the adhesive layer includes bondline thickness and bondline end shapes or spew fillets. In a typical bonding process, the adhesive material which may be initially in a liquid/semiliquid state is consolidated into a solid state. During curing process while the bondline thickness may be controlled using shims or spacers or carrier mats, etc, the shape control of the spew fillets (beads of adhesive formed by overflown/squeezed-out liquid/semiliquid phase of the adhesive from the overlap region to ends of the overlap), becomes quite difficult if not impossible. Moreover, due to the off-set load line an internal bending moment is induced at the ends of the overlap and the overlap region is subjected to rotation, when a SLJ test specimen is subjected to tensile load. Most of the issues related to adhesive bonding technology have been addressed by researchers and reasonably well understood. However, the effect of the spew fillet in a SLJ test geometry has still not been addressed. Some of the analysis carried out on single lap joints with spew fillet [22–24] highlights the importance of circumventing the effect of spew fillet in characterization of adhesives and bonded joints. The inability in controlling the shapes and sizes of the spew fillet make this issue more serious.

1.2 Bonding in composite materials

Composite material is a substance consisting of two or more physically or chemically distinct, suitably arranged or distributed phases with an interface separating them. Its characteristics are not depicted by any of the components in isolation. Fiber-reinforced polymer (FRP) composite material are widely used in the aerospace, civil and structural industries because of several favorable properties such as low density, high specific strength and stiffness. In addition, the fatigue strength-weight ratios as well as fatigue damage tolerances of many composite laminates are excellent. For these reasons, Fiber Rein-

forced Composites (FRC) have emerged as a major class of light-weight structural material. These materials are either used presently or considered as substitutions for metals in many weight critical components.

The first use of modern composite materials on aircraft was about 30 years ago when boron-reinforced epoxy composite was used for the skins of the empennages of the U.S. F14 and F15 fighters [1]. Initially, composite materials were used only in secondary structures (secondary load bearing structures), but as knowledge and information of the materials improved, their use in primary structures (main load bearing structures) such as wings and fuselages, etc., became possible. Table 1.2 reports a list of aircrafts, in which significant amounts of composite materials are used in the manufacture of airframe. Initially, the percentage by structural weight of composites used in manufacturing was very small, at around 2% in the F15, for example. However, the percentage increased considerably, through 19 % in the F18 up to 24 % in the F22. The distribution of various materials used in the manufacture of F18E/F aircraft is shown in Figure 1.1. The AV-8B Harrier GR7 has composite wing sections and the GR7A features a composite rear fuselage. Composite materials are used extensively in the Eurofighter: the wing skins, forward fuselage, flaperons and rudder all make use of composites. Toughened epoxy skins constitute about 75% of the exterior area. About 40 % of the structural weight of the Eurofighter is carbon fibre reinforced polymer composite material [1]. Other European fighters typically feature between about 20 and 25 % composites by weight: 26 % for Dassaults Rafael and 20 to 25 % for the Saab Gripen and the EADS Mako. The B2 stealth bomber is an interesting case. The requirement for stealth means that radar-absorbing material must be added to the exterior of the aircraft with a concomitant weight penalty. Composite materials are therefore used in the primary structure to offset this penalty. Figure 1.2 shows the usage of composites in a typical military aircraft [2].

The use of composite materials in commercial [25, 26] transport aircraft is attractive because reduced airframe weight enables better fuel economy and therefore lowers operating costs. The first significant use of composite material in a commercial aircraft was by

Airbus in 1983 in the rudder of the A300 and A310, and then in 1985 in the vertical tail fin. In the latter case, the 2,000 parts (excluding fasteners) of the metal fin were reduced to fewer than 100 for the composite fin, lowering its weight and production cost. Later, a honeycomb core with CFRP faceplates was used for the elevator of the A310. Following these successes, composite materials were used for the entire tail structure of the A320, which also featured composite fuselage belly skins, fin/fuselage fairings, fixed leading- and trailing-edge bottom access panels and deflectors, trailing-edge flaps and flap-track fairings, spoilers, ailerons, wheel doors, main gear leg fairing doors, and nacelles. In addition, the floor panels were made of GFRP. Composites constitute approximately 28 % of the weight of the A320 airframe. The A340-500 and 600 feature additional composite structures, including the rear pressure bulkhead, the keel beam, and some of the fixed leading edge of the wing. The last is particularly significant, as it constitutes the first large-scale use of a thermoplastic matrix composite component on a commercial transport aircraft.

Composites enabled a 20 % saving in weight along with a lower production time and improved damage tolerance [1]. The A380 uses about 20-22 % composites by weight. The top and bottom skin panels of the A380 and the front, centre and rear spars contain CFRP, which is also used for the rear pressure bulkhead, the upper deck floor beams, and for the ailerons, spoilers and outer flaps (see Figure 1.3). The belly fairing consists of about 100 composite honeycomb panels. The Boeing 777, whose maiden flight was about ten years ago, has around 20 % composites by weight [1], with composite materials being used for the wings fixed leading edge, the trailing-edge panels, the flaps and flaperons, the spoilers, and the outboard aileron. They are also used for the floor beams, the wing-to-body fairing, and the landing-gear doors. Using composite materials for the empennage saves approximately 680 kg in weight. The Boeing 777 will leverage extensive use of composite materials (estimates are as high as 50 %) in the quest for developing an efficient and better performance with reduced weight. Falcon 7X, is one of the new business jet as an example of how new generation aircraft are making greater use of CFRP

composite materials [1]. The excellent strength-to-weight ratio of composites is also exploited in helicopters to maximize payloads and performance at large. Boeing Vertol used composites for rotorcraft fairings in the 1950s and made the first composite rotor blades in the 1970s. Composites are used in major structural elements of many modern helicopters, including the V22 tilt-rotor aircraft, which uses approximately 50 % composites by weight [1]. The formability of composites has been used to particular advantage in helicopter manufacture to reduce the numbers of component parts and therefore cost.

Composite materials have been considered in some applications of the automotive industry as it produces a high-quality surface finish, styling details, and processing options. Manufacturers are able to meet automotive requirements of cost, appearance, and performance by utilizing composites. Today, composite body panels have a successful track record in all categories from exotic sports cars to passenger cars to small, medium, and heavy truck applications. Sports and recreation industry is another major consumer of composite materials, they include golf shafts, tennis rackets, snow skis, fishing rods, etc. These products are light in weight and provide higher performance as compared to engineering alloys or plastics, which helps the user in easy handling and increased comfort. Composite usage in construction and civil structure industries such as bridges, earthquake and seismic retrofit activities is also booming. The columns wrapped by glass/epoxy, carbon/epoxy, and aramid/epoxy show good potential for these applications. The use of composite materials in various other industrial applications is also growing. Composites are being used in making industrial rollers and shafts for the printing industry and industrial drive shafts for cooling-tower applications /citeroller. Filament winding shows good potential for making composite pipes. Injection molded, short fiber composites are used in bushings, pump and roller bearings, and pistons. Composites are also used for making robot arms and provide improved stiffness, damping, and response time.

The development of a good and reliable joining method and its characterization becomes an important issue in light of the development of new modern materials. Currently there are two main techniques being employed in the industry for manufacture of compos-

Table 1.2: List of aircraft in which significant amounts of composite materials are used in the airframe structures [1]

Type	Country	Name of aircraft
Fighter Aircraft	U.S.A. Europe	AV-8B, F16, F14, F18, YF23, F22, JSF, UCAV Harrier GR7, Gripen JAS39, Mirage 2000, Rafael, Eurofighter, Lavi, EADS Mako
Bomber	U.S.A. Russia	B2 MIG29, Su Series
Transport	U.S.A. Europe	KC135, C17, 777, 767, MD11 A320, A340, A380, Tu204. ATR42, Falcon 900, A300-600
General Aviation		Piaggio, Starship, Premier 1
Rotary Aircraft		V22, Eurocopter, Comanche, RAH66, BA609, EH101, Super Lynx 300, S92

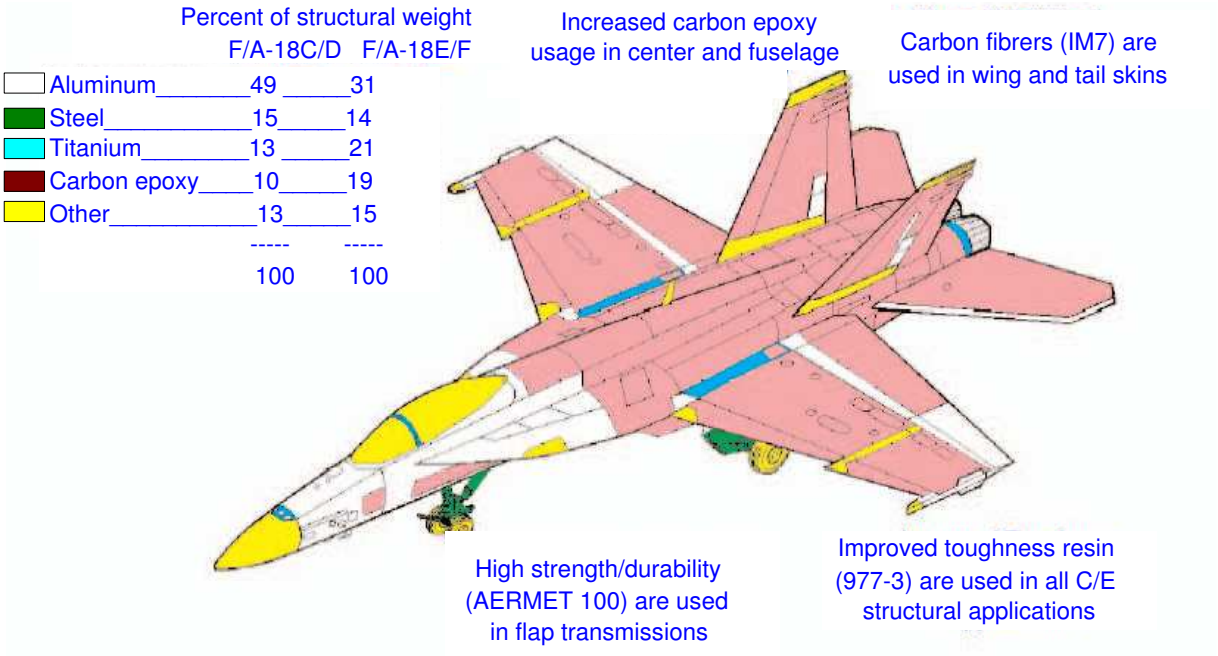

Figure 1.1: Distribution of some of the engineering materials used in the fabrication of structural components in F/A-18C/D and F/A-F18E/F aircrafts [1].

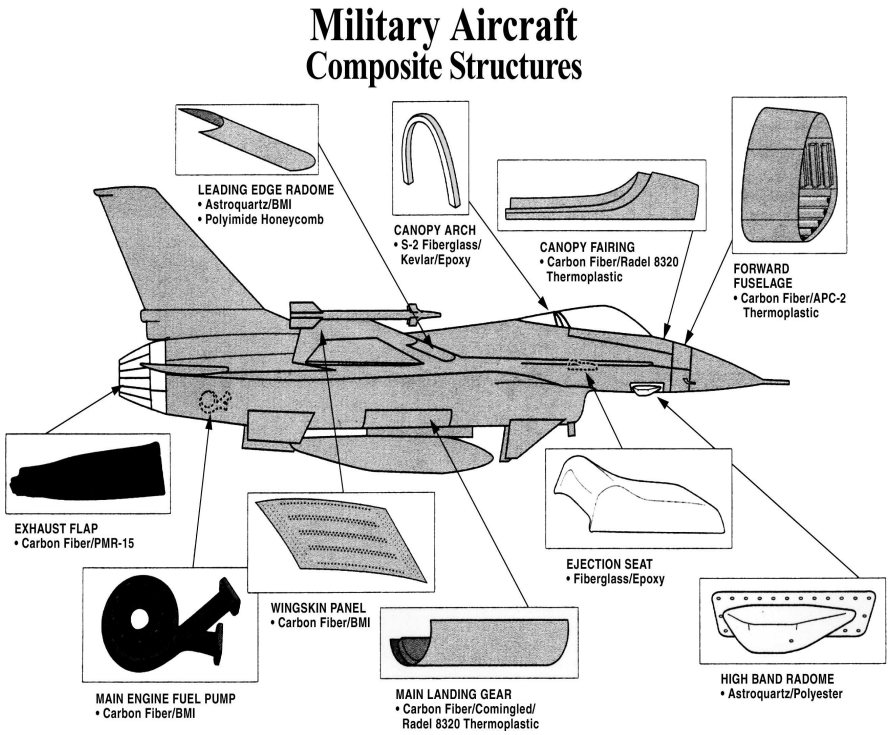

Figure 1.2: Usage of composites structures in a typical military aircraft [2].

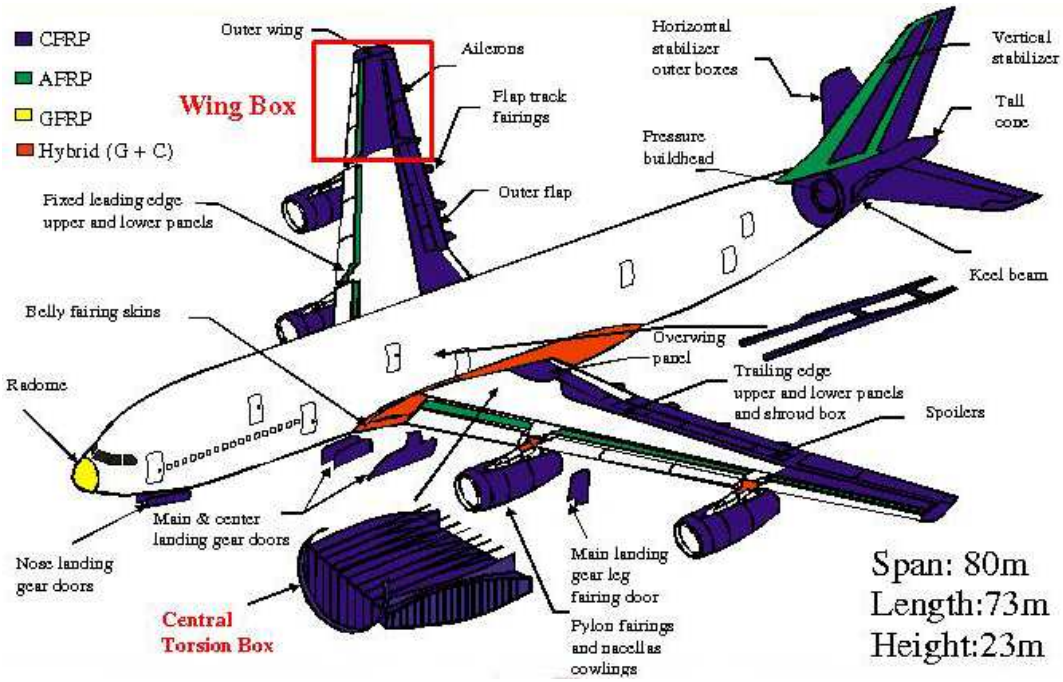

Figure 1.3: Distribution of various composite materials used in fabrication of A380 aircraft [3].

ite structures; these comprise (a) adhesive bonding and (b) mechanical fastening methods such as those using bolts, rivets and screws etc. In weight critical applications such as those with aerospace structures, adhesively bonded joints are gaining preference over mechanical fastening techniques because of their favourable attribute such as almost zero weight penalties. In contrast, mechanical fastening methods employ screws, nuts, bolts and rivets etc, thus adding significantly to the weight of the structures. Mechanical fastening also requires numerous cutouts such as holes to be made in the composite structure; this may induce high stress concentrations locally in the structures, thus reducing their load bearing capacity. In addition, metallic fasteners are often susceptible to atmospheric and stress corrosion, which is another disadvantage of mechanical fastening method. Adhesively bonded joints in contrast enable high load bearing structures by eliminating need to make holes, cut-outs, etc., possess superior sealing properties and provide smooth contour and aesthetic appearance.

There are several configurations of joints, such as butt-joints, lap-joints and scarf-joints (see Figure 1.4) [20], which can be employed when designing, manufacturing or repairing structures. Amongst these, scarf-joints have been found to exhibit the highest structural efficiency since they eliminate eccentricities (which act as stress raisers) in the loading path resulting in a more uniform stress distribution across the joint. A scarf-joint uses a relatively small scarf-angle to transfer load efficiently. Furthermore, a scarf joint adds little additional weight to the structure by way of excess overlap material (such as that found in lap-joints, for example). For aircraft structures, the added advantage is that there is no interference in the aerodynamic profile as flush configuration (with no excess bond overlap) is used in the scarf-joints. The favorable attributes of scarf-joints and adhesive bonding make adhesively-bonded scarf-joints an attractive option for the repair and fabrication of composite structures.

Single lap joints (SLJs) made in accordance with ASTM D 1002 test methods are widely used for various purposes such as to compare different materials, procedures, products, and so on. To the author's knowledge, in all the previous experimental studies carried

out with conventional SLJ (i.e., ASTM D 1002), the effect of spew fillet was neglected. This is a serious error as it is a major contributor of the scatter in the experimental results from those of the analytical and finite element analysis results. Any improvement in this testing method will be a novel contribution, because adhesive manufacturers as well as end users will be able to derive benefits. To solve the current problem, a novel modification is made to the conventional test geometry and measurement of adhesive fracture energy or fracture toughness of structural adhesives in dry condition, aged condition and fatigue life prediction were performed. The effectiveness of the modification was studied by comparing the results with one obtained from conventional SLJ and well established double cantilever beam (DCB) specimens.

Composite bonded structures are often subjected to adverse environmental conditions during service life. Aqueous environment (i.e., exposure to high moisture) is the most common among other environmental conditions. It has been observed that when bonded joints come in contact with an aqueous medium, the polymeric materials absorbs water and a significant change in its glass transition temperature, (T_g), takes place. Due to this change in glass transition temperature the mechanical properties of the polymeric materials normally degrade. To illustrate the use of the modified test geometry in obtaining information from aged specimens a systematic study was made. Using the modified geometry the effect of environmental ageing on a fracture mechanics parameter such as the adhesive fracture energy (which is a material property of the adhesive) was studied and compared with the result obtained from DCB in identical conditions.

An important requirement of a structural adhesive joint is that it continues to support design loads, under service conditions, for the planned life of the structure. The ability of a joint to maintain satisfactory long-term performance, in dry conditions or severe environmental conditions, is of interest and concern. A simple test coupon which produces repeatable design data with reliability will be an important development in this direction. To quantify the effect of the modification in predicting the fatigue life, the new test geometry was tested for fatigue life prediction and the result was compared with SLJ and

analytical results.

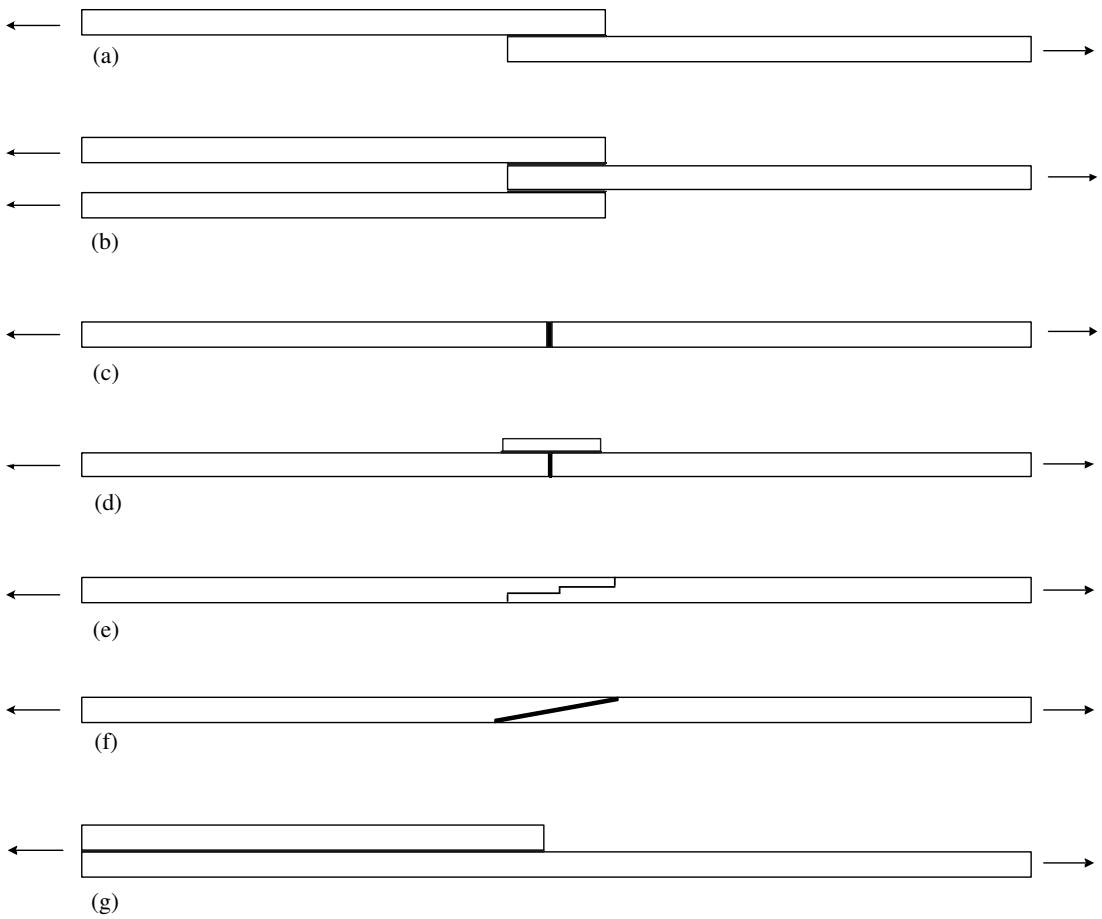

Figure 1.4: Commonly employed structural bonded joints configuration, (a) Single lap joint, (b) double lap joint, (c) Butt joint, (d) Butt strap joint, (e) Step joint, (f) Single scarf joint, and (g) Lap shear joint.

1.3 Objectives

The present PhD research work attempts to address some of the issues which inhibit the wider use of adhesives in high performance applications. The following objectives were identified to achieve the desired goals.

1. To propose and verify a test coupon for studying the behavior and failure mechanisms of adhesively bonded composite scarf joints subjected to uniaxial compressive and tensile loading.

2. To develop a simple and accurate testing method to circumvent the effect of spew fillet on the test results by inventing/modifying a test geometry, and thus facilitate the characterization of the adhesively bonded joint with reasonable accuracy and reliability.

1.4 Scope of the work

A review of the literature pertinent to the scarf joints revealed that currently no standard test geometry exists for characterizing the adhesively bonded scarf joints. It was also felt that the mechanical behavior of this type of joints are still not fully understood and a lot of things need to done in order to exploit its potential usage. To address some of these points, the scarf joint coupons made from composite material substrates and structural adhesive were extensively studied and performance under uniaxial compression and tensile loading was evaluated. The experimental measurements were verified through finite element simulations.

As far as testing using single lap joint is concerned, a well established standard test method exists and enormous amount of advancement has been made by now. The most important drawback in the current SLJ test methods is that it does not take account of variations in the spew fillets present at the ends of the overlap (a practical considerations in the adhesive bonding). Generally, during the bonding process, the adhesive changes its state from film to semi-liquid to solid and it has tendency to overflow or squeeze out due to contact pressure and form a bead at the ends of the overlap (a practical difficulty in adhesive bonding process). Thus, the test coupons generally have inherent beads of adhesive at the ends of the overlap, commonly known as spew fillet. The inability to control the shape, size and nature of bluntness of these adhesive beads formed at the end of the overlap magnify the problems, and as a result a large variation in the experimental measurements was observed by researchers. Due to large scatter in experimental data the interpretation of test results is difficult. Hence, these results cannot be used for design purposes and in any accurate service life prediction models. In the present thesis, these

issues are addressed by conducting experiments and numerical simulations. A simple modification was proposed to conventional single lap joint (SLJ) geometry to circumvent the effect of spew fillet. The new test coupon is referred to as modified single lap joint (MSLJ), and is made by implanting a starter pre-crack in the middle of the bondline at both ends of the overlap.

1.5 Thesis layout

In Chapter 2, the previous literature pertaining to the single lap joint and scarf joint is presented. The analytical solutions, experimental approach and finite element analyses reported on single lap joints were reviewed. Both stress-based as well as fracture mechanics-based solutions are reported. Chapter 3 presents the study performed on scarf joints under uniaxial compression loading. Both experimental as well as finite element simulations were used to investigate the compression behaviour and failure mechanisms. The results of scarf joints subjected to uniaxial tensile loading were investigated in similar manner and are reported in Chapter 4. In Chapter 5, the effectiveness of the modified single lap joint (i.e., MSLJ) is demonstrated by predicting the adhesive fracture energy or fracture toughness, G_a, of the bonded joint and comparing the results with well accepted DCB test methods and conventional single lap joint (SLJ). To further illustrate the use of MSLJ in studying the effect of environmental ageing on adhesively bonded joints, the adhesive fracture energy was calculated after ageing the test specimens. MSLJ results were compared with DCB test results obtained under identical conditions. These results are reported in Chapter 6. The fatigue life calculation which is the final and most important design requirement for structures likely to be subjected to cyclic loading is addressed in Chapter 7. The experimental results obtained by testing the modified single lap joint (i.e., joints with starter pre-cracks) and conventional single lap joint (with spew fillets) subjected to sinusoidal cyclic loading under dry test conditions are reported. Finally, in Chapter 8, major conclusions from the research work carried out are made and scope for further research is outlined.

Chapter 2

Literature Review

This chapter begins with a general overview of the adhesive bonding process. The current status of literature on bonded scarf joints, single lap joints and double cantilever beam (DCB) are reviewed critically with special focus in reference to composite joints. Various assumptions and pros and cons of analytical, experimental and finite element approaches are discussed. Finally, concluding remarks are made and the issues which need to be addressed are highlighted.

2.1 Introduction

Joining is a secondary manufacturing process, in which two or more members are joined together in order to realize a complex configuration or product. Joining is also routinely used to repair the structural damage which may occur during the operation of a product. For a permanent bonded structure one may opt for welding or adhesive bonding. For a non-permanent joint, mechanical fastening is preferred. Joints play a vital role in all practical structures (e.g. primary, secondary or non-structural). The purpose of a joint is to transfer load between the joined components and manufacture intended complex structure, which may not be obtained by net shape forming processes. The possible joining methods of composites can be broadly classified into three categories, namely, mechanical fastening, bonding and combinations of the two. In the mechanical fastening technique components to be joined are held together by additional component(s) such as fasteners, screws or rivets. The fasteners may be used directly to transfer the load between the components to be joined (e.g. as in a bolted, riveted or screwed joints) or indirectly, such as those in friction grip, clamp or strapped joints. Bonded joints can be adhesive bonded

joints, laminated joints, moulded joints, bonded insert joints or cast-in joints. The combined joints can be effected using any combination of the above two techniques. Adhesive joints are generally made by one or more of the commonly used configurations shown in Figure 1.4. A comprehensive description of the various joints configuration can be found in the book by Tong and Steven [20]. Bonded joints used in aerospace applications can be classified single (primary such as fuselage splice and wing/tail root, etc) or multiple (secondary such as stringers, frame and doorframe, etc) load path joints. In the design of bonded composite joints several issues need to be considered as described below:

1. Selection of the appropriate adhesive
2. Pre-bond surface treatment of substrates
3. Application or dispensing of the adhesive
4. Curing
5. Characterization (Mechanical and Thermal)
6. Testing for joint strength and failure mechanism
7. Reliability

These items are described briefly in the following paragraphs. However, a detailed description can be found in a monograph by Petrie [12] and engineered materials handbook [27]. A recently published book by Dillard and Pocius [28] has covered most of the work taken up so far in the area of adhesive bonding technology.

Major factors governing the selection of adhesives are: i) the joint strength to be achieved, ii) environmental exposure (e.g. service temperature, moisture, etc.), iii) surface pre-treatment requirements, iv) cost effectiveness of the adhesive curing cycle, v) adhesive flexibility to account for coefficient of thermal expansion (CTE) mismatch, vi) effect of curing cycle on the substrate, vii) method of application/dispensing of the adhesive, viii) cost of the adhesive, ix) safety factors (e.g. adhesive odor, reaction to human

skin, environmental regulations on waste disposal), x) gap filling requirements, and xi) conformity with in-house company regulations.

The main purpose of surface pre-treatment is to provide a consistent and repeatable/reproducible bonding surface of the adherend such that when bonded, the joint meets the strength and durability required for a specific application. The function of surface pre-treatment are five folds: i) removes impurities from the surface, ii) roughens the surface, iii) allows the adhesive to properly wet the substrate surface, iv) enables the formation of chemical bonds, and v) ensures that the bond is stable over the lifetime of the bonded structure. The wetting effect of the adhesive before and after surface treatment is shown in Figure 2.1. When the angle, θ, between surface tension of solid-liquid, γ_{sl}, and liquid-vapour interface, γ_{lv}, is greater than 90^0 no wetting condition occurs. However, if the angle, θ, between surface tension of solid-liquid, γ_{sl}, and liquid-vapour interface, γ_{lv}, is less than 90^0 liquid placed on the substrate surface can wet the substrate. Surface tension between solid-vapour phase is denoted as γ_{sv}. Commonly used surface pre-treatment methods in adhesive bonding technology are as described below:

1. Basic cleaning, such as, (a) abrasive + solvent wipe (i.e., sand blasting/acetone) (b) vapor degreasing (i.e., use of condensing solvent vapors to dissolve material surface contaminants) (c) ultrasonic scrubbing (i.e., use of high frequency sound wave to initiate the cavitations of bubbles in a solvent bath which cleans the materials surface on impact.)

2. Oxidative treatment

3. Chemical treatment

4. Plasma treatment

After surface preparation, adhesives have to be dispensed/applied on the treated surfaces of the adherends. The dispensing processes can be divided into two categories, namely, i) non-precise dispensing using spatula, manual gun, non-automatic system and

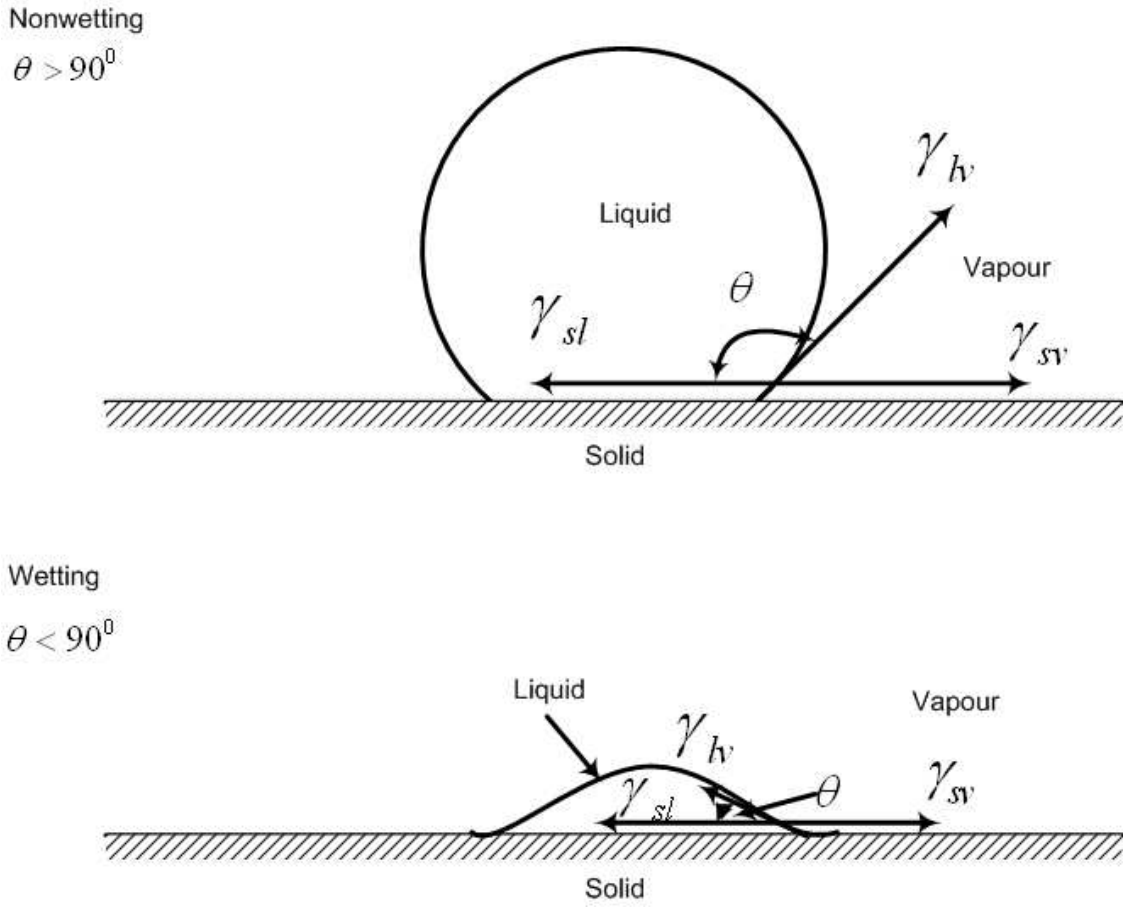

Figure 2.1: Sessile drop configuration explaining the non-wetting and wetting phenomena of a substrate/adherend.

it does not require any specialized equipments. ii) precise dispensing, using specialized equipment with good repeatability.

Curing is viewed as a mechanism that causes change in the state of adhesive from liquid/semi-liquid to solid state, so that it holds the substrates and can carry and/or transfer the applied load. Curing methods are commonly divided into i) room temperature/pressure cure, ii) heat/pressure (e.g. convection oven, hot press, and autoclave), iii) ultraviolet radiation curing, iv) variable frequency microwave curing, and v) electron beam radiation curing. Usually adhesive manufacturers recommend a curing schedule by specifying cure temperature (i.e. room temp. or above room temp.), cure pressure for uniform compaction of resin, cure time (total cure time + post cure time) and curing catalyst. It is important to adhere with the manufacturer's specifications for better results.

Characterization of adhesives refers to obtaining relevant information on properties of the cured adhesive that is useful to the end users. Mechanical characterizations generally refer to the study of tensile and shear stress-strain behavior (i.e. estimation of Young's modulus, shear modulus, Poisson's ratio, and tensile strength, etc.). The study of the temperature dependence of material properties is called thermal characterization. As adhesives are subjected to both mechanical as well as thermal loading during service life, it is important to understand both the mechanical and the thermal behavior of adhesives.

Testing for joints strength refers to characterization of joints experimentally. Joint strength can be estimated analytically, experimentally or numerically. In analytical solution (i.e. close form solution), problems are idealized and governing equations are derived and strength is predicted using a set of equations. In experimental procedures, specimens are fabricated using the same material as is used in actual structures. The specimens are tested using standardized procedures (e.g. standardized coupon test, coupon test, full-scale structural test).

Failure analysis of the adhesively bonded joints is necessary to determine the reliability of the joints. The failure in adhesively bonded joints can be categorized into three separate types: (i) adhesive failure (i.e. failure at the adhesive-adherend interface), (ii) co-

hesive failure (i.e. failure within the adhesive layer) and (iii) adherend failure (i.e. failure in the adherend materials).

The previous research work reported in which various aspects of adhesively bonded joints were studied can be broadly classified into two main categories, i) stress-based approach and ii) fracture mechanics-based approach. Herein, the literature on bonded lap joint and scarf joints was critically reviewed.

2.2 Scarf Joint

The shear stress in the adhesive layer is reasonably uniform in a scarf joint, provided the adherends have equal stiffness and thermal expansion coefficients and the scarf edge is sharp (see Figure 2.2). Peel stresses or transverse stresses, σ_T are normally very low for small scarf angle joints. Simplified theory gives the following equation for shear stress in the adhesive layer

$$\tau = \frac{P \sin\theta \cos\theta}{t} \tag{2.1}$$

and the peel stress or normal stress is given by

$$\sigma_T = \frac{P \sin^2\theta}{t} \tag{2.2}$$

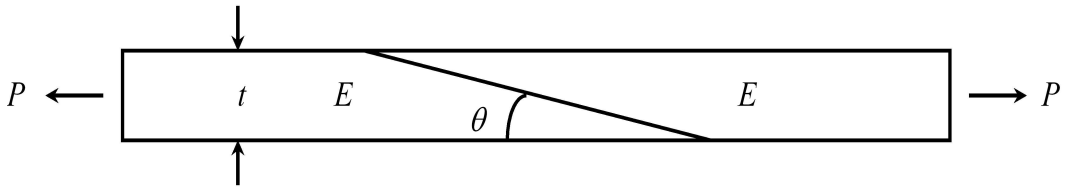

Figure 2.2: Schematic diagram of a single scarf joint (SSJ) with geometric parameters.

2.2.1 Compressive Joint Strength

Composite structures (e.g. Aircraft wings, helicopter rotor blades, etc) consisting of adhesively bonded joints are subjected to compressive as well as tensile loading during their

service life. The compressive strength of carbon fiber reinforced polymer-matrix composites generally varies between 30 – 60% of their corresponding tensile strength [29]. This implies that a bending composite beam such as an aircraft wing structure or helicopter rotor blade which are subjected to both compressive as well as tensile loading is likely to fail in compression rather than in tension [30]. Consequently compression strength is widely used as a "*design-limiting feature*" for continuous fiber composites [31–36].

Soutis and Hu [37, 38] have developed analytical and numerical models to determine the optimum geometry and compressive strength of flush composite repairs. An average stress failure criterion (ASFC) was used with the finite element calculations to estimate the ultimate compressive strength of the three-dimensional repaired configuration. They observed that the simple scarf-joint analysis underestimates the strength of the scarf patch repair by more than 40% and predicts an optimum scarf angle of 4^0 as compared with an angle of almost 7^0 obtained by the ASFC.

2.2.2 Tensile Joint Strength

The uniaxial tensile failure of neat polymer composites (i.e., without joints) and adhesively bonded scarf joints of engineering alloys such as steel and aluminum is reasonably well understood [39–47]. Macander and Mulville [48] and Marcolefas *et al.* [49] have studied uniaxial tensile failure of adhesively bonded scarf joints consisting of a combination of metals and composites. Adkins and Pipes [50, 51] have investigated the improvement of failure strengths of adhesively-bonded composite scarf-joints using different joint preparation techniques (for scarf angles greater than 1^0).

Charalambides and co-workers [52, 53] have investigated adhesively bonded scarf repairs to fibre composite materials. In part I, they performed a series of tests on repair joints, repair panels, the adhesive and the composite substrates. The repair joints were immersed in distilled water at 50^0C for periods of up to 16 months and the effect of the hot/wet environment on the static and fatigue strengths was evaluated. Although changes in the failure modes were observed, no major effect was noticed on the static strengths of

the repair joints. The static strength of the repair joint was somewhat lower than the static strength of the parent, the average efficiency being 84%. However, under fatigue loading, the repair joints do not perform nearly as well as the parent CFRP material. Nevertheless, the parent material had obvious signs of damage fairly early in the fatigue tests, whereas the joints failed catastrophically with no visual signs of damage. The repair panels were found to have similar fatigue performance to the repair joint, as well as similar failure modes. In part II, they carried out finite element analysis and compared with the experimentally observed failure path and strength of the adhesively-bonded repair joints. They reported good agreement between the experimental observations and numerical predictions.

Baker *et al.* [54] have carried out experimental studies to determine the capability of a scarf repair on a 21 ply laminate. The aim of their study was to demonstrate that the repair can withstand a strain capability in the repair of at least 6000 $\mu\epsilon$ when tested under hot/wet conditions. Although their test result showed that some of the specimens were able to sustain the desired strain values, the performance of the joint/repair was marginally lower than expected for the chosen conditions. They also observed some design improvements for this type of joint.

Marcolefas *et al.* [49] have proposed an analytical method to analyze an adhesively-bonded metal-to-composite scarf joint under both tensile and compressive loading conditions. Their analysis led to a numerical procedure capable of evaluating stresses developed by shear failure of the joint for the particular type of scarf joint.

Lubkin [55] has established conditions under which a wide or narrow adhesive scarf joint can have uniformly distributed adhesive stresses, and gave expressions for these stresses under tensile loading conditions. In the analysis, adherend and adhesive were considered as isotropic materials with linear stress-strain behaviour.

Emerson and Fawcett [56] have conducted a series of tests to validate scarf repairs and determine repair limits in heavily loaded GFRP-to-metal and CFRP-to-CFRP joints. This was accomplished using Boeing 777 Stabilizer CFRP main torque box skin panel

sub-components, representative of both trailing edge and forward torque box rib attachment joints, and 99 single and double fastener joint coupons. Their results showed that the two repaired sub-components that were tested at room temperature exceeded the original test values for the same sub-components that had not been repaired and they also exceeded the calculated typical design values. These results enable repairs to be designed for composite/composite and composite/metal joints in the structure.

Odi and Friend [57] have developed a 2D plane stress approach, which allowed them ply-by-ply modeling of composite adherends in a scarf joint under uniaxial tensile loading. They predicted ultimate joint failure load. They found that the approach offered the prospect of accurately modeling more realistic joints.

Objois *et al.* [58,59] have presented some experimental and theoretical analyses incorporating the influence of the scarf angle value upon the micro-mechanical behavior of the scarf-joint bonded structure loaded in uniaxial tension. The specimens studied were made of mild steel adherends and epoxy resin adhesive. They characterized the various stages of the adhesive gradual damage and considered the threshold of the first micro-cracks initiation (symbolized F_d) and the threshold of the start of flaw propagation (symbolized F_g) as the fundamental parameters. The F_d and F_g thresholds were determined by two experimental methods used simultaneously: extensometry with electrical strain gauges and acoustic emission.

Macander and Mulville [48] have experimentally established a failure criterion based on a strain energy release rate formulation to predict the performance of the scarf joint under tensile loading condition. These joints comprised of GFRP and steel adherends and adhesive.

Hart-Smith [60] presented advances in the design of adhesive bonded joints, with particular reference to advanced composite structures. The solutions were largely closed-form analytical results, employing iterative solutions on a digital computer for the more complicated joint configurations. The joints analyzed were double-lap, single-lap, scarf and stepped-lap configurations. Tensile, compressive, and in-plane shear load conditions

were covered. In addition to the usual geometric variables, the following joint parameters were accounted for: adhesive plasticity (using an elastic-plastic shear stress model), adherend stiffness imbalance and adherend thermal mismatch. Of these, the adhesive plasticity increases the joint failure strength dramatically above the predictions of purely elastic analyses because the maximum lap-joint strengths are shown to be defined by the adhesive strain energy in shear. Any dissimilarity between adherends effects a joint strength reduction.

Adams *et al.* [61] presented theoretical stress distributions, obtained from a two-dimensional finite element idealization, in adhesive-bonded lap, bevel and scarf joints between adherends of carbon fiber reinforced plastic. The adhesive was treated both as an elastic and an elastic-perfectly plastic material, with a yield criterion that is dependent on both the hydrostatic and deviatoric stress components. They also estimated the joint efficiency.

Johnson [62] developed a closed-form solution for the stresses in an adhesive-bonded scarf joint comprising laminated composite adherends. Unfortunately, his closed-form solution did not agree well with the finite-element calculations on four and twelve-layer scarf joints having alternating 0^0 and 90^0 plies. The different load-carrying capacity of the oriented plies caused irregular stress distributions whose characteristics were related to the location of each ply within the stack.

Baker *et al.* [63] have also studied scarf joints representative of repairs to graphite/epoxy (gr/ep) honeycomb structure using mechanical testing and finite-element (FE) modelling. The load carrying capacity of such scarf repairs was only marginal when tested under hot/wet conditions and compared to the required design ultimate strain of 5200 $\mu\epsilon$. The analysis of the scarf joint using FE methods predicted that high stresses occurs at ply drop-offs and at the top of the scarf and good correlation was observed between the FE models and experimental results. The shear stress distribution within the adhesive layer is not uniform over the length of the scarf, as would be the case for isotropic adherends, but rather varies with position by up to 250%, due to the varying longitudinal compliances

of the plies within the gr/ep adherends. Their experimental results offer some evidence indicating the occurrence of stress relaxation or creep within the scarf joints. They found that the external patches were effective for temporary repair.

Ishii *et al.* [64] studied adhesively bonded CFRP/metal joints under multi-axial stress conditions by conducting a series of fatigue tests on three kinds of adhesively bonded joint specimens; butt joint, scarf joint and thick-adherend lap-shear joint, where these joints have considerably uniform stress distributions in the adhesive layer. The stress distributions of these joints were analyzed by the finite element method. The results showed that the fatigue limits of respective joints are governed by the maximum principal stress except when negative hydrostatic pressure acts on the adhesive.

Mortensen and Thomsen [65] have developed a unified approach for the analysis and design of adhesive-bonded stepped and scarfed lap-joints. The adherends were modelled as orthotropic beams/plates in cylindrical bending (i.e. $b/L \gg 1$ where b and L is width and length dimensions respectively). Both the linear elastic and inelastic behaviour of adhesives were considered. The governing equations were formulated in terms of a set of first-order ordinary differential equations, which are solved numerically using the 'multi-segment method' of integration.

Du *et al.* [66] have used finite element method for predicting the strength of Al adherends bonded by structural adhesives. Criteria based on maximum strain and stress were used to characterize the cohesive failure within the adhesive and adherend failure respectively. It was observed that their approach is capable of analyzing the entire deformation and failure process of adhesive joints in which different fracture modes may dominate and both adhesive and adherends may undergo inelastic deformation. The finite element predictions of the joint strength agreed well with the experimental measurements.

Gleich *et al.* [46] have studied shear and peel stress distributions in a scarf joint made of two isotropic adherends with blunt adherend tips using a linear elastic analysis by a finite difference method. The adherends were modelled as plates with extensional and bending stiffnesses bonded together with an elastic interlayer. The stresses across the

adhesive layer were assumed to be constant. The current analysis was applied to cases known from the literature which demonstrated good agreement with the shear stresses but the peel stresses were overestimated.

Chui [67] fabricated three hundred joints from oriented strandboard (OSB) and resorcinol formaldehyde adhesive and tested them in tension in a dry condition. These included two nominal thicknesses of OSB (11 mm and 18 mm) from two manufacturers. The joint strengths were compared with the material strengths in tension. The results showed that optimum joint strength was reached when the scarf slope was about 1 in 7 irrespective of manufacturer and thickness. At the optimum joint slope, no loss of strength was observed compared with unjointed material. For slopes less than the optimum slope, normalized joint strength decreased slightly. As the scarf slope increased from the optimum value, normalized joint strength decreased to a value of about 0.35 for a vertical scarf (butt) joint.

In spite of these findings, useful predictions of scarf-joint strengths in tension for commercial unidirectional composites with small scarf-angles appear scarce. For successful use of scarf-joint configurations with unidirectional composites such as those used in helicopter rotor blades, bridges constructions and repair, the mechanical responses of these joints under uniaxial tensile loading conditions need to be understood properly.

2.3 Lap Joint

The new era aircraft utilize a large number of primary structures made of composite materials [68] and the complex airframe structures are manufactured by employing adhesive bonding [69]. Bonded single lap joints prepared according to ASTM D1002 are widely used in adhesive industry for various purposes such as to assess the bond integrity, evaluate the adhesive performance and predict the fatigue life. The lap joint configuration is the most common joints in practice, and the single lap joints (SLJs) are widely used in a variety of standard tests for evaluating adhesive performance and quality control. The two most common methods used for analyzing adhesive joints are the stress-based analysis and the fracture mechanics-based methods. The stress analysis approach is used for

the determination of shear and normal (i.e., peel) stress distribution within the adhesive bondline under static loading conditions [4, 60, 61, 70–72]. Assuming the adherends as a rigid material (i.e., they do not exhibit elastic deformation) and considering that the adhesive deforms only in shear, an expression for apparent shear strength of the single lap joint is given by [4].

$$\tau = \frac{P}{2cB} \tag{2.3}$$

where P is the failure load, B is the width and $2c$ is the overlap length.

2.3.1 Analysis and Joint Performance

Volkersen [4] presented a theoretical analysis of lap joints by considering only the stress arising from the differential straining in the overlap region. The differential straining between the adherends (see Figure 2.3) results in a non-uniform shear stress distribution in the bondline with a maximum at each end of the overlap. The stress concentration factor, η defined as the ratio of maximum to the mean shear stress across the bondline was derived in terms of bond parameters such as adhesive layer thickness, t_a, overlap length, $2c$, adherend's thicknesses and the material properties of adherends and adhesive as below

$$\eta = \frac{X_1}{X_2}\left[\frac{2{X_2}^2 - 1 + \cosh(2X_1X_2)}{\sinh(2X_1X_2)}\right] \tag{2.4}$$

where

$${X_1}^2 = \frac{2c^2G}{E_2t_2t_a}$$

and

$${X_2}^2 = \frac{E_1t_1 + E_2t_2}{2E_1t_1}$$

where E_1, t_1 and E_2, t_2 are the Young's modulus and thickness of upper and lower adherends; G and t_a are shear modulus of adhesive material; and $2c$ is the overlap length.

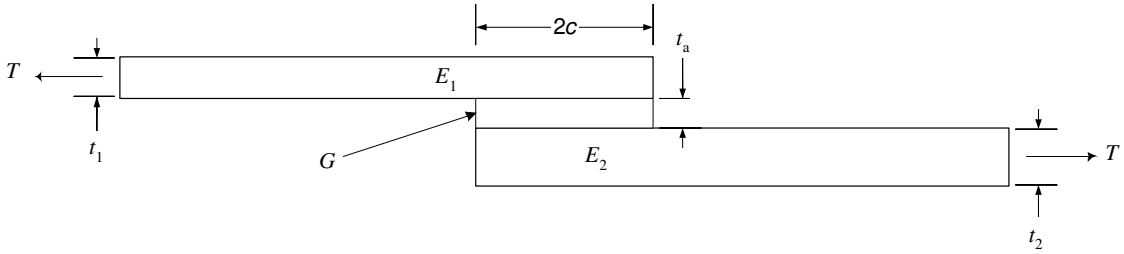

Figure 2.3: Schematic of a single lap joint considered in the Volkersen's analysis [4].

As the science of joining developed, it was found that the Volkersen analysis based on the shear lag model was unsatisfactory in the sense that it was unable to include the peel stress in the bondline at the ends of the overlap occurring due to the load eccentricity. As the Volkersen analysis was unable to describe the stress distribution correctly, the modelling was later refined by adopting a two-parameter elastic foundation approach, in which the adherends are considered as narrow or wide beams (panels) and the adhesive layer was described in terms of uniformly distributed transverse normal and shear springs. This type of model was originally suggested by Goland and Reissner [71] but later formed the basis for many investigations of the structural response of adhesive bonded joints. Goland and Reissner derived an equation to relate the bending moment at the ends of the overlap to an in-plane applied load. The undeformed single lap joint geometry considered in Goland and Reissner analysis with the geometric parameters is depicted in Figures 2.4(a) and 2.4(b). In their analysis they assumed that the adhesive layer is very thin as compared to the adherend thickness ($t_a \ll t$) and thus neglected the adhesive layer presence. The edge bending moment, M_0 in terms of bending moment factor, κ, load per unit width, T and substrate thickness, t is given by

$$M_0 = \kappa \frac{Tt}{2} \tag{2.5}$$

where

$$\kappa = \frac{1}{1 + 2\sqrt{2}\coth(u_1 l)\tanh(u_2 c)},$$

$$u_1 = \frac{\sqrt{12(1-\nu^2)T}}{Et^3}$$

and

$$u_2 = \frac{u_1}{2\sqrt{2}}$$

where E and ν are the Young's modulus and the Poisson's ratio of the adherend material.

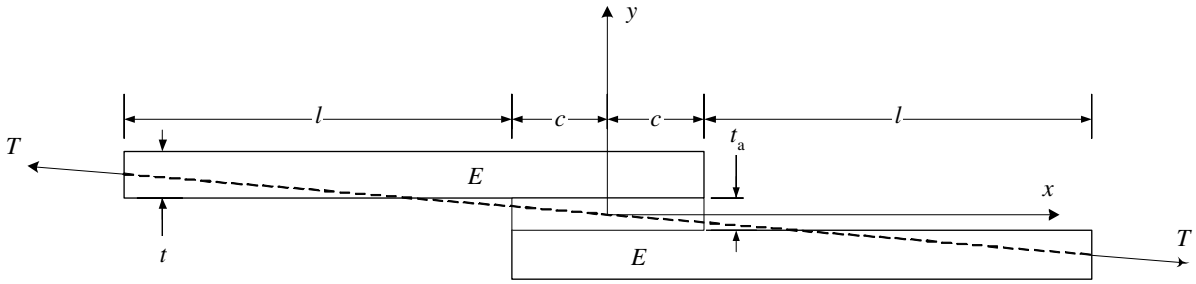

(a) Undeformed geometry

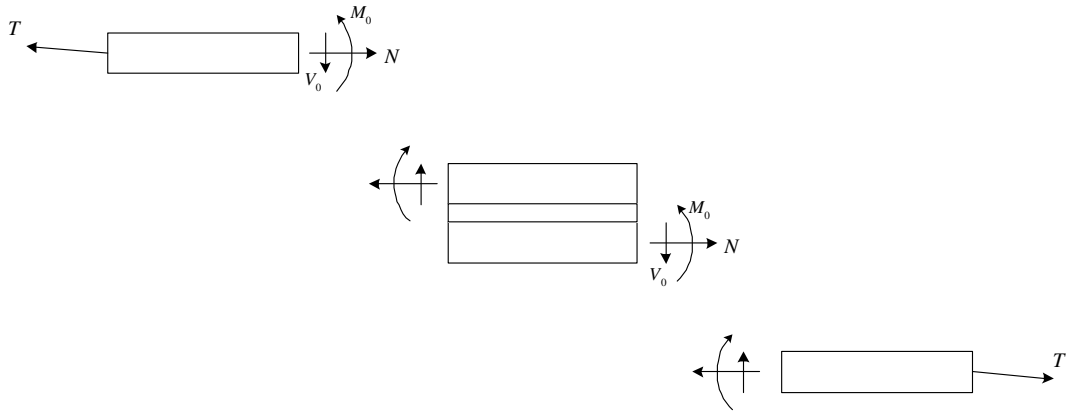

(b) Free-body diagrams

Figure 2.4: (a) Undeformed single lap joint geometry considered in Goland and Reissner's theoretical analysis (b) Free-body diagrams considered in the analysis.

The early research work pertaining to adhesive bonding prior to 1961 was reviewed by Kustcha [73], and developments from 1961 to 1969 was reviewed by Kustcha and Hofer [74]. Matthews *et al.* [75] have published a review paper covering various aspects of adhesively bonded joints made of composite materials. Vinson [76] produced a summary of published work related to adhesive bonding of polymer matrix composite structures in 1989.

Goland and Reissner [71] assumed that the thickness of adhesive layer was so small as compared to the adherend thickness ($t_a \ll t$) that its presence does not have any significant effect on the determination of the bending moment, M_0 at the ends of the overlap. However, Hart-Smith's [77] analysis was able to account the effect of adhesive layer thickness on the bending moment as he coupled the bending moment with the adhesive shear, τ_0, and peel stresses, σ_0. He calculated the edge bending moment at the ends of the overlap in a single lap joint by considering individual deformations of the upper and lower adherends as

$$M_0 \cong T\left(\frac{t+t_a}{2}\right)\frac{1}{1+u_1 c+\frac{u_1^2 c^2}{6}} \tag{2.6}$$

His analysis determines the edge moment, M_0 and the adhesive stresses simultaneously, and takes into account of the effect of large deflection of the free adherends, but ignores the large deflection effect in the joint overlap. Hart-Smith has published a number of notable papers [60, 72] covering various aspects of analysis and design of advanced composite bonded joints.

Adams and Wake [78], Tong and Steven [20] and Messler [6] have published books on structural adhesive joints. Baldan [79, 80] has reviewed various aspects of adhesively-bonded joints and repairs in metallic alloys, polymers and composite materials. Mackerle [81] has published bibliographical review of the finite element analysis and simulations of adhesive bonding, soldering and brazing.

Reis *et al.* [82] studied the mechanical behavior of single-lap joints of polypropylene (PP) reinforced with glass fibres. Failure loads were obtained experimentally for different superposition lengths (15, 30, 45 and 60 mm). They also performed a 2D finite element analysis assuming a plane strain state, a linear elastic orthotropic behavior for the laminates and an elastic-plastic behavior for the adhesive. They observed that the positions where σ_{yy} and τ_{xy} stresses have their maximum values, which were near the extremities of the joint and close to the interface adhesive/adherends, moved inside the joint with increasing load. They proposed an adhesive failure criterion based on equivalent stress

in terms of σ_{yy} and τ_{xy} which is similar to von Mises criteria. This quantity varies 9.7 % with superposition length, which can be considered reasonable therefore can be used as a damage criterion for single-lap joints.

Da Silva *et al.* [83] studied a bismaleimide adhesive, Redux 326 (Hexcel Composites), in two forms: supported (woven glass) film and paste. Different composite manufacturing methods such as vacuum release technique and sheet moulding were evaluated in order to produce adhesive joints and bulk specimens free of defects. They used single lap joint configuration for the evaluation of the manufacturing methods and studied the influence of voids and the carrier support on the joint strength.

Francesco [84] has investigated the effect of Kevlar stitching on the tensile static and fatigue properties of co-cured single-lap joints with cross-ply graphite-epoxy adherends. The variables considered in his study were the overlap length, the stitch spacing, and the off-edge distance. His experimental results indicate that stitching does not improve the static strength, however the stitched joints exhibit much better fatigue performance than unstitched joints.

Yang *et al.* [85] developed an analytical solution for determining adhesive stress distributions within the adhesive-bonded single-lap composite joints. The composite adherends were assumed linear elastic while the adhesive was assumed elastic-perfectly plastic following the von Mises yield criterion. Laminated anisotropic plate theory was applied in the derivation of the governing equations of the bonded laminates. The adhesive was assumed to be very thin and the adhesive stresses are assumed constant through the bondline thickness. The governing equilibrium equations were solved analytically with appropriate boundary conditions using a commercial programming software Maple V. The adhesive stress calculated by analytical model compared well with the finite element simulations.

Kim and Lee [86] have studied the effect of process parameters such as curing pressure and temperature on the tensile load capabilities of tubular single-lap adhesive joints bonded with an epoxy adhesive experimentally. The actual cure finish temperature was determined using thermocouples and dielectrometry. From the experiments, they found

that the actual cure finish temperature of tubular single-lap adhesive joints increased as applied pressure increased, which increased residual thermal stress in the adhesive layer and decreased the load capabilities of adhesive joints. From finite element analysis and experimental results of tubular single-lap adhesive joints, the optimal geometry condition for adhesive joints was also investigated.

Lees and Makarov [87] used single-lap shear test experiments to evaluate the strengths of combined mechanical-connected and adhesive-bonded joining systems for composite materials. They studied the influence of the pin material, diameter, number and configuration on the resulting performance. Their results demonstrated that the potential of pinned/bonded systems as a new method for connecting composite materials. However, they recommended further work is necessary to confirm the sensitivity of the results to changes in parameters such as the fibre architecture, adherend geometry, adhesive interface and joint configuration.

Melograna and Grenestedt [88] have studied single lap joints made from CFRP adherends with wavy geometries. In their experimental studies they observed that it is superior to the conventional single lap joints in terms of strength.

Zou *et al.* [89] developed analytical solutions for adhesively bonded composite and metallic joints. The classical laminate plate theory and adhesive interface constitutive model were employed in their deduction. Both theoretical and finite element analysis studies were conducted to reveal the adhesive peel and shear stresses. They analyzed single-lap and single-strap joints under tensile, moment and transverse shear loadings. They observed good correlation between the FE and theoretical analysis.

Ozel *et al.* [90] have performed elasto-plastic stress analysis of a single lap joint (SLJ) subjected to bending moment using a 2D non-linear finite element analysis. The SLJs, consisting of hardened steel as the adherend bonded by two adhesives, one stiff and another compliant, with very different mechanical behaviors were analyzed. They also determined the effect of geometrical parameters on the performance of the SLJs with four different adherend thicknesses and overlap lengths for each adhesive used. The theory

was verified with experimental measurements. It was observed that there was a significant effect of adherend thickness on the strength of the joint with both adhesives. Their results shows that SLJ bonded with the compliant adhesive has a higher failure load with increasing overlap length.

Van Tooren *et al.* [91] have a applied stress singularity model to predict joint failures in single-lap joints with varying bondline thicknesses. Mechanical characterization of the adhesive was carried out to determine the Young's modulus and Poisson's ratio. Secondly the failure loads versus bondline thickness was measured. Finally they proposed a relationship between the joint strength and bondline thickness in terms of a two-parameter Weibull function.

Narasimhan and Pandey [92] have presented a 3D large strain viscoplastic analysis of adhesively bonded single lap joint. A pressure (mean stress) and effective stress dependent constitutive law for the adhesive was considered. The adherends and adhesive layers were both modelled using 20-noded solid elements and peel and shear stresses in the adhesive layer were estimated.

The effectiveness of surface pre-treatment parameters such as radio frequency plasmas of oxygen, air and argon was studied by Dartevelle *et al.* [93] by employing SLJ. Oxygen plasma treatment had the most marked effect on joint performance: resulting in a 40% increase in initial joint failure strength and a 38 % increase of aged joint failure strength as compared with the contaminated alloy.

Sancaktar and Nirantar [94] have studied the effect of tapering the ends of the adherend on the joint strength and joint deformation behavior of a single lap joint geometry using a non-linear finite element (FE) technique. The FEA results were then compared with the experimental results for different single lap configurations, which had aluminum and steel adherends with different surface etch conditions, bonded using two different adhesives. The FEA results were found to be consistent with the experimental results with the normal and shear stresses significantly decreasing in the modified (tapered) geometries over those in unmodified geometries. The joint strength increased with decreasing

taper angle, reaching a maximum at the smallest value considered (around 10^0).

Hsiao *et al.* [95] have used multiwalled carbon nanotubes (MWCNT) reinforced adhesive to prepare single lap joints with graphite fibre reinforced adherends. The effect of MWCNT weight fraction in epoxy adhesive on the average joint shear strength was measured. A significant enhancement was observed in joint performance as the weight fraction of carbon nanotubes was increased.

Boss *et al.* [96] employed single-lap adhesive bonded joints to examine the effect of modulus and geometry gradation of adherends on joint performance. The modulus grading of the adherend was provided by continuously varying the composite fibre braid angle and geometrical grading was achieved by varying the adherend thickness in the overlap region. The peak stress distribution and transverse deformation at the adhesive mid-thickness calculated using the finite element method were used to assess the effectiveness of modulus grading and geometrical grading. It was noticed that for certain cases, modulus grading provides reduced stress levels compared to geometrical grading. In certain other cases they demonstrate benefits similar to geometrically graded adherends. In case of shear stress reduction, modulus grading provided better performance; however, it is possible to combine modulus and geometrical grading to evolve an overall better performing single-lap joint. A similar study by Ganesh and Choo [97] have shown that the maximum shear stress reduced by about 20% and the shear stress was more uniformly distributed in the adhesive when the adherend modulus was graded. It was also noticed that the joint rotation was minimum in case of adherend grading.

Pires *et al.* [98] studied the application of two types of adhesives with different stiffnesses along the overlap length in single lap joints. A stiff adhesive was applied in the middle portion of the overlap, while a low modulus adhesive was applied towards the edges prone to stress concentrations. Their results showed measurable increase in strength of the bi-adhesive bonded joints compared with those in which single adhesives were used over the full length of the bondline.

Avila and Bueno [99, 100] have studied the tensile joint strength of single-lap and

wavy single-lap joints. They carried out a statistical study by considering the sample size band and the statistical differences between the single-lap and wavy single-lap joints (see Figure 2.5). The analysis showed that wavy joint demonstrated an average increase of nearly 41% in loading carrying capacity under uniaxial tension. They attributed this improvement to the compressive stress field developed inside the wavy-lap joint during loading.

Mahdi *et al.* [101] used single-lap shear tests and double-cantilever beam fracture experiments to evaluate the oven-cured and induction-cured adhesively bonded joints made from woven-fabric composites. They have presented the results of a study on the use of induction heating for bonding composite adherends. It was found that the strength of single-lap shear joints was not significantly affected by the choice of the adhesive hardening method. Furthermore, the critical fracture energy of the oven-cured and induction-cured double-cantilever beams was also found to be only dependent on the adhesive type. Induction-cured specimens were found to be as tough as oven-cured specimens.

Zeng and Sun [102] have studied the strength of wavy lap joints made from cross-ply composite adherends and observed that the design was much stronger than the conventional flat joint under both static and fatigue tensile loading. The main reason for this improvement was reduction in eccentricity in loading path in the case of a wavy joint.

Feih and Shercliff [103] have predicted the failure load and the failure location in a single-L peel joint of composites using a numerically stabilized damage model. The model was validated with experimental results. Their finite element model was found to correlate well with the test results.

Kafkalidis and Thouless [104] have reviewed the mechanics of lap-shear joints followed by detailed analysis of the problem using a cohesive-zone approach. The cohesive-zone model allowed to consider the geometry of the adhesive, cohesive properties of the interface and plastic deformation of the adherends in the analysis. In the first part the authors examined the strength of elastic joints, with an emphasis on the effects of geometry, the cohesive strength of the adhesive and mode-mixedness. In the second part,

the effect of plasticity in the adherends was considered and transition between the elastic and plastic regimes were observed. They made comparison between the predictions of the numerical calculations and experimental observations for a model system consisting of a commercial adhesive used to bond an aluminum alloy. Using cohesive-zone parameters previously determined for this particular combination of materials, the numerical predictions showed excellent agreement with the experimental observations.

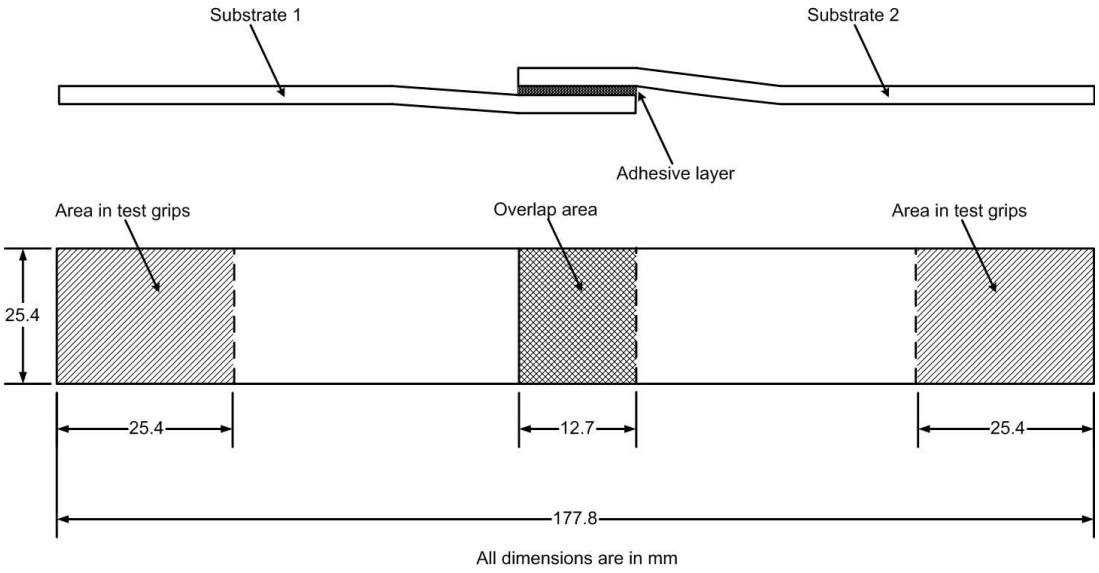

Figure 2.5: Schematic diagram of a wavy joint.

2.3.2 Role of Spew fillet

Apalak and Engin [105] studied the effect of adhesive free-end geometry on the initiation and propagation of damaged zones in adhesively bonded single and double lap joints. Both tensile and bending loading were considered. They showed that as the adhesive fillet size increased, the applied load necessary for the damaged zone initiation also increased.

Adams and co-workers [106, 107] performed stress analysis to study the role of the spew for a wide range of joint parameters. They have studied the stress distribution across the adhesive thickness and found it essentially uniform over a large part of the overlap length. However, near the overlap end, the stress variation across the thickness was very high, resulting in higher stresses and so lower strengths than would be expected consider-

ing average stress levels in the joint.

Tsai and Morton [24] studied a single-lap joint made from laminated composite with and without a spew fillet under tensile loading experimentally and numerically using FEA. They used Moire interferometry to measure the in-plane surface deformation of the overlap region of the test specimens. Experimental and numerical results indicate that the adhesive shear and peel strain (stress) concentrations was reduced greatly in the case of a fillet at the end of the overlap.

Kim and Lee [86] have studied fracture characteristics of single-lap bonded joints in composites experimentally and numerically. The effects of bonding method, surface roughness, bondline thickness and the existence of a fillet on the failure characteristics and strength of bonded single-lap joints were evaluated. They observed apparently different failure process, failure mode and the load-displacement curve for the different bonding methods.

Feih and Shercliff [103] have performed some numerical simulations to study the effect of fillet shape occurring in a single-L composite peel joint on the joint performance. A review of adhesive failure criteria was presented and these criteria were compared with experimental outcome. Their comparative study shows that zone criterion was able to predict the failure load at best for the different fillet shapes. It was also concluded that an alteration in fillet shape enhanced the joint strength significantly.

2.3.3 Estimation of Energy Release Rate

Although characterization of materials based on strength of materials approach is easy, it is not suitable in true sense for flaw prone materials, because it does not take into account the initial flaws present in the material matrix. In contrast, the fracture mechanics approach, which was developed on the basis of Griffith and Irwin theories, takes into account the presence of flaws in the material matrix. Ripling and his co-workers [108–110] have used this method extensively and studied the bonded joints by calculating the fracture toughness using a taper double cantilever beam (TDCB) configuration. Irwin

derived an expression for energy release rate, G_e, as the rate of change in potential energy with crack area A as given by [20]

$$G_e = -\frac{d\Pi}{dA} \tag{2.7}$$

where Π is the potential energy of an elastic body, defined as follows:

$$\Pi = U - W \tag{2.8}$$

where U is the strain energy stored in the elastic body and W is the work done by external forces.

The crack propagation in the solid body occurs when G_e attains a critical value G_c, namely, $G_e = G_c$. Depending upon the type of loading with reference to the crack orientation the crack propagation can be divided into 3 types: mode I; mode II and mode III. The mode I fracture toughness (K_{IC} or G_{IC}) of a material is a measure of its resistance to crack propagation under opening mode loading. Most of the materials perform better under mode II and mode III loading than that of mode I loading because mode I fracture toughness of the material is found to be the lowest ($G_{IC} < G_{IIC} < G_{IIIC}$) [111]. In the case of adhesively bonded systems G_{IC} is replaced by the adhesive fracture energy, G_a. Consequently, in several manufacturing industries such as aerospace, land transportation, building, and marine, the fracture energy, G_a, of an adhesive is regarded as the most important design variable for bonded structures.

Sun and Yang [112] used a fracture mechanics model to estimate the energy release rate of adhesive-bonded single-lap composite joints under tensile loading. The stress distributions within the composite joint were determined by the laminated anisotropic plate theory. Based on the stress resultants, the crack tip forces were obtained and the energy release rate of adhesive-bonded single-lap composite joints with a crack were determined by the classical plate theory version of virtual crack closure (VCC) method. The symbolic computation tool, Maple 8, was used as the mathematical tool. The results from the analytical model showed a good agreement with the finite element solutions.

Qin and Dzenis [113] analyzed the single lap adhesive composite joints with delaminated adherends by developing a simple engineering model for cracked adhesive joints with arbitrary orthotropic laminated adherends. They studied joints with unidirectional and cross-ply adherends. Variations of the strain energy release rates with the crack location and size were calculated. Their analysis results showed that joints with the cross-ply adherends have higher energy release rates than the joints with the unidirectional adherends. The experimental observations of the delamination growth were found to corroborate the theoretical predictions.

Court *et al.* [114] studied the damage evolution in a single lap joint of polymethylmethacrylate (PMMA) and a two-part acrylic adhesive using video imaging techniques. The joints were aged in a hot/wet environment (40^0 C and 95 % humidity) with no applied stress up to 4000 h and tested under tensile loading conditions. Significant reduction in joint failure strength and a change in the failure mode from substrate failure to interface failure was noticed.

Different kinds of coupon specimens such as the double cantilever beam (DCB) [115], and the taper double cantilever beam (TDCB) [116, 117], have been used in the past to calculate the adhesive fracture energy of adhesive bonded joints. There are two shortcomings in DCB test coupons. Firstly, it requires that the crack length be known accurately, which is quite tedious to measure with presently available measuring devices. Secondly, displacement and load at the loadline both are to be monitored accurately. Some of the difficulties in DCB testing methods can be avoided by using the TDCB testing method, as in the case of TDCB only load value need to be measured, but unfortunately, fabrication of the TDCB joint from composite substrates is cumbersome and thus, these benefits can not be exploited.

Recently, calculation of fracture energy of an adhesive in a bonded single lap joint was performed by using the KO-model [5, 16, 18]. Recent studies conducted on single lap joints (SLJ) with naturally occurring spew fillets showed that the fatigue life obtained from the KO-model appeared to fit only modestly with those from analytical and numer-

ical studies on similar adhesives/substrate systems [5, 18, 19]. It was suggested that the discrepancy might be due to the presence of adhesive fillets at the end of the overlap, which exaggerated the magnitude of peel stress developed [22, 23].

Although this ASTM D1002 standard recommends joint preparation with square ends, most of the previous experimental investigations reported on single lap joints have used joints with naturally occurring spew fillets. Spew fillet is a portion of cured adhesive which is squeezed out from the lap area and forms a bead at the ends of the overlap when the two substrates are assembled during bonding process. The spew fillet can take different shape and size (triangular, round, oval etc.) [70] and as of now no standard methods are available to control or eliminate the effect of spew fillets in the bonded joint testing methods. Some commonly occurring spew fillets in single lap joints and square end single lap joint are shown in Figure 2.6. Single lap joints have been studied and analyzed by many researchers, the pioneering work dates back to as early as 1940s [4].

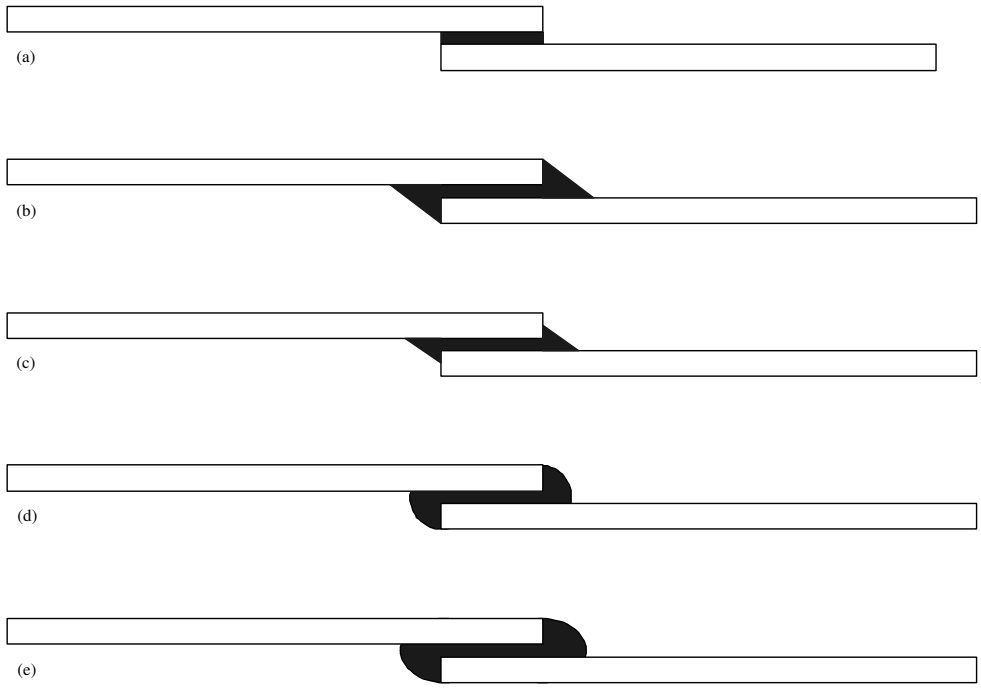

Figure 2.6: Single lap joint (SLJ) without and with commonly occurring spew fillets (a) square ends, (b) full triangular, (c) half triangular, (d) full rounded, and (e) oval.

A modified single lap joint test geometry need to be developed with the aim of reducing the effect of spew fillet on the measured properties (i.e. reducing experimental

scatter in the measurements) such as apparent lap shear strength, toughness, elongation and number of cycles to failure of the bonded joints.

2.3.4 Effect of Moisture

In many engineering applications structural adhesive joints may be exposed to hostile environmental conditions or experience cyclic loading or both. It is well known that the mechanical properties of the polymeric materials (e.g. polymer based composites and adhesives) are adversely affected in the presence of water. Ravi *et al.* [118], have studied the influence of long term moisture absorption on the mechanical properties of Kevlar 49 fabric reinforced composite. Their investigation showed that moisture absorption reduces the tensile strength of Kevlar/epoxy composite. However, the modulus of elasticity was insensitive to the moisture absorption. The fracture toughness was 25% higher than demoisturised composites for small amount of moisture absorption and had very little effect on the fracture toughness of the composite. Lucas and Zhou [119] have studied the water absorption effect on diffusion behavior, moisture induced expansion and fracture properties of thermoset (T330/934) and thermoplastic (IM6/PEEK) composites. In this investigation they have reported that graphite epoxy (T300/934) exhibits both Fickian as well as non-Fickian behavior. However, the graphite thermoplastic (IM6/PEEK) composite showed Fickian behaviour. In width and thickness directions, significant dimensional changes were observed, while no significant expansion along the fiber (longitudinal) direction was observed. The fracture toughness of IM6/PEEK composites was insensitive to the moisture absorption, however they observed significant reduction in the fracture toughness of T300/934 composites with moisture absorption.

Several researchers have studied the effect of environmental factors, such as water on the strength of adhesively bonded joints. Some of the commonly used test geometries are butt joints [120], the wedge specimen [121], T-peel test [122], step lap shear (SLS) [123], double lap joint (DLJ) [124] and single lap joint (SLJ) [125–127]. The pioneering work in this area was undertaken by Mostovoy and Ripling as cited in paper by Kinloch and Shaw

[13]. They used taper double cantilever beam (TDCB) joint made of aluminium substrates and epoxide adhesives. Later on, many investigators have used the test geometry proposed by Mosovoy and Ripling and various other geometries.

The double cantilever beam (DCB) [128], taper double cantilever beam (TDCB) [128], cracked lap shear (CLS) [128], compact tension (CT) [128] and single lap joint (SLJ) [127–130] are commonly used to study the effect of moisture on adhesively bonded joints. Some of the critical research work dedicated to study thew effect of moisture absorption is reported below.

Parker [127] used single lap shear test geometry to study the strength of bonded carbon composite joints exposed to high humidity. The joints were exposed unstressed to $50^0C/69\%$ RH for up to three years and tested at $20^0C, 60^0C$ and 80^0C. The specimens were tested after exposure time of 1000, 4000, 9000, 18000 and 25000 hours. He observed that long-term exposure to high humidity and increased test temperature both reduced the strength of the joints. No interface failure between the adhesive and the composite adherends was observed.

Lee *et al.* [131] measured the strength and modulus of adhesives under hygrothermal environments with respect to the absorbed moisture content and temperature. They also studied the strength of adhesively bonded tubular lap joints with respect to the absorbed moisture content. From the investigation they found that the tensile strength of both the adhesives and tubular joints decreased as the moisture content increased, Also, it was found that chemical surface treatment of the adherends improved the strength retention of the joint under a hygrothermal environment.

Hand *et al.* [132] performed moisture absorption studies on six types (i.e., Hysol EA 9394, LP2-31, MML-3H, MML-14H, MML-16H and MML-96) of adhesives and bonded joints made from them. The moisture level/concentrated saturated within 48 hours. The fracture toughness studies on exposed samples of EA 9394, LP2-31 and MML-3H indicated that the fracture toughness decreased with increased exposed time to the humidity. Adhesive MML-3H was found to have a good balance of moisture absorption resistance,

load bearing capacity and fracture toughness. EA 9394 showed moderately good fracture behavior, despite its rapid water weight gain. LP2-31 showed the lowest values of strength retention and fracture toughness, despite of its low moisture pick-up characteristic.

Although it has been clearly demonstrated by some of these studies that the absorption of water influence the mechanical performance of adhesively bonded joints, these test procedures have several limitations. Most of these testing geometries can not be used to study joints made of composite adherends. So far, only little work has been undertaken to study the adhesively bonded composite joints. With composite adherends, most of the work undertaken has used DCB, the Peel test, and the single lap joint test geometry. Although the single lap joint test geometry has the problem of spew fillets, it is the most popular test configuration for the evaluation of adhesively bonded joints.

An accurate and reliable test methodology for studying the effect of hostile conditions on adhesively bonded joints parameters is needed.

2.3.5 Fatigue Life Calculation

During the service life, most of the components are subjected to cyclic mechanical and environmental loading. Both mechanical as well as environmental loading can cause the deterioration in mechanical and physical properties of materials.Thus, it is important to develop a robust and accurate fatigue life prediction method for evaluating bonded structural assembly service life.

The first step in the prediction of fatigue life of bonded joints/structures is to obtain fracture mechanics data in cyclic fatigue on the adhesive/substrate system of interest. The fracture mechanics data are represented in an expression such as the relationship between the rate of crack growth, da/dN and the maximum energy release rate, G_{max}. Then an expression for G_{max} in terms of crack length should be available. Finally, these expressions are combined and the resulting expression is integrated to predict the long-term fatigue life of the joint or component.

Fracture mechanics data can be obtained by performing fatigue tests on any standard

LEFM test geometry, such as taper double cantilever beam (TDCB), double cantilever beam (DCB) or compact tension (CT) specimens. These tests enable the measurement of the rate of fatigue crack growth, da/dN, for maximum energy release rate, G_{max}, applied during the fatigue cycle. The fracture mechanics tests should be conducted under the same test conditions as joints whose fatigue life is to be predicted. The locus of failure should also be same in both fracture tests and the joint or component of interest.

Kinloch and Osiyemi [16] have reported the use of fracture mechanics data obtained from fatigue testing of double cantilever beam (DCB) to predict the fatigue life of adhesively bonded single lap joint (SLJ) in early 1990's. They developed an analytical model to predict the fatigue life of a single lap joint and generated experimental data by testing SLJ's under tension-tension cyclic loading. They observed a good correlation between the analytical and experimental results (maximum load per unit width versus number of cycle to failure). Recently, many researchers such as Kinloch and Taylor [5], Hadavinia *et al*. [17] and Curley *et al*. [19] have conducted rigorous studies on single lap joints (SLJ) with naturally occurring spew fillets analytically, numerically and experimentally. Their experimental measurements which was plotted as maximum applied load per unit width, T_{max} vs. $\log(N_f)$ curve modestly fitted with both numerical and analytical results. Some recent research work which reports fatigue life prediction of bonded joints are highlighted below.

Curley *et al.* [133] have discussed the use of the relationship between da/dN and G_{max}, which can be obtained in a relatively short timescale, to predict the fatigue lifetime of (no pre-cracked) single-overlap joints subjected to tension-tension cyclic load. An analytical and a finite-element model was derived to predict the number of cycles to failure, N_f, for lap joints, particularly when the latter model was used to deduce the value of the elastic strain-energy release-rate, G, in the lap joints. They observed good agreement between the theoretical solutions and the experimental results. Later on, Curley *et al.* [19] used a fracture-mechanics approach to predict the cyclic-fatigue performance of the adhesively-bonded single-lap joint and a typical bonded component, represented by

an adhesively-bonded top-hat box-beam joint. The joints were tested under cyclic-fatigue loading in either a wet or dry environment, respectively. Firstly, fracture-mechanics tests were used to obtain the relationship between the rate of fatigue crack growth per cycle, da/dN, and the maximum strain-energy release-rate, G_{max}, applied during the fatigue cycle for the adhesive/substrate system, in both a dry and a wet test environment. Secondly, analytical and finite-element theoretical models were developed to describe the variation of the strain-energy release-rate with crack length, as a function of the applied fatigue loads, for the single-lap joint and the top-hat box-beam joint. Thirdly, the experimental results from the short-term fracture-mechanics tests, obtained under similar test conditions and in the same environment as were used for the single-lap or bonded box-beam joints, were combined with the modelling results from the theoretical studies. Finally, the cyclic-fatigue performance of the single-lap or bonded box-beam joints was predicted over relatively long time-periods. The agreement between the theoretical predictions and the experimentally-measured cyclic-fatigue behaviour for the joints was found to be very good.

Hadavinia and co-workers [18] have evaluated the performance of adhesively bonded joints under monotonic and cyclic-fatigue loading. The joints comprised of epoxy-film adhesive and aluminium-alloy substrates. The effects of undertaking cyclic-fatigue tests in (a) a 'dry' environment of 55% relative humidity at 23^0C, and (b) a 'wet' environment of immersion in distilled water at 28^0C were studied. The basic fracture-mechanics data for these different joints in the two environments were measured. Apart from basic data fatigue behaviour of single-lap joints (SLJs) were also assessed. In another paper [17] the authors suggested a method for predicting the lifetime of adhesively bonded joints and components. The prediction method consisted of three steps. First, the acquisition of fracture-mechanics data under cyclic loading in the environment of interest, resulting in an expression which related the rate of crack growth per cycle, da/dN, to the maximum applied strain-energy release-rate, G_{max}, in a fatigue cycle. Second, combining the relationship with an analytical or a computational description of the variation of G_{max} with

the crack length, "a", and the maximum applied load per unit width, T_{max}, per cycle in the joint, or component. Third, the numerical integration of the resulting equation to give a prediction for the cyclic-fatigue lifetime of the bonded joint or component. They compared the theoretical predictions from the above method, using different approaches to describe the variation of G_{max} with the crack length, "a", and maximum applied load per unit width, T_{max}, in the single-lap joint, with the cyclic-fatigue behaviour of the lap joints as ascertained from direct experimental measurements.

Abdel Wahad *et al.* [134] proposed and demonstrated a generalized technique for fatigue life prediction of bonded structures using finite element analysis. The method is based on numerical integration of the fatigue crack growth law from an initial pre-crack to a final crack size. They applied the proposed technique to carbon fibre composite joints bonded with an epoxy adhesive. A crack growth law was determined experimentally using double cantilever beam (DCB) samples. Experimental load-life data were then generated for single and double lap joints (DLJs) manufactured from the same materials as that of DCB samples. The crack growth law determined from the DCB samples was used to predict the load-life response of the single lap and DLJs. They observed a reasonable agreement between the predicted and experimental load-life data.

2.4 Double Cantilever Beam (DCB) and Taper Double Cantilever Beam (TDCB)

Double cantilever and taper double cantilever beam test geometries are used to measure the fracture mechanics parameters of adhesives in a bonded system. Currently, both of these test geometries are widely used in the adhesive industry and in research and development organization. The literature pertinent to measurement of Mode I adhesive fracture energy using DCB and TDCB is reported below.

Blackman and co-workers [115, 116] have reviewed the adhesive fracture energy calculation methods (e.g., area method, compliance method, simple beam theory method,

corrected beam theory and displacement method), from the data obtained by testing double cantilever beam specimens consisting of bonded polymeric fibre-composite substrates. They observed that, the corrected beam theory can be successfully employed for bonded fiber composite joints to obtain an accurate and reliable value of adhesive fracture energy. They have also compared the mode I adhesive fracture energy (G_{IC}) calculated from double cantilever beam (DCB) and taper double cantilever beam (TDCB): (G_{IC}) values were independent of the test geometry, but dependent upon the substrate material used. A similar observation was made by Bell and Kinloch [117]. A separate study by Blackman *et al.* [135] revealed no differences in the values of G_c of adhesive for the mild steel and aluminum alloy joints while the value for the CFRP joints was comparatively lower.

Pereira and Morais [136] have done an experimental study on the strength of adhesively bonded stainless steel joints, prepared with two epoxy and one acrylic adhesive. The mode-I critical strain energy release rate, G_{IC}, was measured in double cantilever beam (DCB) tests. Lap-shear tests were performed on various types of single-lap and double-lap joints. Finite element analyses were used to explain joint strength results. It was found that the strengths of epoxy adhesive joints depended mostly on the level of peel stresses near the bondline edges.

Hosaka *et al.* [137] studied the static and fatigue fracture characteristics of the rubber modified epoxy adhesives under Mode I loading. The fracture toughness under static loading was measured using Double Cantilever Beam (DCB) specimens. The energy release rate was used as a parameter of fracture toughness. The effect of rubber content and adhesive layer thickness on the fatigue crack growth and static strength were examined. The following conclusions are drawn from the study: The rubber modified adhesives show higher fracture toughness and fatigue resistance than the unmodified one. The fracture toughness increased with an increase of adhesive thickness while no effect of adherend thickness was found.

Erpolat *et al.* [138] used double cantilever beam joints to study cohesive and interlaminar crack growth in bonded composite joints under constant and variable amplitude (VA)

loading conditions. A numerical crack growth integration was used to predict the VA fatigue life using constant amplitude data. This method underestimated the fatigue crack growth rate for interlaminar cracks, indicating crack growth acceleration due to load interactions. Similar results were also obtained in the case of cohesive cracks subjected to a moderate initial strain energy release rate (G_{max}). An unstable crack growth regime was also identified for the case of high initial G_{max} cohesive crack propagation.

Tzetzis *et al.* [139] studied the adhesion between an infusion resin and a composite substrate by conducting Mode-I fracture toughness tests using double cantilever beam (DCB). Post-failure examination of the fracture surfaces showed that the locus of failure switched from the interface to the reinforced resin bondline.

Bardis and Kedward [140] studied the significance of surface preparation on the long-term durability of bonded composite joints. Several potential factors were evaluated, including the effects of release fabric usage and grit blasting on the fracture toughness and failure modes of bonded assemblies. The double cantilever beam (DCB) test was employed in the study. DCB tests showed that curing nylon release fabrics against adherend surfaces leads to interfacial failures and intermittent crack propagation, with reduced loads and crack opening displacements. This resulted in lower critical strain energy release rates (G_{IC}) than bonds produced with equivalent PTFE vacuum bag surfaces. Grit-blasted adherends gave higher failure load and G_{IC} values than non-blasted ones, though the mode of failure did not change.

Blackman *et al.* [141] have corrected the beam theory analysis of the adhesively bonded double cantilever beam test specimen to account for the effects of beam root rotation. They also made provision to account for actual test geometry. A number of adhesive-substrate combinations were tested according to a new test protocol and the new analysis method for data reduction is compared critically with the existing simple beam theory and experimental compliance approaches. Correcting the beam theory for root rotation effects is shown to be more important than correcting only for the effects of shear deformation of the substrates. Results from a finite element analysis, using a cohesive

zone model, also showed close agreement with the proposed new corrected beam theory.

Ting and Cottington [142] used a fracture mechanics approach to determine the adhesive fracture energy of various high temperature resistant adhesives such as tetrafunctional epoxy and phthalocyanine resin polymers. Tapered double cantilever beam specimens were used for fracture tests at both room temperatures and 225^0 C. Adhesive fracture behavior of polymers at high temperatures was found to depend on their glass transition temperature, whereas at low temperatures it was related to secondary relaxation processes in the glassy state.

Davalos *et al.* [143] have reported an experimental characterization of the opening-mode (Mode I) fracture toughness of bonded interfaces for hybrid laminates. A bi-layer contoured double cantilever beam (CDCB) specimen was used for the fracture toughness tests of the bonded interfaces. The bi-layer specimen consists of constant thickness adherends bonded to tapered sections of an easily machinable material, and it was contoured to achieve a constant rate of compliance change with respect to crack length. Using linear slope CDCB specimens, Mode I fracture tests for wood-wood and Fiber Reinforced Plastic (FRP)-wood bonded interfaces were performed to determine the critical loads for crack initiation and crack arrest, and from the critical loads measured, the critical strain energy release rates (G_{IC}) were evaluated by making use of the experimentally verified constant compliance rate change over defined crack lengths.

Korenberg *et al.* [144] calculated adhesive fracture energy, G_c, of aluminium alloy and steel joints bonded with a rubber-toughened epoxy adhesive using monotonically loaded tests. Tests were conducted at different levels of relative humidity, and two types of surface pretreatment were employed on the substrates prior to bonding: a simple grit-blast and degrease (GBD) pretreatment or a silane primer (GBS) pretreatment. The G_c was plotted against the crack velocity, and three distinct regions of fracture behaviour were visible. They observed the following phenomena, i) at low rates of displacement the crack grew in a stable manner, visually along the interface, and relatively low crack velocities could be readily measured. This was termed “Region I”, and the value of the

adhesive fracture energy was relatively low and decreased steadily as the relative humidity was increased. ii) at relatively high rates of displacement the crack grew in a stick-slip manner mainly cohesively in the adhesive layer at approximately 20 km/min. This was termed "Region III", and the value of G_c was relatively high and independent of the relative humidity. In this region the crack was considered to grow faster and the water molecules were able to reach the crack tip, which explains the independence of G_c upon the test environment. iii) in between Region I and Region III, a transition region was observed, which was designated "Region II". The major effect of the GBS pretreatment, compared with GBD pretreatment, was to increase the value of G_c both in Regions I and III, although the presence of the silane primer had the greater effect in Region I.

Halliday *et al.* [145] have studied the ageing behaviour of adhesively bonded joints comprising carbon fibre-reinforced plastic adherends and epoxy adhesive using high-frequency dielectric analysis and mechanical shear/cleavage experiments. The joints were aged at 70^0C and 100% humidity. The results exhibited significant loss of strength over a prolonged period of exposure. A good correlation was observed between the extent of change of the joint structure as characterised by the dielectric data and the loss of mechanical strength. There was an evidence of toughening due to plasticisation of the adhesive from the fracture toughness data.

Wylde and Spelt [146] studied fracture strength degradation of two epoxy adhesives using an accelerated aging test. They prepared open-faced specimens by applying adhesive to aluminum plates and, after curing, exposed them to a range of temperatures and humidities. At various times, the adhesive layer (in either the wet or dry states) was bonded to a second aluminum adherend to form a double-cantilever-beam fracture specimen. The critical strain energy release rate was then measured at several mode ratios by ensuring that the crack followed a path in the 'primary' adhesive.

Frantzis [147] has reported the effect of environmental attack on adhesive joints using an extended version of double torsion (DT) test method. The toughness of the rubber-modified and unmodified DT adhesive joints exposed to distilled water environment at

$25^0C, 40^0C$ and 55^0C was studied with incubation time and it was found that fracture toughness increased with increasing test temperature. The incubation time of rubber-modified DT adhesive joints was found to decrease with test temperature. However, with an increase in incubation time an increase in temperature was observed for DT joints made from unmodified adhesive.

Abdel Wahab *et al.* [148] analysed and discussed fatigue crack propagation in adhesively bonded joints using double cantilever beams, single lap joints and double lap joints. They made experimental samples from carbon fibre composite substrates and epoxy adhesive. The joints were tested in constant amplitude fatigue at different loads to obtain the load against number of cycles to failure curve. A crack propagation law was then derived from the experimental results of the double cantilever beam and implemented in a finite element based predictive tool in order to predict the number of cycles to failure for single lap and double lap joints subjected to cyclic fatigue loading. The prediction technique is based on numerically integrating the crack growth law along the bonding line from an initial crack length to a final crack length. A comparison of mode I strain energy release (G_I) and total strain energy release rate (G_T) as failure criteria in the prediction procedures were presented.

Abou-hamda *et al.* [149] measured fatigue crack growth rates for an adhesive material along the bondline in a double cantilever beam specimen containing a cohesive crack. They conducted tension-tension tests with a stress ratio of 0.5 at a frequency of 5 Hz. Debond growth rates were measured using a experimental compliance method. Corresponding changes in the J-integral were computed assuming elastic-plastic behavior of adhesive. Three bondline thicknesses were evaluated. The computed J values were plotted against the measured debond growth rates, to obtain a power law relationship which characterizes the debond behavior for a given bondline thickness. The increase in bondline thickness showed a significant effect on fatigue crack growth and the larger the bond line thickness, the higher was the fatigue crack growth resistance.

Mall and Ramamurthy [150] carried out experimental investigation on composite to

composite bonded joints and studied the effect of bond thickness on debond growth rate under cyclic loading and critical strain energy release rate under static loading. Double cantilever beam specimens of graphite/epoxy adherends bonded with EC 3445 were tested under mode I loading. A different behavior of fracture and fatigue strength was observed with variation of bondline thickness.

2.5 Numerical methods

The numerical methods available to predict the strain energy release rate from FE analysis can be mainly categorized as: virtual crack extension method, virtual crack closure method, modified virtual crack closure method, and contour integral or J-integral method. Using virtual crack extension method the mode-I strain energy release rate can be calculated as,

$$G_I = \frac{\Delta U}{\Delta a} = \frac{U_2 - U_1}{\Delta a} \tag{2.9}$$

where ΔU is the amount of energy released due to crack extension, Δa, and, U_1 and U_2 are the strain energies associated with crack lengths a and $a + \Delta a$ respectively. In this case, to calculate the strain energy release rate, two runs of FE analysis are needed to be performed on two different crack lengths which differ by an incremental Δa. A virtual crack closure integral method can be used to calculate the strain energy release rate from a single FE analysis [151–154]. In this approach, strain energy release rate can be calculated from the knowledge of nodal forces and displacements at the crack tip. With reference to Figure 2.7(a) the mode I and mode II strain energy release rates G_I and G_{II} can be expressed respectively as:

$$G_I = \frac{1}{2\Delta a}[F_{yi}(u_{yk} - u_{yk'})] \tag{2.10}$$

$$G_{II} = \frac{1}{2\Delta a}[F_{xi}(u_{xk} - u_{xk'})] \tag{2.11}$$

where F_{xi} , F_{yi} are the nodal forces in the x and y-directions at node i; u_{xk}, u_{yk}, $u_{xk'}$ and $u_{yk'}$, are the displacements in x and y directions at node k and k' respectively, and Δa is the elemental length at the crack tip. Sethuraman and Maiti [155] proposed a modified crack closure integral method to compute the strain energy release rate, which can account for stress singularity. They expressed the equations for opening and sliding mode as stated below;

$$G_I = \left[\frac{(u_{yk} - u_{yk'})}{\Delta a}\right](F_{yj} + (1.5\pi - 4)f_{yi}) \tag{2.12}$$

$$G_{II} = \left[\frac{(u_{xk} - u_{xk'})}{\Delta a}\right](F_{xj} + (1.5\pi - 4)f_{xi}) \tag{2.13}$$

where F_{xi}, F_{yi} are the nodal forces; f_x and f_y are the crack closure forces; u_x and u_y are the crack sliding and opening displacements; and i, j and k are the nodes near the crack tip (see Figure 2.7(b)).

Rice [20] proposed a completely different approach to predict the strain energy release rate as stated below;

$$J = \int_{\Gamma} (Wdy - T_i \frac{\partial u_i}{\partial x} ds) \tag{2.14}$$

where Γ is an arbitrary path beginning from the bottom of the crack face and ending on the top the face. W is the strain energy density, T_i are the traction components, u_i are the corresponding displacement components and ds is the increment of arc length along the contour Γ. It should be noted that the J-integral is widely accepted as a fracture mechanics parameter for both linear and non-linear material response. A bibliographical review of FE methods in adhesive bonding using fracture mechanics principles was given by Mackerle [81].

2.6 Conclusions

The literature review has revealed that although the compressive strength of composite materials is considered as a "*design limiting feature*" in the design of composite struc-

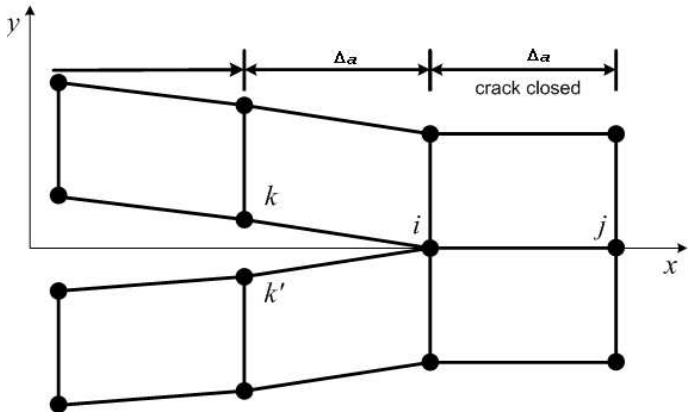

(a) Crack closure method

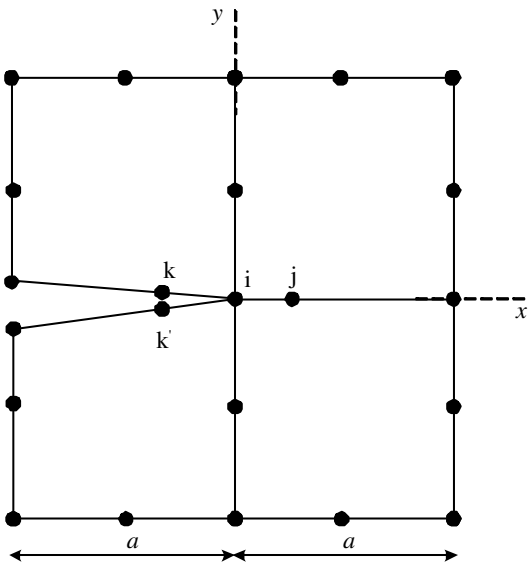

(b) Modified crack closure method

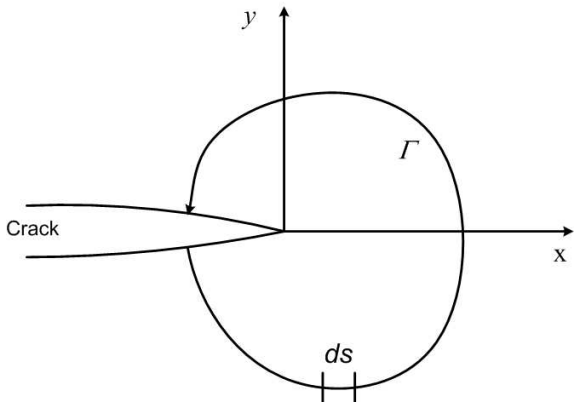

(c) An arbitrary contour around a crack tip illustrating J-integral calculation

Figure 2.7: The physical interpretations various symbols used in equations for calculating strain energy release rate with numerical approaches.

tures, very little research effort has been devoted to study the compressive behavior of adhesively bonded scarf joints of composites. The review of previous research under taken to study the tensile behavior of bonded scarf joint also showed that there is a lack of understanding of the failure mechanisms of joints made of unidirectional fiber composites (which forms the basis for the other types of laminates). A thorough search of literature dealing with single lap joint (SLJ) indicated that researchers have neglected an important issue (i.e., formation of bead at the ends of overlap during curing commonly known as spew fillet) in the experimental studies and it is the root cause of scatter in data when employing SLJ in the studies. Single lap joint has drawn great attention and is the most popular in the adhesive bonding community, because of its simplicity, economical to prepare and closest resemblances to the practical joints. It was found that several researchers have used SLJ to study fatigue life prediction of bonded joints/structures. Some researchers have reported the improvement in the load carrying capacity because of the presence of spew fillets. However, to accurately measure the parameters a method must be suggested to counteract the effect of spew fillets. In the present thesis, the first two issues were addressed by investigating compressive and tensile behavior of scarf joints ranging from $0^0 - 5^0$. The third issue was addressed by suggesting a novel modification to SLJ. The new test geometry was referred to as modified single lap joint (MSLJ), which is capable of overcoming the existing problem in the conventional SLJ test geometry. MSLJ was used to predict the mode - I adhesive fracture energy in dry conditions, the effect of environmental ageing on mode - I adhesive fracture energy and for fatigue life prediction of bonded joints for the first time.

Chapter 3

Compression Failure of Bonded Composite Scarf-Joints

3.1 Introduction

The understanding of compressive failure of long fiber composites has improved tremendously in recent times [31–36] and good design database exists. However, the design information needed for scarf-joints remains a persistent curiosity. In this chapter, the issue has been addressed by conducting critical experiments and finite element analysis to improve the understanding of failure mechanisms and failure strength prediction of adhesively-bonded scarf joints under uniaxial compressive loading condition.

3.2 Experimental Set-up and Testing Procedures

3.2.1 Test material

Experiments were conducted on joints of CFRP laminates made from commercially available carbon fiber epoxy prepregs (Fiberdux-913CHTA, from Hexcel Corporation). To fabricate the composite laminate, 16 plies of prepreg (each of size 300 mm x 300 mm and 0.125 mm in thickness) were hand-laid to obtain a unidirectional lay-up and cured by vacuum bag molding to obtain a composite laminate of 2 mm nominal thickness. Teflon sheets and breather cloth were used to control the resin content and prevent the epoxy from adhering to the bagging material while ensuring that the vacuum was well distributed within the whole vacuum bag. The order of stacking of prepregs, teflon sheets, breather cloths and other bagging materials were as shown in Figure 3.1. The vacuum bag was

maintained at a vacuum pressure of 0.08 MPa and the stacked prepregs were cured at 120^0C for about 2 hrs. The laminates were cooled to room temperature and later post-cured for 4 hrs at the same temperature and pressure as above.

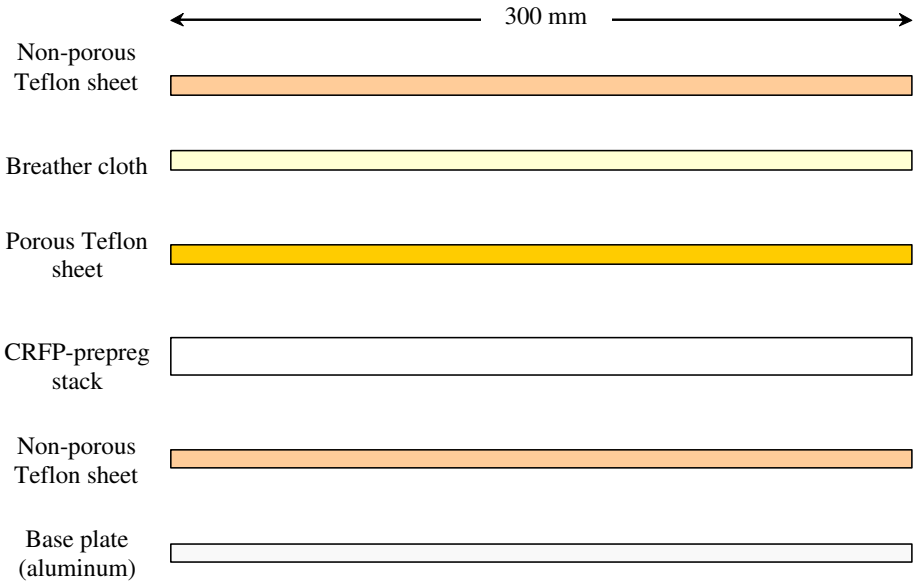

Figure 3.1: Order of arranging the prepreg stack and other materials in vacuum bagging before commencement of curing process

3.2.2 Preparation of Scarf Joints

The composite laminates were cut to the required specimen dimensions with a high speed diamond bench cutter. A high-speed (2800-3000 rpm) Dormer (Type-S281) TiCN, 10 mm end-mill cutting tool was used to machine the scarf to nominal angles ranging from 0.5^0 – 5^0 (with respect to the loading axis). A metal back plate of 10 mm thickness was used as a support to prevent the laminate from bending during the scarffing process. A photograph of adherend with back plate support is presented in Figure 3.2, to illustrate the scarffing process. The composite adherend and the metal plate were tightly secured in the vice of the milling machine and the workpiece was fed against the rotating tool at the desired angle. The resulting scarf angles were verified using a Starret Sigma vertical optical profile projector (VF600). Figure 3.3 shows a photograph of the vertical profile projector used in the current experimental studies. To avoid the contamination from loosely held

debris after the machining process, the mating scarf-joint surfaces were degreased by wiping them with a cotton-tissue wetted with acetone and subsequently dried for about 2 hours before applying the film adhesive strip.

After surface preparation, a strip of film adhesive AF-163-2 [156] was placed on each of the two previously prepared substrates/adherends. AF-163-2 is a rubber filled solid film industrial adhesive with a nylon scrim cloth support. The nylon scrim cloth support within the adhesive film has no significant effect on the adhesive property but provides better control of adhesive bond-line thickness. The mating surfaces were brought in contact with each other to commence the bonding process. The whole composite scarf-joint assembly was sandwiched in a silicon rubber mold, and cured at 120^0 C for an hour in a hot press maintained at the pressure of 0.12 MPa. The silicon rubber mold was needed to maintain a uniform pressure distribution across the adhesively-bonded joint during the curing. The nominal film thickness of adhesive before curing was measured to be 0.325 mm but reduced to 0.15 mm after the curing process. Upon completion of the adhesive bonding process, the composite laminates with scarf-joints were carefully machined into specimens appropriate for compression testing.

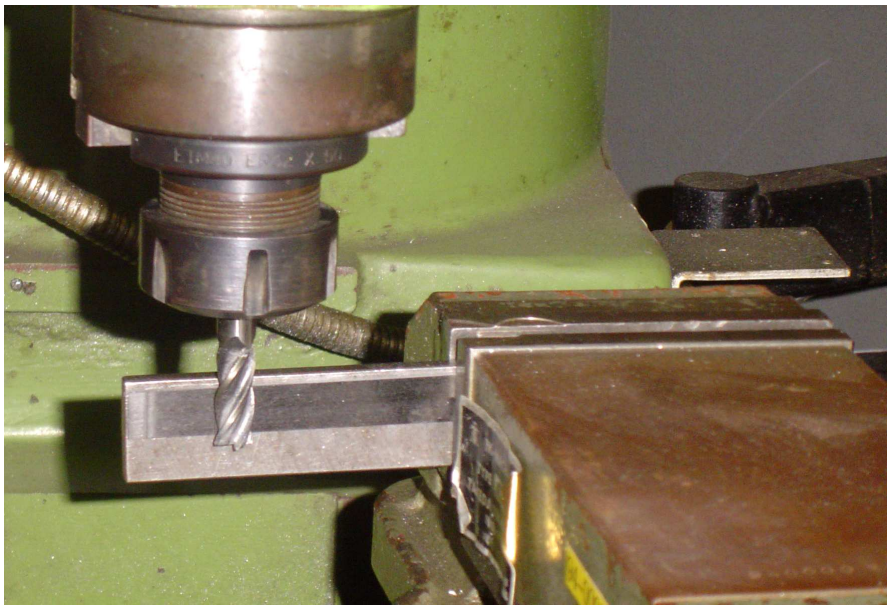

Figure 3.2: The composite adherend and the backing metal plate held in the vice of the milling machine and the workpiece was fed at desired angle during scarffing process.

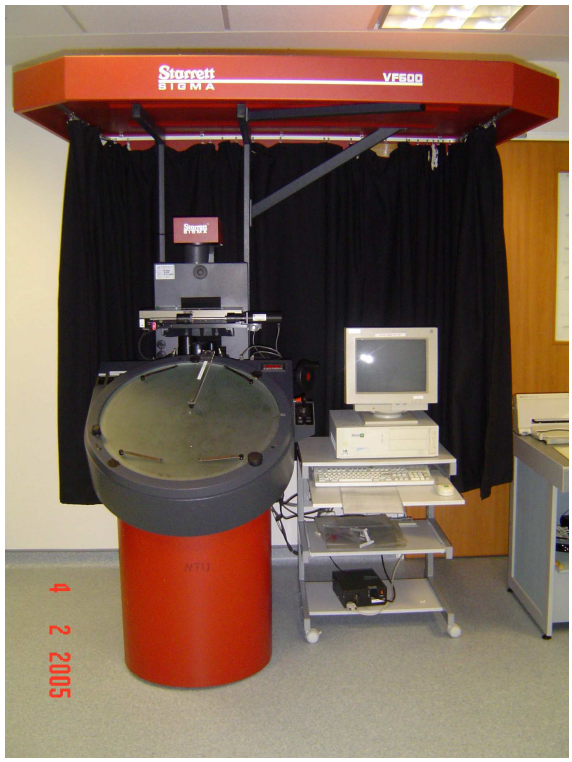

Figure 3.3: A photograph of Starret Sigma vertical optical profile projector (VF600).

3.2.3 Specimen Design and Mechanical Testing

Scarf Joint

A schematic diagram of the test specimens along with geometrical dimensions is shown in Figure 3.4. All specimens were made from composite laminate with unidirectional lay-up and were nominally 2 mm thick. They were 12.5 mm wide and the gauge-length was 10 mm in order to ensure that there was a compromise between the need to overcome Euler buckling and end-tab effects. If the gauge length was too short, the end-tabs would become too close to each other and will not allow uniform distribution of stresses in the central region. Whereas, if the gauge-length was too long, Euler buckling becomes significant [36]. Each specimen was loaded using the standard Illinois Institute of Technology Research Institute (IITRI) test-rig (see Figure 3.5), and compressed using a 100 kN Instron screw-driven testing machine at a crosshead speed of 1 mm/min. An engineer's right-angle was used to ensure proper alignment of the specimen especially between the lower and upper wedge grips.

Annealed aluminum tabs (1 mm thick) were bonded to the end of the specimens with a modified epoxy (redux) film adhesive to enable a smooth transfer of load to the specimen. The mating surfaces of the aluminum end-tabs and composite were abraded using emery cloth and were chemically cleaned with acetone. Moreover, since the compressive testing of these high-strength composites may cause the specimen to slip at the grips, the use of annealed aluminum end-tabs ensured that the knurled surfaces of the IITRI wedge grips bite firmly into the specimen end-tabs, thereby preventing slippage at the grips. The gauge section of the compression test specimens was waisted along the width direction to prevent premature failure at the end-tabs due to stress-concentration effects [36, 157]. After waisting, the specimens were found to have a nominal width of 8.0 mm in the center of the gauge-length region. Strain gauges of length 1 mm were placed back-to-back on each face of the specimens (i.e. within the gage length section) to detect the presence of significant bending effects (if any). All the test specimens were kept at standard laboratory environment (i.e. 23 ± 2^0C and 50 ± 5% relative humidity) for about 48 hours before the mechanical testing commenced. Load and displacement measurements were recorded using a computerized data logging system and the fractured specimens were examined using optical and scanning electron microscopy (SEM). A total of five tests were performed for each scarf-angle ranging from $0^0 - 5^0$ and the results were averaged.

Mechanical characterization of Adherends and Adhesive

To obtain the compressive properties of the base composite in longitudinal and transverse direction, test specimens were prepared according to ASTM D 3410/D 3410M. To measure the in-plane shear properties of the composite material, specimens were extracted from $\pm45^0$ laminates as per ASTM D3518/D3518M. For measurement of out-of-plane shear properties specimens were prepared as per ASTM D 5379/D 5379M. The compression tests were conducted on an Instron universal testing machine fitted with 100 kN load cell using IITRI test fixture. Strain gauge rosettes were mounted in the middle of the specimens and strains in both longitudinal and transverse directions were monitored

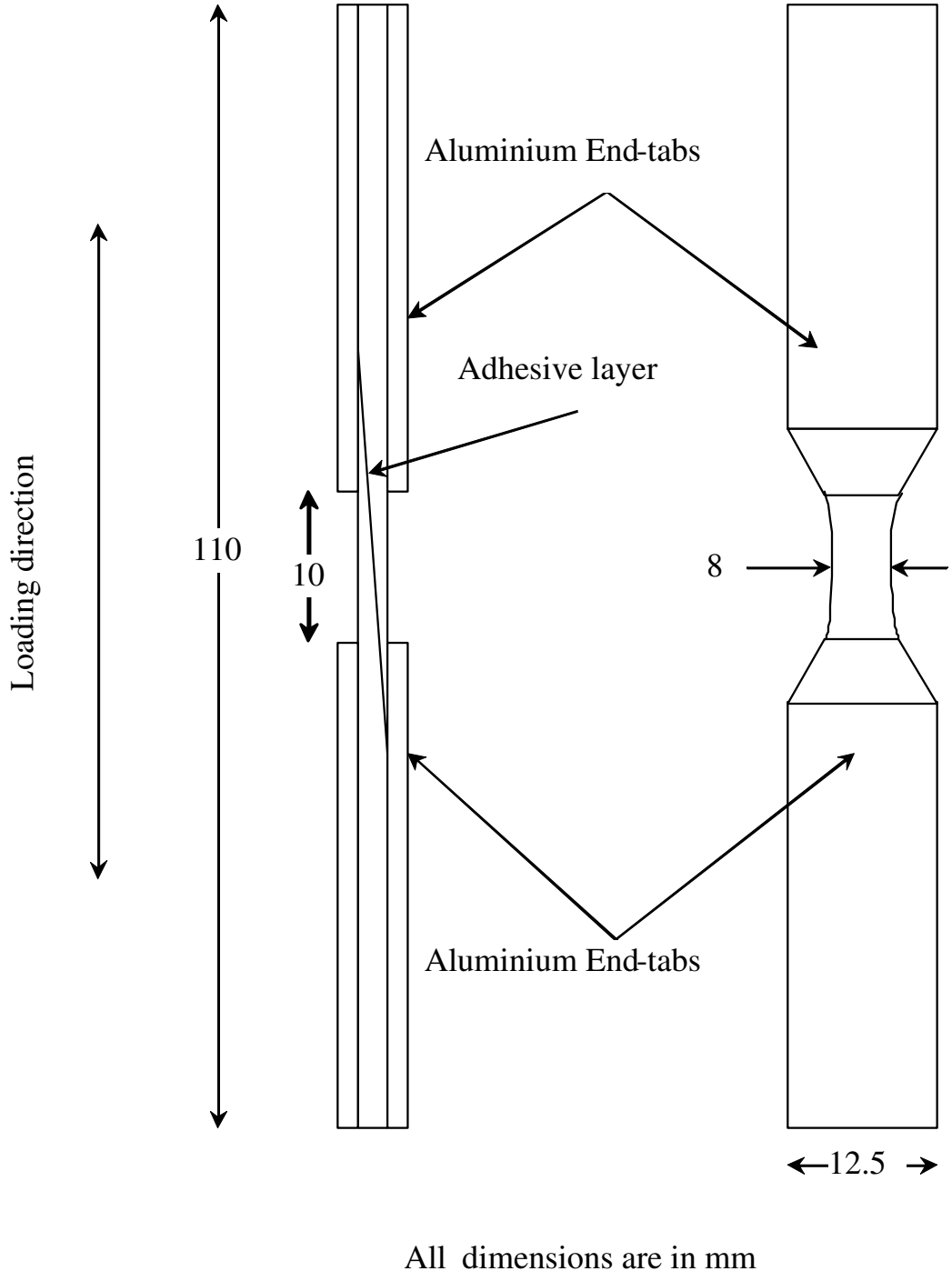

Figure 3.4: A schematic diagram of compression test specimen geometry.

Figure 3.5: A photograph of Illinois Institute of Technology Research Institute (IITRI) compression test-rig.

simultaneously using a portable data logger. The measured strains were used to calculate the Poisson's ratio of the material tested. Standard test methods were adopted for both in-plane and out-of-plane shear tests. The test results are summarized in Table 3.1.

The mechanical properties of the adhesive (epoxy film adhesive (AF-163-2) from 3M Corporation) used in this study were measured by conducting tests on flat coupons (dog-bone shape) specimens prepared according to ASTM D 638. Ten layers of the adhesive film ($100 \times 100mm$) were stacked to achieve a nominal thickness of 3 mm and cured under a hot press at 120^0C for 1 hr. The required flat shaped specimens were machined out using a high speed profile cutting machine (TensileKut, Model 10-86).

The specimens were tested on a 50 kN Instron universal testing machine. An Instron extensometer (No. 2620-601) with range, ± 5 mm and gauge length of 12.5 mm was used to measure tensile strain. Cross-head ramp speed was fixed to 1 mm/min. A non-linear tensile stress-strain behavior was observed (see Figure 3.7(a)). Tensile strength of the adhesive was found to be approximately 31.5 MPa with a corresponding failure strain of 3.5%. The Young's modulus of the adhesive was measured to be 1.818 GPa. Adhesive material was also tested in shear mode using the thick adherend test geometry

Table 3.1: Fiberdux-913CHTA composite material properties under compressive loading

Property	Value
Longitudinal compressive elastic modulus, E_{11}^c	126 GPa
Transverse compressive elastic moduli, E_{22}^c and E_{33}^c	9.80 GPa
Shear elastic moduli, G_{12} and G_{13}	1.07 GPa
Shear elastic modulus, G_{23}	3.92 GPa
Poisson's ratio, ν_{12} and ν_{13}	0.26
Poisson's ratio, ν_{23}	0.25
Longitudinal compressive strength, σ_{11}^c	1000 MPa
Transverse compressive strength, σ_{22}^c	155 MPa
Interlaminar shear strength, τ_{13}	100 MPa

Table 3.2: Mechanical properties of AF-163-2 film adhesive

Property	Value
Tensile elastic modulus, E	1.82 GPa
Shear strength of sandwiched adhesive, τ	32.5 MPa
Poisson's ratio, ν	0.34
Ultimate tensile strength, σ_u	31.5 MPa
Yield strength, σ_y at 0.2% offset strain	21.0 MPa

(see Figure 3.6). Shear stress-strain behavior of the adhesive is depicted in Figure 3.7(b). The measured mechanical properties of the adhesive material are summarized in Table 3.2.

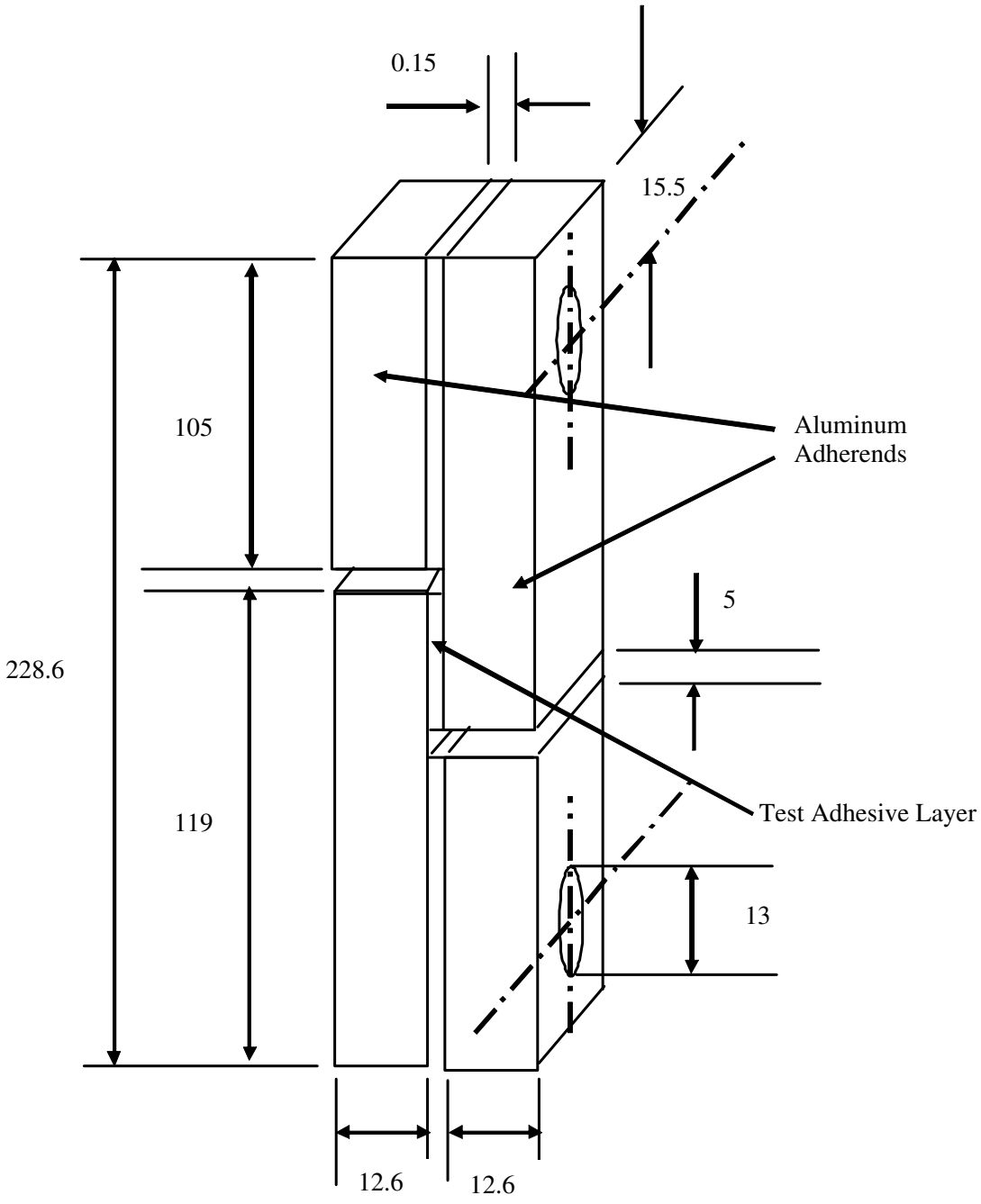

Figure 3.6: Schematic diagram of a thick adherend shear test specimen used for characterizing the shear properties of the adhesive material.

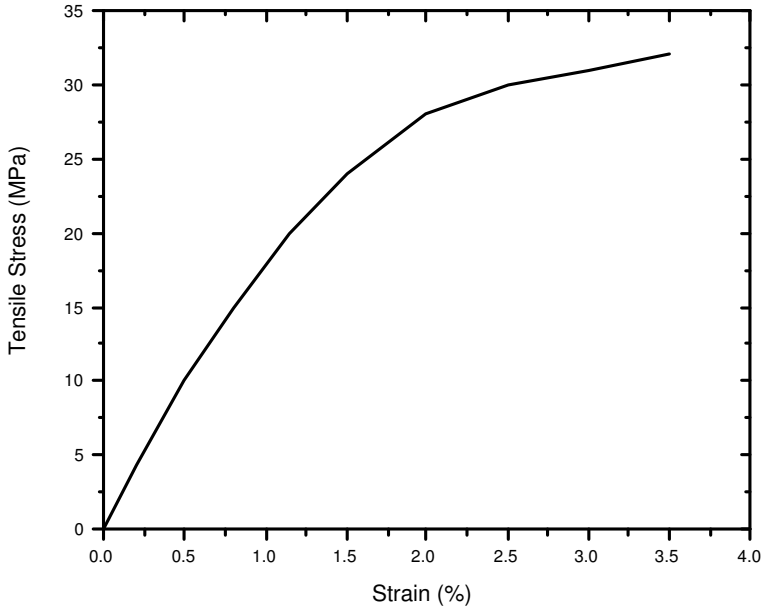

(a) Tensile stress-strain graph

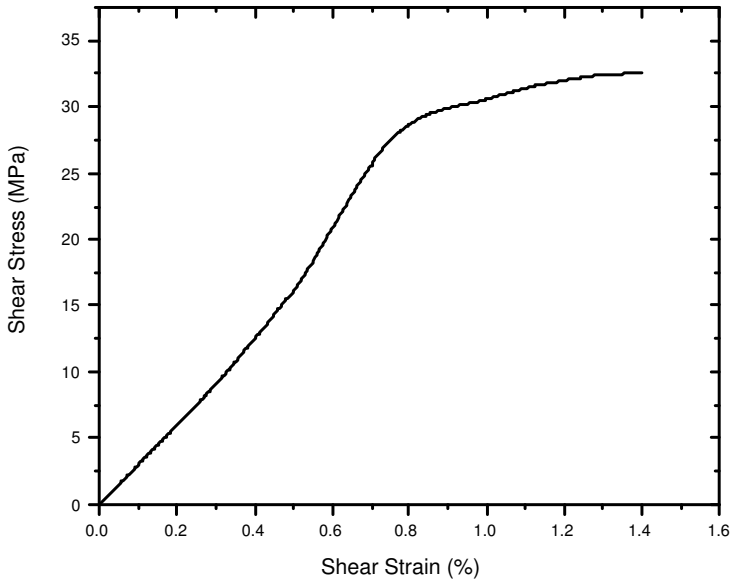

(b) Shear stress-strain graph

Figure 3.7: Experimentally measured stress-strain response of the cured film adhesive, AF-163-2.

3.3 Experimental Results and Discussion

3.3.1 Failure Modes

The failure modes observed in the present experiments can be classified into two main categories: Mode A_c: Failure predominantly by fiber microbuckling; Mode B_c: Failure predominantly by cohesive shear deformation through the adhesive layer with attendant fiber microbuckling (see Figure 3.8). Table 3.3 shows the frequency of occurrence of the two types of failure modes in relation to scarf angle. Failure mode A_c was observed for scarf angles less than about 3^0 while failure mode B_c was observed for scarf angles greater than 3^0. There appears to be a consistent trend in failure, which switches from modes A_c to B_c as the scarf-joint angle (with respect to the loading axis) increases from 0^0 to 5^0.

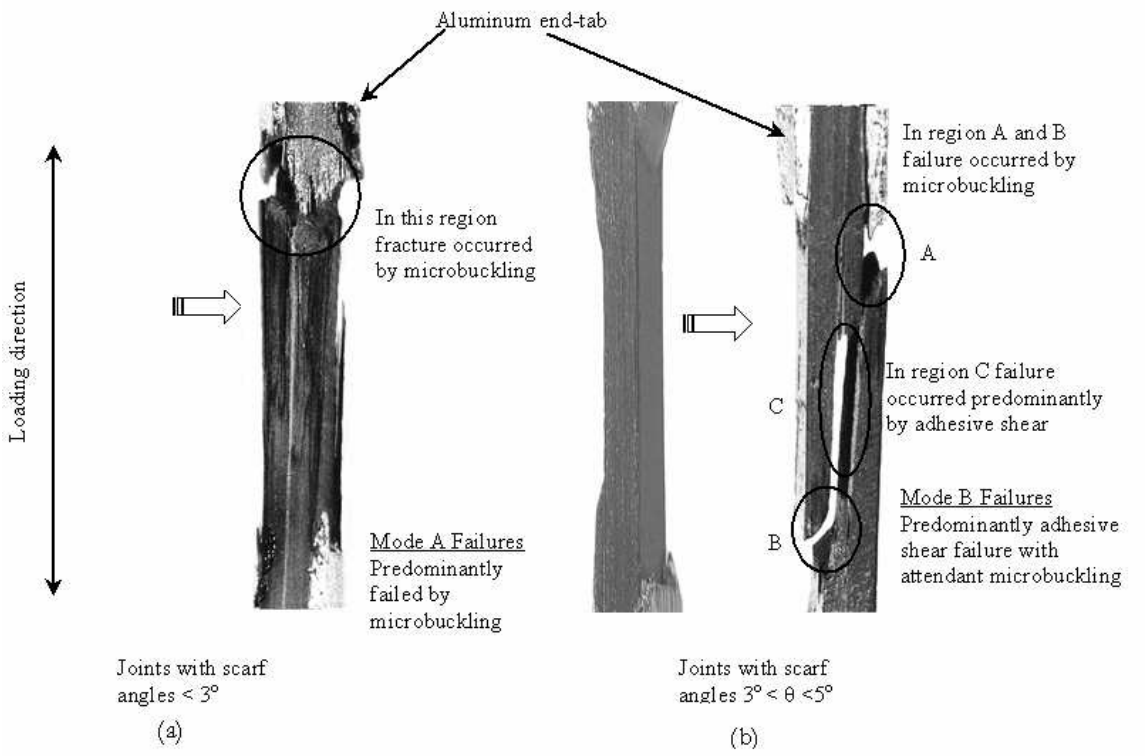

Figure 3.8: Stereo photomicrograph of specimens before and after fracture, illustrates the two competing failure modes noticed in scarf joints in compression at varying scarf angles, ranging from 0^0 to 5^0: (a) adherend failure, and (b) adhesive shear failure with attendant microbuckling.

Table 3.3: Frequency of Occurrence of Failure Modes A_c and B_c

Scarf Angle (Degrees)	Mode A_c No. of Specimens that failed predominantly by microbuckling	Mode B_c No. of Specimens that failed predominantly by adhesive shear failure with attendant microbuckling in the composite
0.6	100%	-
1.7	100%	-
2.7	close to 100%	-
3.5	about 33%	about 67%
4.7	-	close to 100%

3.3.2 Load versus Displacement response

The shape of the load displacement response is similar for both types of failure modes (A_c and B_c) for different scarf angles. Figure 3.9 shows typical load-displacement curves in which it was observed that the load increased in an almost linear manner to a peak value. With increasing load, there were no visible signs of impending failure for both failure modes (A_c and B_c). Upon reaching the peak, the load dropped suddenly indicating catastrophic fracture. The slight stiffening of the curve with increasing load is due to the wedge grips of the IITRI jig, which slip into the hollowed out tapered rectangular collets during the compression test. The gradual slipping motion between the split-collet grips and the rectangular tapered collets resulted in an increasing wedging effect, which assumes that the split collet grips 'bite' firmly into the end-tabs and prevented specimen slippage as the compressive load increased. In Figure 3.10, the compressive stress-strain curves for scarf joints with scarf angle 0.6^0 are shown. It shows wide experimental scatter in the measured compressive failure strength of the joint, similar to that of the composite materials.

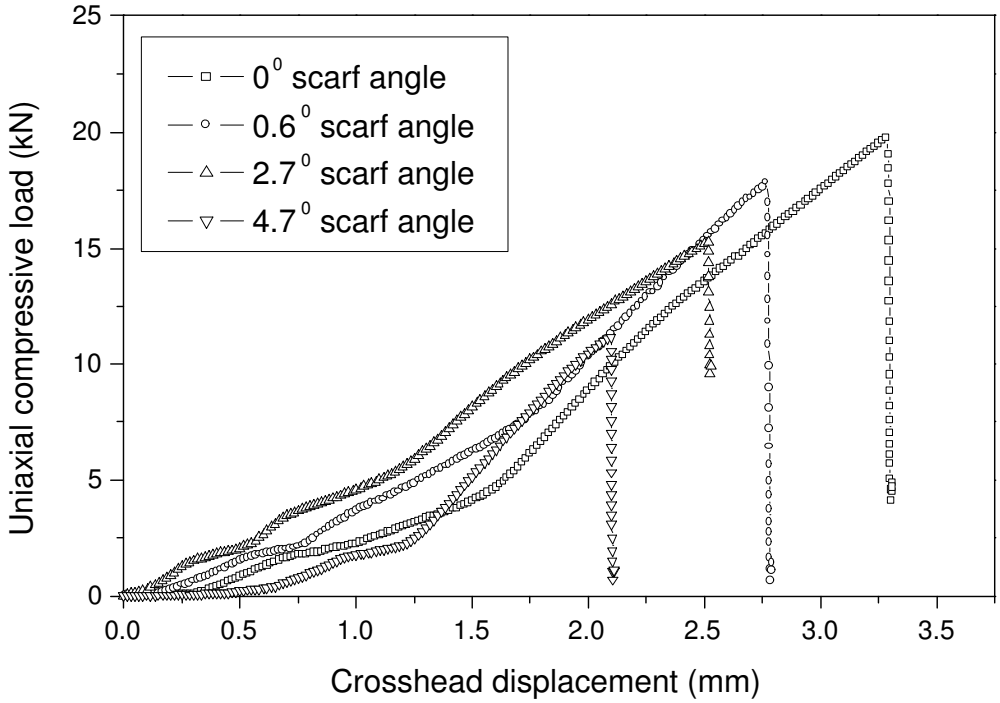

Figure 3.9: Experimentally measured load-displacement response for adhesively bonded scarf joint with different scarf angle.

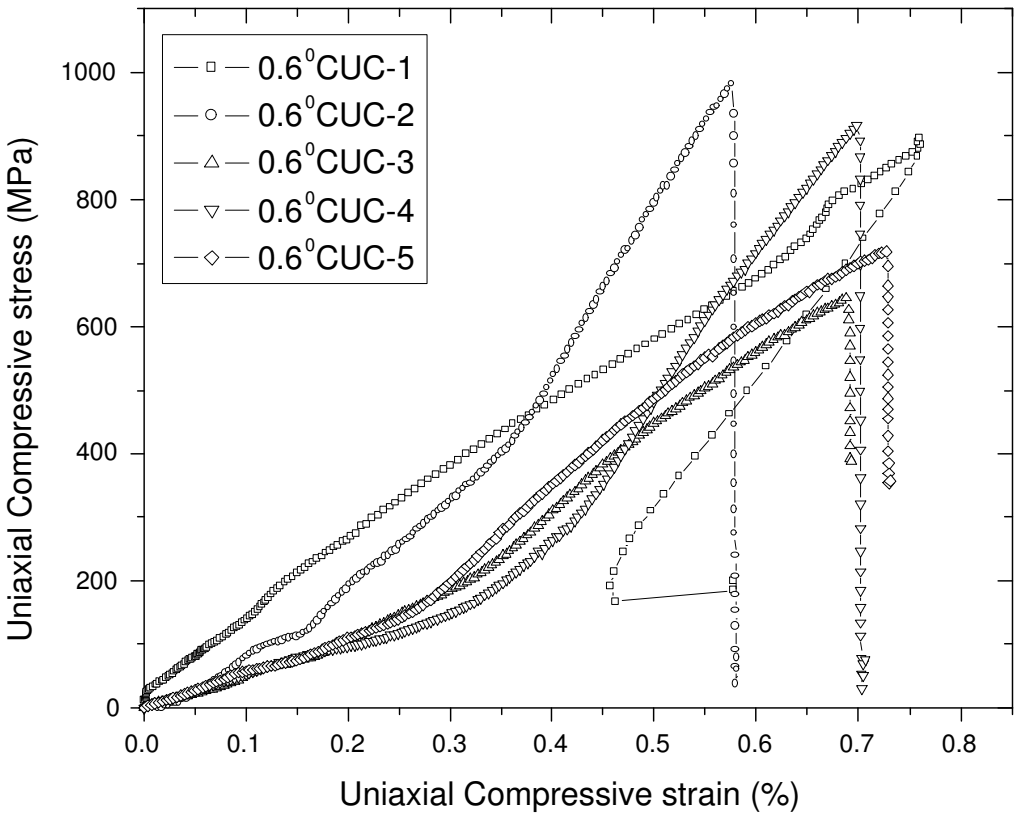

Figure 3.10: Scatter in the experimentally measured stress-strain response for adhesively bonded scarf joints with 0.6^0 scarf angle.

3.3.3 Microbuckle failure

In the present study, it was observed that composite joints with scarf angles less than about 3^0 failed in compression via out-of-plane microbuckling across the joint (see Figure 3.12(a)). For such scarf-joint configurations, the normal to the fracture surface was inclined at an angle of about 18^0 to the fiber direction similar to the compressive failure mode of neat unidirectional composites with no scarf joint [36, 157]. It was also noticed that fracture did not take place predominantly along the scarf length and the failed specimens did not separate neatly into two portions along the scarf length (see Figure 3.8(b)). Instead the fractured surfaces remained loosely bonded to each other when unloaded as the residual bridging tractions of the mangled microbuckled debris held the two fractured portions of the specimen together. A micrograph of the microbuckled scarf-joint fracture surface obtained using scanning electron microscopy (SEM) is shown in Figure 3.12(a).

These observations may be explained from the point of view that the continuous fibre reinforcements in these composites were not perfectly aligned and possessed local areas of misalignment believed to arise from the composite manufacturing process itself [30, 158]. Madhukar *et al.* [158] have demonstrated that significant residual stresses were set-up in the fiber during the curing process of graphite-epoxy composites. These residual stresses resulted from matrix thermal contraction and cure shrinkage and may be responsible for distorting fiber alignment. Direct evidence to support the presence of local fiber waviness in aligned fiber polymeric composites were found from the experimental measurements made by Yurgartis [159] and Kyriakides [160]. When loaded in compression, such imperfections trigger microbuckling where the fibers underwent cooperative kinking, and the supporting matrix material deformed in non-linear shear. This type of compressive failure mechanism has been referred to in earlier studies as plastic microbuckling [33–35, 160–162] and its resultant effect is reduced strength in compression compared to that in tension. In adhesively bonded composite scarf-joints, the inclined adhesive layer in the composite knocked down the shear-yield strength of the bonded composite and acted as an additional imperfection, which reduced the compressive strength of

the bonded composite (when matrix material deformed non-linearly). At a certain loading stage, the process became unstable at larger strains due to decreasing stiffness of the non-linear matrix and adhesive layer, leading to deformations that caused failure through the formation of kink bands (see Figures 3.12(a-c)). Thus, the larger the scarf angle (with respect to the loading axis), the greater the knockdown in the shear-yield strength of the composite and hence the compressive strength.

As shown in Figure 3.12(b), the material above the microbuckle band slides over that below it. The out-of-plane microbuckling is believed to occur in preference to in-plane microbuckling because the specimen thickness of 2 mm was much less than the specimen width of 12.5 mm. Hence there was much less constraint in the through-thickness direction, thus resulting in out-of-plane microbuckling.

In the present study, it was observed that the kink-band angle, β, ranged from 15^0 to 25^0 with an average of 18^0. The average fiber rotation angle, Φ, was about 40^0. Thus on average, the fibre rotation of band-width, w, equals to 2.2β (see Figure 3.11). These observations are in good agreement with the theoretical models based on volume conservation proposed by Chaplin [163] and Evans and Adler [164]. These models state that $w = 2\beta$. The overall kink-band width ranges from 35 μm to about 48 μm. Recently, observations of microbuckle propagation in unidirectional composites (with no adhesive-bonded scarf joints) showed that microbuckles advanced with broadening of the microbuckle-band behind its tip [157]. The broadening of the microbuckle-band ultimately led to the formation of multiple kink-bands as the fiber fracture sets the width of each of the individual kink bands. Eventually a steady state of band-broadening is attained at constant load. In general, band broadening may be construed as an example of steady-state buckle propagation, whereby unbuckled fibers are convected into a buckled state under a constant remote stress. In this present study on adhesively-bonded composite scarf-joints loaded in compression, the optical microscopy examination of the microbuckle band also revealed the presence of multiple kink bands associated with band broadening [157] as shown in Figure 3.12(c). Micrographs of these distinct kink bands show vividly that the boundary of

each of these multiple kink bands is actually separated by fiber fracture at two locations. The width of each individual kink band can be inferred to be approximately constant at about an average value of 42 μm, which corresponds to about 8 fiber diameters (8d). This observation is in reasonable agreement with the value of 10-15 fiber diameters predicted by couple stress theory [165].

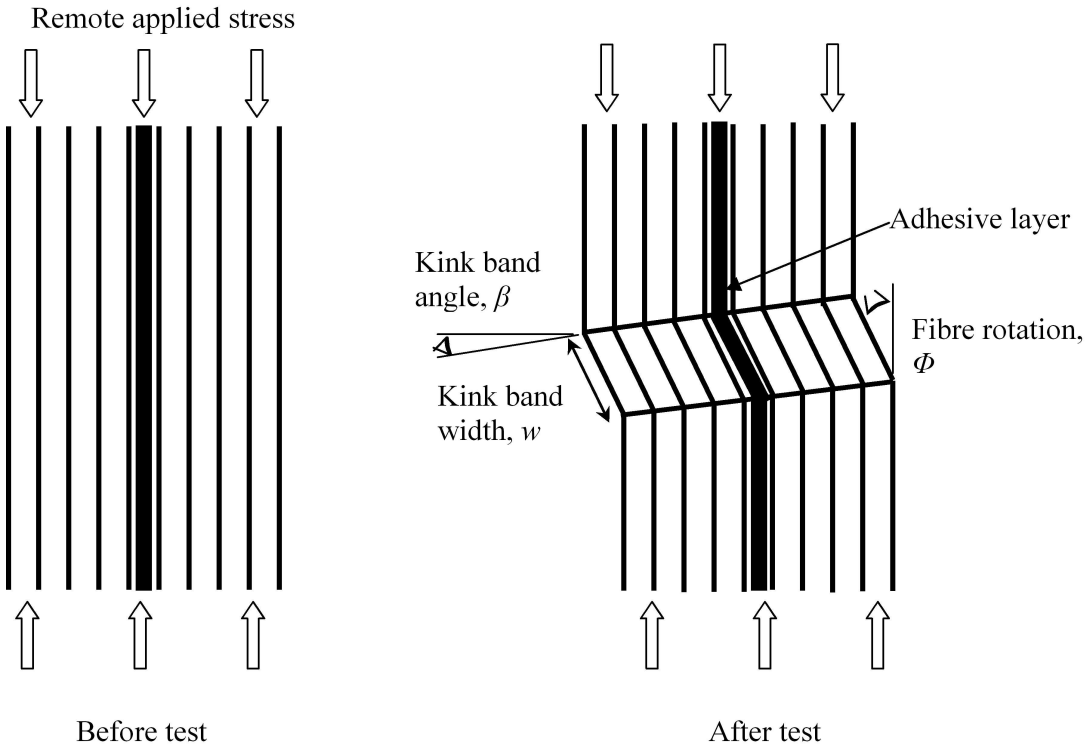

Figure 3.11: Schematic of out-of-plane microbuckling in bonded scarf joint for scarf angle less than 3^0 under uniaxial compressive loading.

3.3.4 Microbuckling with cohesive shear failure

In the present study, the adhesively-bonded unidirectional composites with scarf angles greater than about 3^0 (with respect to the loading axis), failed predominantly in compression by cohesive shear failure of the adhesive along the scarf joint. In addition, there was attendant out-of-plane microbuckling failure on both sides of the scarf length. The fracture surface ran mainly along the scarf length of the failed specimens, which separated

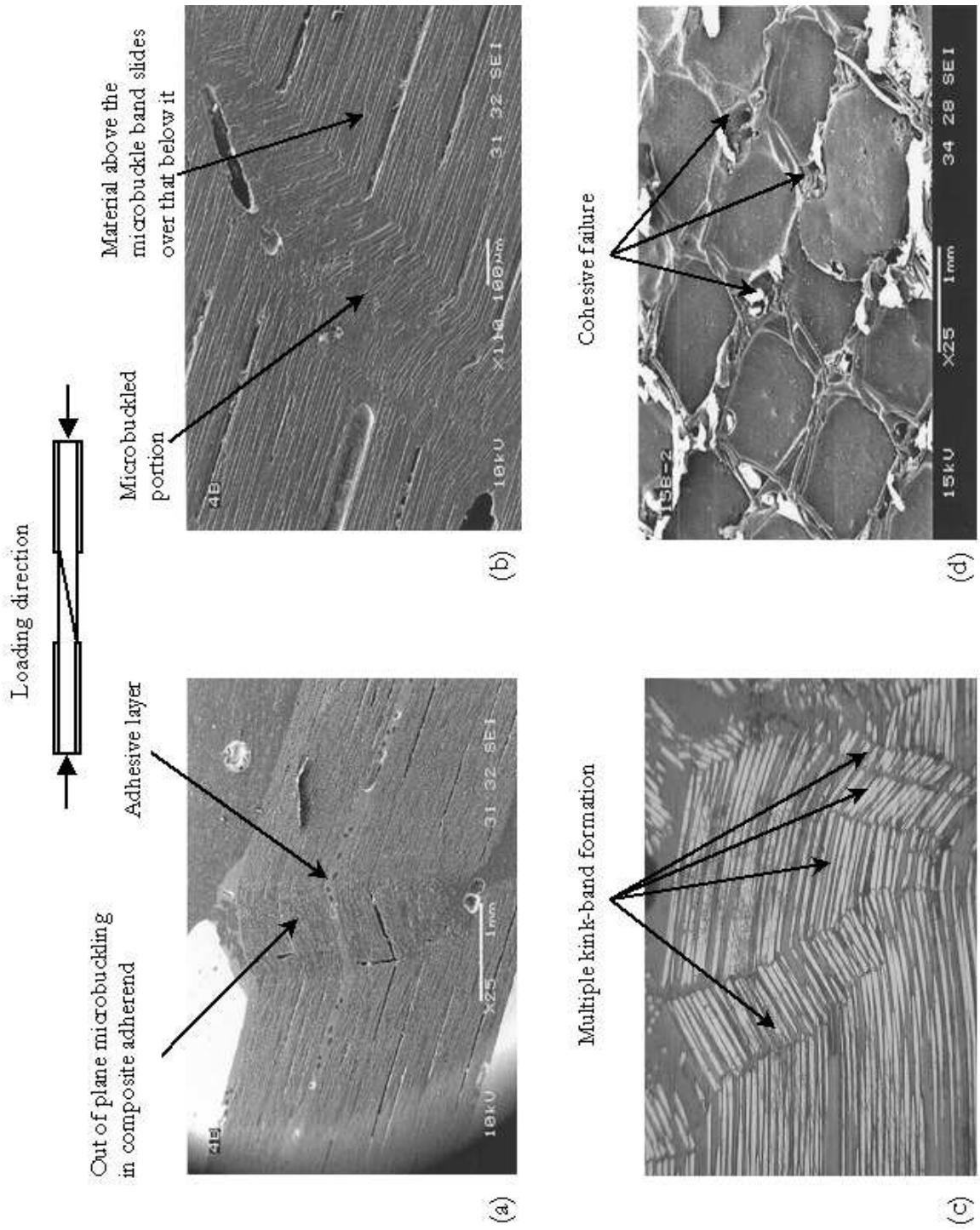

Figure 3.12: (a) SEM micrograph showing clear evidence of out-of-plane microbuckling in the adherend, (b) SEM micrograph illustrating microbuckle band sliding, (c) an Optical micrograph showing multiple kink bands associated with band broadening, and (d) SEM micrograph showing failure in the film adhesive (cohesive failure).

almost neatly into two portions along the scarf length (see Figure 3.8(b)). The SEM micrograph in Figure 3.12(d) shows that the failure in the film adhesive was cohesive in nature (i.e. failure occurring within the adhesive layer) and not of an interfacial one (i.e. occurring along the interface between the composite and the adhesive). The lattice like structures is in the adhesive material itself. The grids formed by the fabrics of the mat support clothe which appears to be square lattice on the fracture surfaces of the adhesive.

3.3.5 Effect of Scarf angle on Compressive joint strength

Figure 3.13 shows the effect of the scarf angle on the uniaxial compressive joint strength as a function of scarf angle, θ. As shown in Figure 3.13, smaller (i.e. steeper) scarf angles yielded higher compressive joint strengths in comparison to those with larger scarf angles. The knockdown in compressive strength is most prominent for scarf joint angles less than about 1^0 . As the scarf angle of the joint increases, the additional reduction in compressive strength becomes more gradual. The observed reduction of compressive strength as a function of scarf angle agrees with the general experimental observations reported by Sivashanker and Osiyemi [166], Kozey [167], Hancox [168], Soutis [36], Khamesh and Wass [169], where studies showed knockdown in compressive strengths of epoxy composites with a variety of imperfections. It is noteworthy that an adhesively-bonded joint with a scarf-angle of only 1^0 (i.e., about the size of initial fiber misalignments in neat long fiber composites) can cause a further drop in compressive strength of a unidirectional carbon epoxy composite laminate by as much as an additional 20%. For the largest scarf-angle of 5^0 used in the current experiments, the compressive strength dropped by 50%. These findings reflect the importance of imperfections in reducing the compressive strength of composites, and the importance of fabrication, machining and processing controls and techniques to minimize the knockdown in compression strength of fibre reinforced composite joints. Clearly, a scarf-joint with as small as possible scarf-angle yields the highest compressive strength but it is also apparent that relatively smaller scarf-angles are more challenging to machine and fabricate in practical applications.

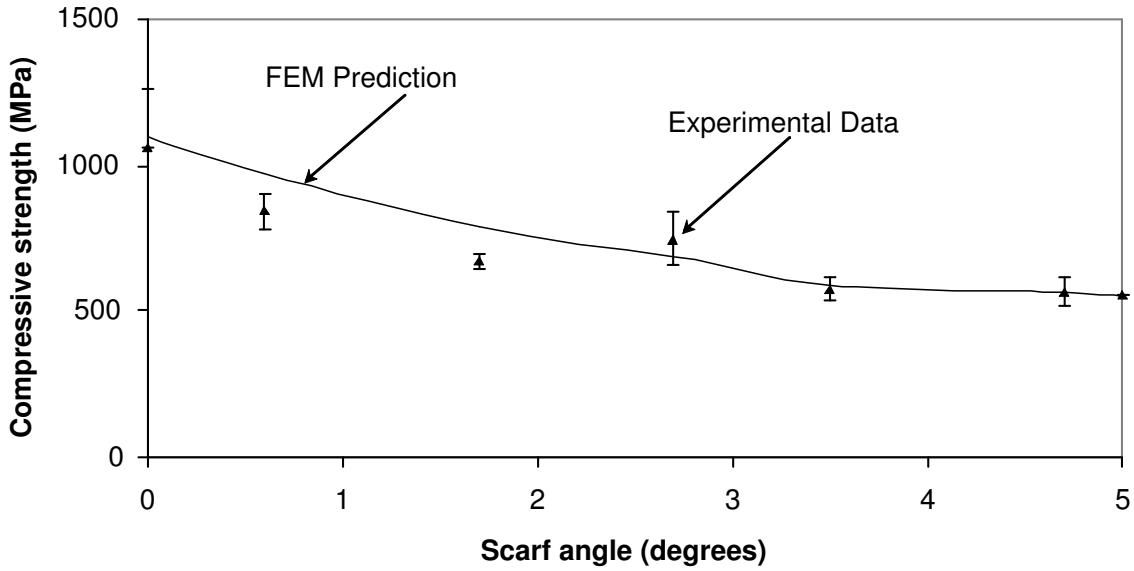

Figure 3.13: The variation of scarf joint compressive strength with scarf angle: experimental measurements were compared with numerically simulated results.

3.4 Comparison with Numerical predictions

In this section, the experimental measurements of the strengths of the scarf joints are compared with finite element (FE) simulations. The commercial FE package ABAQUS [170] was used for the numerical simulations of the adhesively bonded composite scarf joints. To adequately simulate the behavior of adhesively bonded structural members, the material properties of both adherends and adhesives must be accurately known. The appropriate material modeling technique must also be adapted, so that the results are accurate enough and at the same time the solution is not computationally extensive. In the present studies, the unidirectional composite laminate adherends are modeled as homogeneous orthotropic continuum material with material properties as shown in Table 3.1. Modeling the composite laminate as layers of laminae requires each laminae to be modelled using a single element through the thickness of the laminae, resulting in a mesh which is computationally improbable. Due to the same reason, the heterogeneous nature of the composite laminate was approximated as an orthotropic material and on macroscopic scale the fiber and matrix are not distinguished as discrete entities. Although this approach does not

capture the fiber microbuckling failure mode in composite laminates, it is sufficient to capture the macroscopic behavior of the laminates.

3.4.1 Materials Constitutive Models

In the FE analysis of the adhesively-bonded scarf joints, the composite laminate (adherend) was assumed to be linearly elastic orthotropic and the adhesive layer was considered as an elasto-plastic isotropic material. A three-dimensional failure criterion proposed by Hashin and Lee [171, 172] was used as a USER SUBROUTINE in the ABAQUS finite element program to account for the onset of damage in CFRP composite laminate. Hashin and Lee's failure criteria for composite laminates are briefly described in Appendix A. The adhesive film layer was assumed to be perfectly bonded to the composite laminate adherends and its uniaxial tensile stress-strain response, resembles that of an elastic-plastic material. The mechanical properties of the film adhesive AF-163-2 were taken from Table 3.2. Elastic behavior of the adhesive material was defined by Young's modulus and Poisson's ratio. A finite strain version of the J_2 flow theory with isotropic hardening was used to describe the constitutive behavior of the adhesive film. Post yield behavior was defined by inputting the true stress-strain plastic curve. This model is inbuilt in the ABAQUS code.

3.4.2 Geometry

Figure 3.14 shows a schematic representation of a typical scarf joint along with the significant geometric parameters. The scarf joint was modelled as a three-dimensional problem with geometric length scales similar to that used in experiments so that the FE simulation closely represents the test conditions. The finite element model of the tested specimen (see Figure 3.15(a)) corresponded to a mesh of length 3000d along the fiber direction and width of 1000d in the transverse direction (where d is the fiber diameter). The finite element mesh consisted of three-dimensional solid-continuum reduced integration (C3D8R) elements with three degrees-of-freedom at each node (two in-plane displacements and

one normal to the plane of deformation). In Figure 3.15(b) mesh design in adhesive and substrates material is depicted.

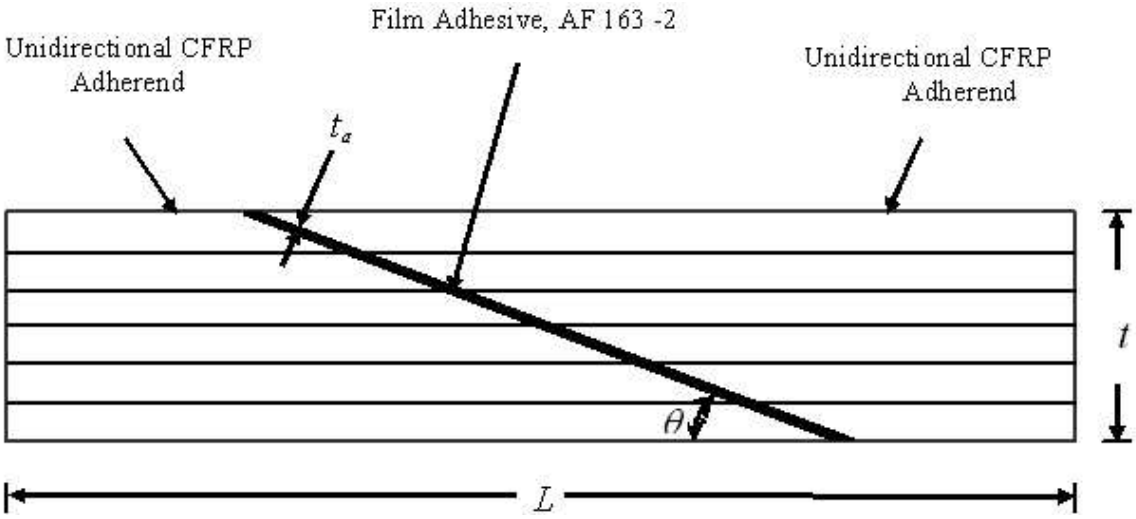

Figure 3.14: Schematic representation of a typical scarf joint along with the significant geometric parameters used in numerical simulations.

3.4.3 Boundary and Loading Conditions

The applied boundary conditions in the finite element model are such that the portion of the specimen in the grips was constrained to move only along the loading direction. In order to simulate uniaxial compressive loading, axial displacements were imposed on the nodes in the grip section of the specimen. Mesh refinement was carried out to the extent that no significant changes in the load-displacement response were observed with further mesh refinement. The simulation output included for the duration of loading, the displacement, stress, strain fields and reaction forces at the nodes on which the displacement loading was imposed. At each load increment, the sum of the reaction forces yielded the total applied load, which was divided by the original cross-sectional area (mm^2) of the specimen to calculate the applied stress. The corresponding displacement increment divided by the original gauge length yielded the strain.

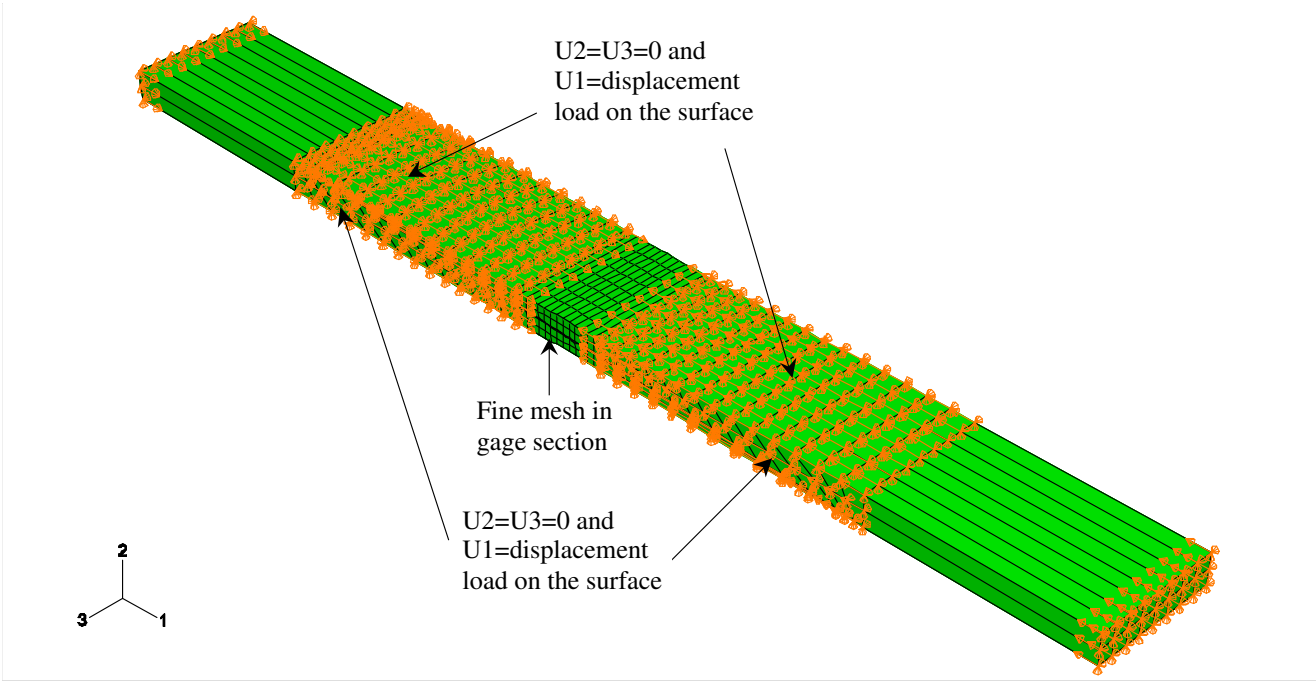

(a) Mesh design, load and boundary conditions

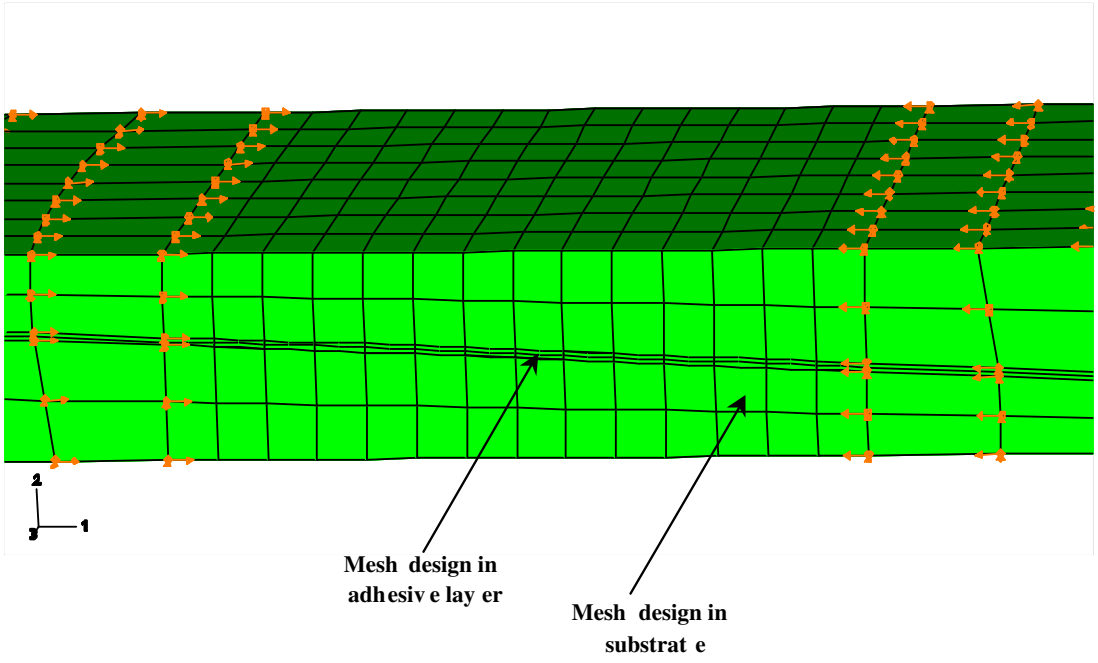

(b) Zoomed in FE mesh in gauge length section

Figure 3.15: Finite element mesh, load and boundary conditions and a zoomed in FE mesh in gauge section in the FE simulation of the joint with the scarf angle 2.7^0.

3.4.4 Numerical Results

Numerically predicted uni-axial compressive stress-strain curves as a function of scarf angles (see Figures 3.16) show that the compressive failure strength decreased with increasing scarf angle. The stiffness value was almost constant at about 125 GPa. The compressive strength was calculated as the maximum load recorded divided by area of cross-section in gauge-length. Figures 3.17(a)-3.17(c) compares the predicted uniaxial compressive stress (σ_{11}) - strain (ε_{11}) response with the corresponding experimental response for 0^0, 2.7^0 and 4.7^0 joints. As can be seen from the figure, the results from the numerical simulations and experiments are in reasonable agreement if some allowance is made for experimental scatter. Figure 3.18 shows the simulated uniaxial compressive stress (σ_{11}) line contour at 0.77% of uniaxial compressive strain (ε_{11}) for 0^0 scarf angle joint. From this line contour it was observed that the stress value reached around 1265 MPa near the end tab which exceeds the compressive strength of the laminate and from that region the failure initiates and finally fracture occurred. In Figure 3.19(a) and (b) uniaxial compressive stress (σ_{11}) band contour and von-Mises band contour at 0.77% of uniaxial compressive strain (ε_{11}) are depicted for 4.7^0 scarf angle joint. The stress level in the adhesive layer has reached a value higher than 32 MPa as can be seen in Figure 3.19(b) and has exceeded the ultimate strength of the adhesive, however, the stress level has just exceeded the longitudinal compressive strength of composite in a small portion of region "A" and "B", where microbuckling starts and final failure takes place as shown in Figure 3.8. The point where significant plastic deformation starts in the curves as shown in Figure 3.16 corresponds to joint failure. Failure strain is not constant as shown in Figure 3.16. The first curve failed at about 1% of strain. The second, third, fourth, fifth and sixth curves show 0.8%, 0.6%, 0.7%, 0.5% and about 0.5%. The last curve (4.7^0 case) changed its slope at about 0.5% of strain. A number of analysis was carried out with refined mesh design for the 4.7^0 scarf joint but there was no change in the results.

The finite element predictions of joint strength are compared with the present experimental data in Figure 3.13. The knockdown in compressive strength with increasing

scarf-angle is well described by ABAQUS FEM predictions and a good quantitative correlation with experimental measurements was observed.

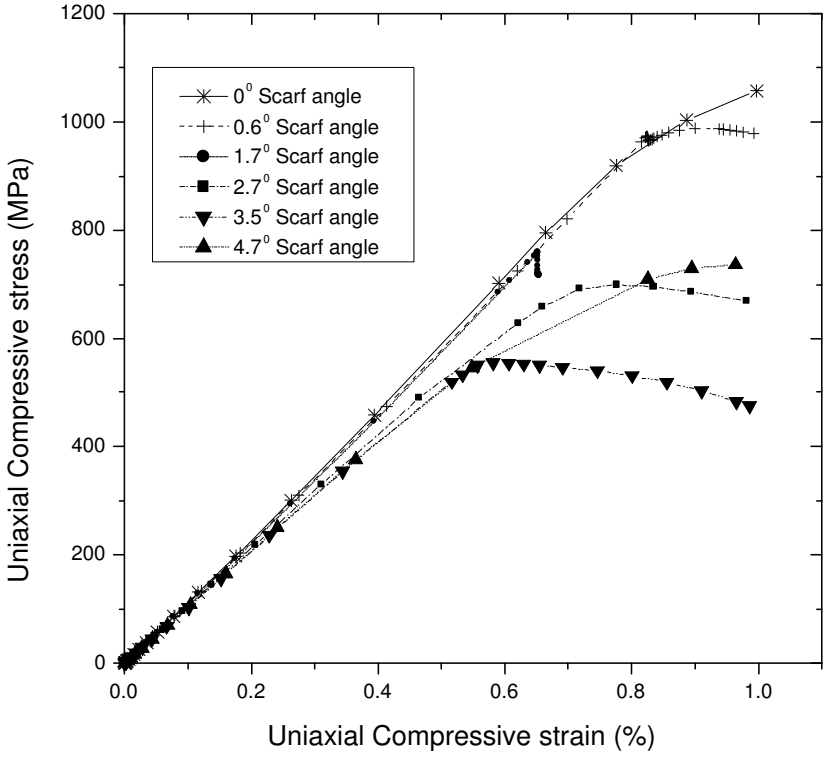

Figure 3.16: Numerically simulated stress-strain curves of scarf joints with scarf angle ranging from 0^0 to 5^0.

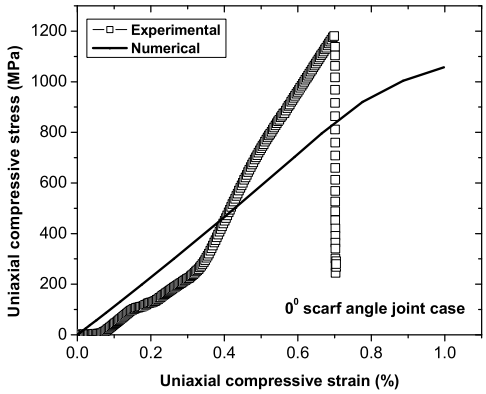

(a) 0^0 scarf joint

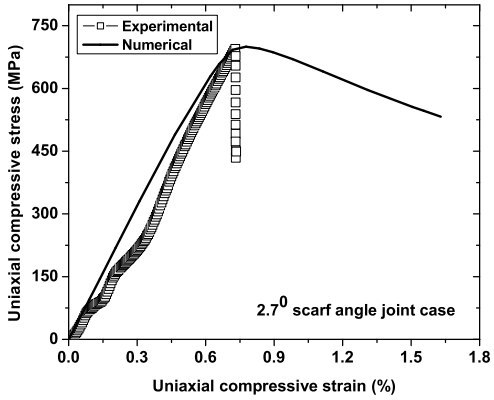

(b) 2.7^0 scarf joint

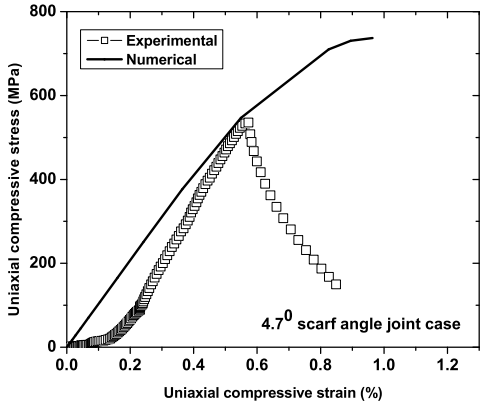

(c) 4.7^0 scarf joint

Figure 3.17: Comparison of the numerical compressive stress (σ_{11}) versus strain (ε_{11}) responses with the experimental data for a joint with scarf angle 0^0, 2.7^0 and 4.7^0.

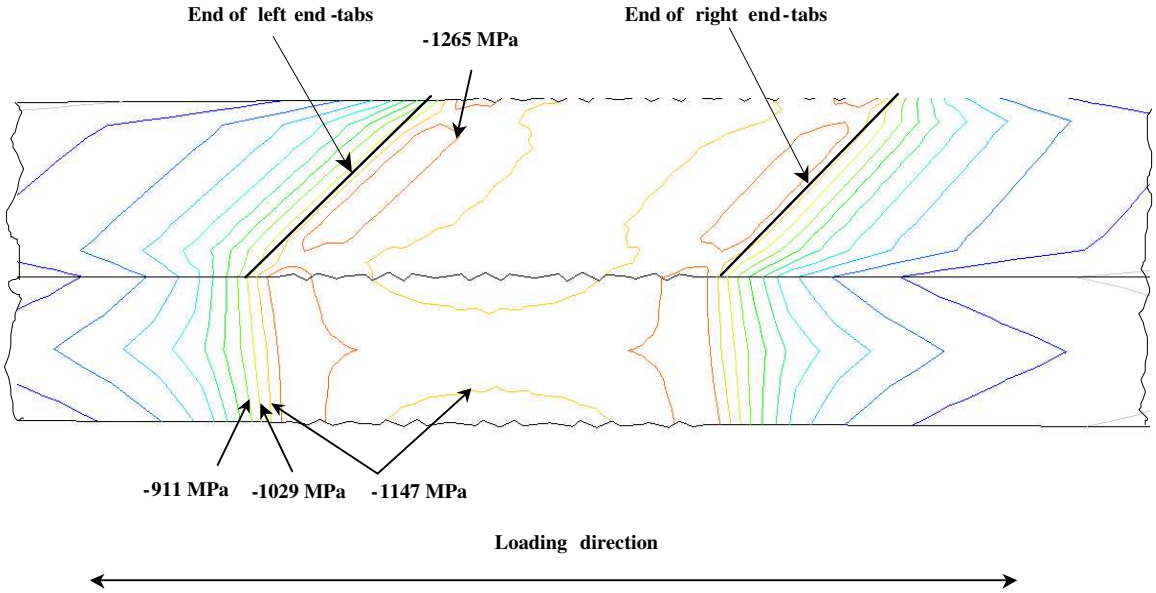

Figure 3.18: FE simulated uniaxial compressive stress (σ_{11}) line contour at 0.77 % uniaxial compressive strain (ε_{11}) for 0^0 (neat specimen) under uniaxial compressive loading.

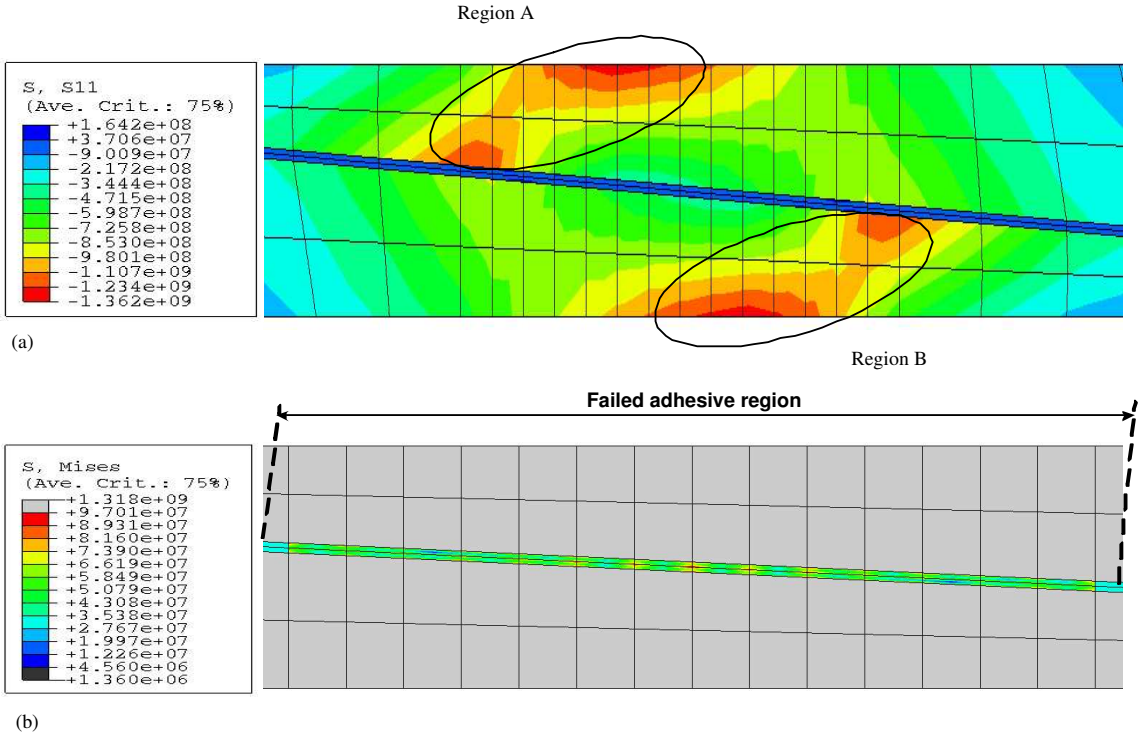

Figure 3.19: (a) FE simulated uniaxial compressive stress (σ_{11}) band contour at 0.77% uniaxial compressive strain (ε_{11}) for 4.7^0 scarf angle, and the (b) corresponding von-Mises stress contours.

The effect of pre-existing, random background waviness was neglected in the above finite element simulations. The strong dependence of compressive joint strength on the scarf-angle and the consistent pattern of failure in the vicinity of the scarf-joint suggest that the presence of the scarf-joint in the composite is a more serious defect in comparison to the random inherent initial waviness observed in composites. The presence of the scarf joints reduced the compressive strengths by 20 – 50% below the infinite band collapse response observed in neat composites. It is therefore expected that including pre-existing, random background waviness in the composite adherends in the numerical analysis will not significantly affect the predicted compressive strength.

3.5 Conclusions

The compression test results on the adhesively-bonded scarf joints comprising unidirectional carbon fibre reinforced polymer (CFRP) laminate and "AF-163-2" structural film adhesive showed that the compressive strength of the joints increased as the scarf angle decreased. The failure mechanism switched from predominantly fiber microbuckling for joints for scarf angles below 3^0, to cohesive shear deformation through the adhesive layer coupled with some traces of attendant fiber microbuckling for joints with scarf angles above 3^0. The compressive strengths of the scarf joints *reduced* by 20 – 50% below the value of the infinite band collapse response in compression. A comparison of numerical and experimental values of the joint strengths showed that the knockdown in compressive strengths increased with the scarf angle. These findings are useful for predicting the overall knockdown in compressive strength of adhesively bonded composite scarf joints used in high performance industrial applications (e.g., aerospace and space, missiles etc).

Chapter 4

Bonded Composite Scarf-Joints under Uniaxial Tensile Loading

4.1 Introduction

In the present study, failure of adhesively bonded aerospace composite scarf joints in uniaxial tension was investigated both experimentally and numerically. The scarf angles studied range from $0^0 - 5^0$. The aim of the study was to predict the joint-strengths and understand their failure mechanisms under tensile loading. The experimental measurements of the composite scarf-joint tensile strengths were validated with numerical predictions carried out using the ABAQUS finite element (FE) program in combination with a in-house user subroutine for the composite adherend failure.

4.2 Experimental Techniques

4.2.1 Test material and preparation of scarf joints

The scarf joints were made from carbon fiber reinforced polymer matrix composite adherends (CFRP) bonded to each other with AF-163-2 film adhesive. CFRP composite laminates were fabricated as described in Chapter 3. An identical method of fabrication as described in Chapter 3 was followed to fabricate the joints. In the present case a gauge length of 130 mm was maintained as opposed to 10 mm for compression specimens. The final dimensions of joints satisfied the requirements for tensile testing in accordance with ASTM standards D3039/D3039M [173].

4.2.2 Specimen Design and Mechanical Testing

Figure 4.1 shows the typical specimen geometry of the tensile test specimens; cut to dimensions 12.5 mm width, 2 mm thickness and 130 mm gauge length. Each specimen was loaded on a standard 100 kN screw-driven INSTRON-5565 universal testing machine fitted with mechanical wedge grips (suitable for flat specimens) at a crosshead speed of 2.5 mm/min. Annealed aluminum end-tabs of 1 mm thickness were bonded to the end of the specimens using a modified epoxy (Redux) film adhesive to enable a smooth transfer of load to the specimen. The mating surfaces of the aluminum end-tabs and composite adherends were abraded using emery cloth and chemically cleaned with acetone. The use of annealed aluminium end-tabs enabled the knurled surfaces of the grips to 'bite' firmly into the specimen tabs, thus preventing slippage between the specimen and grips. In addition, end-tabs distributed the pressure applied by the grips evenly over the surface of the specimen, thus preventing local damage in the laminate. Load and strain measurements were recorded using a computerized data logging system. A total of five tests were performed for each scarf-angle ranging from 0.5^0 – 5^0 degrees and the average failure strength values were calculated.

Tensile mechanical properties of Adherends

To obtain the tensile properties of the base composite in longitudinal and transverse direction, test specimens were prepared according to ASTM D 3039/D 3039M. To measure the in-plane shear properties of the composite material, specimens were extracted from 450 laminates as per ASTM D3518/D3518M. For measurement of out-of-plane shear properties specimens were prepared as per ASTM D 5379/D 5379M. The tests were conducted on an Instron universal testing machine fitted with 100 kN load cell. Strain gauge rosettes were mounted in the middle of the specimens and strains in both longitudinal and transverse directions were monitored simultaneously using a portable data logger. The measured strains were used to calculate the Poisson's ratio of the material tested. Shear properties of the base composite material were measured by following the procedures

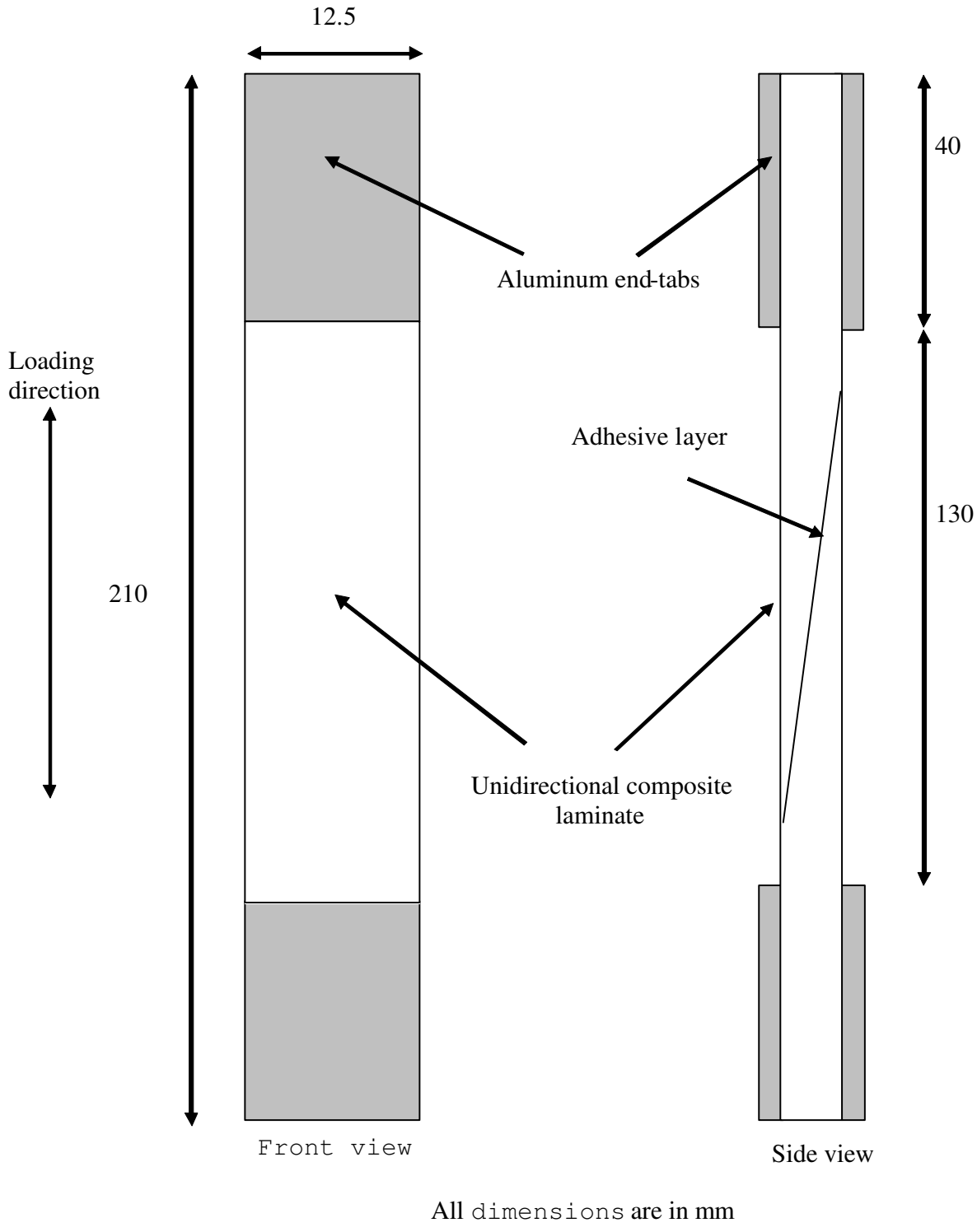

Figure 4.1: A typical adhesively bonded scarf joint specimen geometry used for tensile testing.

Table 4.1: Fiberdux-913CHTA composite material properties under tensile loading

Property	Value
Longitudinal tensile elastic modulus, E^t_{11}	150 GPa
Transverse tensile elastic moduli, E^t_{22} and E^t_{33}	9.50 GPa
Shear elastic moduli, G_{12} and G_{13}	1.07 GPa
Shear elastic modulus, G_{23}	3.92 GPa
Poisson's ratio, ν_{12} and ν_{13}	0.26
Poisson's ratio, ν_{23}	0.25
Longitudinal tensile strength, σ^t_{11}	1900 MPa
Transverse tensile strength, σ^t_{22}	57 MPa
Interlaminar shear strength, τ_{13}	100 MPa

described in section 3.2.3. The test results are summarized in Table 4.1.

4.3 Experimental Results and Discussion

4.3.1 Failure Modes & Load versus Displacement responses

The failure modes observed in the experiments are classified into two main categories: (i) Mode A_t - Failure predominantly by fibre fracture and pullout, (ii) Mode B_t - Failure predominantly by cohesive shear failure in adhesive film with little or no fibre fracture and pullout (see Figure 4.2). Figures 4.3(a) and (b) show actual specimens from fractured scarf-joints in uniaxial tension corresponding to Modes A_t ($< 2^0$ scarf angle) and B_t ($> 2^0$ scarf angle) failure respectively. A photograph of a fractured base composite specimen is shown in Figure 4.4. Figure 4.5 shows that the adhesive shear failure was cohesive and not interfacial in nature. Table 4.2 shows the frequency of occurrence of the two types of failure modes in relation to scarf angles. Mode A_t type failure was observed for scarf angles less than about 2^0, while Mode B_t type failure was observed for scarf angles more than 2^0. A consistent pattern of failure was observed, which switched from Modes A_t to B_t as the scarf-joint angle (with respect to the loading axis) increases from 0^0 to 5^0. The

Table 4.2: Frequency of Occurrence of Failure Modes A_t and B_t

Scarf Angle (Degrees)	Mode A_t No. of Specimens that failed predominantly by fibre fracture and pullout	Mode B_t No. of Specimens that failed predominantly by adhesive shear failure in adhesive film with little or no fibre fracture and pullout
0.5	100%	-
1.8	-	close to 100%
2.9	-	close to 100%
4.0	-	100%
4.7	-	100%
5.0	-	100%

shapes of the load- displacement responses are similar for both types of failure modes and the various scarf angles ranging from 0^0 to 5^0. Figure 4.6 shows several typical stress-strain curves and it can be seen that the stress increases in a linear manner to a peak value before dropping precipitously upon catastrophic fracture.

4.3.2 Effect of scarf angle on tensile joint strength

Figure 4.7 shows the effect of scarf angle on the uniaxial tensile strength of the joint. As shown in the Figure 4.7, a clear scarf angle effect is evident. Smaller (i.e. shallow) scarf angles yielded higher tensile strength as compared to those with larger (steep) scarf angles. The knockdown in tensile strength was most prominent for scarf angles less than about 1^0. As the scarf angle of the joint increases, the quantum of additional knockdown in tensile strength becomes progressively more gradual. The observed reduction in tensile strength as a function of scarf angle is consistent with the experimental work carried out by other researchers working on a similar geometrical configuration with other material systems/combinations [44, 174, 175]. The experimental work only considered scarf joint with 0.15 mm adhesive layer thickness. No experimental studies were performed for scarf

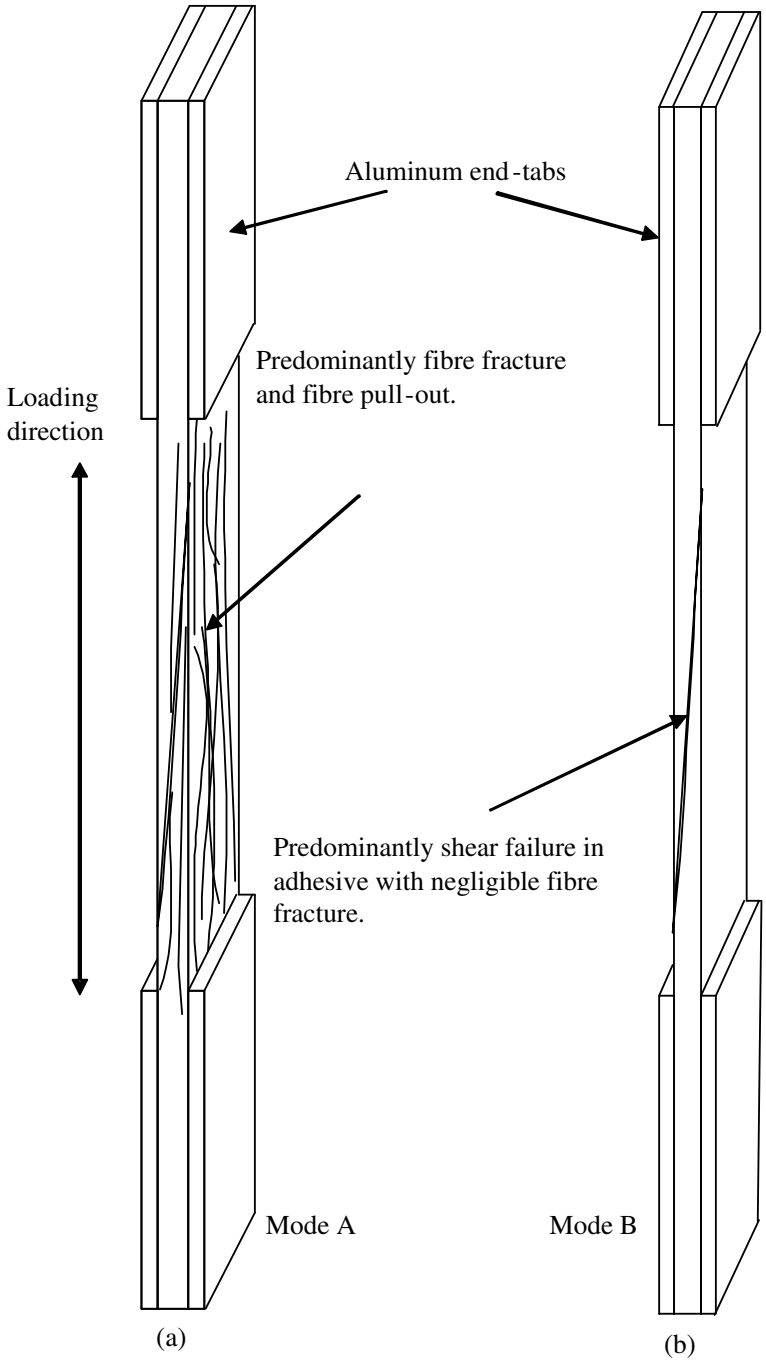

Figure 4.2: Schematic illustration of the two competing failure modes noticed in the scarf joints subjected to tensile loading at varying scarf angles: (i) adherend failure, (ii) cohesive failure.

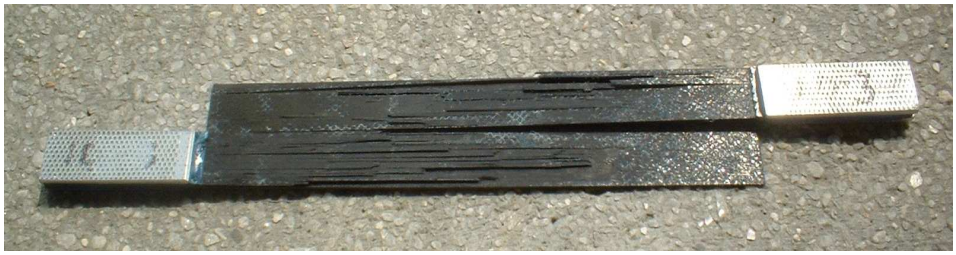

(a)

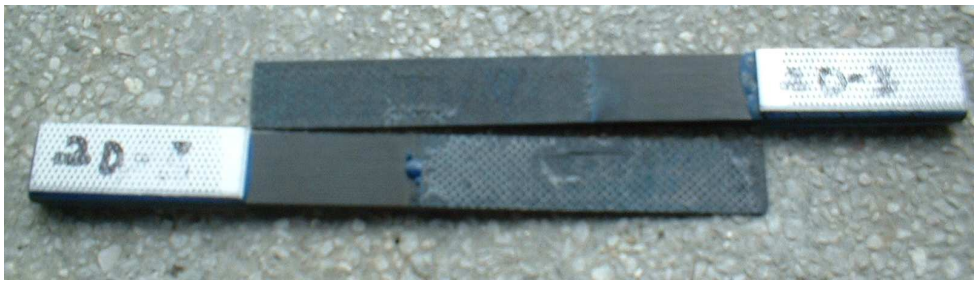

(b)

Figure 4.3: Fracture surfaces (a) with scarf angle 0.5^0: Significant damage in the composite adherends was observed thus illustrating fibre fracture and fibre pull-out in the joint area, (b) with scarf angle 2.9^0: No significant damage in the composite adherends was observed. The joint separated by cohesive failure in the adhesive.

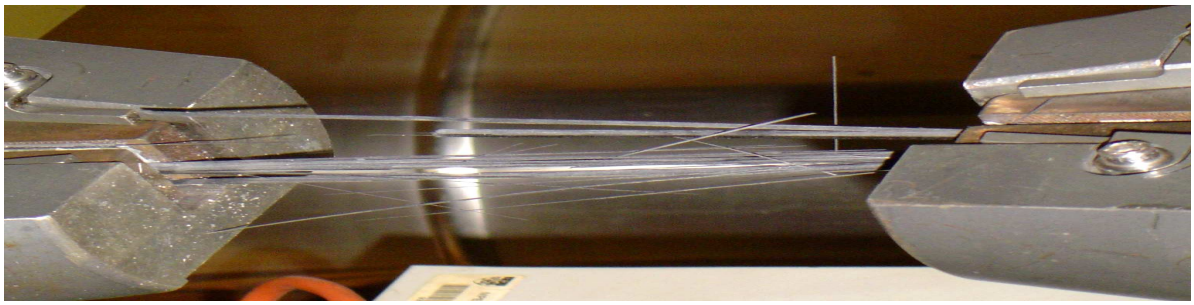

Figure 4.4: Fractured morphologies of the base composite specimens (i.e. with 0^0 scarf angle): A catastrophic failure in the composite specimen was observed.

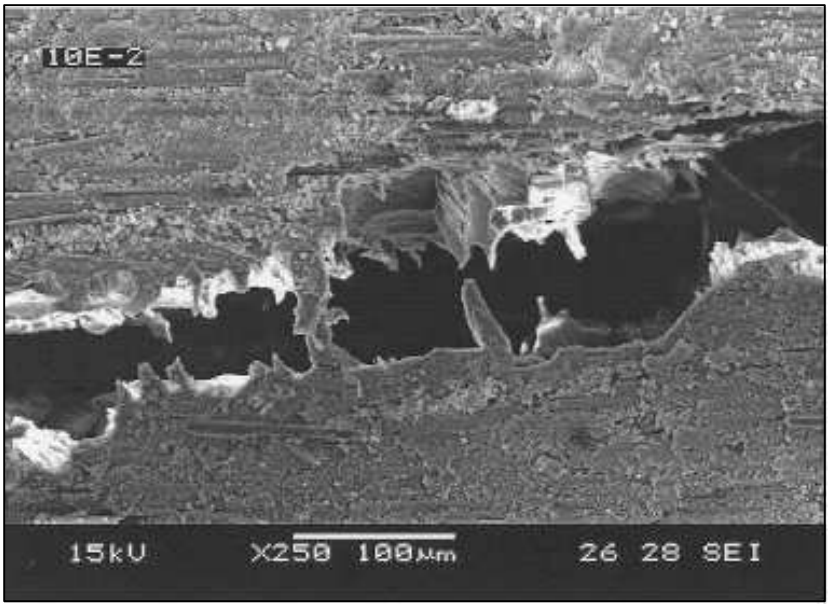

Figure 4.5: SEM micrograph of a typical fracture observed in the adhesive region of the scarf-joint illustrating cohesive failure.

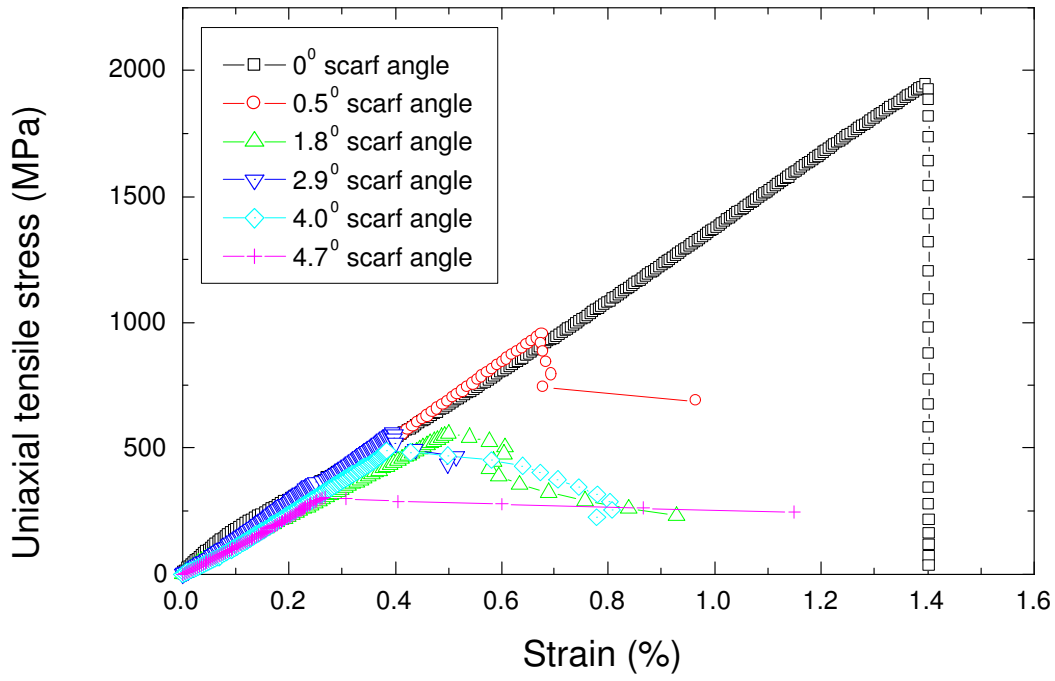

Figure 4.6: Experimentally measured stress-strain responses for adhesively bonded scarf-joints with different scarf angles.

joints with adhesive layer thicknesses of 0.230 and 0.50 mm because of time limitation.

It is noteworthy that an adhesively-bonded joint with a scarf-angle of only 1^0 (symbolizing a small imperfection in the long fiber composites) causes a knockdown in tensile strength of a unidirectional CFRP composite by as much as 60%. For the largest scarf-angle of 5^0 used in the present experiments, the tensile strength drops by 89%. These findings highlight the significance of imperfections in reducing the tensile strength of composites and emphasize the importance of fabrication, machining and processing techniques, which minimize such imperfections. Evidently a scarf joint with shallow scarf angle resulted in higher tensile load bearing structure than that of one with steeper scarf angle. However, relatively smaller scarf-angle joints are much more difficult to machine and fabricate in practical applications. Thus, it is believed that the findings would be useful in predicting the overall knockdown in tensile strength of adhesively bonded scarf-joints of unidirectional CFRP composites such as those required in aerospace and other high performance industries being worth putting in extra effort.

4.4 Comparison with Numerical Predictions

ABAQUS Finite Element Analyses (FEA) were carried out on the scarf-joint configurations in order to assess the numerical prediction of the experimental results. In the present studies, the unidirectional composite laminate adherends were modeled as a homogeneous orthotropic continuum material as described in Chapter 3 with material properties listed in Table 4.1. The adhesive layer sandwiched between adherends was modelled as an isotropic solid with mechanical properties of film adhesive AF-163-2 shown in Table 3.2.

4.4.1 Finite Element Geometry

The scarf joints were analyzed as a three-dimensional problem with geometric length scales similar to those used in the experiments so that our FEM model closely represented

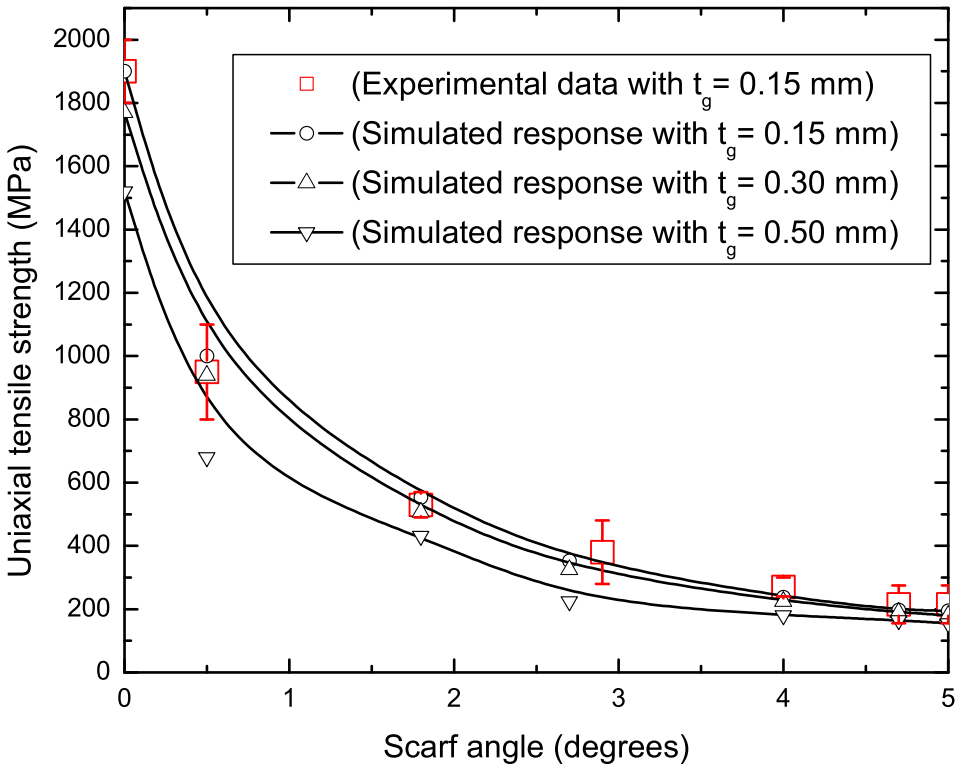

Figure 4.7: Comparison of experimental measurements of joint tensile strengths and scarf angles with the numerical results.

the test conditions. The finite element model of the specimen (shown in Figure 4.8) corresponded to a mesh of length 18000d along the fiber direction and width 1600d in the transverse direction (where d was the fiber diameter). The finite element mesh consisted of three-dimensional solid-continuum reduced integration (C3D8R) elements with 3 displacement degrees-of-freedom at each node (i.e., two in-plane displacements and one normal to the plane of deformation). Material constitutive model and load and boundary conditions were similar to that of one adapted in Chapter 3.

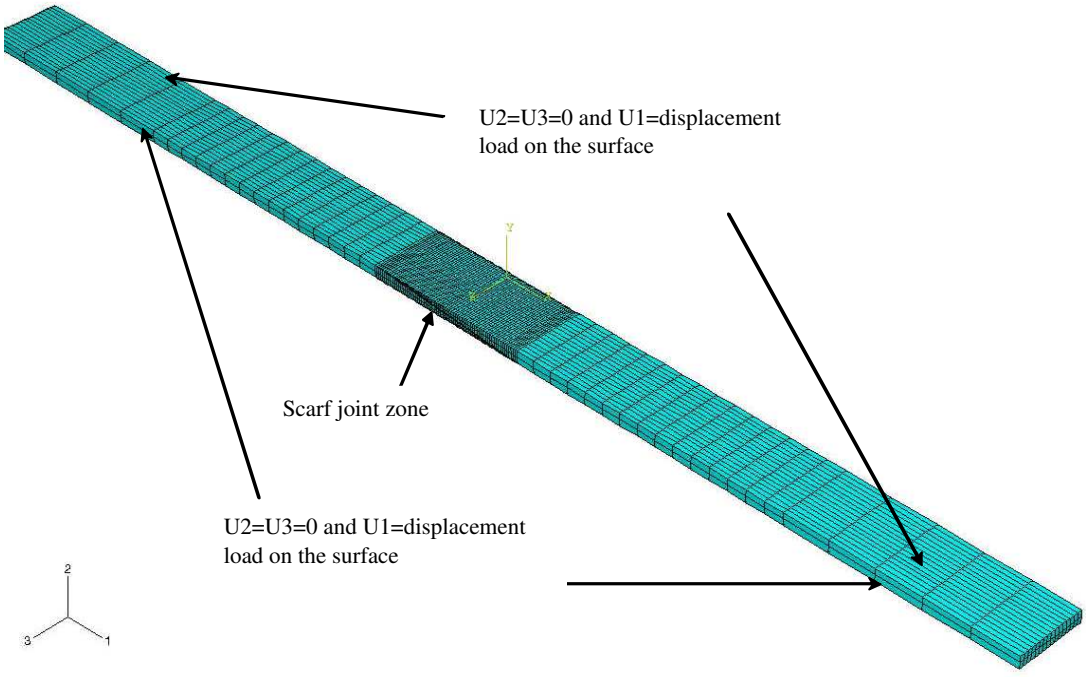

Figure 4.8: Illustration of the typical mesh used in the numerical analysis of the bonded scarf joint.

4.4.2 Numerical Results

Finite element predictions were carried out for scarf joints with angles ranging from 0^0–5^0 using the ABAQUS/Standard solver. The numerically simulated stress-strain responses for the various scarf angles from 0^0 – 5^0 (shown in Figure 4.9), showed that while failure load decreased with increasing scarf angle, the stiffness remains constant (within limits of numerical scatter) at about 145 GPa. The point where significant plastic deformation

starts in the curves as shown in Figure 4.9 corresponds to the joint failure. The failure in base composite occurred at about 1.5% engineering strain. The 0.5^0, 1.8^0, 2.9^0 4.0^0 and 4.7^0 scarf joints failed at about 0.7%, 0.4%, 0.25%, 0.17% and 0.15% engineering strain. When joint fractured abruptly the drop was sudden implying brittle nature of failure. However, when joints fractured gradually the drop was slow implying ductile failure i.e. cohesive failure in the adhesive layer. Figure 4.10 shows that the numerically simulated stress (σ_{11}) - strain (ε_{11}) response of a typical scarf joint in uniaxial tension is in reasonable agreement with the experimental response. Figure 4.11 shows the von-Mises stress contours for the FE model of a 4^0 scarf-joint in the bonded zone of the joint showing cohesive joint failure. The comparison of finite element predictions of the scarf-joint strength in uniaxial tension with experimental values (see Figure 4.7) showed that the knockdown in tensile strength with increasing scarf-angle could be well described by the FEM predictions. Thus, from these FEM predictions, a reasonable quantitative correlation was observed with the experimental measurements.

4.4.3 Effect of adhesive layer thickness

The effect of the adhesive layer thickness on the performance of the scarf joint strength was investigated numerically by adopting the above described numerical procedures. The analysis was performed with three different adhesive bondline thickness values (i.e., 0.15 mm, 0.3 mm and 0.5 mm). Uniaxial stress, σ_{11} (MPa) versus uniaxial strain,(ε_{11}) (%) curves show that the joint strength and stiffness decreased by increasing the bondline thickness of the adhesive layer (see Figures 4.12 - 4.16). For shallow scarf angle (i.e. 0.5^0 scarf angle) the knockdown in strength was higher than that of steeper scarf angle (i.e. 4.7^0 scarf angle). The reduction in the joint strength with increasing bondline thickness for scarf joint 2.9^0 and above is only marginal. The failure mode in the scarf joint with scarf angle of 0.5^0 changed from 100% adherend to mixed (i.e. adherend + cohesive) with increasing bondline thickness. The failure modes observed in the simulated study is summarized in Table 4.3. The percent of failure modes were calculated by studying the

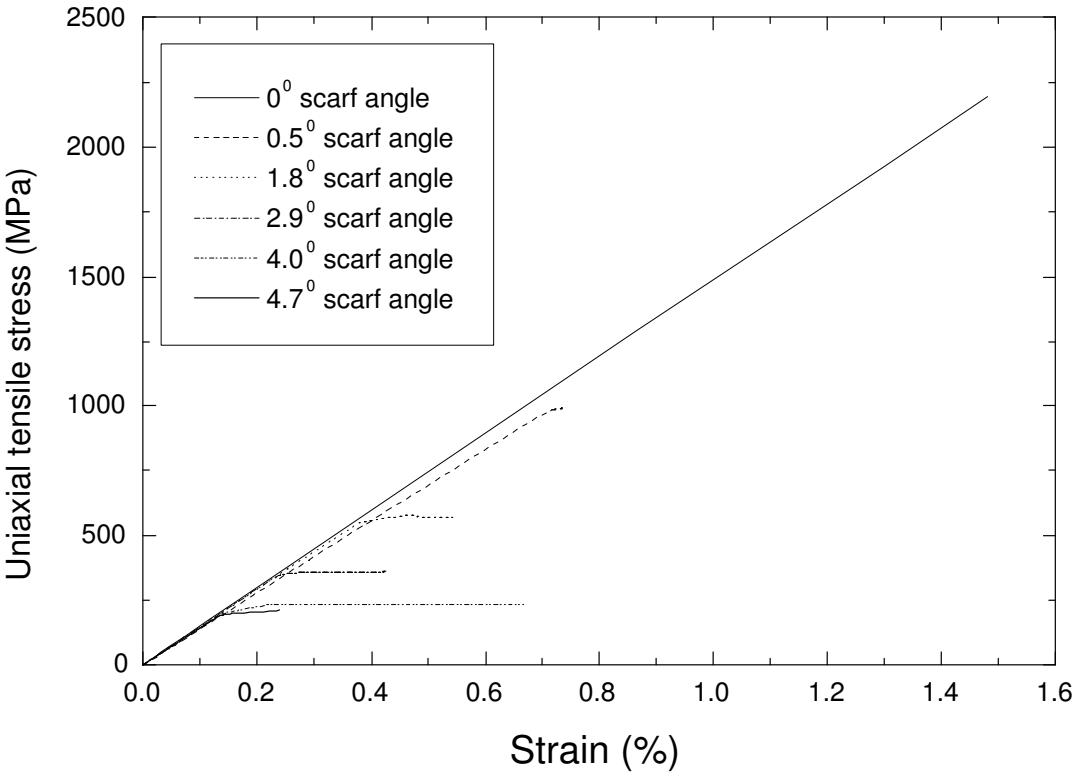

Figure 4.9: Numerically simulated stress-strain curves for different scarf angle geometries under tensile loading.

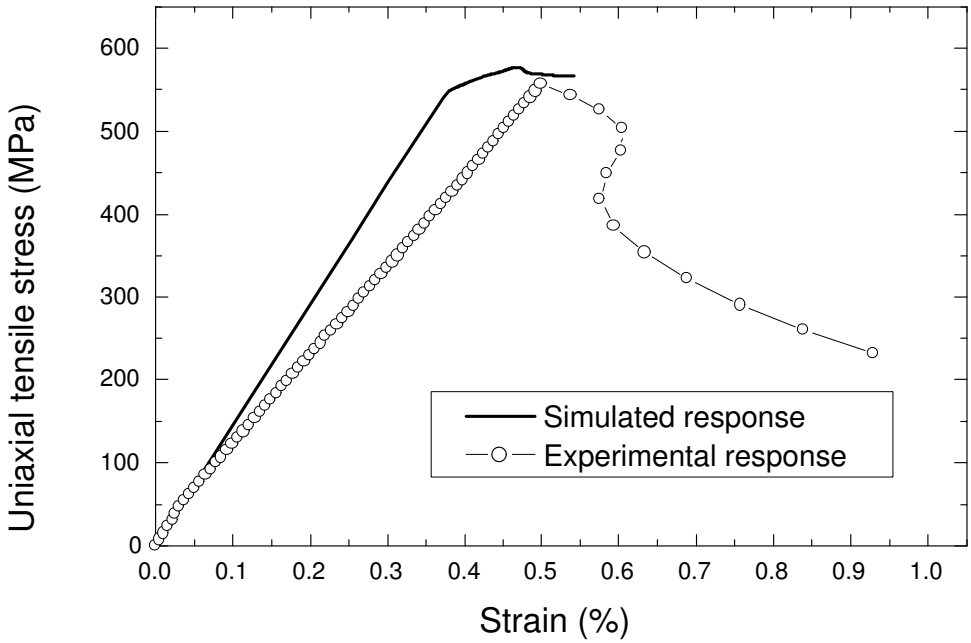

Figure 4.10: Comparison of the experimental and numerical stress-strain responses of a joint with a scarf angle of 1.8^0 subjected to uniaxial tensile loading.

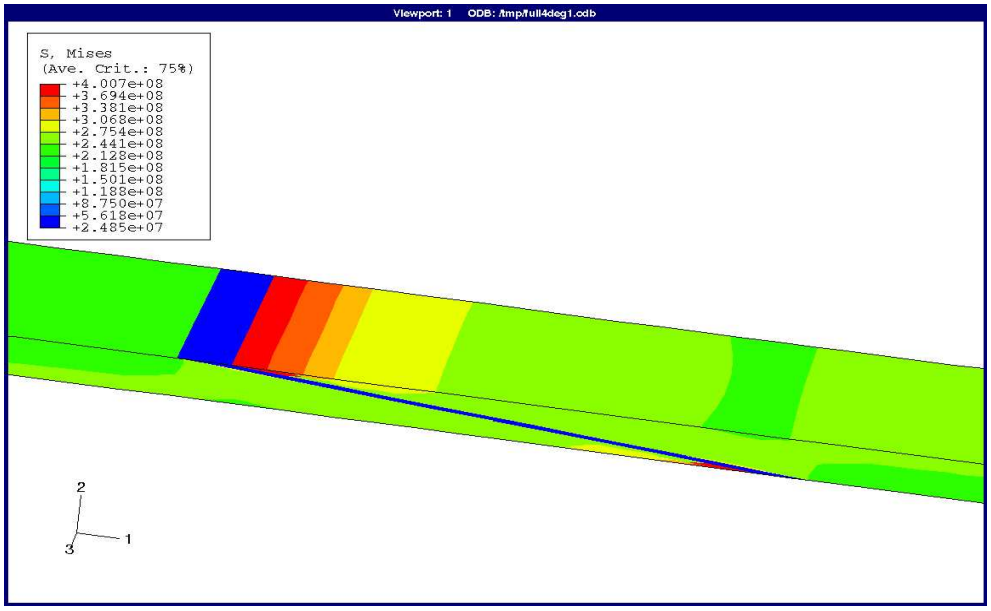

Figure 4.11: Enlarged view of the von-Mises stresses from FE analysis for cohesive failure of a joint with a scarf angle of 4^0 subjected to uniaxial tensile loading.

Table 4.3: Summary of joint strength and failure modes, A_t or B_t with scarf angle for adhesive layer thickness of 0.15, 0.3 and 0.5 mm

Bondline Thickness (mm)	Scarf Angle (Degrees)	Joint Strength (MPa)	Mode A_t Adherend Failure	Mode B_t Cohesive Failure
0.15	0.5	1012	100%	-
	1.8	549	25%	75%
	2.9	348	-	100%
	4.0	250	-	100%
	4.7	214	-	100%
0.3	0.5	922	95%	5%
	1.8	508	30%	70%
	2.9	332	-	100%
	4.0	237	-	100%
	4.7	207	-	100%
0.5	0.5	672	85%	15%
	1.8	451	40%	60%
	2.9	297	-	100%
	4.0	214	-	100%
	4.7	204	-	100%

von-Mises stresses in the elements used to mesh the adhesive layer. If all the elements used for meshing the adhesive layer exceed the yield strength 100% cohesive failure is assumed.

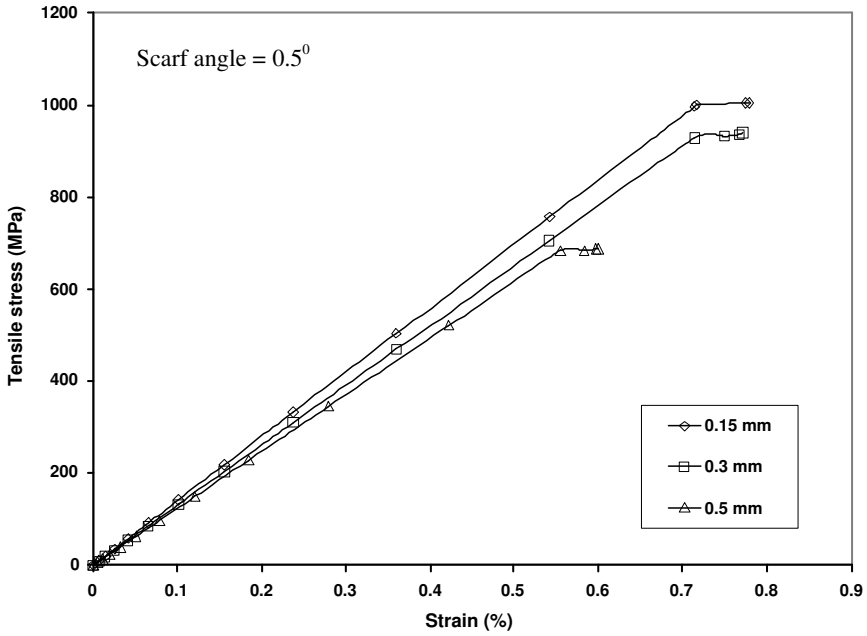

Figure 4.12: Uniaxial stress-strain curve for scarf joint with scarf angle 0.5^0 for different adhesive layer thickness subjected to uniaxial tensile loading.

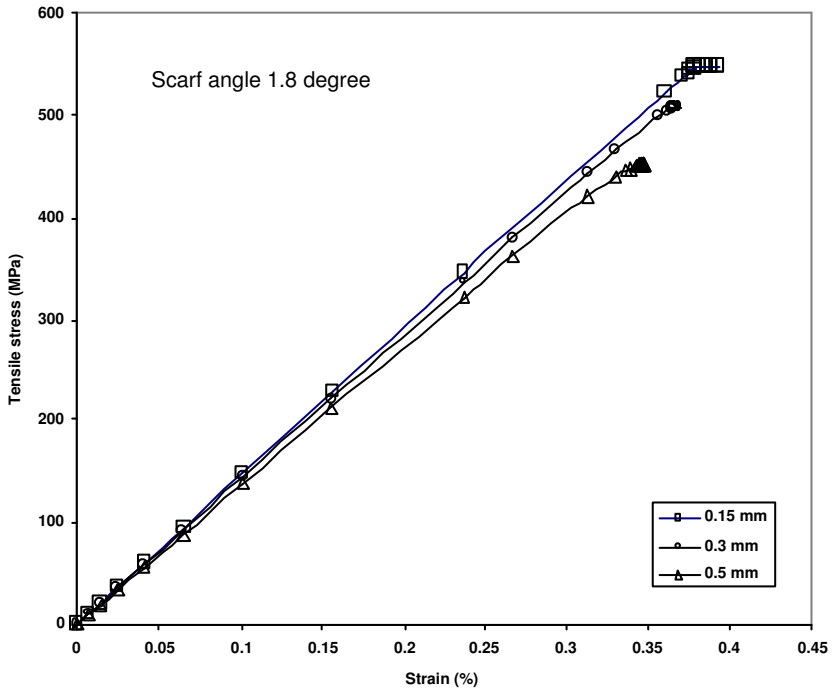

Figure 4.13: Uniaxial stress-strain curve for scarf joint with scarf angle 1.8^0 for different adhesive layer thickness subjected to uniaxial tensile loading.

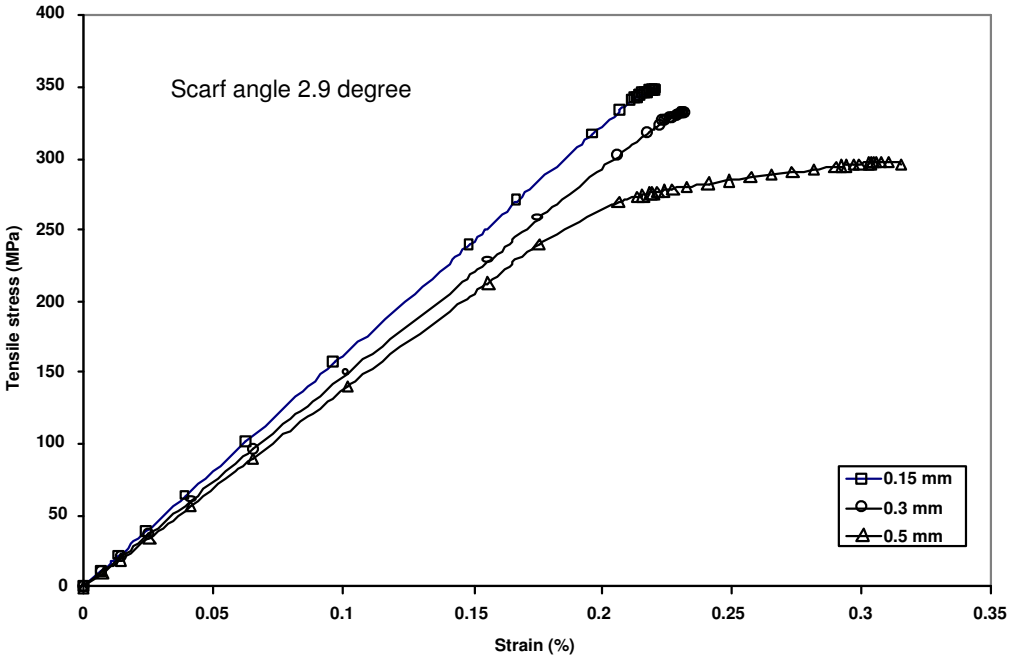

Figure 4.14: Uniaxial stress-strain curve for scarf joint with scarf angle 2.9^0 for different adhesive layer thickness subjected to uniaxial tensile loading.

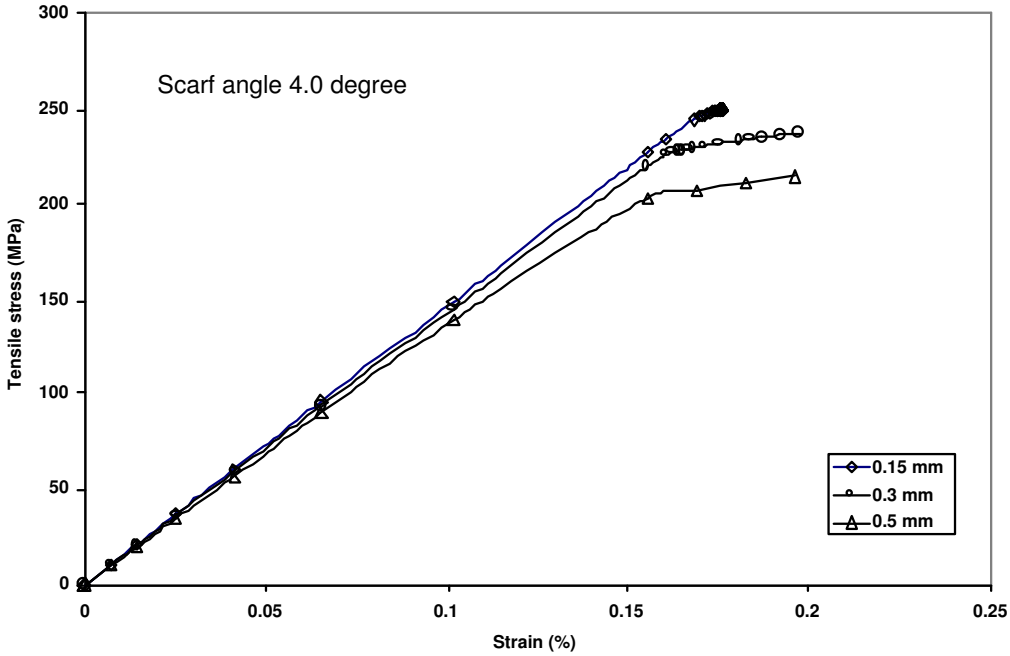

Figure 4.15: Uniaxial stress-strain curve for scarf joint with scarf angle 4.0^0 for different adhesive layer thickness subjected to uniaxial tensile loading.

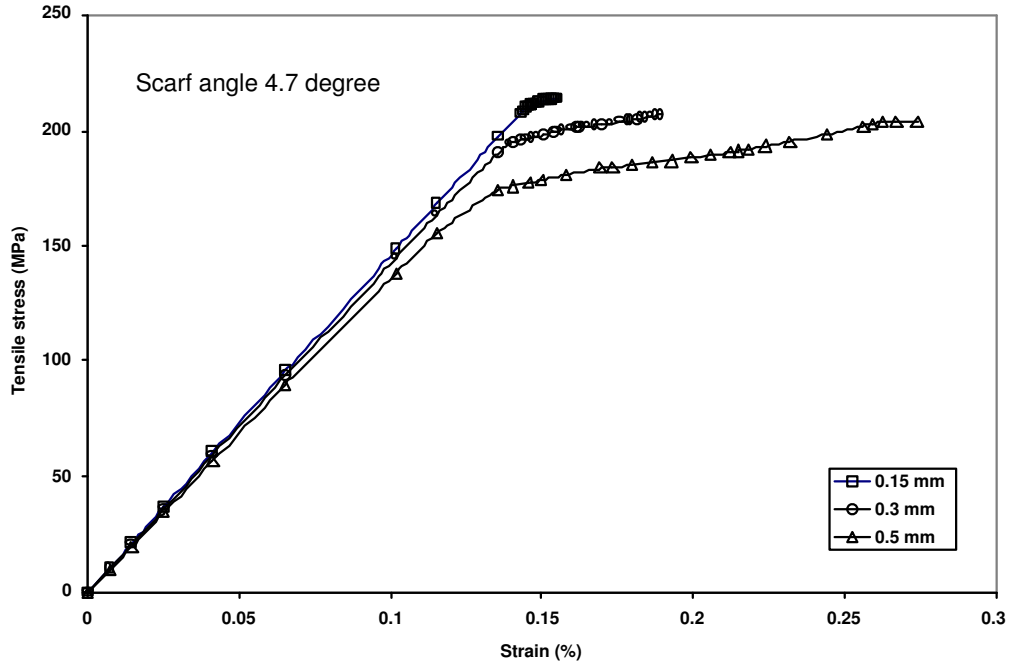

Figure 4.16: Uniaxial stress-strain curve for scarf joint with scarf angle 4.7^0 for different adhesive layer thickness subjected to uniaxial tensile loading.

4.5 Conclusions

The investigation of the adhesively bonded unidirectional CFRP scarf joints in uniaxial tension revealed two main failure modes: (i) failure predominantly by the fibre fracture and fiber pull-out (Mode A_t), and (ii) failure predominantly by the cohesive shear in adhesive film (Mode B_t). The failure Mode A_t was observed for scarf angles less than about 2^0, while Mode B_t was observed for scarf angles greater than 2^0. We observed a consistent pattern of failure that switched from Modes A_t to B_t as the scarf-joint angle increases from $0^0 - 5^0$. A clear scarf angle effect was noticed with smaller (i.e. shallow) scarf angles yielding higher tensile joint strengths in comparison to those with the larger (steeper) scarf angles. The knockdown in tensile strength was most prominent for scarf angles less than about 1^0. The adhesively-bonded joint with scarf-angles of 1^0 or lower (symbolizing a small imperfection in long fiber composites) caused a knockdown in tensile strength of a unidirectional CFRP composite by as much as 60%. For the specimen with the largest scarf-angle of 5^0 used in the present experiments, the tensile strength dropped by 89%.

The knockdown in tensile strength with increasing scarf-angle was well described by the FE predictions, which model the unidirectional composite as a homogeneous orthotropic continuum with negligible fiber bending resistance in the longitudinal direction. The adhesive film was assumed to be an elastic-plastic solid perfectly-bonded to the composite laminate.

Chapter 5

Measurement of Mode I Adhesive Fracture Energy, G_a

5.1 Introduction

In the present work, a modification has been proposed for the traditional single lap joint (SLJ) configuration, in order to overcome the wide scatter in the values of strength and fracture toughness measurement due to adhesive fillets. This new specimen, referred to as Modified Single Lap Joint (MSLJ), is made by implanting end pre-cracks in the adhesive layer at the center of the bondline in a conventional SLJ. The objective of inserting the pre-crack was to ensure that during testing, a sharp crack propagated from both ends of the overlap and reduced the effect of spew fillets and hence the scatter in the data on the fracture toughness measurements. Thus, in this study, experiments were carried out to investigate the effect of the modification on the SLJ on the accuracy of the measured adhesive fracture energy. In addition, the results obtained from MSLJ specimens were compared with those obtained from SLJ and DCB specimens.

5.2 Experimental

5.2.1 Materials and specimen preparation

In the present study, unidirectional composite laminates, $[0]_8$, made from 913C - HTA 12K 5-34% carbon prepreg and three types of Redux film adhesives (all supplied by Hexcel Composites, UK) were used. Prepreg sheets were cut from the material roll and 8 sheets of prepregs were stacked together to fabricate a laminate of 1.6 ± 0.125 mm thick-

ness. The stacked system was then pressed on a hot press at a pressure of 700 kPa and maintained at a temperature of 120^0C for 1 hour as recommended by the composite manufacturer. Figure 5.1 illustrate the order of arrangement of stacked prepregs, other moulding materials and mould dimensions. To prevent laminate warpage and obtain thermal stress free laminate, the cured laminate was allowed to cool down to room temperature in the hot press machine overnight (12 hr). Later the laminate panel was post cured at the same temperature and pressure for about 4 hours. The molded composite laminates which had a volume fraction of around 60% were cut into pieces with dimensions of 230x230x1.6 mm. The three types of adhesive used in the current investigation are Redux 322, Redux 335K and Redux 319A. Redux 322, 300 gram per square meter (gsm) is a high performance modified epoxy film adhesive with 300 gsm areal weight and has nylon scrim cloth support. The nylon cloth provides better bondline thickness control. Redux 335K, 150 gsm is a film adhesive with areal weight of 150 gsm. This adhesive comes with knit carrier support which controls the adhesive layer thickness during curing process and provides easy handling. Redux 319A is a film adhesive suitable for bonding aluminium to aluminum, fibre reinforced composite (FRP) to FRP and sandwich construction. This adhesive has areal weight of 73 gsm and is supported on a woven nylon carrier, which provides better control of bondline thickness during curing.

Preparation of MSLJ and SLJ

Three sets of modified single lap joints (MSLJs) samples were prepared from the $103.6 \times 230 \times 1.6mm$ unidirectional CFRP laminate panels as recommended for SLJ specimens in ASTM D 1002-01. The first set was prepared using Redux 322, 300 gsm structural film adhesive. The second set was prepared using the Redux 335K, 150 gsm film adhesive and the third set was prepared using Redux 319A, 73 gsm film adhesive. The mating surfaces were pre-treated with grit blasting followed by degreasing with a white cotton cloth slightly wetted with acetone. The degreasing process was done to remove any contamination present whatsoever on the grit blasted surface. After the surface pre-

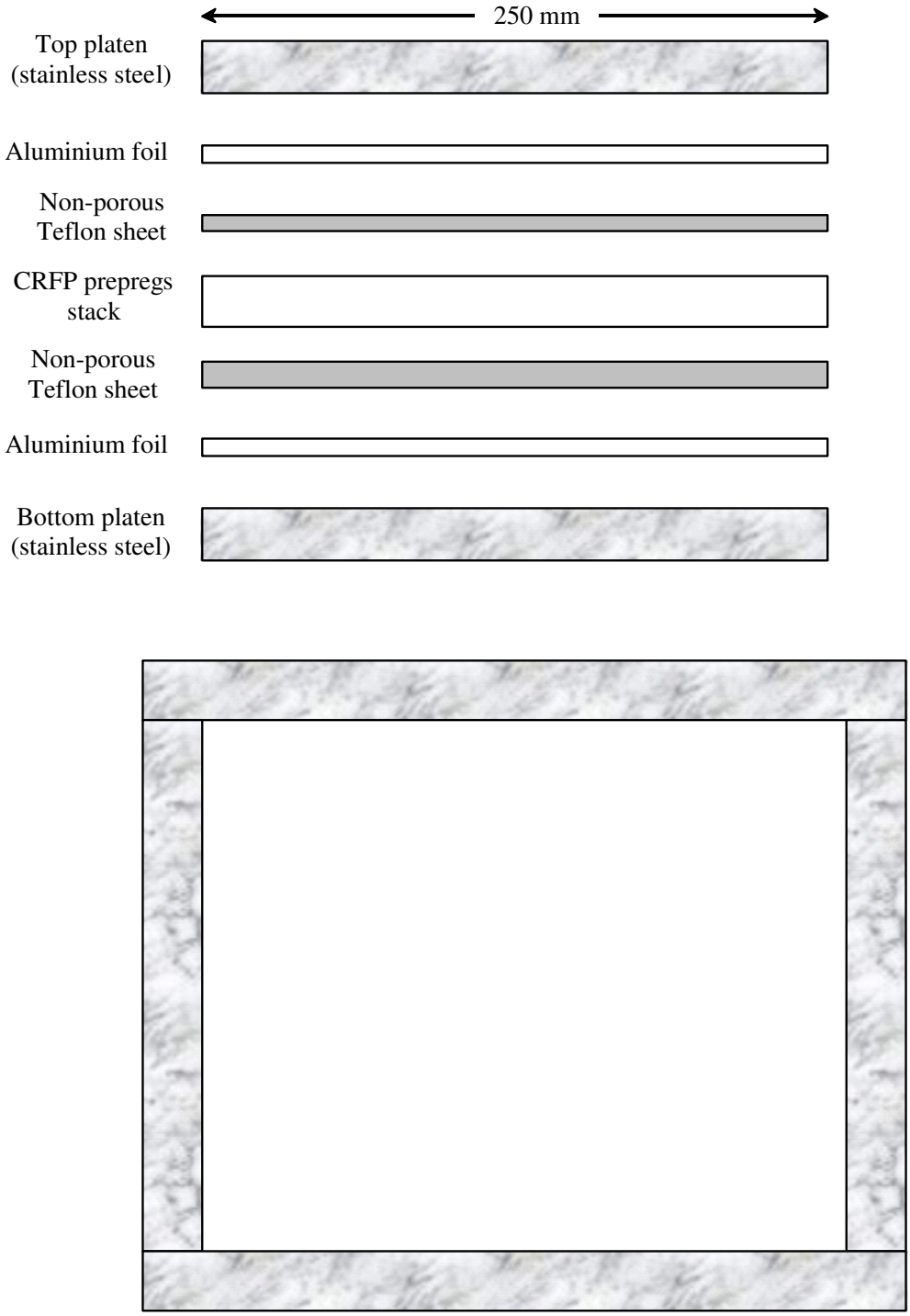

Figure 5.1: Schematic diagram of order of arrangement of stacked prepregs and mould dimensions.

treatment, the composite panels were dried at 80^0 C for an hour. Two strips of adhesives with width of 16.7 mm were cut and applied to the pre-treated surface of the panels. To create the pre-crack two stencils of size 300x30x0.02 mm were cut from the household aluminum foil roll. A typical placement order is shown in Figure 5.2(a). An opening of size 12.7x225x0.02 mm was cut symmetrically from the middle of each stencil, and the remaining portion was then precoated with mold release agent (see Figure 5.2(b)). The precoated aluminium foil was then placed on the top of each adhesive film, which were previous placed on the substrates (see Figure 5.3) such that it ensured a 2.0 mm pre-crack, (δ), at both ends of the bonded overlap. The aim of using these precoated stencils was to create a sharp starter crack in the middle of the bondline. This set-up prevented the slippage of the aluminium foil during adhesive curing process thus allowed to maintain a constant overlap length of 12.7 ± 0.25 mm in all specimens. The two mating parts of the substrate were then brought together symmetrically for the bonding process to commence as shown in Figure 5.2(a). The assembled system was then placed in a convection oven on a horizontal base plate. Contact pressure (applied through dead weights) and temperature was maintained as recommended by the adhesive manufacturer for the respective adhesive. The cured joint was allowed to cool down overnight inside the oven. The bonded panel was then cut to the size of the test specimens using a high-speed diamond bench cutter. For comparative studies of the test results, three sets of SLJ specimens were also prepared by following similar procedures and recommendations of the ASTM D 1002-01 standard.

A reflective optical microscope was used to measure the adhesive layer thickness. It was found that most of the specimens had adhesive layer thickness between 0.3 - 0.5 mm. The overlap length of the joint was measured after fracture using a digital Vernier caliper with 0.01 mm as its least count. All other short dimensions were measured using a suitable micrometer. For convenience the various batches of the specimens are named as MSLJ-Redux322, MSLJ-Redux335K, MSLJ-Redux319A, SLJ-Redux322, SLJ-Redux335K, and SLJ-Redux319A. MSLJ-Redux322 stands for modified single lap

joint made from Redux 322 adhesive.

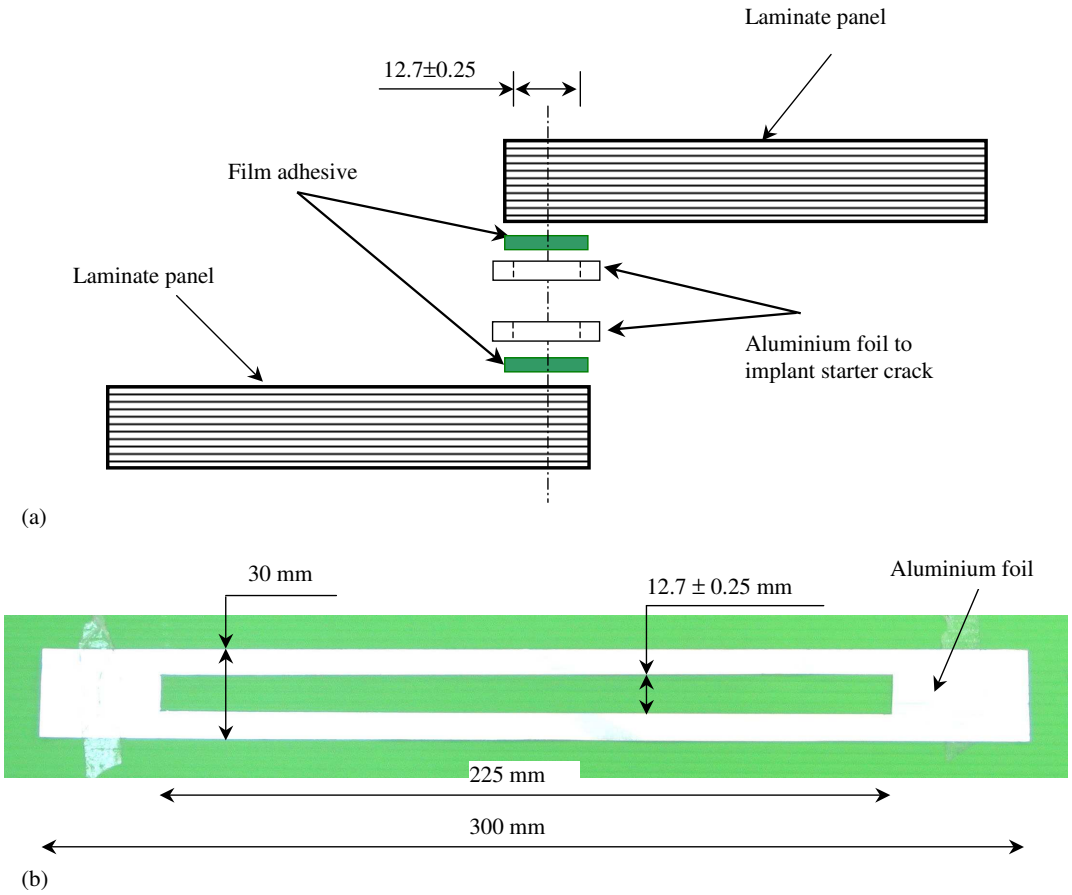

Figure 5.2: Schematic diagram which illustrates the placement of aluminium foil and adhesive during the preparation of MSLJ configuration; (b) A photograph of mould release coated aluminium stencil: opening of size 12.7x225x0.01 mm was cut out from the middle of the stencil.

Preparation of DCB

Three sets of DCB test specimens each consisting of three samples were prepared in accordance with the ASTM standard D 5528 - 01 as shown in Figure 5.4. The width and length of the specimens were maintained at around 25.4 mm and 200 mm respectively. Before applying the adhesive film to the substrates, the substrates were pretreated by grit-blasting/acetone wipe and then dried at 80^0 C for 60 min. A sheet of adhesive film (Redux 322 or Redux 335K or Redux 319A) was placed on the pretreated surface of each composite panel. A pair of release coated aluminum foil of length 75 mm was used as a starter pre-crack. The mating parts were brought together and cured in an

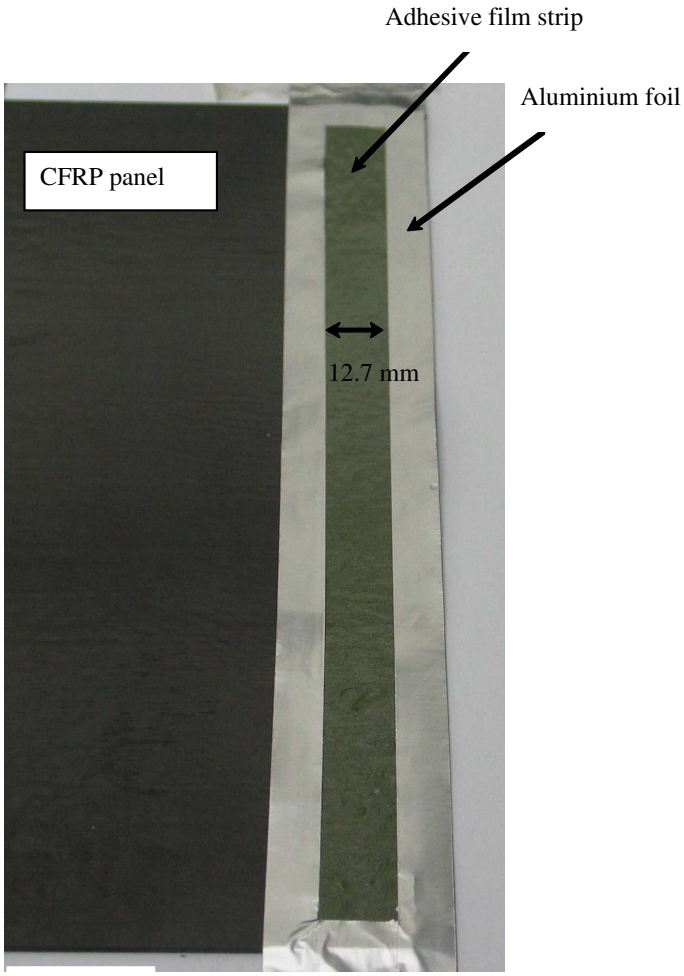

Figure 5.3: (a) Photograph of mould release coated aluminium stencil placed on previously applied adhesive layer on pretreated substrates, so that a starter pre-crack of length, 2 mm at both ends is obtained.

oven at temperature, contact pressure (applied through dead weights) and curing cycle recommended by adhesive manufacturer. The cured assembly was cooled down to room temperature in about 12 hr and then cut to the required specimen size. Piano hinges were then bonded to the end of the DCB specimens in the region where the release coated aluminium foil had been placed. A high performance film adhesive "Scotch-Weld AF163-2k.085" was used to bond the piano hinges to the substrates at 120^0 C for 1 hour and at a pressure of 125 kPa. The thickness of the adhesive layer sandwiched between the two substrates in DCB joint after curing was between 0.3 - 0.5 mm. In order to monitor the position of the crack front, the side of the DCB specimen was painted lightly using typewriter correction fluid, and marked at an interval of 5 mm. The DCB specimens made from Redux 322, Redux 335K and Redux 319A were named as DCB-Redux322, DCB-Redux335K and DCB-Redux319A respectively.

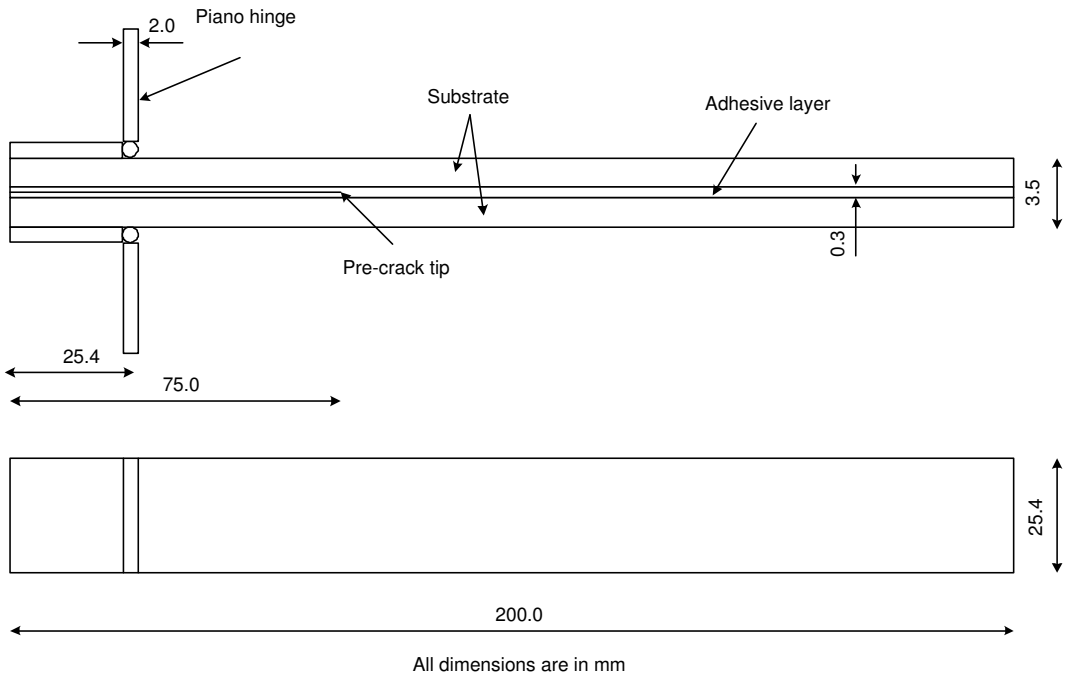

Figure 5.4: Schematic diagram of a typical double cantilever beam (DCB) test specimens.

5.2.2 Data Reduction

Adhesive fracture energy measurement

Ripling *et al.* [108] and Mostovoy *et al.* [109] have used linear elastic fracture mechanics (LEFM) based tests to measure the mode-I adhesive fracture energy, G_a, of adhesively bonded joints. There are several methods reported in the literature, which can measure mode-I adhesive fracture energy of the adhesive in a bonded joint. The most common ones are the Double Cantilever Beam (DCB), the Taper Double Cantilever Beam (TDCB) and the single Lap Joint (SLJ) [16, 115, 116, 141]. These methods have their own limitations and inherent problems. For example, in case of the DCB test methods we need to precisely track the crack length extension, load and the displacement simultaneously, and read the data precisely. Therefore, the calculated mode-I adhesive fracture energy, G_a, depends on the preciseness of crack length reading and it is a quite cumbersome task with the presently available facilities. The TDCB test methods overcome some of these problems of DCB, but it imposes stringent requirements on the shape and size of the test specimens, and requires very high amount of labor and probably it will be too tedious to manufacture substrates of composites with the required taper. Although, with the single lap joint (SLJ) technique as proposed by Kinloch and Osiyemi [16] (known as KO model) one can overcome most of the problems encountered in the above two methods, the presence of squeezed out surplus adhesive at the ends of the overlap length, commonly known as spew fillet, occurring during the curing process, renders this technique imprecise as spew fillet introduces a wide variation in the experimentally measured data. Lang and Mallick [23] and Frostig [22] have performed numerical studies and reported the effect of various types (shape and size) of spew fillets on the stress distribution in the adhesive layer of single lap joint. Because of the limitation and the problems related with the above test geometries (i.e. DCB, TDCB and SLJ), a new test geometry referred to as the modified single lap joint (MSLJ), is proposed and its accuracy is investigated so that it can help industrialists in evaluating the bonded joints performance accurately.

Modified Single Lap Joint (MSLJ)

In the overlap region of both SLJ and MSLJ, shear as well as peel stresses are induced when they are subjected to tensile load. However, it is possible to separate the contribution from peel and shear with careful analytical formulation. Herein, the steps involved in deriving the analytical formula for the calculation of the mode-I adhesive fracture energy of bonded MSLJ configuration due to peel stress at the end of the overlap are described. Consider the schematic diagram of MSLJ shown in figure 5.5(a). When this joint is subjected to a quasi static load T per unit width, then the overlap region of the joint rotates and take a shape shown in figure 5.5(b)). The induced bending moment causes high normal or peel stresses in addition to the shear stress distribution at the crack tip. Thus, it is believed that the joint fails due to normal or peel stress developed at the crack tip instead of shear stress. The transverse tensile stress or peel stress, which acts as operative load at the overlap ends can be given as reported by Hart-Smith [176]:

$$\sigma_{22} = M_e \sqrt{\frac{E_a}{2t_a S}} \tag{5.1}$$

where E_a and t_a are the Young's modulus and thickness of the adhesive respectively. The substrate bending stiffness per unit width, S, is given by:

$$S = \frac{E_s h^3}{12(1-\nu^2)} \tag{5.2}$$

where E_s, ν and h are the longitudinal Young's modulus, Poisson's ratio and thickness of the substrate material. The bending moment per unit width, M_e at the ends of the overlap is given by:

$$M_e = \frac{KT(h+t_a)}{2} \tag{5.3}$$

where K is the bending moment factor and is given by following expression:

$$K = \frac{1}{1+ec} \tag{5.4}$$

where c is the half of the overlap length of the joint and e, the eccentricity is given as:

$$e = \sqrt{\frac{T}{S}} \tag{5.5}$$

where T is the load applied per unit width of the joint. Now, by considering equation for calculating the constant strain energy release rate in a cracked beam from the knowledge of bending moment at the crack tip is proposed by Williams [177] for MSLJ. The equation for Mode-I strain energy release rate, G_I, for the modified single lap joint configuration can be given as:

$$G_I = \frac{12S(M_e^2)}{B^2h^3E_s} \tag{5.6}$$

where B is the width of the specimen. Now by substituting equation (5.3) into equation (5.6) and using equation (5.2) and (5.4), the expression for mode I adhesive fracture energy can be expressed as below:

$$G_a = \frac{12}{E_s h^3}\left[\frac{T_f(h+t_a)}{2}\right]^2 \frac{1}{(1+ec)^2} \tag{5.7}$$

where T_f is the failure load per unit width for the modified single lap joint. Then, by measuring the value of T_f, the value of G_a can be calculated using the above equation for the known values of E_s, h, t_a, c.

5.2.3 Testing and Data Collection

Prior to testing the bonded joints, the adherend and adhesive materials were tested in order to characterize their mechanical properties.

Tensile tests of composites

Tensile specimens were prepared from composite panels produced in the laboratory with the method described in section 5.2.1. The specimens for measuring longitudinal and transverse properties were prepared as per ASTM D3039/D3039M. For measurement of

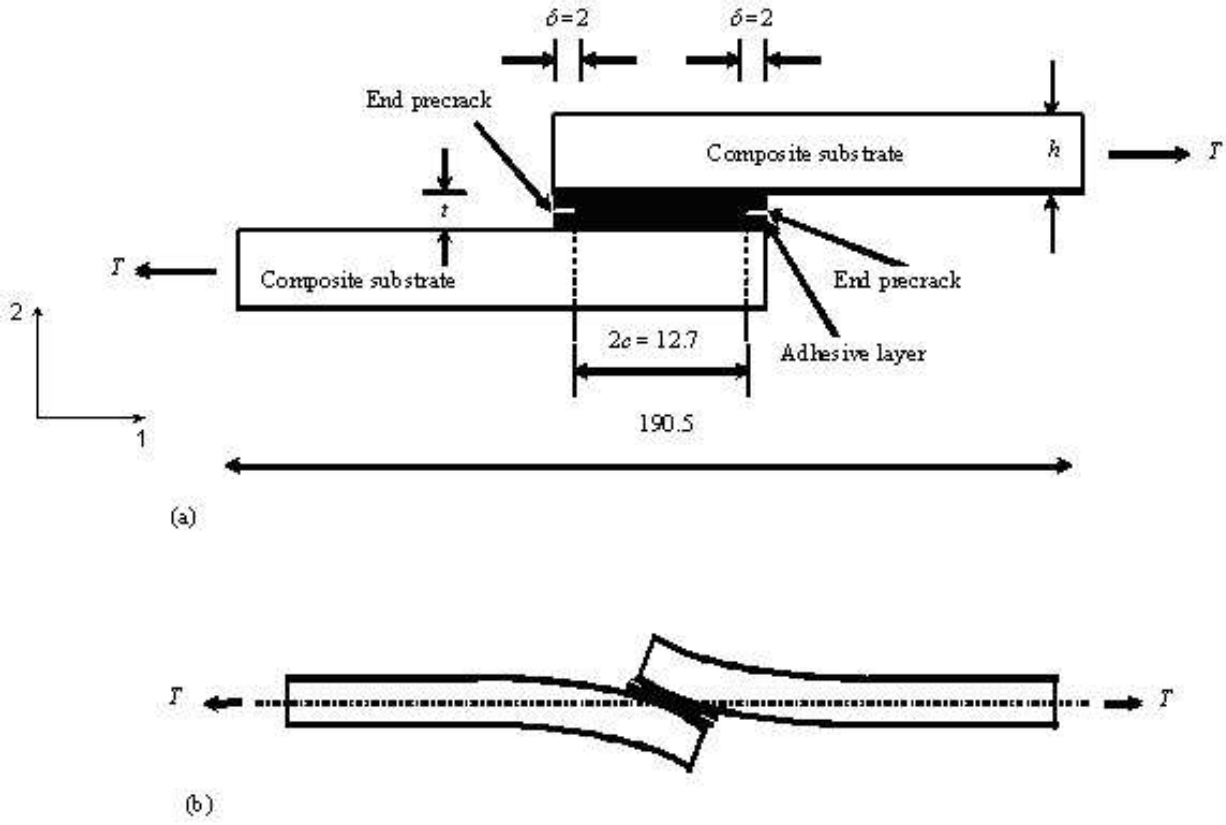

Figure 5.5: (a) Schematic diagram of MSLJ configuration with geometric parameters (All dimensions are in mm), (b) Typical deformed geometry of MSLJ during loading.

in-plane properties specimens were extracted from $\pm 45^0$ laminates. Uniaxial tensile tests were conducted on the CFRP laminate using an Instron universal tensile testing machine fitted with 50 kN load cell to measure its longitudinal Young's modulus and Poisson's ratio. A strain gauge rosette was mounted in the middle of the specimens and strains in both longitudinal and transverse directions were monitored simultaneously using a portable data logger. The measured strains were used to calculate the Poisson's ratio of the material tested. The longitudinal Young's modulus (E_{11}) was measured to be 140 GPa and the Poisson's ratio as 0.35. The average longitudinal uniaxial tensile strength of the tested CFRP laminate was 1800 MPa with a scatter of around 188 MPa. The mechanical properties such as longitudinal tensile strength, σ^t_{11} ,transverse tensile strength, σ^t_{22}, in-plane shear strength, τ_{12}, longitudinal tensile modulus, E^t_{11}, transverse tensile modulus, E^t_{22}, in-plane shear modulus, G_{12}, and minor Poisson's ratio, ν_{23} of the composite material are summarized in Table 5.1.

Adhesive properties

The mechanical properties of Redux 322 adhesive material were obtained by performing tensile testes on dog-bone shaped specimens made according to ASTM D 638. Specimens were prepared from cured adhesive panels manufactured using the hot pressing technique. Uniaxial tensile tests were conducted on the coupons extracted from the cured adhesive panel using an Instron universal tensile testing machine fitted with 50 kN load cell to measure mechanical properties. A strain gauge rosette was mounted in the middle of the specimens, and strains in both longitudinal and transverse directions were monitored simultaneously using a portable data logger. The tensile Young's modulus and Poisson's ratio were calculated to be 4.08 MPa and 0.44 respectively. The tensile fracture strength was 41 MPa. The shear properties of the bonded adhesive were measured according to the specified method in the established standard ASTM D3165. A schematic diagram of the specimen used in the present investigation is shown in Figure 5.6. The substrate and adhesive materials were the same as for the MSLJ and DCB specimens. The tensile

strength, shear strength, tensile modulus, shear modulus and Poisson's ratio of the cured adhesive material were measured as tabulated in Table 5.2.

Modified single lap joint specimens

Modified single lap joint specimens were tested on a screw driven Instron universal testing machine fitted with a 50 kN load cell. Flat face mechanical wedge grips were used to hold the specimen and the loading was applied by moving the cross-head under displacement control at a constant rate of 0.5 mm/min. All the specimens were loaded to final fracture. On an average six specimens were tested from each batch and the load required to cause final fracture was measured.

Single lap joint specimens

Six single lap joint specimens (i.e. specimens with naturally occurring spew fillets of adhesive formed at the ends of the overlap) were tested from each batch to failure. The specimens were loaded one by one into flat face mechanical wedge grips of the Instron machine and tested in a similar manner as the MSLJ specimens. The failure load of the single lap joint was measured. The test results from the SLJ experiments were compared with those from the MSLJ specimens in order to investigate the benefits of the proposed specimen modification.

Double cantilever beam specimens

Three DCB specimens from each batch (Redux 322, Redux 335K or Redux 319A) were tested on an Instron universal testing machine equipped with 500 N load cell at a constant displacement rate of 0.5 mm/min. During each test three parameters namely, load, crosshead displacement and crack length were monitored. A travelling microscope was used to monitor and measure the crack length in the adhesive layer. The measurements of load and displacement were taken at every 5.0 mm extension of crack length. The fracture toughness of the adhesive in the DCB geometry was calculated using the protocol

Table 5.1: Mechanical properties of 913C - HTA 12K 5-34% CFRP composite substrate

Property	Value
Longitudinal tensile elastic modulus, E^t_{11}	140 GPa
Transverse tensile elastic moduli, E^t_{22} and E^t_{33}	7.8 GPa
Shear elastic moduli, G_{12} and G_{13}	12 GPa
Shear elastic modulus, G_{23}	3.92 GPa
Poisson's ratio, ν_{12} and ν_{13}	0.35
Poisson's ratio, ν_{23}	0.25
Longitudinal tensile strength, σ^t_{11}	1800 MPa
Transverse tensile strength, σ^t_{22}	48 MPa
Interlaminar shear strength, τ_{13}	186 MPa

Table 5.2: Mechanical properties of Redux 322 adhesive

Property	Value
Tensile elastic modulus, E_a	4.08 GPa
Shear elastic modulus, G	1.34 GPa
Poisson's ratio, ν	0.44
Tensile strength, σ_a	41.0 MPa
Shear strength, τ	18.0 MPa

developed by Kinloch and his coworkers [178].

All these tests were conducted in dry conditions, i.e. at 23 ± 2^0 C and approximately 50 ± 5% relative humidity.

5.2.4 Experimental Results and Discussion

MSLJ and SLJ test results

Test data obtained from all the six batches of samples (i.e. MSLJ-Redux322, MSLJ-Redux335K, MSLJ-Redux319A, SLJ-Redux322, SLJ-Redux335K, and SLJ-Redux319A) were analyzed. A typical load versus displacement plots from each batch of tested joints is

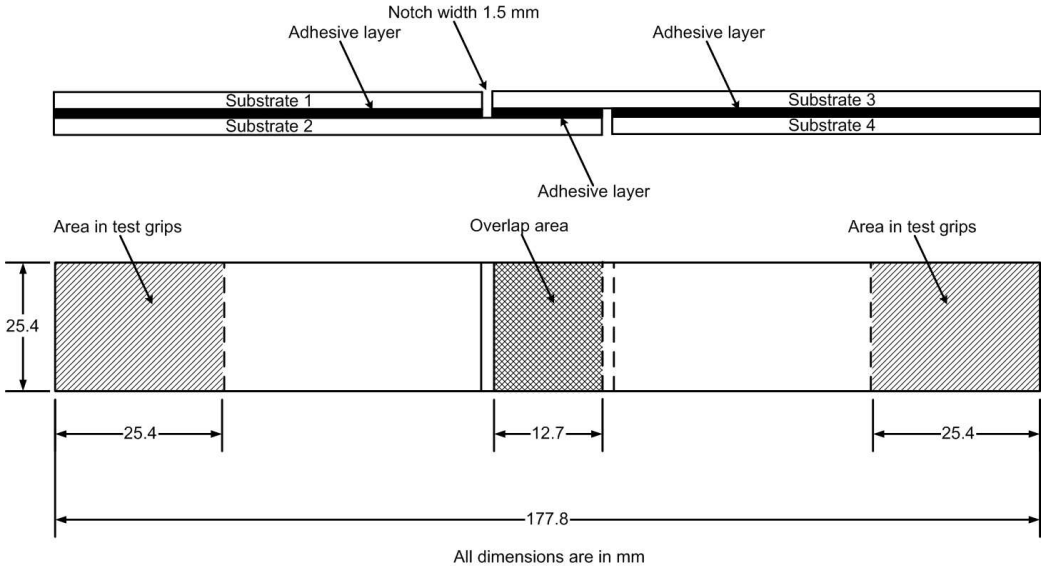

Figure 5.6: Schematic diagram of shear specimen for studying shear properties of sandwiched adhesive.

depicted in Figure 5.7. It was observed that the load increased monotonically with the displacement for MSLJ-Redux322, MSLJ-Redux319A, SLJ-Redux322, and SLJ-Redux319A and finally fractured catastrophically implying brittle failure of joints. The load vs. displacement traces for MSLJ-Redux335K and SLJ-Redux335K specimens showed slight deviation from linear behaviour implying ductile nature of Redux 335K adhesive. Finally upon reaching a maximum value of load the test specimens failed catastrophically. The mean tensile lap shear strength along with the scatter in the tensile lap shear strength measurement for both MSLJ and SLJ types of joints made from Redux 322, 335K and 319A are shown in Figure 5.8. It is noteworthy that the data points are much closer to the average value for MSLJ configuration than that of SLJ, and the reduction in the scatter can be attributed to the starter pre-crack implanted in the MSLJ test geometry. The test data reveal that among the three adhesives tested Redux 335K is the strongest with a mean lap shear strength of 15 MPa and Redux 319A is the weakest with around 8 MPa average tensile lap shear strength.

The adhesive fracture energy of the bonded MSLJ and SLJ specimens was calculated using equation (5.7). This equation is programmed in the Microsoft excel spreadsheet along with the other required parameters for each specimen tested and the average and

Table 5.3: Comparison of test results obtained from MSLJ and SLJ for all the three adhesives (i.e. Redux 322, 335K and 319A) investigated

Adhesive name	SLJ		MSLJ		DCB	
	Adhesive fracture energy $G_a(J/m^2)$	Standard deviation (J/m^2)	Adhesive fracture energy $G_a(J/m^2)$	Standard deviation (J/m^2)	Adhesive fracture energy $G_a(J/m^2)$	Standard deviation (J/m^2)
Redux 322	434	34	252	25	250	21
Redux 335K	847	142	408	57	430	156
Redux 319A	358	59	150	22	163	4

the standard deviation was calculated and listed in Table 5.3. Figure 5.9 compares the fracture toughness values for the tested adhesives using MSLJ and SLJ test geometries. Among three adhesives investigated in this study, Redux 335K is the toughest one with an average adhesive fracture energy of 408 J/m^2 and Redux 319A has the lowest average adhesive fracture energy of approximately 150 J/m^2. It is worth mentioning that SLJ test geometry consistently provided higher values than MSLJ test geometry with a wider scatter band (i.e., large standard deviation) for all the 3 types of adhesives used in the present investigation. In MSLJ joints,during loading, crack propagated from the starter pre-crack tip. There by modified test geometry circumvented the effect of spew fillets, thereby reducing the scatter band in the measured properties. The visual study of fracture surfaces revealed that all the test specimens failed in a cohesive manner (i.e., the crack propagated through the adhesive layer) as shown in Figures 5.10(a)-(f) which is a necessary criterion for meaningful characterization of adhesive properties.

DCB Test Results

The DCB specimens failed in a linear-elastic manner during the tests as observed from the load versus displacement graphs, depicted in Figure 5.11. In the beginning the load in-

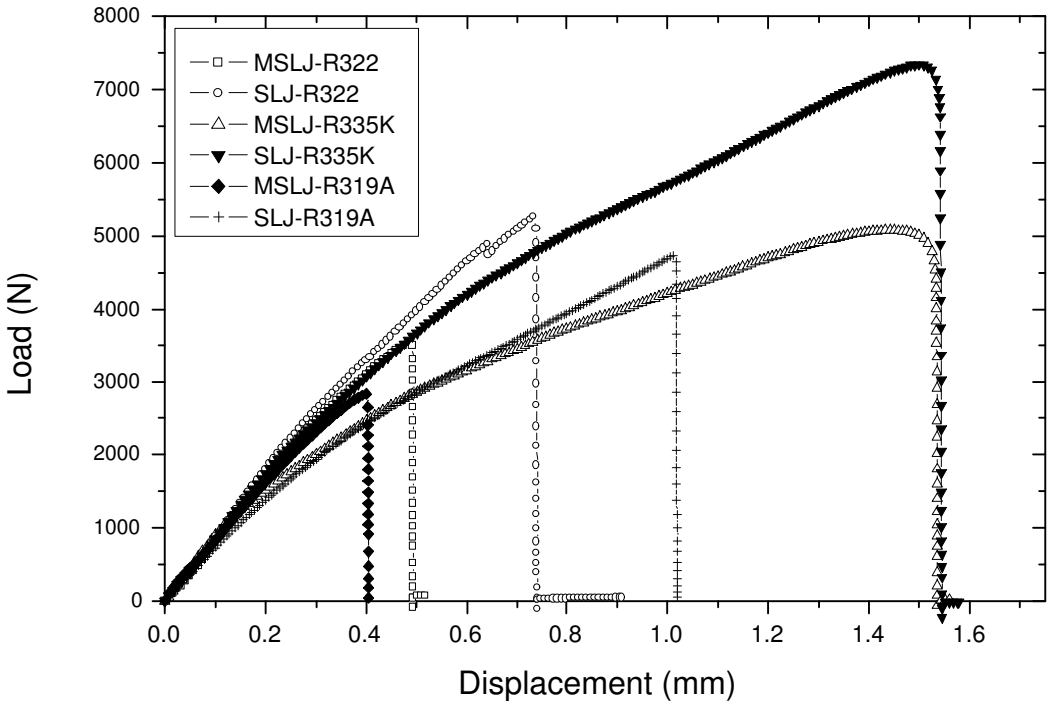

Figure 5.7: Typical load versus displacement curves of MSLJ and SLJ made from Redux 322, 300 gsm, Redux 335K, 150 gsm and Redux 319A, 244 gsm adhesives. The curves illustrate the brittle failure of the adhesively bonded joints.

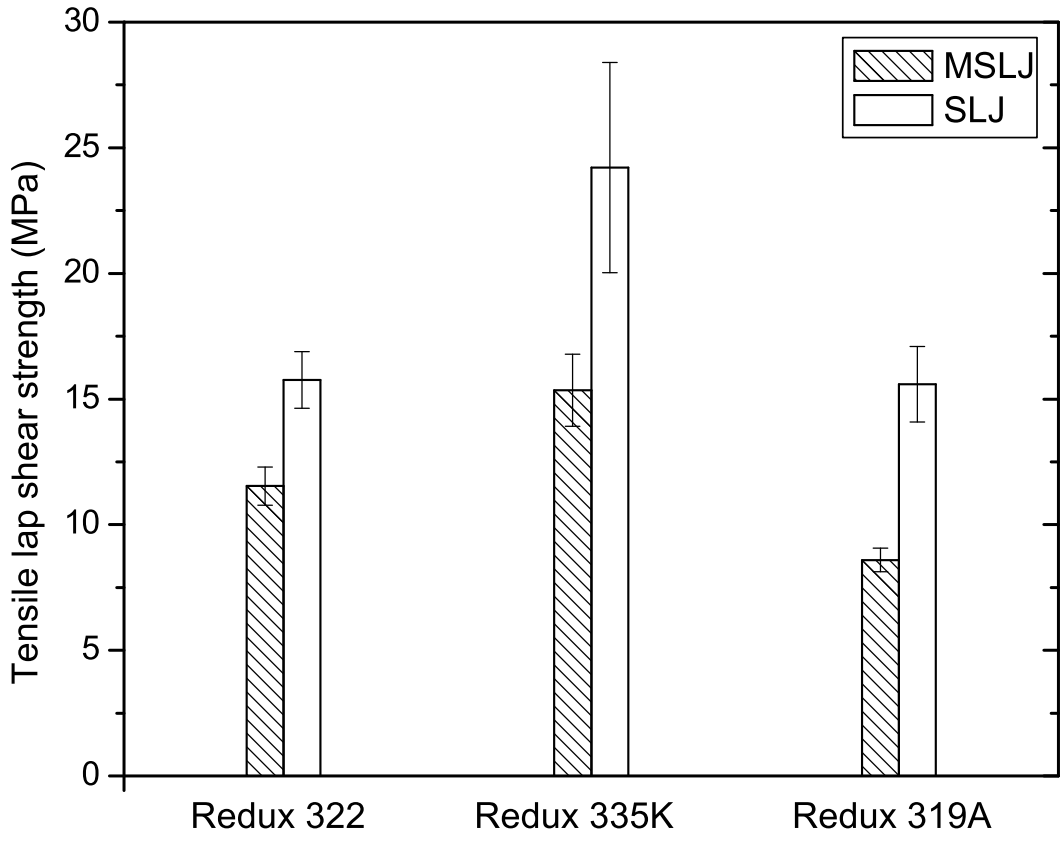

Figure 5.8: Variation in tensile lap shear strength of MSLJ and SLJ specimens made from (a) Redux 322, (b) Redux 335K, and (c) Redux 319A. Notice the reduction in experimental scatter in MSLJ configuration.

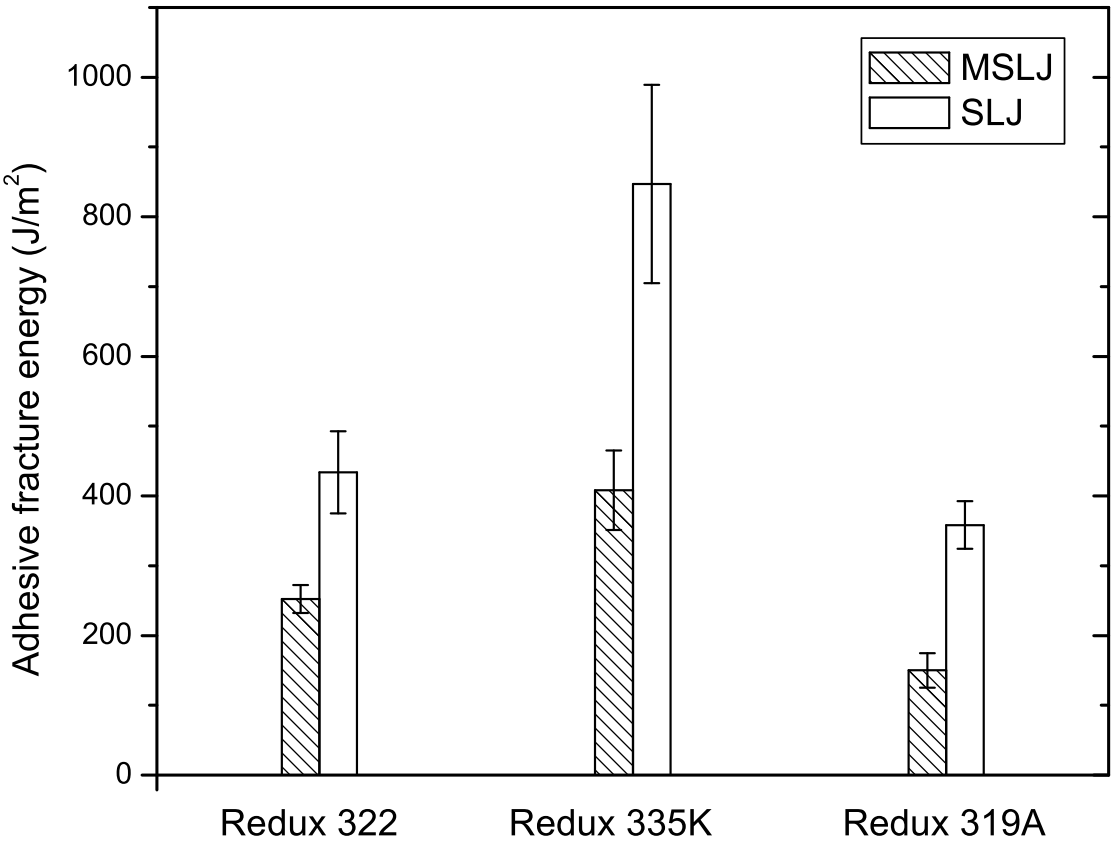

Figure 5.9: Mean adhesive fracture energy (J/m^2) with variation in measurements for MSLJ and SLJ joint made from (a) Redux 322, (b) Redux 335K, and Redux 319A. Notice the reduction in experimental scatter in MSLJ configuration.

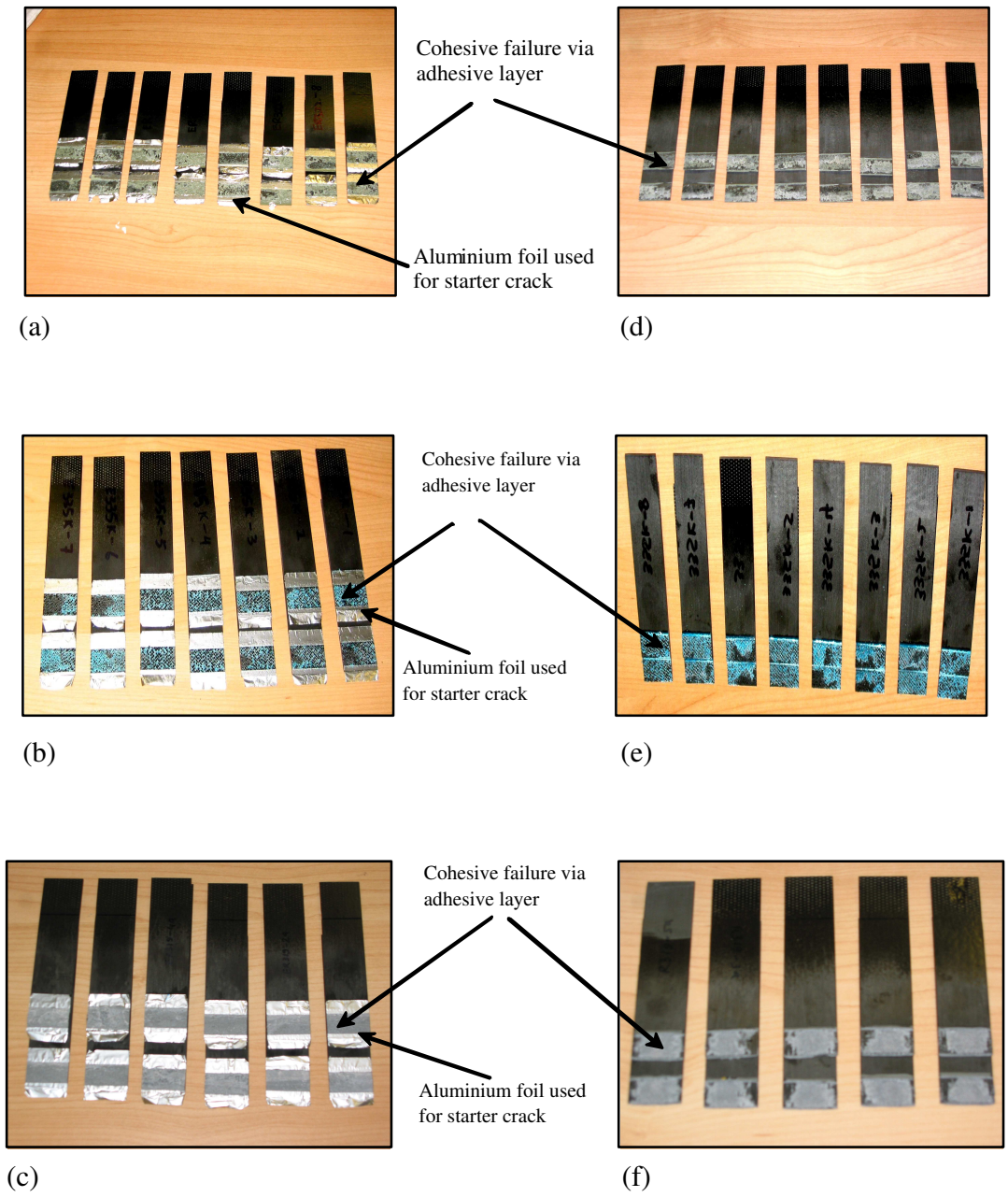

Figure 5.10: Photographs of fractured surfaces of MSLJ specimens showing cohesive failure via adhesive layer, (a) Redux 322 (b) Redux 335K, and (c) Redux 319A; Photograph of fractured surface of conventional SLJ specimens showing cohesive failure via adhesive layer, (d) Redux 322 (e) Redux 335K, and (f) Redux 319A.

creased monotonically with displacement until the crack propagation started in the adhesive layer. As soon as the crack started to propagate the load started to decrease depending on the nature of crack propagation. In the joints made from Redux 322 (DCB-Redux322) and Redux 319A (DCB-Redux319A) the crack propagated in a stable manner. The DCB joint made of Redux 335K film adhesive fractured in stick-slip manner. In all cases, as soon as the elastic strain energy of the system exceeded the required energy needed to open the crack, the crack propagated and the load dropped. This process continued until the crack extended the entire length of the specimen and the test data/information were measured at several predetermined crack-lengths. The information contained in the load-displacement traces together with the crack length data can be analyzed using four different methods to measure the adhesive fracture energy, namely, the "area method", "simplified beam theory (SBT)", "corrected beam theory (CBT)" and "experimental compliance method (ECM)" [115, 116]. In the present investigation, the experimental compliance method (ECM) was used because it is a simple and powerful method, which can compute the adhesive fracture energy directly from the load versus displacement trace and crack length (i.e. distance measured from load line to the crack tip) recorded during the static test, without involving correction factors. The values of the adhesive fracture energy calculated using DCB joints are summarized in Table 5.3 and compared with MSLJ results for all the three adhesives studied. The adhesive fracture energy measured using MSLJ and DCB test geometries are in good agreement. This shows that the foil inserted (starter pre-crack) in the MSLJ circumvented the effect of spew fillets present at the ends of overlap. As is evident from the photographs shown in Figure 5.12, all the DCB joints failed in a cohesive manner via the adhesive layer of the bonded joints.

5.3 Numerical Simulation

To demonstrate the existence of high peel stress at the starter pre-crack tip a 2-dimensional finite element analysis was performed using a commercial FE software program ABAQUS. The modelling details and material model used in the analysis are briefly described in the

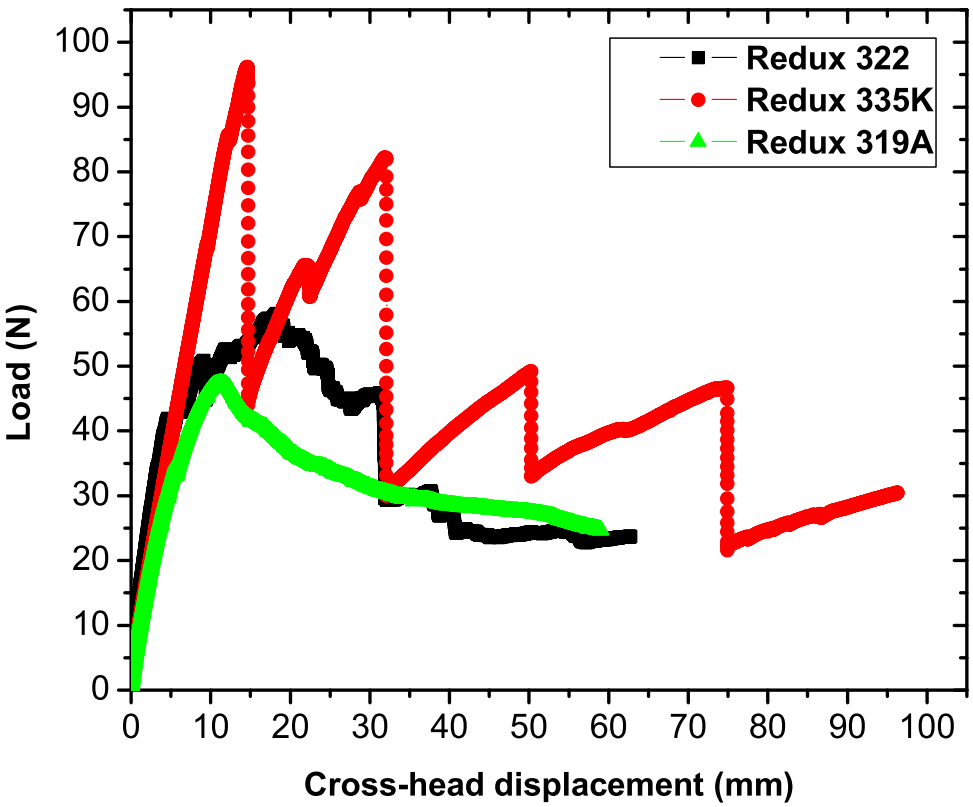

Figure 5.11: Typical load vs. displacement response of tested adhesives under double cantilever beam (DCB) configuration.

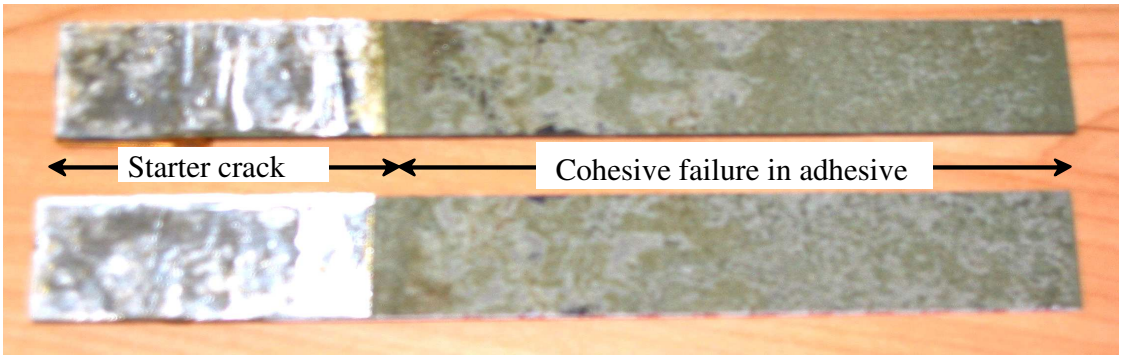

(a)

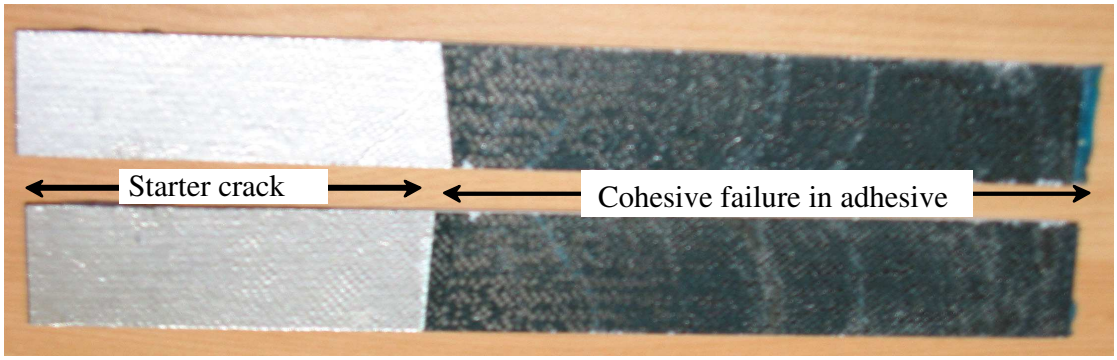

(b)

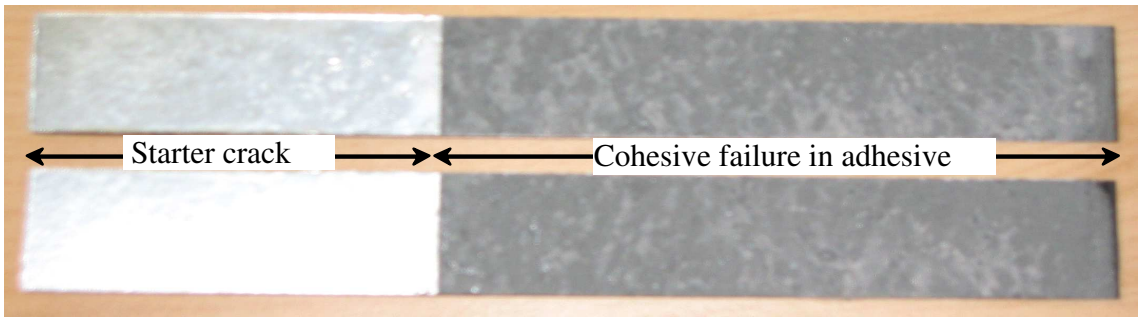

(c)

Figure 5.12: Photographs of fractured surfaces of DCB specimens showing cohesive failure (i.e. crack propagated through adhesive) in joints tested with (a) Redux 322, 300 gsm adhesive, (b) Redux 335K, 150 gsm adhesive, and (c) Redux 319A, 244 gsm adhesive.

following sections.

5.3.1 Finite Element Analysis

Finite Element Analysis (FEA) was performed on MSLJ specimens geometry made from Redux 322 adhesive and CFRP composites to study the normal (peel) and shear stress in the bondline. The CFRP substrates were treated as a orthotropic homogenous material with the elastic properties as shown in Table 5.1. The adhesive layer sandwiched between the substrates in the MSLJ was treated as an isotropic material with elastic properties as listed in Table 5.2.

As significant rotation occurs in the overlap length of the MSLJ test geometry the non-linear geometric option in-built in the program was activated. The applied boundary conditions in the finite element model are such that a portion of the specimen in the grips was constrained to move only along the loading direction. In order to simulate uniaxial tensile loading, normal displacements were imposed on the nodes in the grip section of the specimen. As this problem is a case of finite-strain or large-strain problem (when geometric nonlinearities are included) the use of small strain singular elements at the crack-tip are not advisable. Instead, a reasonably fine mesh was used in the overlap region to capture the expected high strain gradient in the analysis (see Figures 5.13(a) and 5.13(b)). Mesh refinement was carried out to the extent that no significant changes in the stress distribution were observed with a change of mesh size. A total of 5048 elements (4-node bilinear plane stress quadrilateral, reduced integration) consisting of 5705 nodes with 14 layers of elements in the through-thickness of the adhesive layer were used. Stress distribution (i.e., normal/peel stress and shear stress in the middle of the adhesive layer) is plotted along the overlap length of the MSLJ. As shown in Figure 5.14, the normal stress at the pre-crack-tip is observed to be about twice of the corresponding shear stress. The analysis clearly demonstrates that mode-I loading is dominant at the crack-tip. The total displacement in the deformed model (see Figure 5.13(a)) shows the opening of the pre-crack in the simulated study.

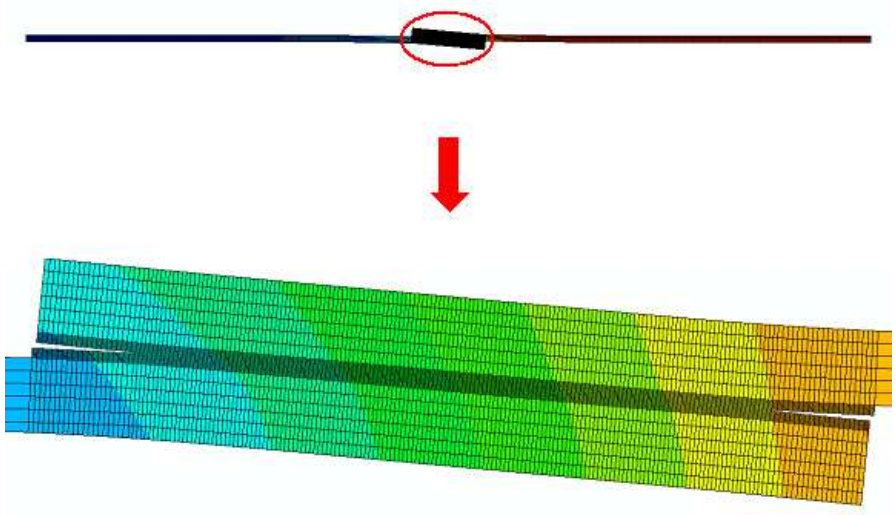

(a) In overlap length

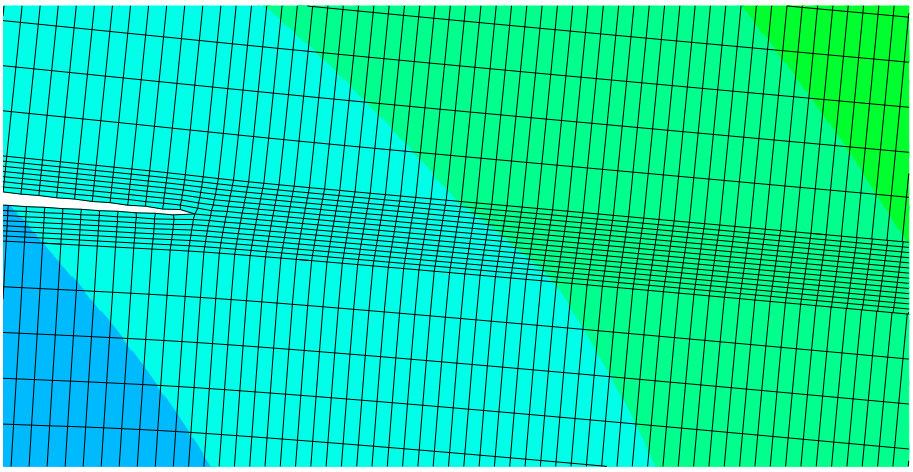

(b) Near pre-crack tip

Figure 5.13: Mesh design, total displacement contour and deformed shape of the MSLJ test geometry from finite element analysis.

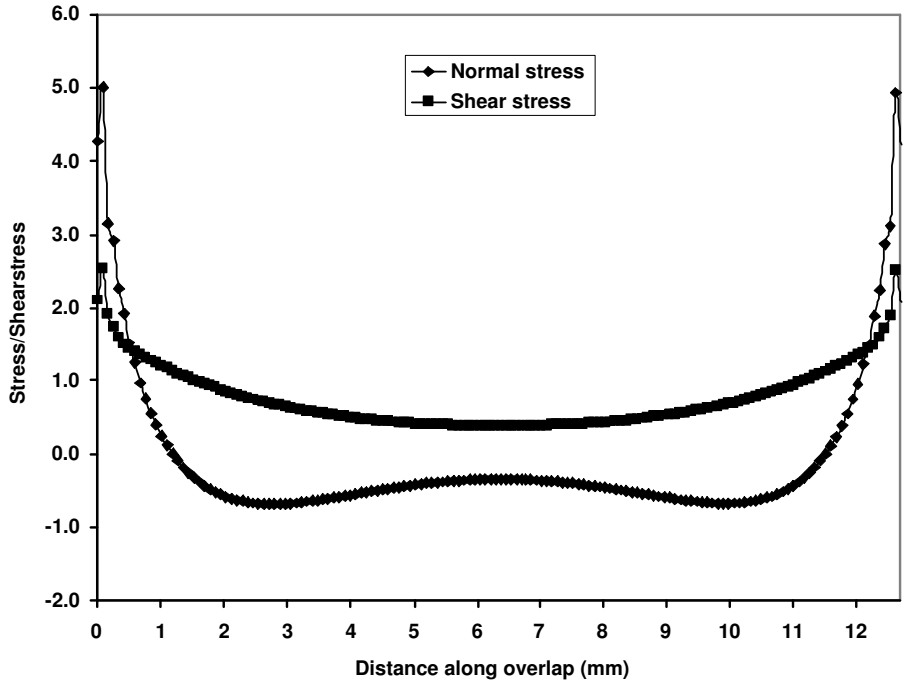

Figure 5.14: Normalized normal/peel and shear stress distribution in the overlap length of the MSLJ geometry

Dominance check for mode I loading

Analysis of the 2-Dimensional finite element analysis results performed with modified single lap joint (MSLJ) geometry revealed a high peel stress at the pre-crack tip. The peel stress, σ_{22} at the pre-crack tip is about twice of the shear stress, τ_{12} in the middle of the adhesive layer (see Figure 5.14). These two stresses at the pre-crack tip can be used to calculate the ratio of mode II and mode I fracture toughness as suggested by [179]

$$\theta = \tan^{-1}\left[\frac{K_{II}}{K_I}\right] = \tan^{-1}\left[\frac{\tau_{12}}{\sigma_{22}}\right] \tag{5.8}$$

where K_I and K_{II} are mode-I fracture toughness and mode-II fracture toughness respectively. On the basis of the numerical value obtained from the FE simulation and equation (5.8), the ratio of mode-II to mode-I fracture toughness at the pre-crack tip was found to be about 0.5.

5.4 Conclusions

In this experimental study, a new test geometry referred to as modified single lap joint (MSLJ) was proposed to measure the adhesive fracture energy of adhesively bonded composite joints. The MSLJ was made by implanting two end pre-cracks in the middle of the bondline in a conventional SLJ. In addition, tests were also conducted on SLJ and DCB specimens made from the same composites and adhesives systems. In all these tests, the unidirectional composite substrates were made from 913C - HTA 12K 5-34% prepregs supplied by Hexcel Composites. The film adhesives, Redux 322, 300 gsm, Redux 335K, 150 gsm and Redux 319A, 78 gsm were also supplied by the same supplier. An Instron universal testing machine was used to load the specimens under tensile loading.

The SLJ joints made from Redux 322, 335K and 319A film adhesive gave mean values of 434 J/m^2, 847 J/m^2 and 358 J/m^2 respectively. While the MSLJ joints made from Redux 322, 335K and 319A film adhesive gave mean values of 252 J/m^2, 408 J/m^2 and 150 J/m^2 respectively. The adhesive fracture energies measured using MSLJ and DCB

test geometries are in good agreement. The standard deviation data revealed that there was a reduction in scatter of the results by as much as 30-60% when the MSLJ specimens were used in place of the SLJ to estimate the fracture energy of the joints. Thus, the results from this investigation showed that the KO-model was valid for an accurate estimation of the mode I adhesive fracture energy of the adhesive in an MSLJ test specimen. These results are especially useful in the critical design of structural components for aerospace and defense applications as a typical design engineer can use the value of G_a obtained from the model to design for how long an adhesively bonded joint will last when subjected to external stresses. In addition, by using the KO-model, manufacturers of adhesives may, in future, be able to include details on the fracture properties of adhesives as an invaluable design tool in their product specification.

Chapter 6

Environmental Ageing Effect on Adhesively Bonded Composites Joints Performance

6.1 Introduction

In the present study, an attempt is made to reduce the effect of spew fillets on the performance evaluation of adhesive bond parameters. Modified single lap joints (MSLJs) prepared by implanting the starter pre-crack at the both ends of the overlap in the middle of the adhesive layer in the conventional SLJ. Aged MSLJs were tested to fracture and the effect of moisture on adhesive fracture energy was quantified. In addition to MSLJ testing, limited tests were performed on aged DCB specimens. In Chapter 5, MSLJ configuration was used to determine the adhesive fracture energy of adhesively bonded joints in dry conditions: the simple modification to the conventional SLJ was able to reduce the scatter in the measurement of adhesive joint strength and adhesive fracture energy by as much as 30 % as compared to SLJ. The influence of moisture ingression on the mechanical properties of the Redux 322 adhesive, CFRP composite substrate and lap joints was also carried out.

6.2 Experimental Details

This section describes test materials, specimens preparation methods and the experimental procedure used in the current investigation.

6.2.1 Materials and Design of test specimens

Unidirectional composite laminates, $[0]_8$, made from 913C - HTA 12K 5-34% carbon prepreg and an aerospace grade Redux 322, 300 gsm film adhesive (supplied by Hexcel Composites, UK) were used to prepare all the specimens. Prepreg sheets were cut from the material roll and 8 or 10 sheets of prepregs were stacked together to fabricate a laminate of 1.6 or 2.0 mm thickness respectively. The stacked system was then pressed on a hot pressing machine at a pressure of 700 kPa and maintained at a temperature of 120^0C for an hour as recommended by the composite manufacturer. To prevent laminate warpage and obtain thermal stress free laminate, the cured laminate was allowed to cool down to room temperature in the hot press machine overnight (12 hrs). The molded composite laminates had a fiber volume fraction of around 60%.

Preparation of MSLJ and DCB

To study the effect of moisture absorption on mode-I adhesive fracture energy, G_a, of adhesively bonded joints, six sets of modified single lap joints (MSLJ), each set consisting of 6-8 specimens, were prepared. These modified single lap joints (MSLJ) samples were prepared from the 103.6x230x1.6 mm CFRP laminate panels as described in Chapter 5. Similarly six sets of DCB test specimens, each set consisting of 3 samples were prepared in accordance with the ASTM standard D 5528-01. The width and length of the specimens was maintained at around 25.4 mm and 200 mm respectively. Figures 5.5(a) and 5.4 depicts the photograph of a typical MSLJ and DCB specimen respectively. The details of specimen preparation method is described in the previous Chapter 5.

Composite specimens

Six sets of test specimens, each set consisting of 5 to 6 specimens were prepared to evaluate the effect of moisture on the mechanical properties of CFRP composites. To study the effect of high moisture ageing on the longitudinal and transverse Young's moduli, tensile strength and Poisson's ratio of composites, tensile specimens were prepared ac-

cording to ASTM D 3039/D 3039M-00. Unidirectional $[0]_8$ specimens were cut to size of 240x12.5x1.6 mm in the direction of the fiber from the unidirectional composite laminate panel using a high speed diamond bench cutter. A schematic diagram of the unidirectional tensile specimens for studying the longitudinal properties is shown in Figure 6.1(a). Transverse tensile specimens were also prepared by cutting the strips from unidirectional panel ($[90]_{10}$) into pieces with size of 175x25.4x2.0 mm, but the direction of cutting was kept perpendicular to the fiber direction. In Figure 6.1(b), a schematic diagram of transverse specimens is depicted. To study the effect of water absorption on in-plane properties, tensile specimens were prepared according to ASTM D 4255/D 4255M-01. These specimens were cut to the size of 230x15x2.0 mm (see Figure 6.1(c)) from $[\pm 45]_{10}$ symmetric laminate panels. Test specimens were prepared according to ASTM D 5529/D 5229 -92 to study the moisture intake in the composite laminate. Five specimens of size 103x25.4x1.6 mm were prepared from the unidirectional panel.

Adhesive specimens

Six sets of test specimens, each set consisting of 3 to 4 specimens were prepared to evaluate the effect of high moisture ageing on mechanical properties of the bulk adhesive. The specimens were cut to the size (see Figure 6.1(d)) according to ASTM D 638-03 from a panel made of adhesive material. Adhesive panel was fabricated by curing Redux 322, 300 gsm sheets. Adhesive sheets were cut from the material roll and 12 sheets of adhesive were stacked together to fabricate an adhesive panel of about 1.5 mm thickness. The stacked system was then pressed on a hot pressing machine at a pressure of 300 kPa and maintained at a temperature of 175^0C for an hour as recommended by the adhesive manufacturer. To prevent panel warpage and obtain thermal stress free panel, the cured panel of adhesive was allowed to cool down to room temperature in the hot press machine overnight (12 hrs).

Six sets of bonded test coupons were prepared according to ASTM D3165 to evaluate the effect of moisture absorption on shear properties (shear strength, SS and shear

modulus, SM) of the sandwiched adhesive. Each set consisted of 3 to 4 specimens. A schematic diagram of the specimen is shown in Figure 5.6.

For studying moisture absorption characteristic and dimensional changes of bulk adhesive material, wafers were cut with dimensional scale, 25.4x25.4x1.5 mm from the same panel. Five test specimens were used in this current study.

6.2.2 Environmental conditioning and moisture absorption

All specimens were demoisturised by keeping the specimens in an oven for around 24 hours before immersing in distilled water. Six sets of specimens for each type of testing were fully immersed in a bucket filled with distilled water (23 ± 2^0 C and 100% relative humidity) at ambient temperature (ASTM D570 [180]) to simulate the moisture absorption in high humidity environment.

6.2.3 Testing and Data collection

Moisture absorption experiment

The composite specimens, the adhesive specimens and the MSLJ specimens were taken out of the distilled water bucket at the intervals of 7 days of ageing. The specimens were carefully wiped with tissue paper and allowed to reach the laboratory temperature before starting the measurements. An analytical balance (AND HM-202, made in Japan), capable of measuring 0.0001 g was used for measuring the weight of the specimens. The length of specimens was measured with a digital vernier calliper (Mitutoyo, made in Japan) with 0.01 mm least count. To study the change in width and the thickness a digital micrometer (Mitutoyo, made in Japan) was used. After measuring the weight and dimensions they were immediately put back into aqueous medium (i.e. bucket filled with distilled water). This type of ageing environmental condition was chosen for simplification purposes.

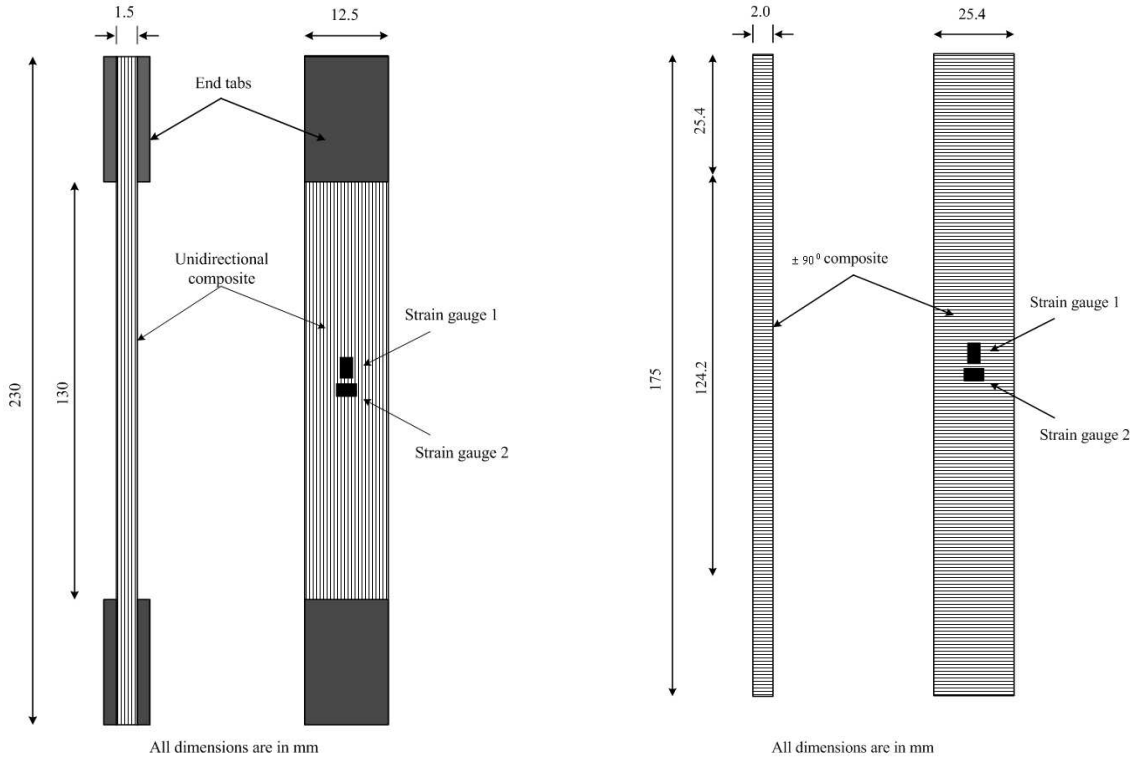

(a) Longitudinal specimens

(b) Transverse specimens

(c) Shear specimens

(d) Adhesive tensile specimens

Figure 6.1: Schematic diagram of tensile specimens for studying mechanical properties of CFRP and adhesive (a) longitudinal (b) transverse (c) shear, and (d) test specimens for adhesive properties.

Mechanical testing

At the end of every 28 days of ageing, a set of specimens from all types of intended tests were taken out from the distilled water medium and brought down to laboratory conditions before conducting the tests. The specimens were kept at standard laboratory environment for about 48 h before commencing the mechanical testing, to ensure that all the specimens have attained laboratory temperature properly. The aged modified single lap joint (MSLJ) specimens were tested at the scheduled intervals on a screw driven Instron universal testing machine fitted with a 50 kN load cell. Flat face mechanical wedge grips were used to hold the specimen and the loading was applied by moving the cross-head under displacement control at a rate of 0.5 mm/min. An automated data logger was used to capture the load sensed by the load cell and extension was obtained by reading the cross-head movement. The specimen was loaded to failure. On an average six specimens were tested and a mean value of failure load was calculated.

Three aged DCB specimens from each batch at the scheduled intervals were tested on an Instron universal testing machine fitted with 500 N load cell at a constant displacement rate of 0.5 mm/min. In order to monitor the position of the crack front, the side of the DCB specimen was painted lightly using typewriter correction fluid, and marked at an interval of 5 mm. Piano hinges attached to the DCB specimen were gripped into the flat mechanical wedge grips and each specimen was tested in tensile mode. During each test load, crosshead displacement and the crack length were monitored. A travelling microscope was used to monitor and measure the crack in the adhesive layer. The measurements of load and displacement were taken at every 5.0 mm extension of crack length. The fracture toughness of the adhesive in the DCB geometry was calculated using the protocol developed by Kinloch and co-workers [178].

All the tensile specimens (composites and adhesive) after exposure to distilled water for intended period were also tested on a screw driven Instron universal testing machine fitted with a 50 kN load cell. Flat face grips were used to hold the specimen and the loading was applied by moving the cross-head under displacement control at a rate of 0.5

mm/min. An automated data logger was used to capture the load sensed by the load cell and an extensometer was used to monitor the longitudinal strain. To precisely measure the longitudinal and transverse strain simultaneously "foil strain gauges" were used. All the specimens were loaded to failure. On an average five specimens were tested and a mean value was calculated. The moisture absorption was monitored for 168 days.

6.3 Results and Discussion

6.3.1 Moisture absorption

The percentage weight gained by MSLJ and the adherends/substrates (almost identical two substrates which were used to prepare the corresponding MSLJ) were calculated from the moisture absorption data and initial weight. The moisture absorption in the sandwiched adhesive was calculated as the difference between the percent moisture absorbed in MSLJ and the percent moisture absorbed in the two identical substrates as in the corresponding MSLJ. Figure 6.2(a) shows the plot of the moisture absorption data (i.e., weight gained %) vs. square root of time for the water immersion experiment for the adhesive layer (i.e., adhesive sandwiched between two substrates) in the modified single lap joint (MSLJ) and bulk adhesive material. It is observed that the rate of moisture diffusion in the sandwiched adhesive is slower than the bulk adhesive possibly due to much lesser exposed surfaces (about 5% of the bulk adhesive), and longer diffusion path as compared to the bulk adhesive. It is also noticed that the sandwiched adhesive achieved state of saturation much earlier than the bulk adhesive as the material matrix volume of sandwiched adhesive layer is only 13% of the bulk adhesive samples. The state of saturation is well demonstrated by the plateau in the moisture uptake graph (see Figure 6.2(a)) for the adhesive layer sandwiched between the two composite substrates. The bulk adhesive reached saturation state at about 5.5% moisture absorption by weight, whereas sandwiched adhesive's saturation state reached at 0.45% by weight only. It is believed that the sandwiched adhesive layer contained less epoxy resin as compared to the bulk adhesive consequently

denser than the bulk adhesive material. In other words, the bulk adhesive would be more porous than the sandwiched adhesive. It is speculated that the distilled water might have got trapped into the pores of the bulk adhesive material, resulting in higher moisture absorption. The uptake behavior of bonded joints in the current experimental investigation is well supported by work reported by Hand *et al.* [132] and Parker [130].

The moisture absorption behavior of CFRP composite laminate is shown in Figure 6.2(b). The diffusion plot of composite laminate tested in water immersion experiment showed a maximum of 1.2% weight gain over a period of 168 days without reaching the saturation point. The moisture absorption behavior of CFRP composite shown in the diffusion plot is similar to the work reported by Gibson [181] on AS/3501-5 graphite/epoxy composite system. In the time frame of the intended study the CFRP laminate did not reach the saturation point and still it was absorbing the moisture, which is clearly indicated by the monotonically increasing weight gain plot. The weight gain curves of bulk adhesive and sandwiched adhesive demonstrated an initial linear region, an intermediate region, followed by a plateau.

Normally a plot of fraction uptake (M_t/M_∞) against square root of time from the moisture experiment is made and the diffusion coefficient is calculated. The diffusion coefficient is related to the slope of the linear uptake region of the equation

$$\frac{d(M_t/M_\infty)}{d(\sqrt{t})} = \frac{4}{\sqrt{\pi}}\left[\frac{\sqrt{D}}{l}\right] \tag{6.1}$$

where M_t is the mass uptake of water as a function of time, M_∞ is the mass uptake at equilibrium, D is the diffusion coefficient, t is the time and l is the specimen thickness. A further manipulation of equation (6.1) gives a simplified expression for calculating the diffusion coefficient in differential form as shown below:

$$D = \frac{\pi}{16}\left(\frac{l}{M_\infty}\right)^2\left[\frac{M_2 - M_1}{\sqrt{t_2} - \sqrt{t_1}}\right]^2 \tag{6.2}$$

and in this case the diffusion coefficient can be calculated directly from the moisture uptake vs. square root of time plot. The diffusion coefficients of bulk adhesive and sand-

Table 6.1: Diffusion coefficient of the adhesive and CFRP laminate

Entities	Diffusion coefficient, $\times 10^{-13}(m^2 s^{-1})$	$M_\infty(\%)$
Bulk adhesive	1.83	5.50
Sandwiched Adhesive	1.39	0.45

wiched adhesive calculated using equation (6.2) are reported in Table 6.1. The diffusion coefficient of CFRP laminate is not reported because the weight gain in the laminate did not reach the equilibrium conditions during this period.

In polymeric materials moisture absorption also causes hygroscopic expansions or contractions analogous to thermal strains. The moisture-induced strains in isotropic materials can be expressed in terms of moisture concentration, C (defined as the ratio of the mass of moisture in a unit volume to the initial dry mass of the material in a unit volume) as

$$\varepsilon_i{}^M = (\beta)C \tag{6.3}$$

where β is the coefficient of hygroscopic expansion (CHE).

Figure 6.3(a) reports the dimensional changes observed in bulk adhesive during the moisture absorption experiment. The dimensional change in length and width were almost same and saturates at a maximum of 1.1 %. In the thickness direction the maximum dimensional change was approximately 2.2 %, indicating twice that of width and length dimensions in this particular adhesive. In all the cases, the dimensional change (%) vs. time (h) plot showed an initial linear region followed by a plateau indicating saturation of moisture absorption.

The dimensional changes occurred in CFRP composite material due to moisture-induced expansion and swelling. Experimental evidence of moisture expansion and swelling in carbon epoxy composite is reported in Figure 6.3(b). The dimensional change of the

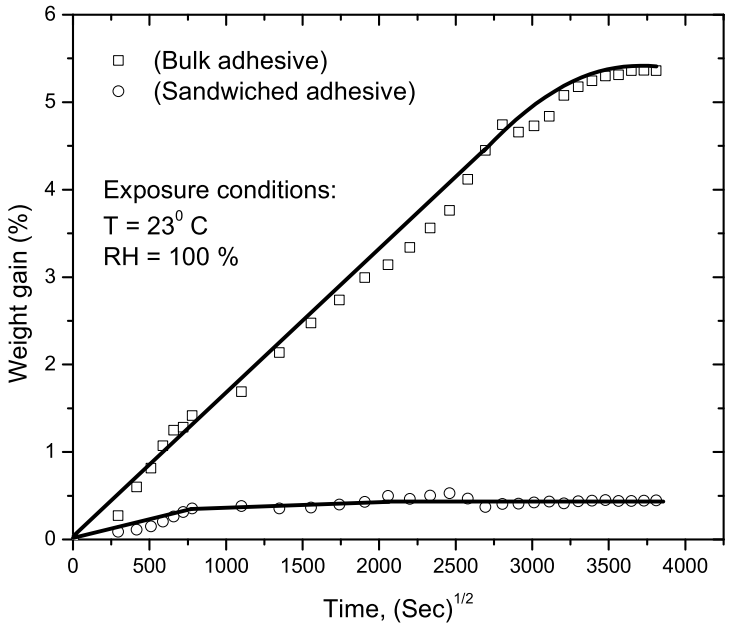

(a) Moisture absorption in Redux 322 adhesive

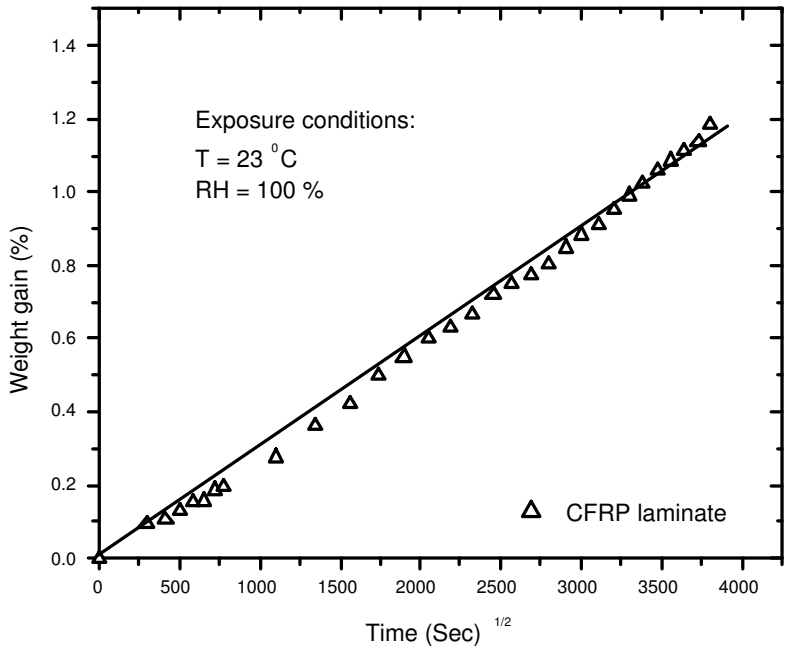

(b) Moisture absorption in CFRP substrate

Figure 6.2: The moisture absorption behavior of adhesive and CFRP laminate.

composite is smallest in the direction where the fibre strength and stiffness dominate. The high dimensional stability of the composite in the fibre direction (longitudinal direction) is mainly due to the high strength and stiffness of the carbon fibres and less sensitivity to the moisture absorption. The study of the width dimension of the laminate after moisture absorption revealed that moisture-induced expansion increased linearly and around 1.1 % expansion was noticed after approximately 4000 h exposure to distilled water (see Figure 6.3(b)). As can be seen in Figure 6.3(b) a highest expansion of around 2.4 % was observed in the thickness direction after some 4000 h of exposure. It was observed that the dimensional changes were highest in the thickness direction of the composite laminate as compared to the width direction because of resin-rich layer that exists in the thicknesses direction as a consequence of progressing. Since resin-rich layer is not constrained by the reinforcing fibers, this layer is free to expand to a greater extent by moisture absorption. Experimental studies performed by Lucas and Zhou [119] with T300/934 composite showed similar results and support the conclusions.

6.3.2 Load versus displacement response and failure modes

DCB and MSLJ joints

The load vs. displacement traces obtained by testing DCB specimens showed that the load increased linearly with the displacement to the point just before when the crack started to propagate from the sharp tip of the pre-crack in all the cases (see Figure 6.4). As the elastic strain energy of the system surpassed the critical elastic strain energy level of the adhesive the crack started to propagate through the adhesive layer in the DCB test specimen and the load dropped and the crack got arrested. In this manner, whenever the elastic strain energy of the system exceeded the energy required to propagate the crack, the crack propagation occurred and load dropped and the system compliance also reduced as can be seen from the graphs shown in Figure 6.4. The trend observed in the present investigation is in agreement with the previous literature. All DCB specimens were tested till enough data points of load and load-line displacement in the stable crack propagation region were

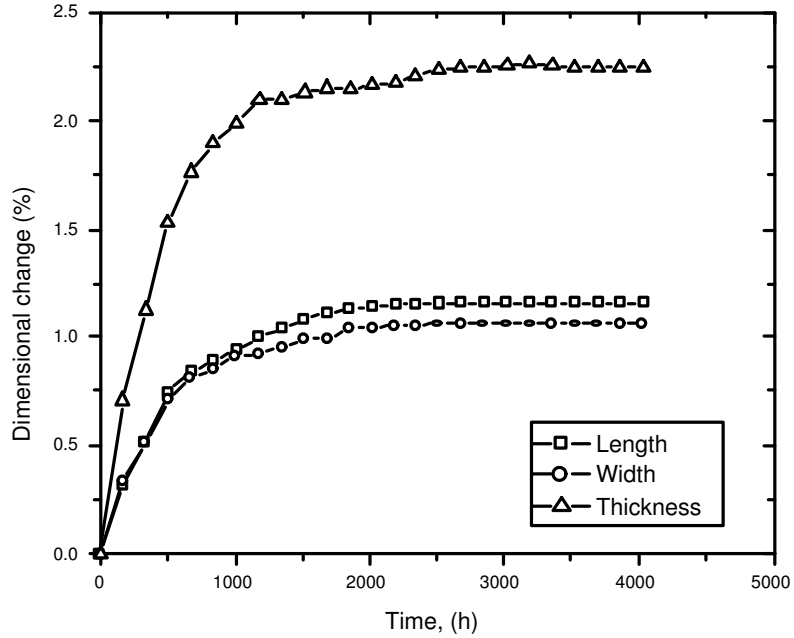

(a) Dimensional changes in the bulk adhesive (Redux 322)

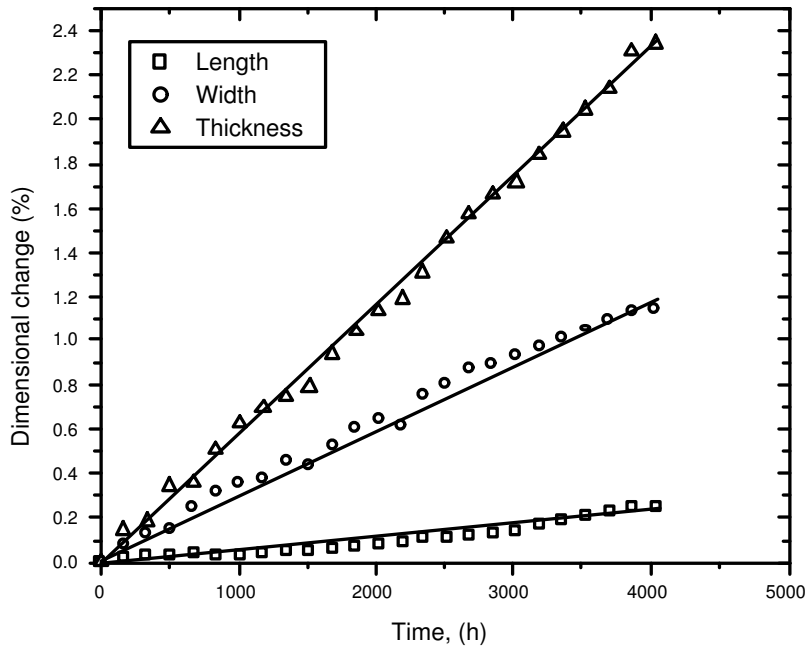

(b) Dimensional changes in CFRP substrate

Figure 6.3: The moisture-induced dimensional expansion and swelling of bulk adhesive material and CFRP laminate.

obtained. The adhesive fracture energy, G_a, was calculated using experimental compliance method from the experimental data. All the specimens considered for analysis failed by stable crack growth and fracture occurred in cohesive manner (i.e., via adhesive layer) as shown in Figures 6.5(a)-(f).

Typical load vs. displacement curves shown in Figure 6.6 from each batch of MSLJ tested specimens evidently indicate that the fracture took place in a linear elastic manner as the load proportionately increased with the displacement till final fracture of the specimens. In Figures 6.7(a)-(f) the photographs of the fractured surfaces of MSLJ specimens are shown, which clearly demonstrate the cohesive failure (i.e., fracture through the adhesive layer) in the bonded MSLJ specimens.

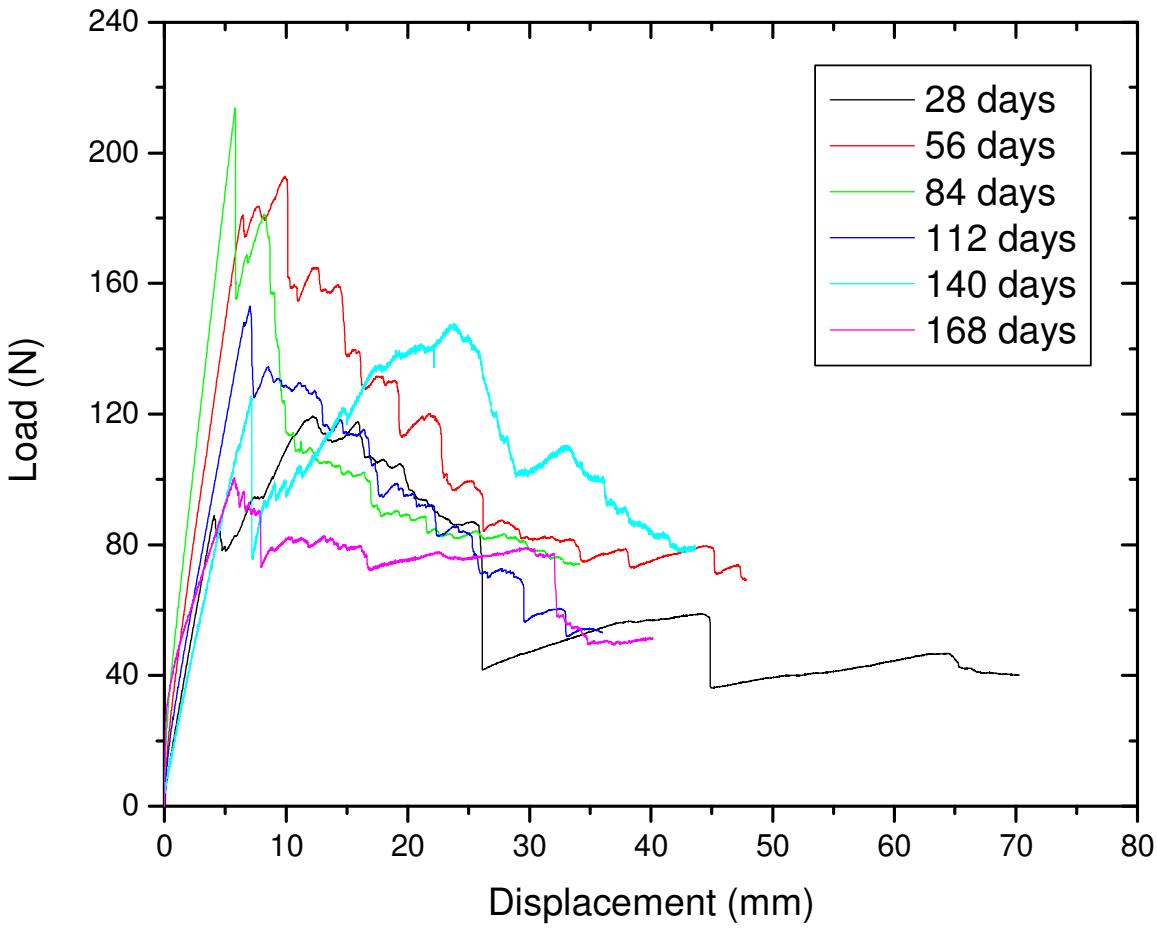

Figure 6.4: The load displacement traces of typical DCB joints after exposure to distilled water for various time periods.

(a)

(b)

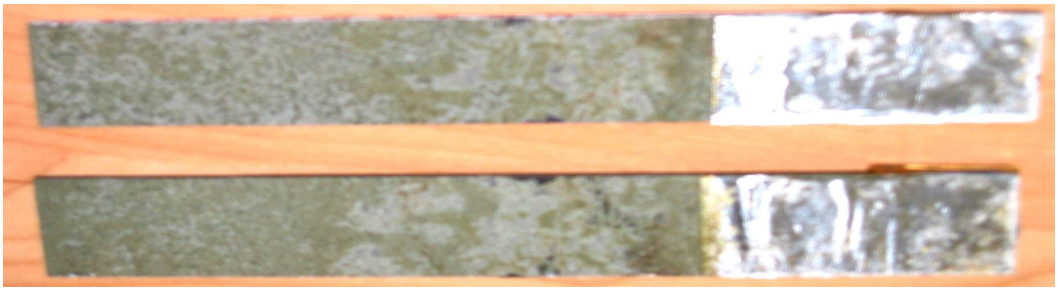

(c)

(d)

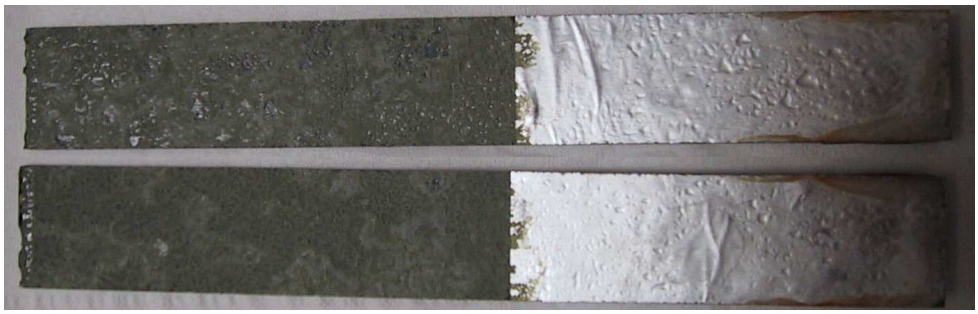

(e)

(f)

Figure 6.5: The fractured surface of adhesive layer in DCB joints after exposure to distilled water gives evidence of cohesive fracture in adhesive layer (a) 28 days, (b) 56 days, (c) 84 days, (d) 112 days, (e) 140 days and (f) 168 days.

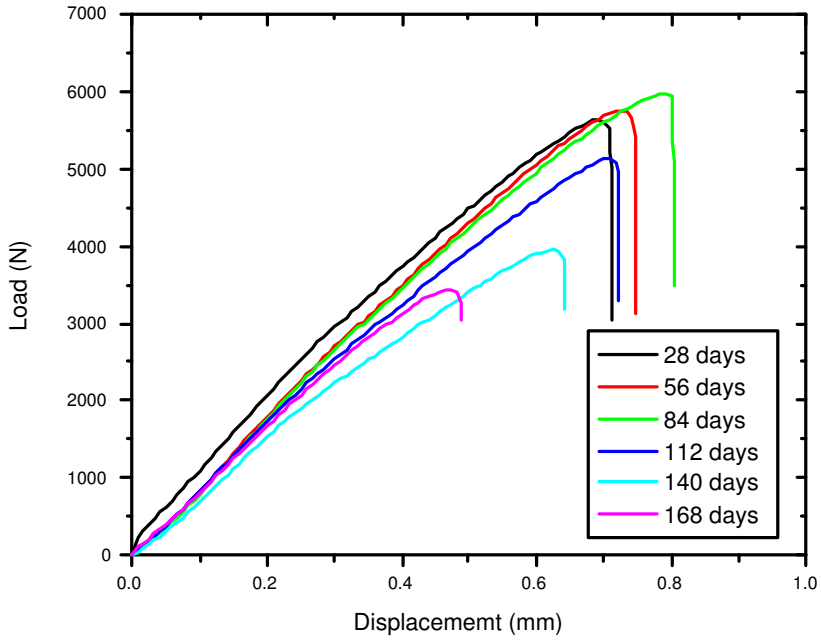

Figure 6.6: Typical load displacement graph of MSLJ joints after exposure to distilled water for various time periods. All the curves indicate brittle failure

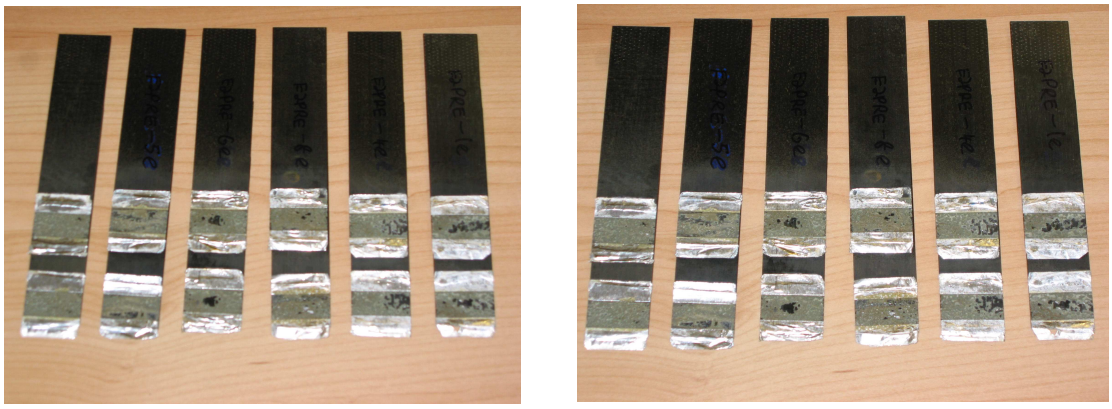

(a) (b)

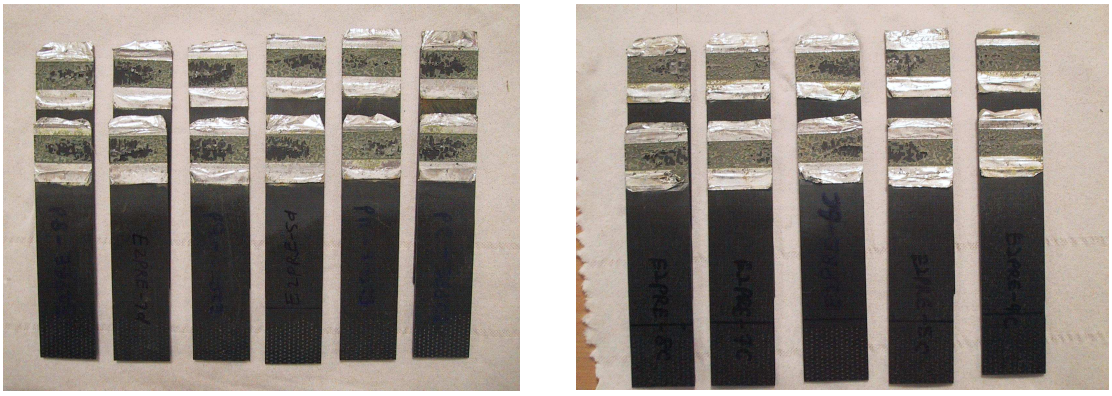

(c) (d)

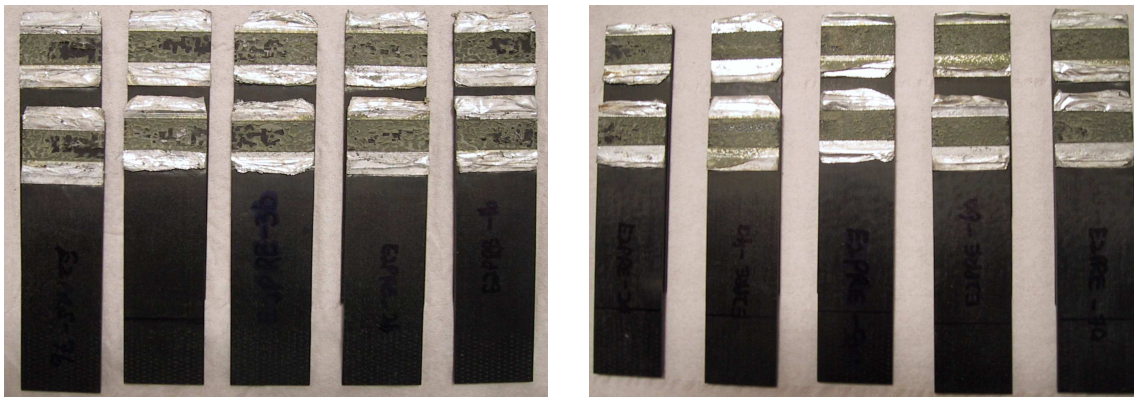

(e) (f)

Figure 6.7: The fractured surface of adhesive layer in MSLJ joints after exposure to distilled water (a) 28 days, (b) 56 days, (c) 84 days, (d) 112 days, (e) 140 days and (f) 168 days.

Composites and Adhesive

Figure 6.8(a) reports some typical load vs. displacement plot for dry and aged longitudinal (0^0) unidirectional CFRP composite laminate. The load vs. displacement curves of transverse (90^0) unidirectional and $\pm 45^0$ balanced and symmetric CFRP laminate, which is used for the in-plane shear properties calculation are shown in Figures 6.8(b) and 6.8(c) respectively. The load displacement curve of longitudinal (0^0) unidirectional composite test coupons showed linear response till the final fracture. The coupons ruptured catastrophically in a brittle manner. The transverse (90^0) unidirectional CFRP composite laminate showed a slight non-linearity in the load-displacement response but the final fracture occurred catastrophically and load dropped abruptly upon fracture. The test specimens cut from $\pm 45^0$ balanced and symmetric CFRP laminate, which is used for studying the in-plane shear properties of the laminated composite showed significant plasticity in the load-displacement curve. The load increased linearly up to around 4 mm of cross-head displacement in all cases. As load was increased the load-displacement behavior deviated from the linear relationship and material started to behave in a non-linear manner. The longitudinal (0^0) unidirectional results showed typical fiber dominated behavior of CFRP composite. A slight non-linearity in the load-displacement response of transverse (90^0) unidirectional CFRP composite laminate tests occurred mainly due to the influence of resin matrix. The non-linear response of $\pm 45^0$ balanced and symmetric CFRP laminate is a result of the combined influence of the resin matrix and the fiber-matrix interface of the composite.

The tensile test results obtained from dry and aged bulk adhesive specimens indicated almost linear elastic behavior of the adhesive material as can be seen in the load-displacement response (see Figure 6.9). The load increased monotonically with the applied displacement and upon reaching the maximum load the test specimens broke into two parts almost in the middle of the gauge region with flat surfaces. The load-displacement curves indicate typical brittle failure of adhesive. The specimens which were aged in distilled water for 28 days, 56 days and 84 days fractured at a higher load

than that of the dry specimens. The rest of the aged specimens fractured at a lower load than the days specimens.

6.4 Effect of exposure time on mechanical properties

6.4.1 Mode-I Adhesive fracture energy of DCB and MSLJ

To obtain the mode-I adhesive fracture energy, the experimental data obtained by testing a DCB specimen may be analyzed using four different methods as described in Chapter 5. In the present investigation, the experimental compliance method (ECM) was used to obtain the adhesive fracture energy, as it is simple and does not involve any correction factors. Kinloch and his co-workers [178] have programmed this solution technique in MS-Excel spread sheet. As shown in Figures 6.5(a)-(f), all the DCB joints chosen for the analysis failed in a cohesive manner via the adhesive layer. The mode-I adhesive fracture energy was calculated from the MSLJ test configuration using the method described in section 5.2.5. The values of the adhesive fracture energy from the DCB joints were compared with those from the MSLJ and are summarized in Table B.1. Since the DCB test is well established for the estimation of adhesive fracture energies, the result obtained from the tests were used as the benchmark for judging the accuracy of the KO-model to obtain the fracture energy of the adhesive in the MSLJ joints. Table B.1 shows the mean adhesive fracture energies for the MSLJ and DCB joints. The graphical analysis (see Figure 6.10) of the data revealed that adhesive fracture energy increased initially with maximum at around 84 days of exposure. The adhesive fracture energy decreased after 84 days of exposure to distilled water. Both MSLJ and DCB specimens which were tested after exposure of 112 and 140 days gave a smaller value of adhesive fracture energy than those of 28, 56 and 84 days. The specimens aged for 168 days gave an adhesive fracture energy value lower that of the dry one.

The observed initial increase followed by decrease in the measured adhesive fracture energies is consistent with previously reported results for Cybond 4523GB epoxy adhe-

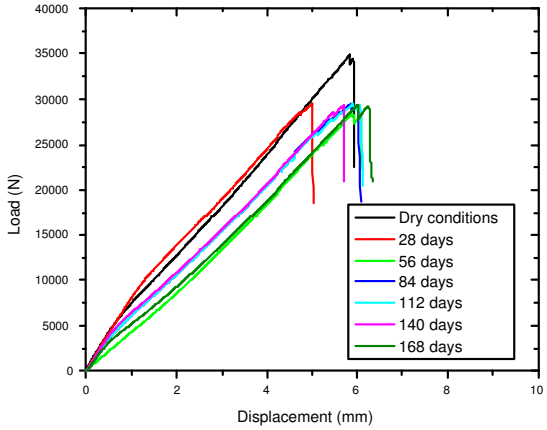

(a) Longitudinal (0^0) unidirectional laminate

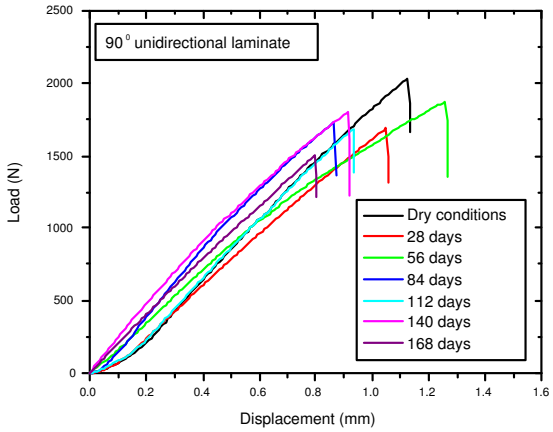

(b) Transverse (90^0) unidirectional laminate

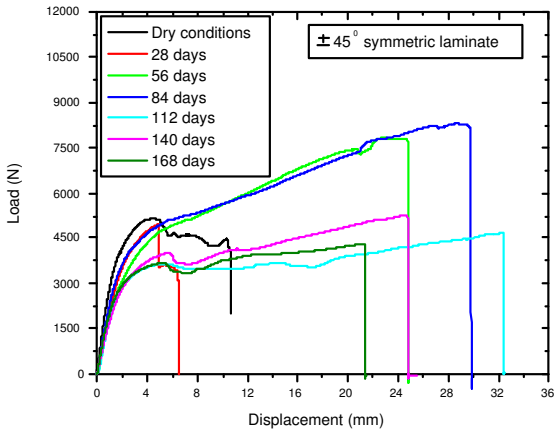

(c) Off-axis $\pm 45^0$ laminate

Figure 6.8: Typical load vs. displacement traces of CFRP laminate for dry condition and after exposure to distilled water till 28 days, 56 days, 84 days, 112 days, 140 days and 168 days.

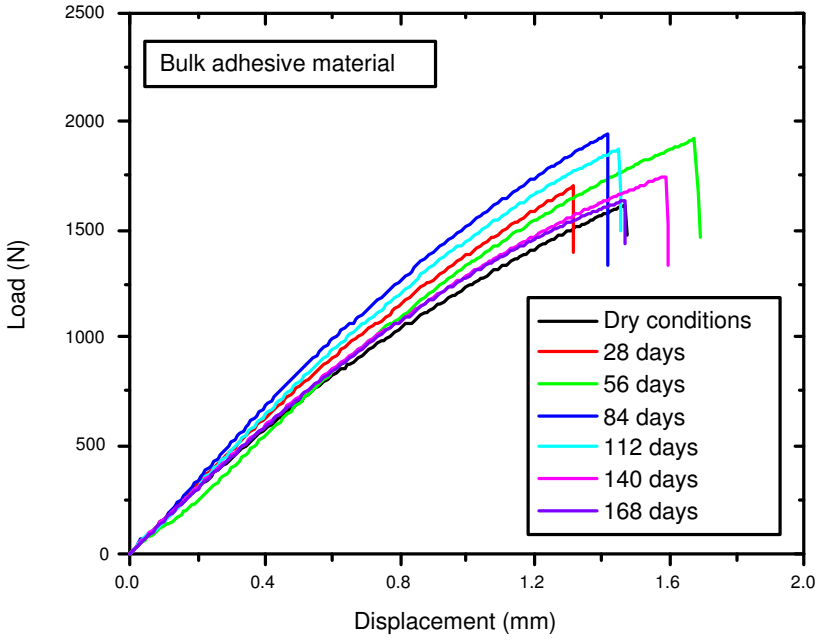

Figure 6.9: Typical load vs. displacement traces of bulk adhesive for dry and after exposure to distilled water till 28 days, 56 days, 84 days, 112 days, 140 days and 168 days.

sive [146]. It is believed that the initial increase in adhesive fracture energy with exposure occurred due to plasticisation of adhesive by absorbed distilled water. The absorbed water in the adhesive may have caused two things to happen in the adhesive layer, namely, (a) relaxation of internal stresses developed during curing process itself and (b) softening of the adhesive, which caused redistribution of stresses over a large region of the bond. The decease in adhesive fracture energy is attributed to degradation in the adhesive material with absorption of distilled water as expected. The adhesive fracture energy obtained from the DCB is in excellent agreement with the MSLJ results. This shows that the starter pre-crack in the MSLJ circumvented the effect of spew fillets and ensured that the values of adhesive fracture energy measured from the MSLJ are in good agreement with the mode-I fracture energy measured using the DCB test configuration.

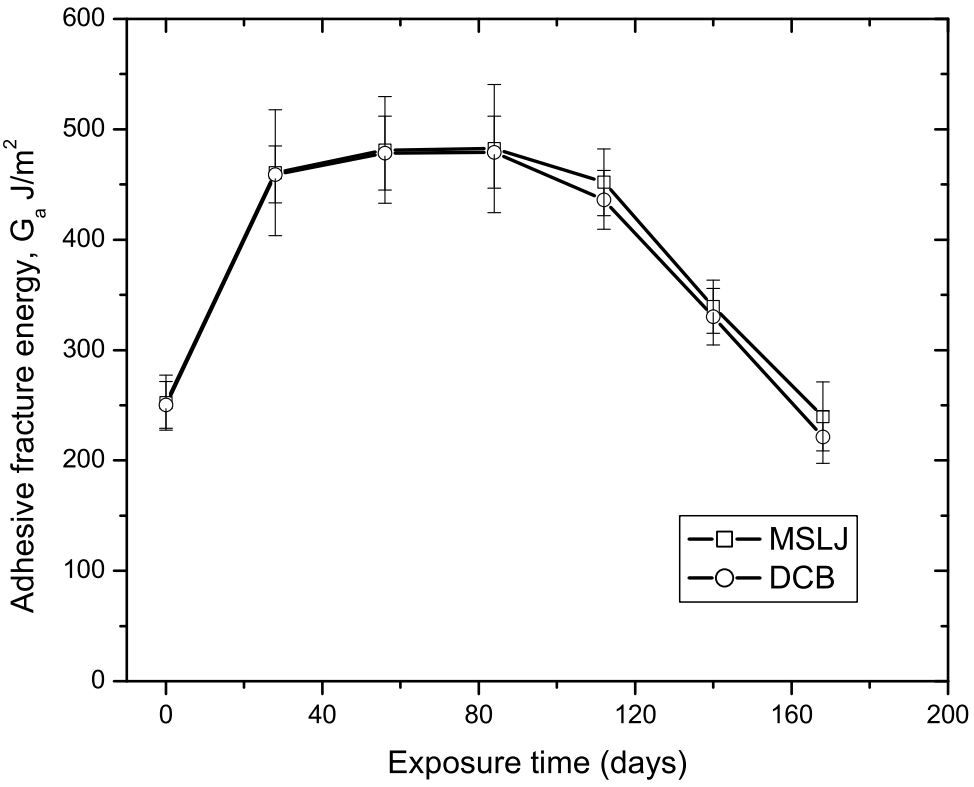

Figure 6.10: The variation in adhesive fracture energy with exposure time in distilled water.

6.4.2 Scanning Electron Microscopy Examination

A scanning electron microscopic (SEM) study was performed by extracting rectangular samples from the tested MSLJ and DCB specimens after testing. Rectangular samples were cut from ruptured specimens consisting complete fractured adhesive surfaces using a high speed diamond cutter. SEM samples were carefully gold plated using a sputtering machine to make the samples conductive. Fracture morphologies in the adhesive material near the pre-crack tip in the failed MSLJ specimens tested in dry conditions and after ageing for 168 days at the intervals of 28 days suggest that fracture occurred due to mode I loading (see Figures 6.11). The failure mode observed on the fractured surface near the pre-crack tip in the MSLJ is similar to those observed in the fractured surfaces of the adhesive material in the DCB joint as shown in Figures 6.12.

(a)

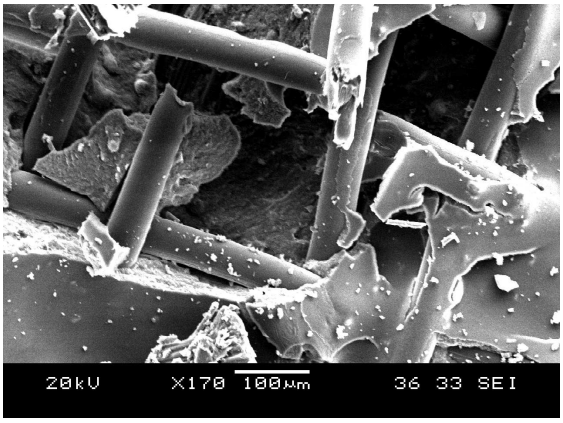

(b)

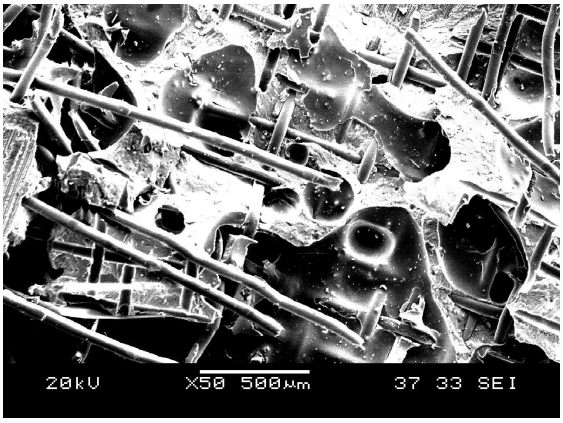

(c)

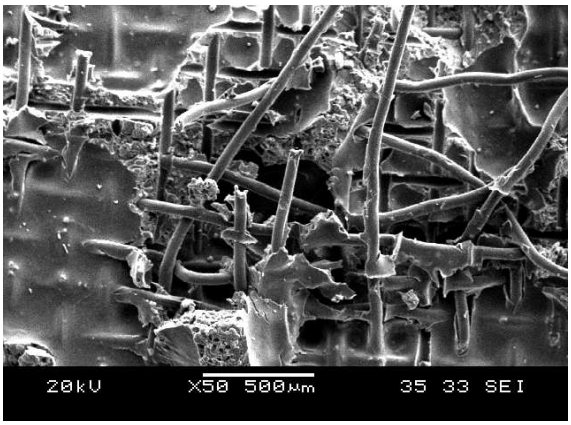

(d)

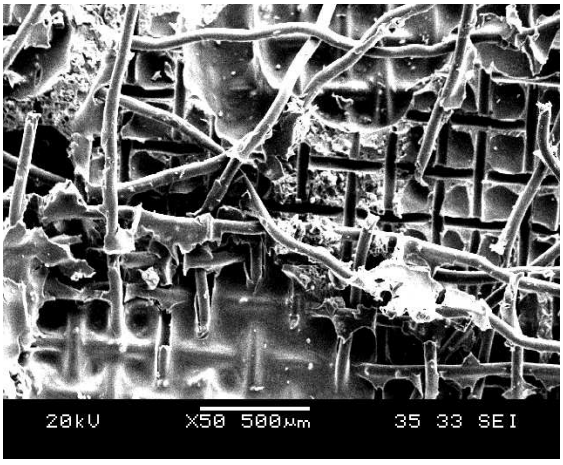

(e)

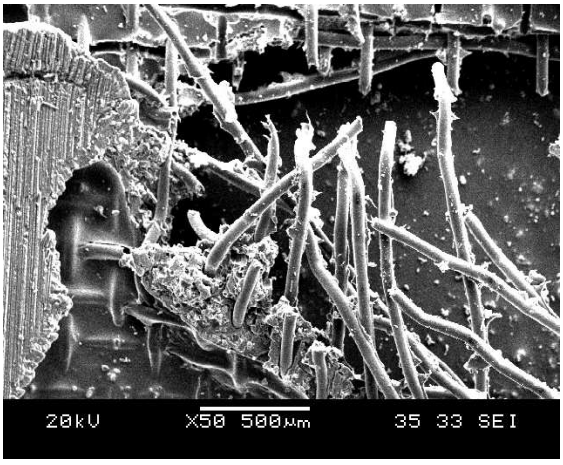

(f)

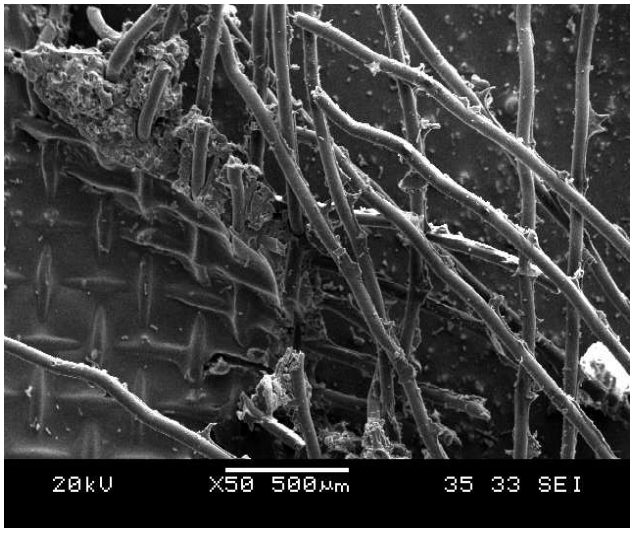

(g)

Figure 6.11: Scanning electron microscopy (SEM) photomicrograph of ruptured adhesive material in MSLJ test specimens in (a) dry condition, (b) after 28 days of ageing, (c) after 56 days of ageing, (d) after 84 days of ageing, (e) after 112 days of ageing, (f) after 140 days of ageing and (g) after 168 days of ageing.

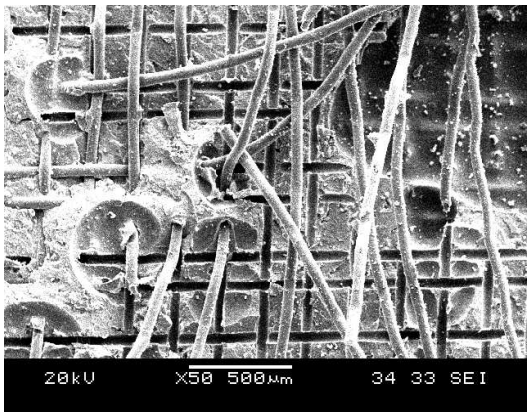

(a)

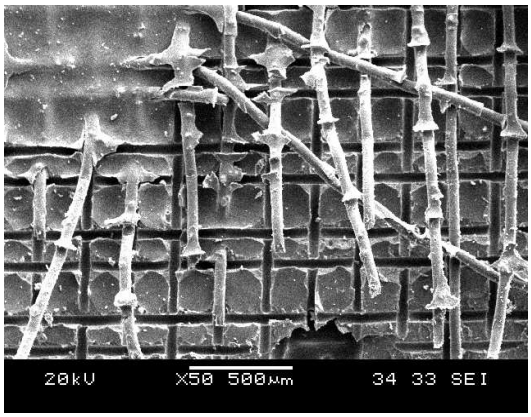

(b)

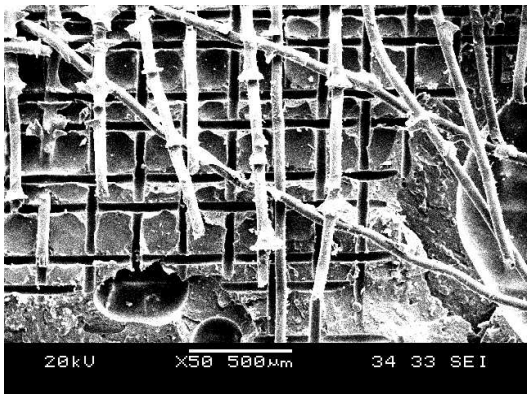

(c)

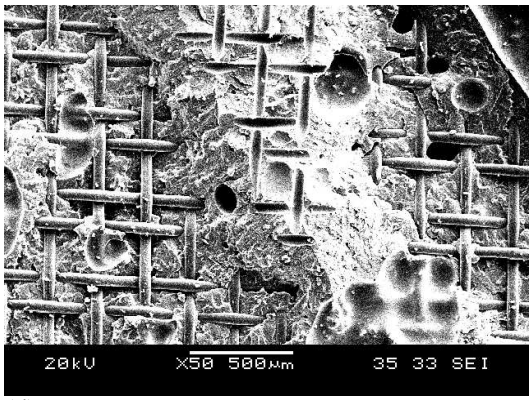

(d)

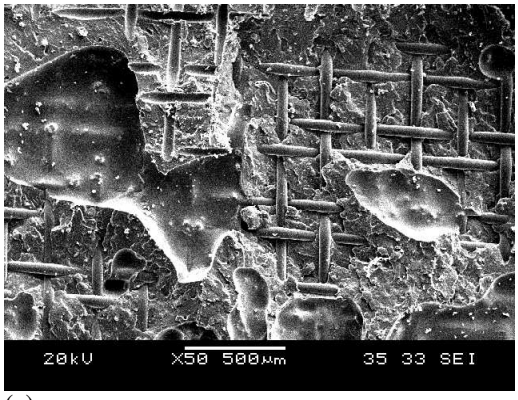

(e)

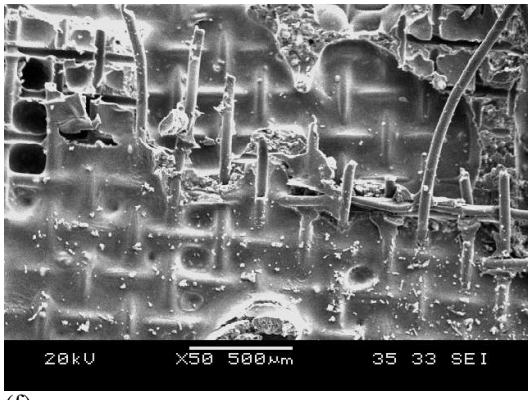

(f)

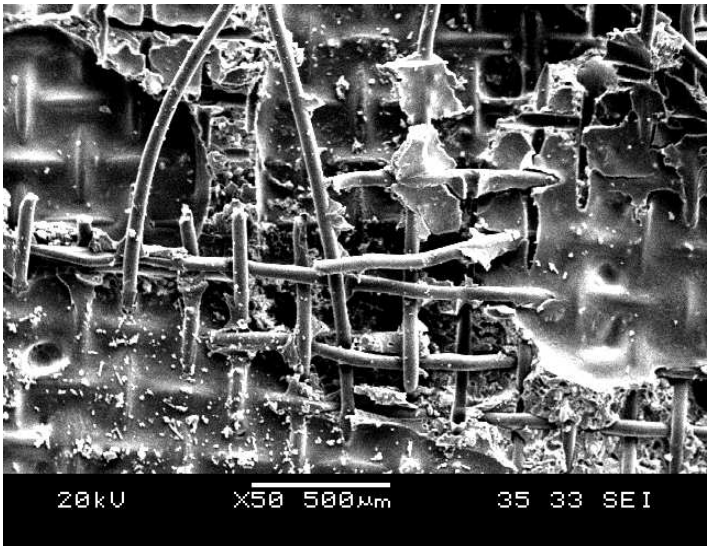

(g)

Figure 6.12: Scanning electron microscopy (SEM) photomicrograph of ruptured adhesive material in DCB test specimens in (a) dry condition, (b) after 28 days of ageing, (c) after 56 days of ageing, (d) after 84 days of ageing, (e) after 112 days of ageing, (f) after 140 days of ageing and (g) after 168 days of ageing.

6.4.3 Composites and Adhesives

The data captured by the automatic data logger and the strain gauges were analyzed and various mechanical properties were calculated. The strain in the middle of the gauge region at each increment of the cross-head was monitored by an extensometer. The mechanical properties such as longitudinal tensile strength (LTS), σ^t_{11}, transverse tensile strength (TTS), σ^t_{22}, in-plane shear strength (IPSS), σ_{12}, longitudinal tensile modulus (LTM), E^t_{11}, transverse tensile modulus (TTM), E^t_{22}, in-plane shear modulus (IPSM), G_{12}, and Poisson's ratio (PR), ν_{12} of the composite material are summarized in Table B.2 with its standard deviation. The effect of the exposure time was studied by plotting various mechanical properties as shown in Figures 6.13(a)-(g). The longitudinal tensile strength of aged composite reduced by about 28% as compared to the dry composite. The reduction was observed mainly between dry and 28 days exposure. The strength was nearly constant for the other exposure periods (see Figure 6.13(a)). The transverse tensile strength reported marginal decrease with exposure time as shown in Figure 6.13(b). All other

properties were almost insensitive within the scatter of the experiment for the exposure period considered in this investigation (see Figures 6.13(c)-(g)).

The mechanical properties of the cured adhesive were obtained by testing the specimens extracted from cured adhesive panel and exposing to the distilled water in the identical conditions to that of composite substrate/MSLJ/DCB specimens. Tensile strength (TS), shear strength (SS), tensile modulus (TM), shear modulus (SM) and Poisson's ratio (PR) of the cured adhesive material were evaluated. As can be seen in Figures 6.14(a) and (c) an initial increase followed by a drop was observed in the tensile strength and the tensile modulus. However, the shear strength and the shear modulus showed a decreasing pattern throughout the exposure period (see Figure 6.14(b) and (d)). The Poisson's ratio was more or less insensitive to the exposure time as shown in Figure 6.14(e). Summary of all these properties is given in Table B.3.

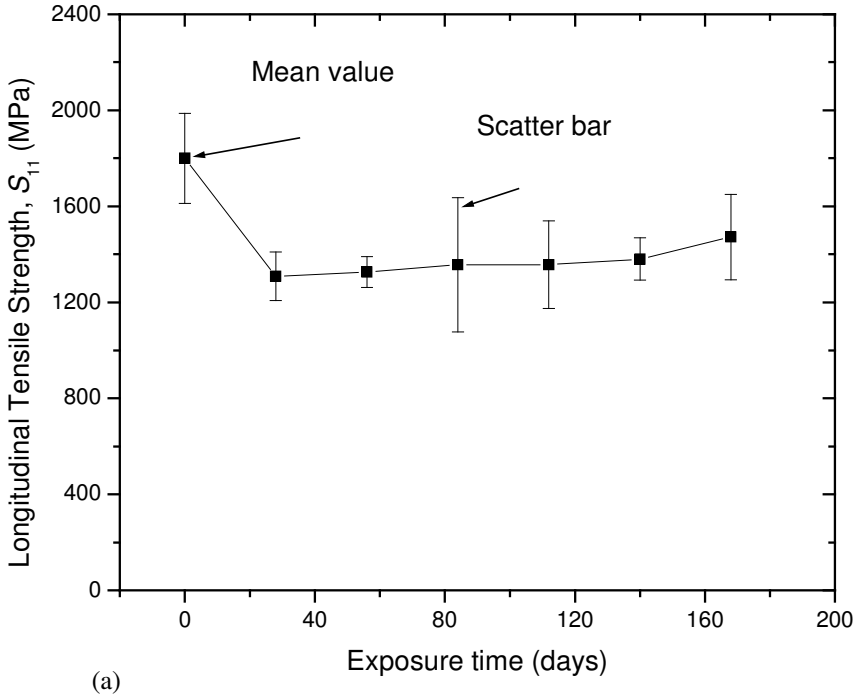

(a)

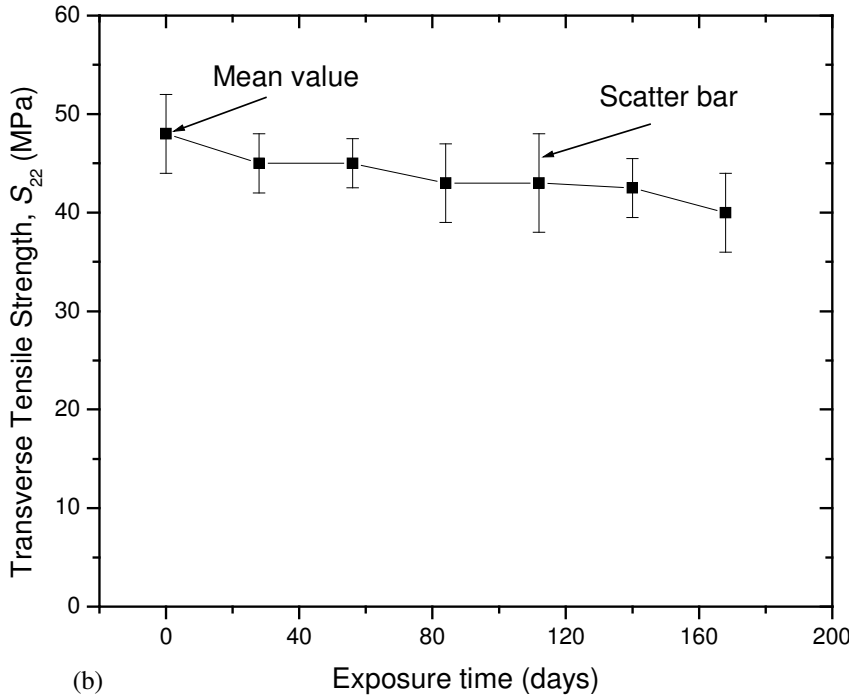

(b)

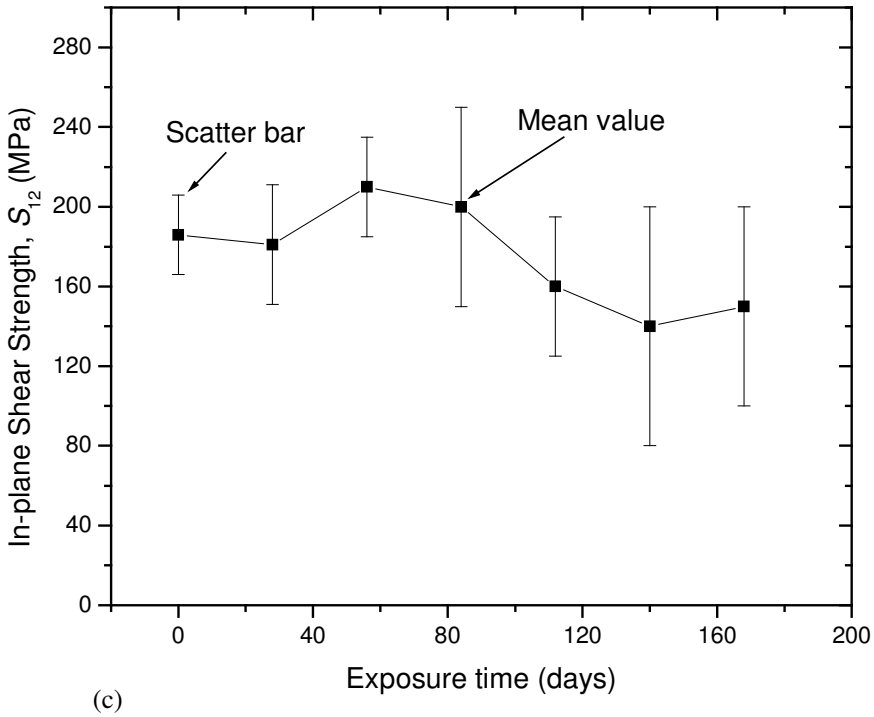

(c)

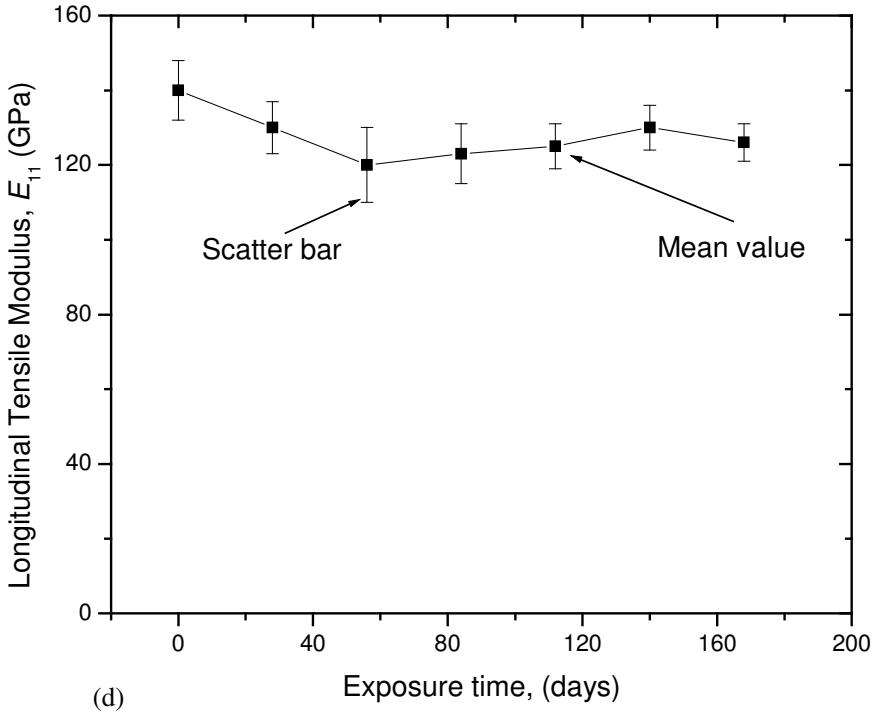

(d)

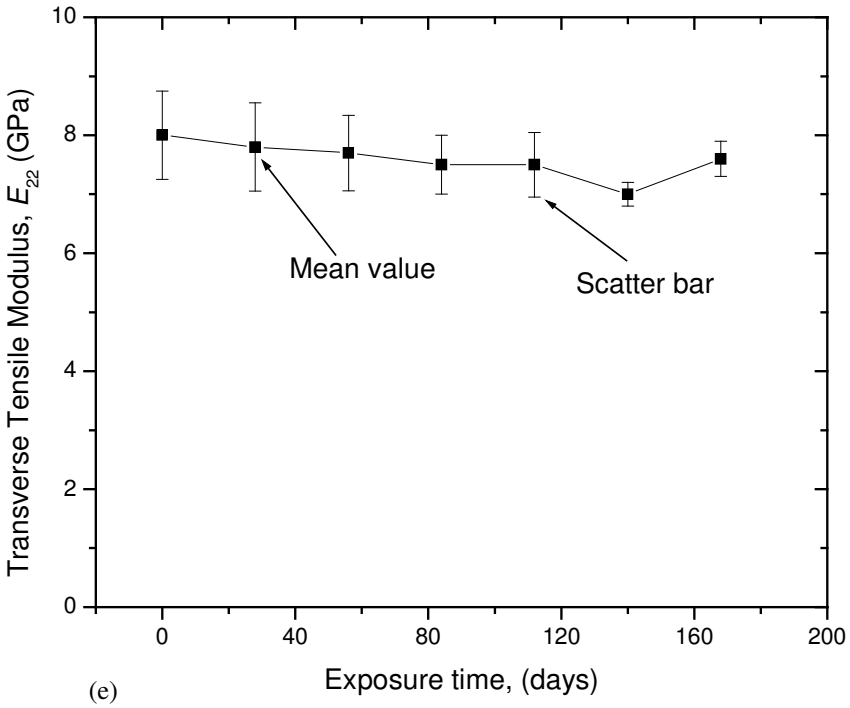

(e)

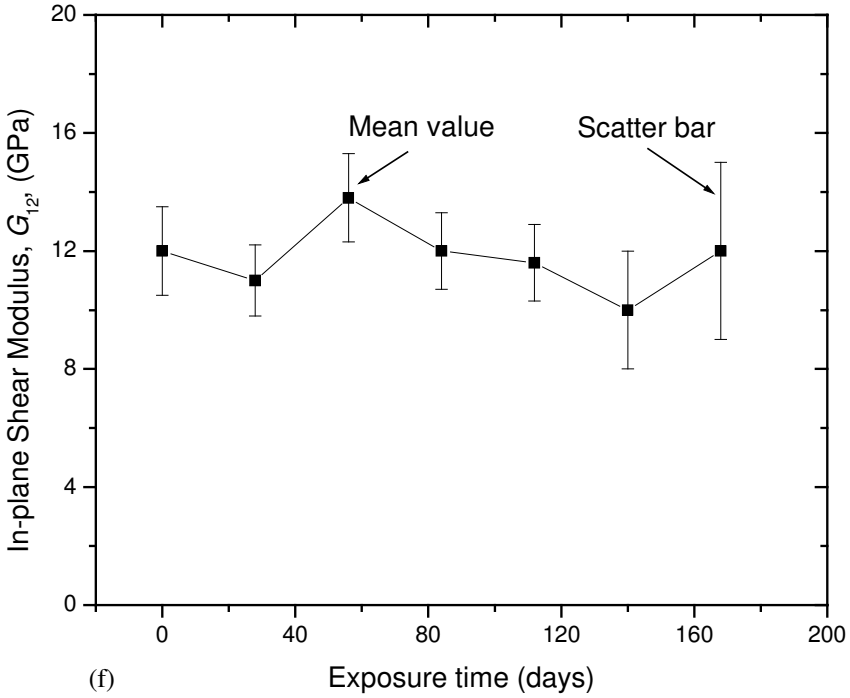

(f)

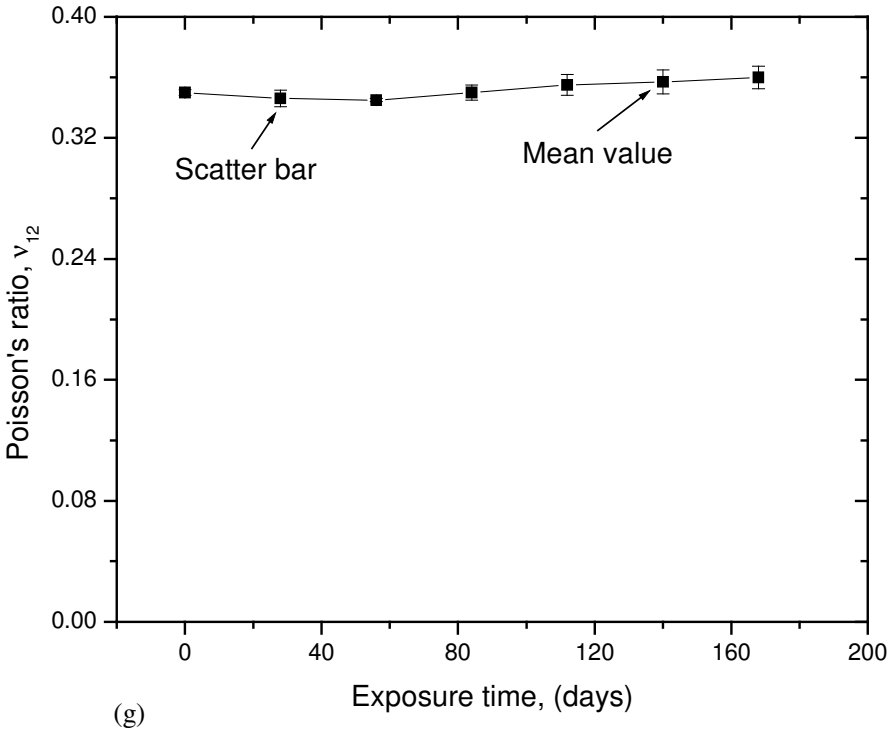

(g)

Figure 6.13: The variation in mechanical properties of CFRP composite with exposure to distilled water (a)longitudinal tensile strength (b) transverse tensile strength (c) in-plane shear strength (d) longitudinal tensile modulus (e) transverse tensile modulus (f) in-plane shear modulus (g) Poisson's ratio.

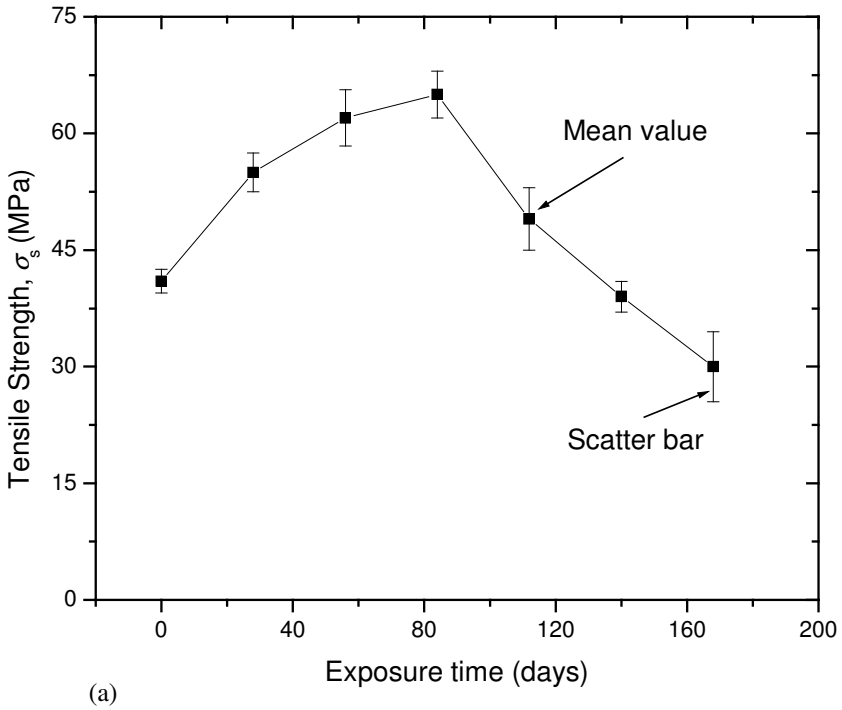

(a)

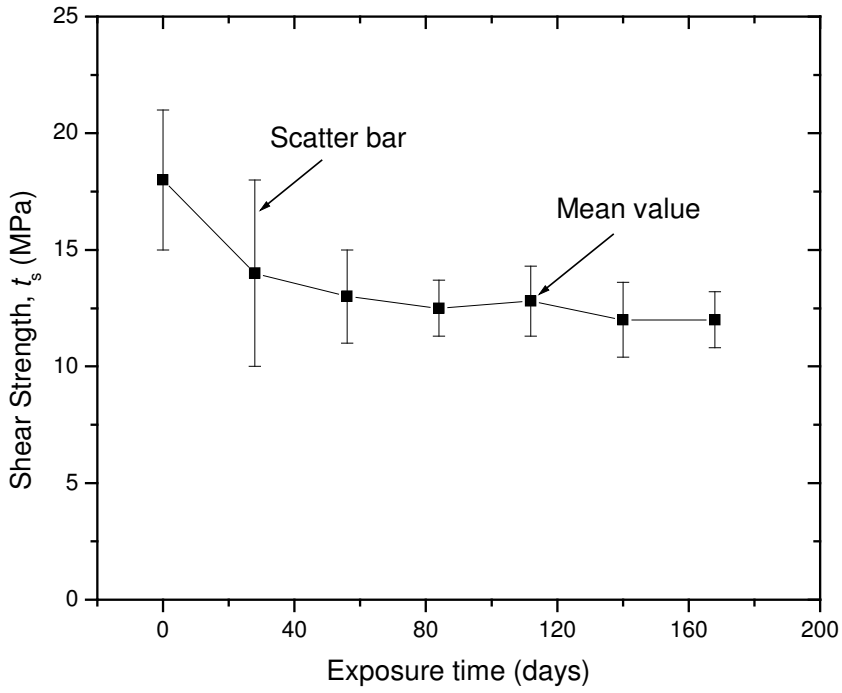

(b)

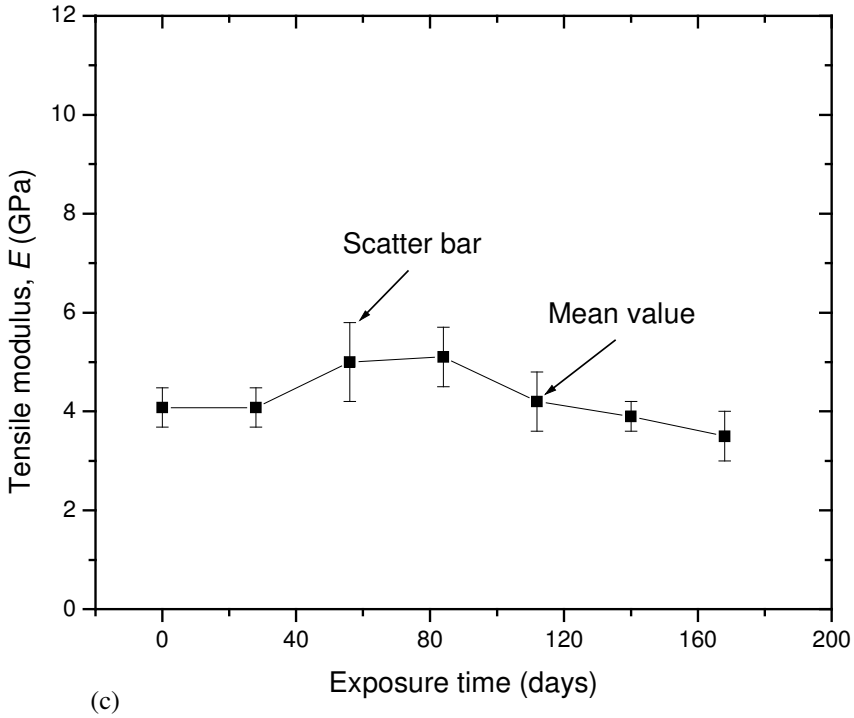

(c)

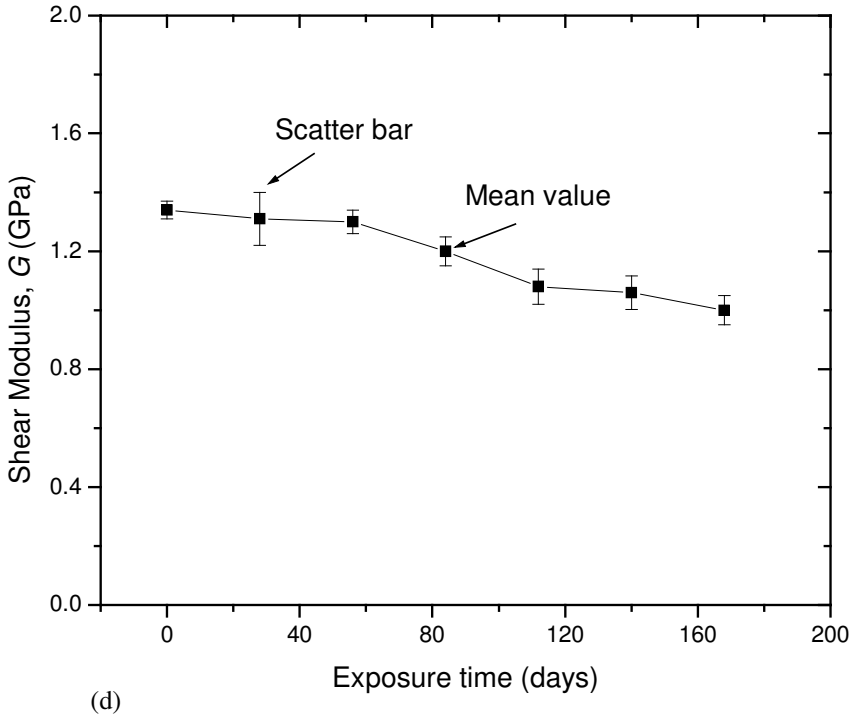

(d)

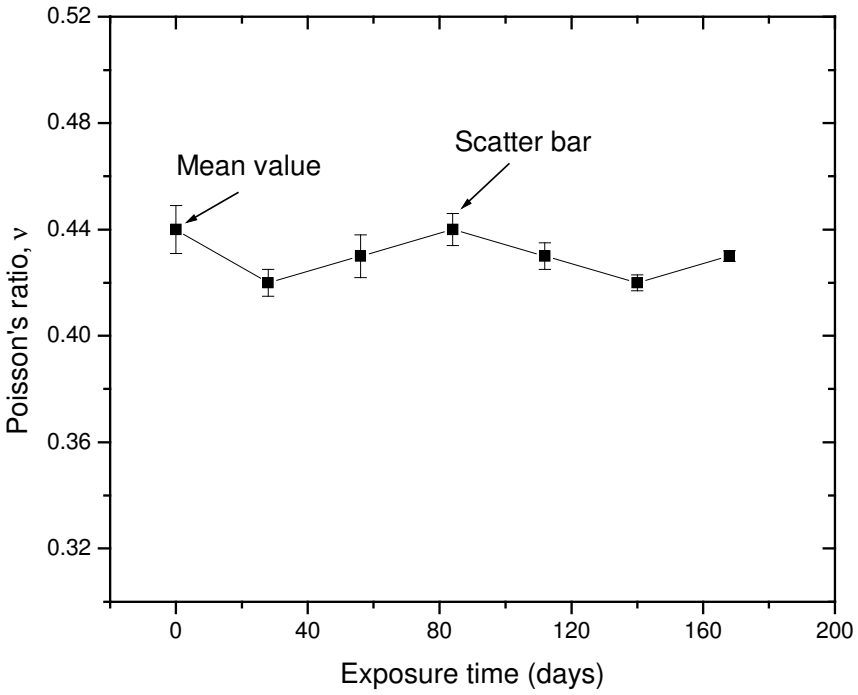

(e)

Figure 6.14: The variation in mechanical properties of adhesive with exposure to distilled water (a) tensile strength (b) shear strength (c) tensile modulus (d) shear modulus (e) Poisson's ratio.

6.5 Conclusions

The effects of moisture absorption on the adhesive fracture energy of bonded joints were studied using a new test geometry referred to as modified single lap joint (MSLJ). The results from experimental measurement showed that most of the water weight gain by the adhesive layer took place in the first few weeks of the exposure time.

These new MSLJ specimens were made by implanting two starter pre-cracks at the ends of the overlap within the middle of the bond line in a conventional SLJ. Tests were conducted on MSLJ and DCB specimens made from the same composite and adhesive combinations in dry conditions and after exposure to distilled water medium. The composite substrates were made from 913C - HTA 12K 5-34% prepregs. The adhesive used in this study was an aerospace grade film adhesive (Redux 322, 300 gsm). Tests were carried out to measure the fracture load and using this fracture load the adhesive fracture energy was calculated by using the KO model. It was observed that the fracture energy

measured using MSLJ and DCB test geometries were in good agreement (see Table B.1). In the beginning of the exposure (for example, for the first three months of the exposure) an increase in the adhesive fracture energy was observed with exposure time, however, from months four onwards a reduction in the adhesive fracture energy was observed. This observation is consistent with previous reported result on anhydride epoxy adhesive by Hand *et al.* [132].

The results from this investigation also showed that the KO-model [16] is a valid model for studying the effect of moisture on the mode-I fracture energy of the adhesive in a MSLJ. These results are especially useful in the critical design based on fracture mechanics concepts for structural components required in aerospace and defense applications. A typical design engineer can also use this test geometry to evaluate and select the adhesive/pretreatment processes in hostile environmental condition more accurately. In addition, this test geometry can be employed to investigate the fatigue life of bonded structures in dry and wet conditions.

Chapter 7

Fatigue Life Prediction of Bonded Structures

7.1 Introduction

In the present Chapter, an attempt is made to illustrate the usefulness of MSLJ in predicting the fatigue life of bonded joints. Modified single lap joints (MSLJs) prepared by implanting the starter pre-crack at the both ends of the overlap as described in Chapter 5. In addition to MSLJ specimens SLJ and DCB specimens were also prepared. The fatigue life of MSLJ and SLJ were measured experimentally. The measured fatigue lives were compared with analytical fatigue life of MSLJ obtained by a fatigue life prediction model. In Chapters 5 and 6, MSLJ test configuration was used to determine the adhesive fracture energy of adhesively bonded joints in dry conditions and wet conditions. The simple modification to the conventional SLJ was able to reduce the scatter in the results by as much as 30 % as compared to SLJ. The influence of moisture ingression on adhesive fracture energy of bonded MSLJ composite joints were in good agreement with adhesive fracture energy of DCB joints.

7.2 Parameters in a typical fatigue testing

Fatigue behavior of any engineering material is dependent upon several factors, which adversely affects it in many different ways. Usually complex fatigue conditions are approximated by simplified laboratory experiments in which the effect of one variable is studied in turn, whilst all the other parameters are held constant. The most important of

these are as listed below [13]:

1. cyclically varying stress with stress amplitude, $\sigma_{amp} = (\sigma_{max} - \sigma_{min})/2$;
2. a corresponding fluctuating strain amplitude, $\epsilon_{amp} = (\epsilon_{max} - \epsilon_{min})/2$;
3. a stress range, $\Delta\sigma = (\sigma_{max} - \sigma_{min})$;
4. a mean stress level, $\sigma_m = (\sigma_{max} + \sigma_{min})/2$;
5. a stress ratio, σ_R, or displacement ratio, δ_R, (σ_R=($\sigma_{min}/\sigma_{max}$) or δ_R=($\delta_{min}/\delta_{max}$));
6. a frequency, f of applied cyclic load;
7. characteristic wave form for both stress and strain (e.g. sinusoidal, square, etc.);
8. operating environments (e.g. temperature, moisture or both);
9. specimen geometry.

Conducting tests with the above mentioned parameters presents a tremendous task to the experimentalists since fatigue tests are very expensive by nature and generation of a single set of data point takes a long time. Thus, a simple test geometry which can predict fatigue life accurately and can capture the effect of the above parameters will be very useful in the design and analysis of structures.

7.3 Fatigue data presentation methods

The aim of generating fatigue data is to use the information to rank and predict the service life of an engineering structure or component. The fatigue data can be conveniently presented in different forms. The most popular and accepted forms are listed below:

1. A plot of the maximum applied stress versus the number of cycles to failure (i.e. S - N curves).
2. The plot of residual properties of the material such the modulus, strength with respect to the number of cycles or time.

3. A plot of the maximum applied strain energy release rate versus the number of cycles to failure (i.e. G_{max} - N curves).

4. A plot of the crack growth rate versus the applied strain energy release rate or stress intensity factor (da/dN versus G_{max} curves).

5. A plot of the maximum applied load per unit width versus the number of cycles to failure (i.e. T_{max} - N curves).

These methods were discussed in detail by Osiyemi [111]. He has recommended the use of G_{max} versus N curves instead of ΔG versus N because the debris at the fractured surfaces normally prevent the crack from closing fully during unloading cycles, thereby the effective ΔG is lower than actually it should be. The use of G_{max} versus N curve was first suggested by O'Brien *et al.* [182] as a method of predicting the threshold value, G_{th} accurately. They found that the fatigue data for composites and adhesives could be represented as a plot of G_{max} versus N curve analogous to $S-N$ curves in metals. They also proposed that by choosing a suitable value of N, it was possible to specify a suitable value for the threshold value, G_{th}. In their investigation it was assumed that when a test was performed in displacement control, in which the crack growth rate decreases as the crack grew, a point is reached when the $G_{max}-N$ curve will be asymptotic. If at the point no crack is seen to grow further for another one million cycles, then this lower bound value of G_{max} could be considered as the threshold value, G_{th}. From these curves it is possible to obtain the threshold value of strain energy release rate, G_{th}, which is a very useful property for quality assurance and design purposes.

7.4 Data reduction methods

The first step in the analysis of fatigue test results is to obtain the crack growth rate (i.e., da/dN) from the measurements of the crack length from load line for corresponding number of cycles of testing performed on DCB joints. The basic experimental data consists of a set of discrete and finite crack length measurement and cycles count (i.e., N_i and a_i

measurements). Various methods are suggested to analyse the data such as "the graphical method", "the secant method", and "incremental polynomial method". Osiyemi [111] has analysed all these methods and recommended the use of the incremental polynomial method. The second step is to correctly calculate the maximum strain energy release rate (i.e., G_{max}) from the experimental data. To evaluate the maximum strain energy release rate four methods can be used those are "area method", "compliance method", "load method" and "displacement method". The compliance method is simple and superior to others, as G_{max} can be obtained directly from the load versus displacement values recorded from the fatigue tests, without involving any correction factor.

7.5 Analytical formulation

The important steps involved in deriving the analytical formula for the prediction of the fatigue life of bonded MSLJ configuration are now described. Consider the schematic diagram of MSLJ shown in Figure 5.5(a). When this joint is subjected to a quasi static load P then the overlap region of the joint rotates and takes the shape similar to the one shown in Figure 5.5(b). The induced bending moment causes high normal or peel stresses in addition to the shear stress distribution at the crack tip. Thus, it is believed that the joint fails due to the normal or peel stress developed at the crack-tip instead of shear stress. The transverse tensile stress or peel stress, which acts as operative load at the crack-tip can be correlated with the mode I elastic strain energy release rate as derived in Chapter 5.

Now for fatigue case, it is well known that in the linear zone of the $\log(da/dN)$ and $\log(G_{max})$ plot a relationship between da/dN and G_{max} can be written as proposed by Paris:

$$\frac{da}{dN} = D[G_{max}]^n \tag{7.1}$$

where the constants D and n are obtained by curve fitting the above equation to the experimental data (i.e., linear portion of $\log(da/dN)$ versus $\log(G_{max})$ curve obtained from DCB joints). However, the complete relationship between logarithmic da/dN and G_{max}

is usually of sigmoidal form. The complete relationship can be expressed by a modified Paris Law [111]:

$$\frac{da}{dN} = D[G_{max}]^n \left\{ \frac{1 - (\frac{G_{th}}{G_{max}})^{n_1}}{1 - (\frac{G_{max}}{G_a})^{n_2}} \right\} \tag{7.2}$$

where G_{th} and G_a are the values of the cyclic-fatigue threshold and constant displacement-rate adhesive fracture energy respectively. The empirical constants n_1 and n_2 are obtained by fitting the above expression to the experimental data i.e., complete sigmoidal da/dN versus G_{max} curve obtained from DCB joints.

Assuming that a crack will grow by a length, a, from both ends of the lap joint through the bonded-overlap region parallel to the bond line in the deformed geometry, the effective overlap length will be reduced from $2c$ to $2(c - a)$. Then by substituting $c - a$ for c and T_{max} for T in equation (5.7) an expression for maximum strain energy release rate during the cycling loading is given by:

$$G_{max} = \frac{12}{E_s h^3} \left[\frac{T_{max}(h + t_a)}{2} \right]^2 \frac{1}{(1 + e(c - a))^2} \tag{7.3}$$

Now, by substituting the above expression for G_{max} in equation (7.2) and integrating after some simplification, it gives the expression for the expected number of cycles to failure, N_f, of the modified single lap joint for a maximum load per unit width of the specimen applied during the cyclic loading, T_{max} in integral form. The number of cycles to failure, N_f, can be written in integral form as:

$$\begin{aligned} N_f = \int_{a_0}^{a_f} & \frac{[E_s h^3 [1 + e(c - a)]^2]^{(n - n_2)}}{D {G_a}^{n_2} [3[T_{max}(h + t_a)]^2]^{(n - n_1)}} \\ & \times \frac{[G_a E_s h^3 [1 + e(c - a)]^2]^{n_2} - [3[T_{max}(h + t_a)]^2]^{n_2}}{[3[T_{max}(h + t_a)]^2]^{n_1} - [G_{th} E_s h^3 [1 + e(c - a)]^2]^{n_1}} \cdot da \end{aligned} \tag{7.4}$$

the lower integration limit is the initial flaw size, a_0, which can be calculated using the given formula below for the plane strain case:

$$a_0 = \frac{E_a G_a}{\pi {\sigma_a}^2 (1 - \nu^2)} \tag{7.5}$$

The upper limit of the integrand, the length of the fatigue crack when fast fracture occurs may be calculated using the formula derived for the cases plane strain

$$a_f = \left(c - \frac{1}{e}\left[\sqrt{\frac{3[T_{max}(h+t_a)]^2}{E_s h^3 G_a}} - 1\right]\right) \tag{7.6}$$

In order to predict the fatigue life of the modified single lap joint, equation (7.4) can be integrated numerically using Simpson's method. This way it is possible to determine the number of cycles to failure, N_f as a function of the applied maximum load per unit width of the specimens, T_{max} during the fatigue cycle.

7.6 Experimental Details

7.6.1 Materials Used

Unidirectional composite laminates, $[0]_8$, made from 913C - HTA 12K 5-34% carbon prepreg and Redux 322 film adhesives (both supplied by Hexcel Composites, UK) were used. Prepreg sheets were cut from the material roll and 8 sheets of prepregs were stacked together to fabricate a laminate of 1.6 mm thickness. The stacked system was then pressed on a hot pressing machine at a pressure of 700 kPa and maintained at a temperature of 120^0C for 1 hour as recommended by the composite manufacturer. To prevent laminate warpage and obtain thermal stress free laminate, the cured laminate was allowed to cool down to room temperature in the hot press machine overnight (12 hrs). The molded composite laminates which had a volume fraction of around 60% were cut into pieces with dimensions of 230x230x1.6 mm. Redux 322, 300 gsm is a high performance modified epoxy film adhesive with 300 gsm areal weight and has nylon scrim cloth support. The nylon cloth provides better bondline thickness control.

7.6.2 Preparation of MSLJ, SLJ and DCB specimens

Three sets of modified single lap joints (MSLJ) each consisting of seven samples were prepared from the 103.6x230x1.6 mm CFRP laminate panels and Redux 322, 300 gsm structural film adhesive as described in Chapter 5. The cured bonded assembly was then cut to size of test specimens using a high-speed diamond bench cutter. Annealed aluminum tabs of 25.4x25.4x1.0 mm dimensions were bonded to the ends of the specimens with a AF-163-2K epoxy film adhesive (supplied by 3M, Singapore) to enable a smooth transfer of load and to prevent any crushing of the laminate in the grip region. A schematic diagram of the MSLJ test specimen is shown in Figure 7.1(a). The mating surfaces of the aluminum end-tabs and composite were abraded using emery cloth and were chemically cleaned with acetone. Most of the specimens had an adhesive layer thickness between 0.3 - 0.5 mm. Three sets of SLJ specimens were also prepared in accordance to ASTM D 1002-01 specifications using the same substrate and adhesive materials for performing fatigue testing. In SLJ joints excess squeezed out adhesive normally took a shape of triangle (see Figure 7.1(b)) at both the ends of overlap.

For acquisition of the fracture mechanics parameters (e.g. D, n, n_1, n_2, G_a and G_{th}, double cantilever beam (DCB) specimens were prepared in accordance with the ASTM D 5528 - 01 standard method as described in Chapter 5. The thickness of the adhesive layer after curing these specimens were measured and found to be in the range 0.3 - 0.5 mm. They were 220 mm long and 25.4 mm wide. A pre-crack of around 60 mm was implanted in the middle of the adhesive layer from one side in the length direction. Aluminium spacers (see Figure 7.2) were bonded to each piano hinge because the MTS wedge grips did not have the facility to close completely, rather it maintained a gap of 3 mm in the locked position.

7.6.3 Constant Rate of Displacement Tests

To calculate the value of maximum strain energy release rate, G_{max} and maximum load per unit width, T_{max} to be applied during the fatigue cycle a few modified single lap joint

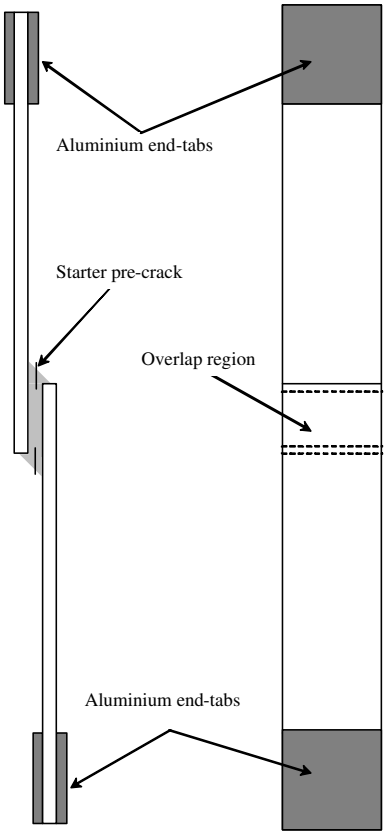

(a) modified single lap joint (MSLJ) test specimen

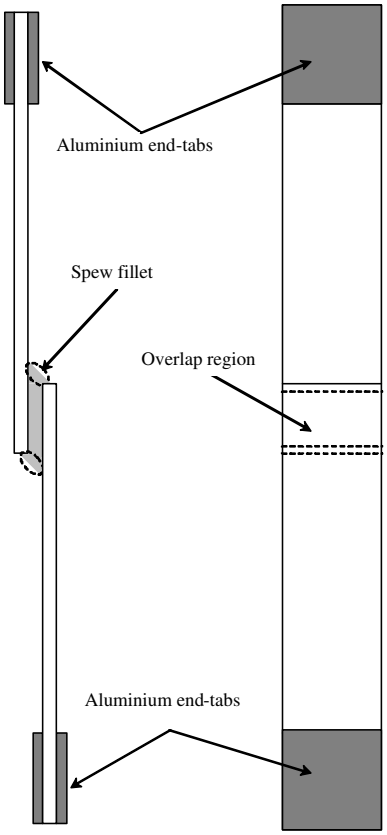

(b) single lap joint (SLJ) test specimen

Figure 7.1: A schematic diagram of the modified single lap joint (MSLJ) and single lap joint (SLJ) test specimen with naturally occurring spew fillet.

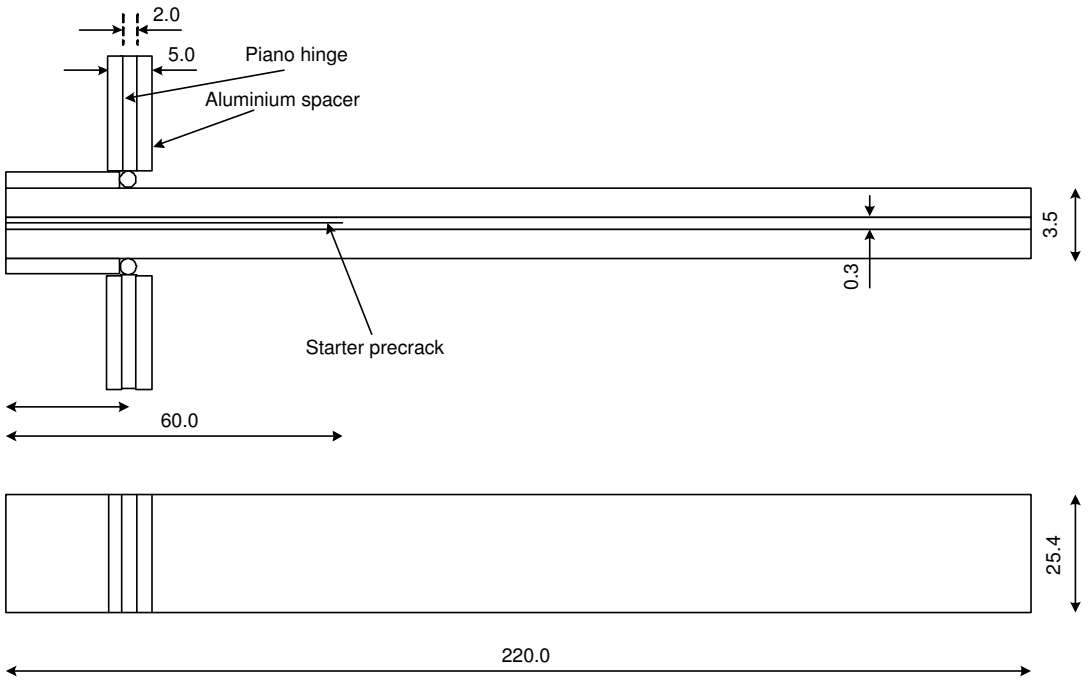

Figure 7.2: A schematic diagram of the double cantilever beam (DCB) test specimen with aluminium spacer bonded to piano hinges.

specimens were tested on a screw driven Instron universal testing machine fitted with a 50 kN load cell at constant rate. Flat face grips were used to hold the specimen and the loading was applied by moving the cross-head under displacement control at a rate of 0.5 mm/min. The specimen was loaded to failure. In addition to MSLJs, some single lap joint specimens (i.e. specimens with naturally occurring spew fillets of adhesive formed at the ends of the overlap) were also loaded and tested in a similar manner as the MSLJ. The failure load of the single lap joint was also measured. A total of three specimens were tested from each type of test specimens and a mean value was calculated. These tests were conducted in "dry" conditions, i.e. at 23 ± 2^0 C and approximately 55 ± 5% relative humidity.

7.6.4 Cyclic Fatigue Tests

MSLJ and SLJ Specimens Testing Procedure

A total of fourteen modified single lap joints (MSLJ) were tested on a servo-hydraulic driven, 810 materials testing system (MTS). The specimen was secured with a pair of 647 series hydraulic wedge grips with flat wedges fitted to the piston. Before securing the specimen, the wedge grips were aligned by holding a steel alignment strip between the grips. After that a specimen was positioned between the grip wedges carefully and hydraulic pressure was applied to the preload chamber. The pressure applied pulled the wedge chamber towards the piston, forcing the wedges to clamp the specimen. The preload chamber locks all moving grip parts in position firmly and thus backlash during cycling is eliminated. The annealed aluminum end-tabs bonded onto the ends of the substrates ensured that the knurled surfaces of the wedge grips bite firmly into the specimen end-tabs, thereby preventing slippage at the grips.The end-tabs also prevented any localized crushing and early failure of substrates in the gripped region by uniformly distributing the gripping pressure. Specimen gripping pressure was adjusted to give a pressure of 8 MPa so that any damage in the specimen or the slippage of specimen could be prevented during the test. The grips provided a constant, hydraulically actuated gripping force regardless of the applied test loads. The grips were aligned properly using aligning bar before loading each specimen. The test machine was run under load control and a tension-tension cyclic load (see Figure 7.3) was applied in sine wave form at a frequency, f, of 5 Hz. The load ratio (T_{min}/T_{max}) was set to 0.5 in all tests. The number of cycles to failure, N_f required to fracture the modified single lap joint was measured as a function of the maximum load per unit width, T_{max} applied during each fatigue cycle. Similar fatigue tests were also conducted on the SLJ test specimens with identical test parameter and environmental conditions and the number of cycles, N_f required to fracture the single lap joints was measured as a function of the maximum load per unit width, T_{max} applied during each fatigue cycle.

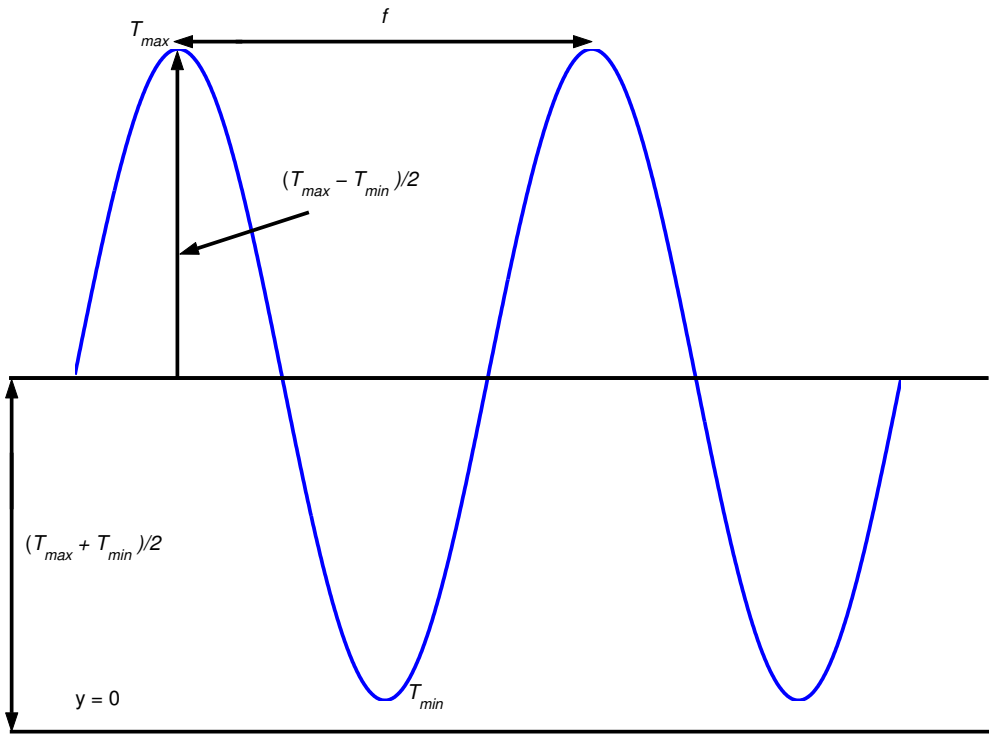

Figure 7.3: Schematic of fatigue load applied in the experimental studies.

DCB specimen testing procedure

DCB specimens were loaded on 810 materials testing system (MTS) equipped with servo-hydraulic testing systems. DCB tests were also performed using sinusoidal waveform at a frequency, f, of 5 Hz and at a displacement ratio of $\delta_{min}/\delta_{max} = 0.5$. A range of maximum displacement values were employed to cover the complete range of applied maximum strain energy release rate, G_{max}. The growth of the crack was monitored by using a travelling microscope at various intervals during the test. From these tests a set of discrete and finite crack length measurements and fatigue cycle count values (i.e., a_i and N_i measurements) were obtained. In addition, the load-displacement data were also collected from the tests. These tests were performed at ambient conditions (i.e., 23 ± 2^0C and $50 \pm 5\%$ relative humidity).

7.7 Results and Discussion

7.7.1 Experimental Observation

The analysis of fracture surfaces of MSLJ and SLJ specimens tested revealed a cohesive failure (i.e., crack propagated via adhesive layer) of joints with little or no sign of interfacial and/or adherend failure. Photographs of fractured surfaces (see Figures 7.4 and 7.5) give clear evidence of cohesive failure in the bonded region of MSLJ and SLJ specimens. The test data (i.e. no. of cycles to failure) obtained from fatigue tests performed on MSLJ and SLJ were analysed by plotting on a semi log scale. When specimens survived for more than one million (10^6) cycles an infinite life was assumed and fatigue tests were terminated. In Figure 7.6, maximum load per unit width (N/m) against number of cycles to failure, N_f, curve is presented. It is noticed that for the same applied maximum load per unit width of the specimen during the fatigue cycling, SLJ specimens survived a higher number of cycles as compared to MSLJ. A curve fit to the MSLJ and SLJ data points revealed a difference in fatigue life of bonded joints as much as around 20%. This observed difference in the fatigue life is almost equal to reported result in a recent paper

by Kinloch and Taylor [5] as shown in Figure 7.7. The disagreement observed in their studies between the experimental and analytical results are about the difference observed in the present MSLJ and SLJ results. This augments the initial presupposition that SLJ made according to ASTM D 1002-01 are likely to over predict the fatigue life because of the presence of naturally occurring spew fillets at the end of the overlap.

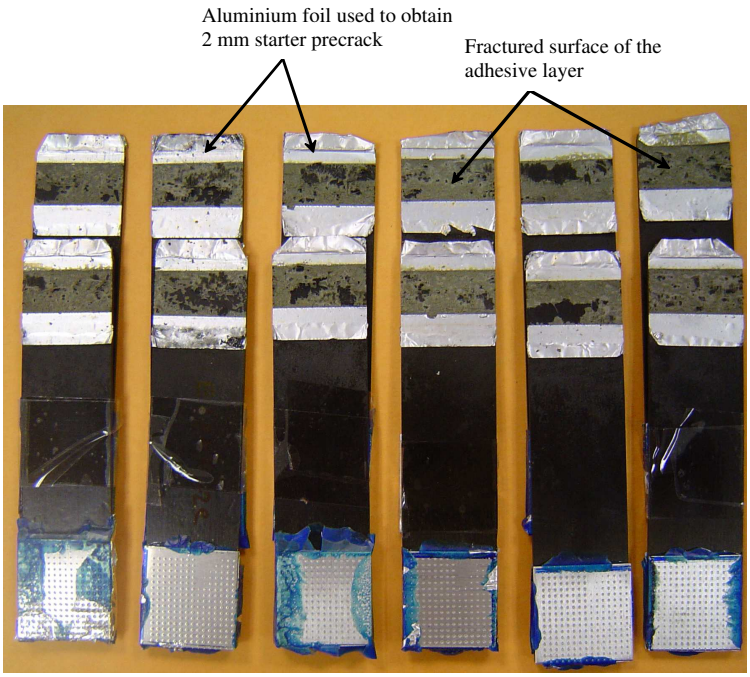

Figure 7.4: Photograph of fractured surfaces of adhesive in the modified single lap joint (MSLJ) test specimen.

7.7.2 Comparison with the Analytical Model

To calculate the fatigue life of adhesively bonded MSLJ configuration analytically the procedure described in this section was followed. The experimental data (i.e., crack length measurements and corresponding number of fatigue cycles) obtained by testing DCB specimens (see Figure 7.8) were analyzed by using the incremental polynomial method as per ASTM E647. It involves estimating the crack growth rate, da/dN by fitting a second order polynomial (i.e. a parabola) to sets of (2g+1) successive data points, where g is usually 1, 2, 3 or 4. In the present work 'g' is assumed to be 3 as recommended

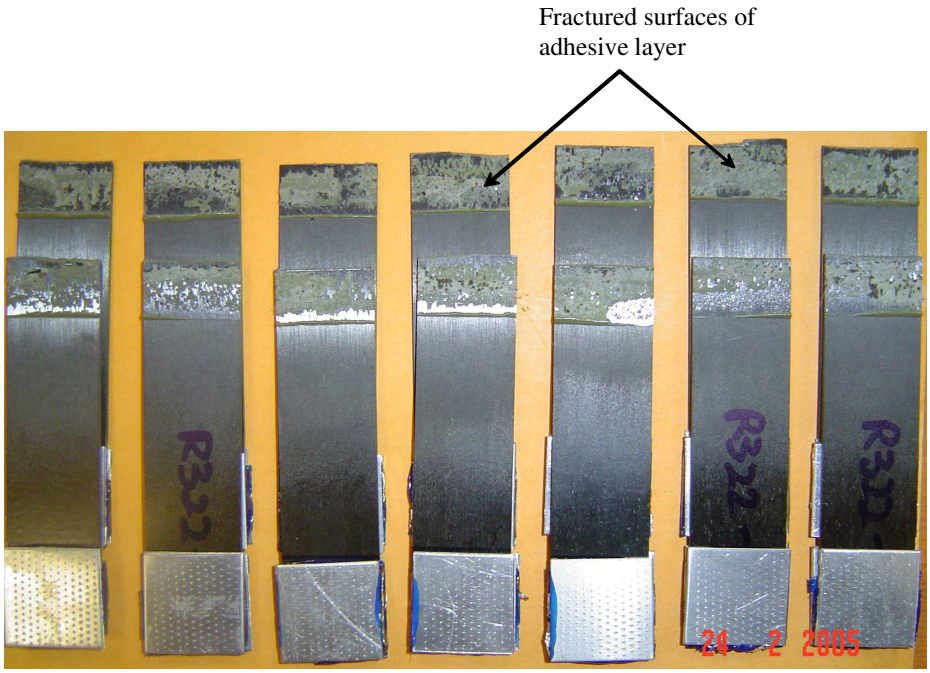

Figure 7.5: Photograph of fractured surfaces of adhesive in the single lap joint (SLJ) test specimen.

by Osiyemi [111]. A quadratic form of equation for the local fit is considered as

$$\hat{a}_i = b_0 + b_1\left(\frac{N_i - C_1}{C_2}\right) + b_2\left(\frac{N_i - C_1}{C_2}\right)^2 \tag{7.7}$$

where

$$-1 \leq \left(\frac{N_i - C_1}{C_2}\right) \leq +1 \tag{7.8}$$

and b_0, b_1, and b_2 are the regression parameters that are determined by the least squares method (i.e. minimization of the square of the deviations between observed and fitted values of crack size) over the range $a_{i-3} \leq a \leq a_{i+3}$. The value $\hat{a}_i$ is the fitted value of crack size at N_i. The parameters $C_1 = 1/2(N_{i-3} + N_{i+3})$ and $C_2 = 1/2(N_{i+3} - N_{i-3})$ are used to scale the input data, thus avoiding numerical difficulties in determining the regression parameters. The rate of crack growth at N_i were obtained from the derivative of the above parabola, which is given by the following expression:

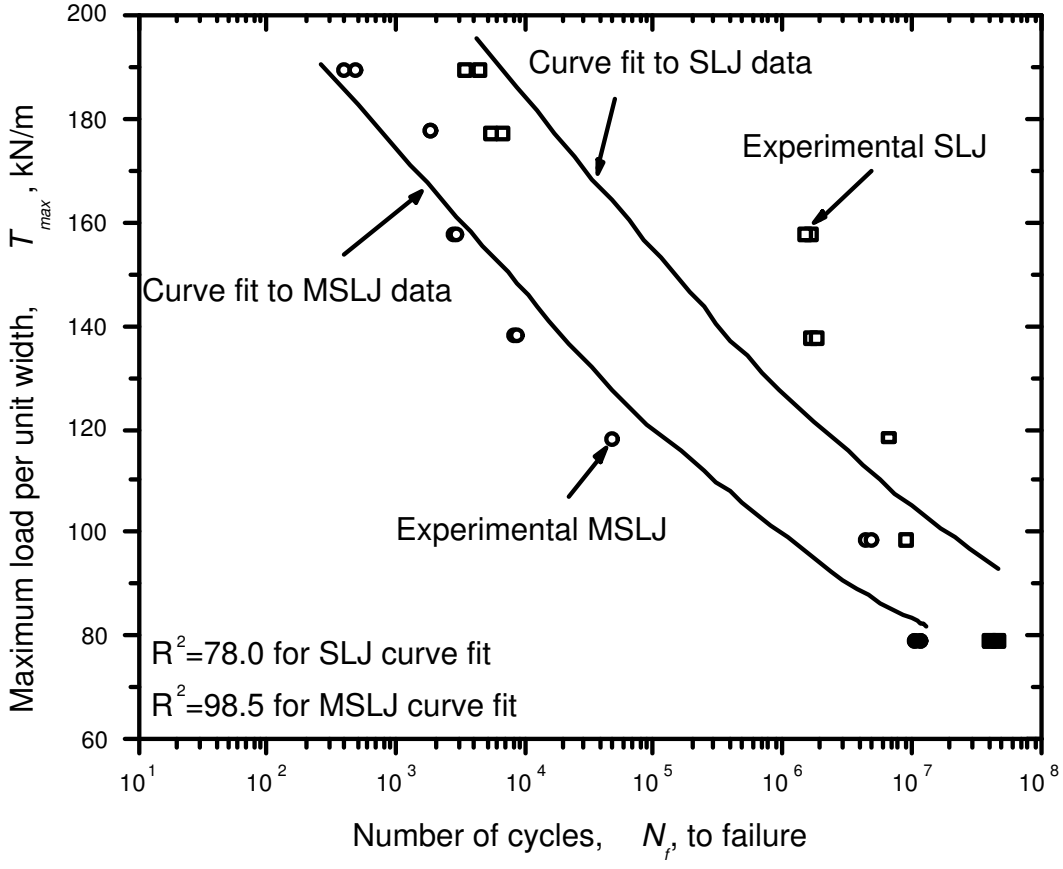

Figure 7.6: Plot of number of cycles to failure, N_f, as a function of the maximum load per unit width, T_{max}, applied during fatigue cycling. The open symbols indicate that joint failed and the filled symbols represent joint did not fail during the testing. The joint which did not fail after about millions of fatigue cycles, an infinite life was assumed. The lines represent curve fitted to the test data.

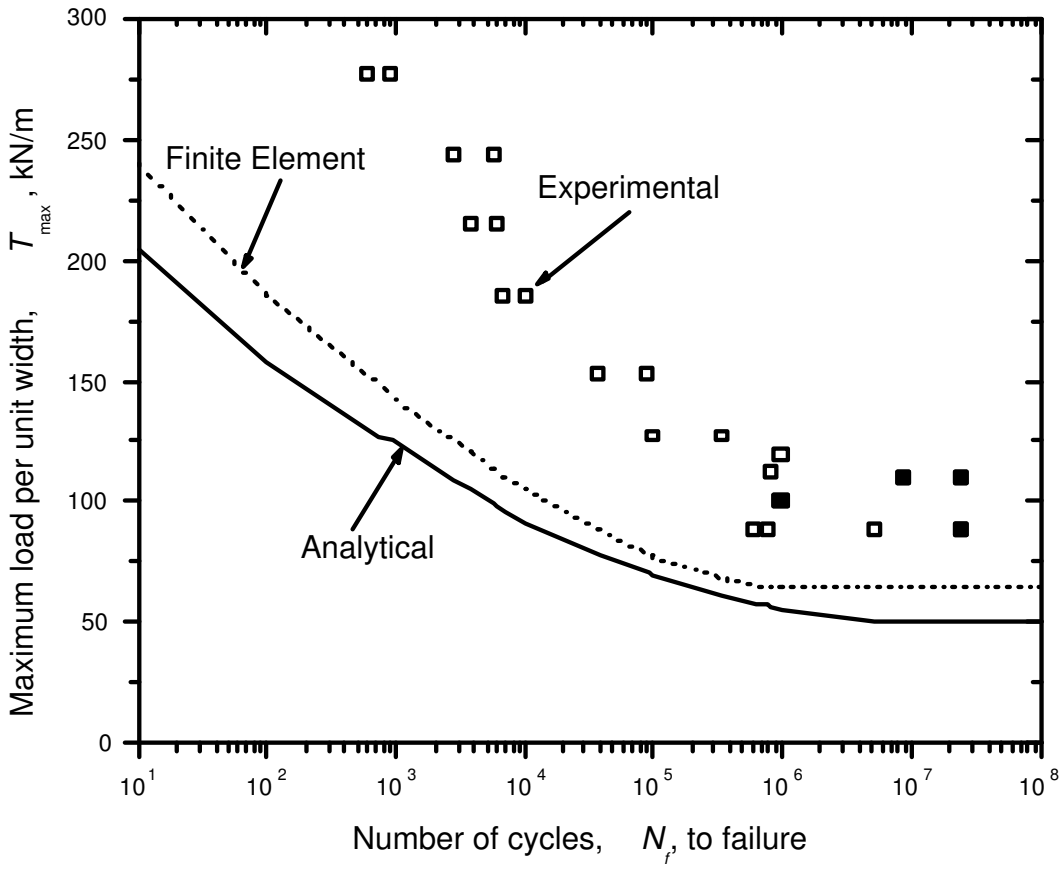

Figure 7.7: The number of cycles to failure, N_f, for the single lap joint as a function of the maximum load per unit width, T_{max}, applied during fatigue cycling. The open symbols indicates the joints that failed and the filled symbols represent joints that did not fail during the testing. The joint which did not fail after about millions of fatigue cycles, an infinite life was assumed. The finite element prediction and analytical results are represented by lines, using $a_0 = 85\mu m$. All the results were taken from Kinloch and Taylor [5].

$$(da/dN)_{\hat{a}_i} = b_1/C_2 + 2b_2(N_i - C_1)/{C_2}^2 \tag{7.9}$$

A computer program was written to obtain the value of da/dN for each data point.

The compliance vs. crack length plot was of obtained from thew experimental data. The maximum strain energy release rate, G_{max} was calculated for each data point using experimental compliance method as described in Chapter 5. A plot of da/dN vs. G_{max} was drawn from experimental data points as shown in Figure 7.9(b). The fracture mechanics parameters (e.g. D, n, n_1, n_2, G_c and G_{th}) were calculated from the da/dN versus G_{max} plot. Firstly, experimental data from the linear portion of the da/dN versus G_{max} plot "Region II" (see Figure 7.9(b)) were fitted with a linear slope of gradient, n and intercept, D. The values of n_1 and n_2 were obtained by fitting the modified Paris equation to the complete experimental data (see Figure 7.9(b)). The values of n_1 and n_2 represent the acuity of the change in the gradient of $\log da/dN$ versus $\log G_{max}$ curve, due to the transition in fatigue data from threshold "Region I" to the linear portion "Region II" and due to the transition in data from the linear "Region II" to the near fast fracture "Region III". The values of n_1 and n_2 were constrained in their range of possible values as suggested by Taylor [183] such that $0.1 \leq n_1, n_2 \leq 10$. The value of n_2 was taken to be equal to that of n_1 [17] as it was not possible to capture data from the near fast fracture region because the crack growth rate is too fast to be measured accurately. Table 7.1 summaries the calculated test parameters. The fractured surfaces observed in the adhesive layer of the DCB joint are shown in Figure 7.10: again cohesive failure in the adhesive layer was noticed. The lower integration limit is the initial flaw size, a_0, and the upper integration limit, a_f of equation (7.4) was calculated from equations (7.5) and (7.6) respectively. Then equation (7.4) was integrated numerically using Simpson's rule which gave the number of cycles to failure. The number of cycles, N_f was represented in terms of the maximum applied load per unit width, T_{max} during the fatigue cycles. The analytical fatigue life values are plotted as T_{max} versus N_f curve, together with experimental results from both MSLJ and SLJ test specimens.

Table 7.1: Values of the Paris law and modified Paris law fitting constants

Property	Symbol and units	Value
Strain energy release rate at threshold	G_{th}, (J/m^2)	56
Mode I adhesive fracture energy	G_a, (J/m^2)	252
Threshold region curve-fitting constant	n_1	10
Fast fracture region curve-fitting constant	n_2	10
Paris Law exponent	n	3.98
Paris Law coefficient	D	9.011×10^{-20}

The analytically predicted fatigue life using MSLJ was compared with the MSLJ test results (see Figure 7.11). It was observed that the results are in good agreement. Moreover the trendline plotted to fit the MSLJ result gives an accuracy level of 98.5%, however the SLJ results gives only 78%. The results clearly demonstrate the usefulness of the new test geometry and proves its superiority. The starter pre-cracks in MSLJ were effective in reducing the scatter in the experimental measurements as compared to SLJ.

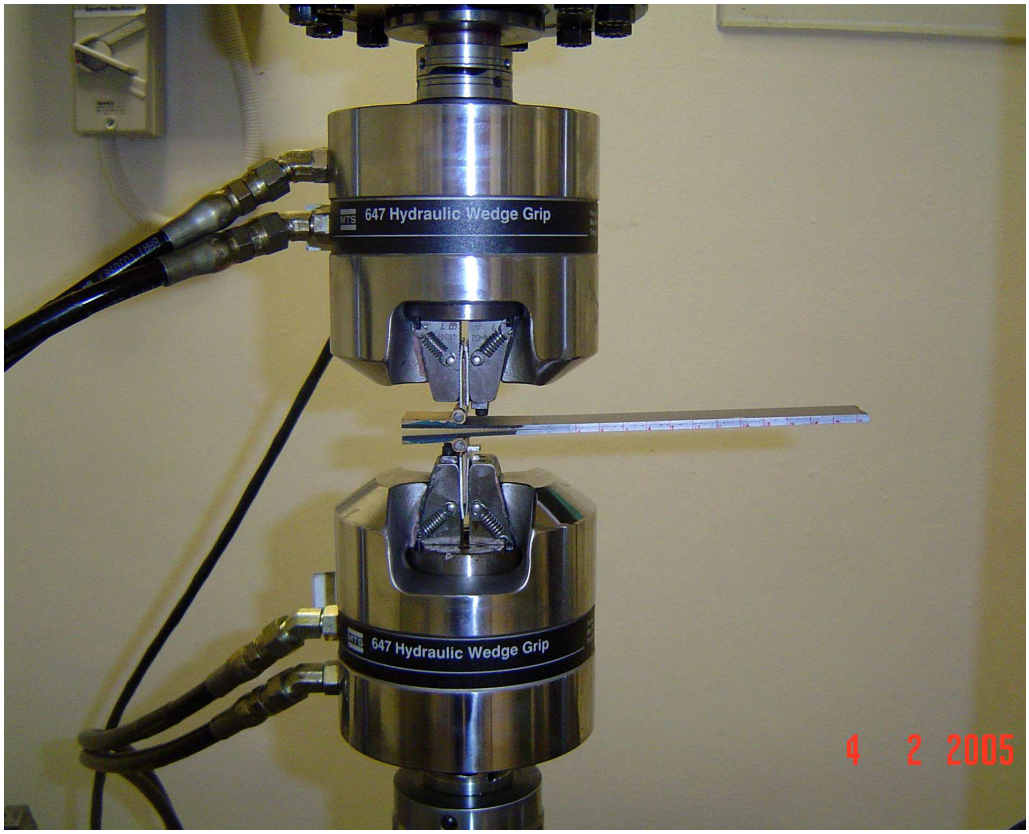

Figure 7.8: Photograph of MTS testing machine with DCB test specimen secured in the hydraulic wedge grip.

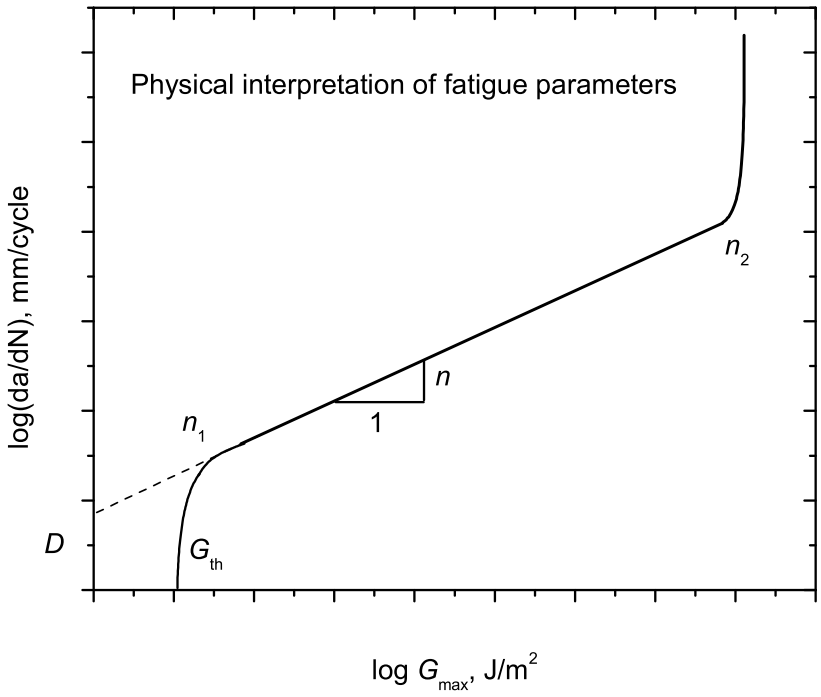

(a) Fracture parameters

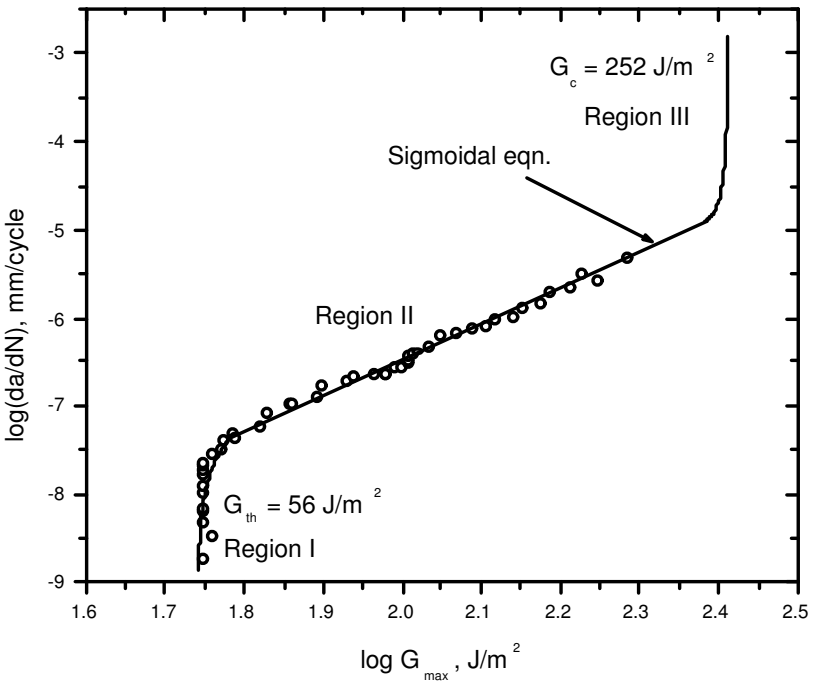

(b) da/dN versus G_{max} curve

Figure 7.9: (a) Physical interpretation of fracture parameters and (b) Variation of G_{max} with crack growth, da/dN for DCB test geometry.

Figure 7.10: Photograph of fractured surfaces of adhesive layer in the double cantilever beam (DCB) test specimen.

7.8 Conclusions

A simple modification was proposed to the single lap joint test geometry and this new test geometry is referred to as modified single lap joint (MSLJ) test geometry. The service life of MSLJ were evaluated analytically using the crack growth rate model. The fatigue life of bonded MSLJ were recorded experimentally and compared with those of SLJ results. Remarkable difference in the fatigue life measurements of SLJ and MSLJ was noticed. This difference in the experimental measurements may be attributed to the spew fillet, which forms during the curing process at the end of the overlap. These experimental results were also compared with analytical results obtained on the basis of fracture mechanics approach. A good agreement between MSLJ experimental results and analytical solution was observed (see Figure 7.11). Thus, it is concluded that the MSLJ test geometry is superior to the conventional SLJ test geometry and can be employed to perform various type of studies related to the bonded joints/components.

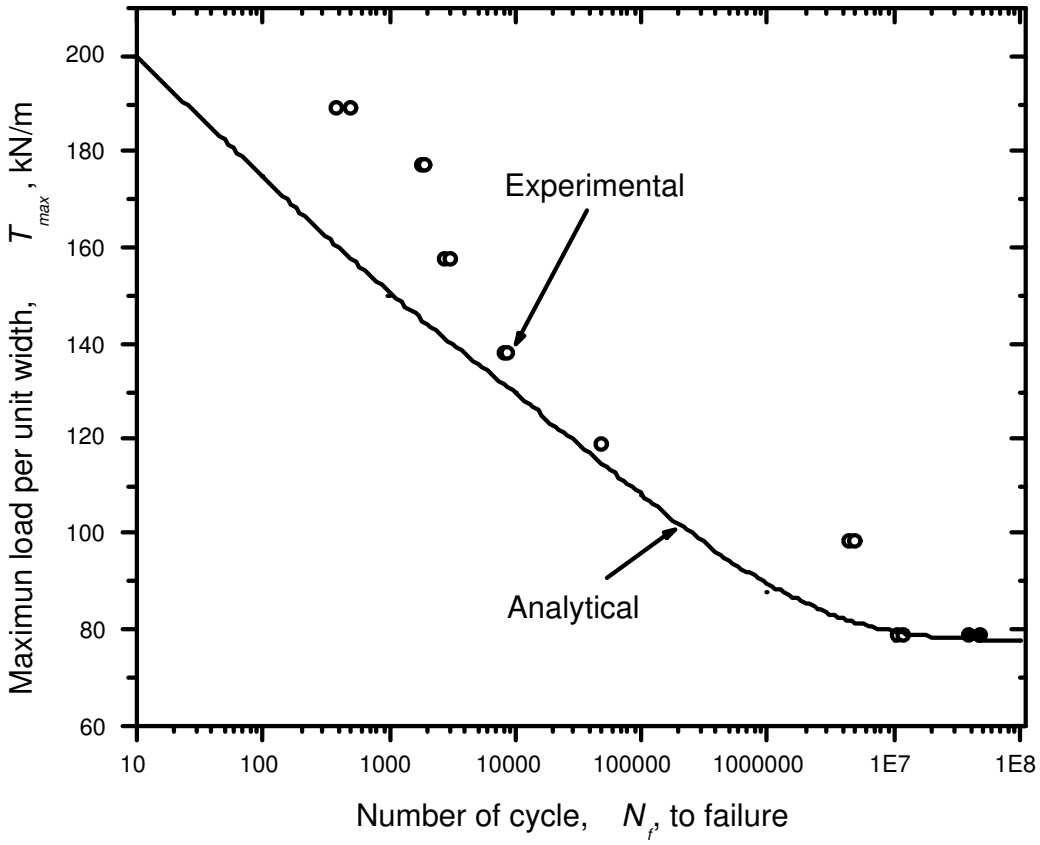

Figure 7.11: The number of cycles to failure, N_f, as a function of the maximum load per unit width, T_{max}, applied during fatigue cycling for the modified single lap joint. The open symbols indicates that the joints failed and the filled symbols represent joint did not fail during testing. The joints which did not fail after about millions of fatigue cycles, an infinite life was assumed. The analytical result is represented by a line, using $a_0 = 82\mu m$.

Chapter 8

Conclusions and Recommendations

8.1 Conclusions

On the basis of the research work reported in the previous chapters the following conclusions are drawn:

1. Quasi static uniaxial compression tests (i.e., constant rate of displacement tests) were performed on the adhesively-bonded scarf joints comprising unidirectional carbon fibre reinforced polymer (CFRP) laminate adherends and "AF-163-2" structural film adhesive. The tests showed that the compressive strength of the joints increased as the scarf angle decreased. The failure mechanisms switched from predominantly fiber microbuckling (Mode A_c) for joints with scarf angles below 3^0, to cohesive shear deformation through the adhesive layer coupled with some traces of attendant fiber microbuckling (Mode B_c) for joints with scarf angles above 3^0. The compressive strengths of the scarf joints reduced by $20-50\%$ below the value of the infinite band collapse response in compression. The experimental results compare well with numerical predictions. In FE analysis unidirectional composite substrate was model as a homogeneous orthotropic continuum material. The adhesive film was assumed to be an elastic-plastic solid perfectly-bonded to the composite laminate.

2. The investigation of adhesively bonded unidirectional CFRP scarf joints in uniaxial tensile loading revealed two main failure modes: (i) failure predominantly by fibre fracture and pull-out (Mode A_t), and (ii) failure predominantly by cohesive shear in

adhesive film (Mode B_t). Mode A_t was observed for scarf angles less than about 2^0, while Mode B_t was observed for scarf angles greater than 2^0. A consistent pattern of failure mode that switched from Modes A_t to B_t as the scarf-joint angle increases from $0^0 - 5^0$ was observed. A clear scarf angle effect was noticed with smaller (i.e. shallow) scarf angles yielding higher tensile joint strengths in comparison to those with larger scarf angles. The knockdown in tensile strength was most prominent for scarf angles less than about 1^0. The adhesively-bonded joint with scarf-angles of 1^0 or lower (symbolizing a small imperfection in long fiber composites) caused a knockdown in tensile strength of a unidirectional CFRP composite by as much as 60%. For the specimen with the largest scarf-angle of 5^0 used in the present experiments, the tensile strength dropped by 89%. The knockdown in tensile strength with increasing scarf-angle was well described by FE predictions.

3. Experimental studies were performed on a new test geometry referred to as modified single lap joint (MSLJ) to measure the adhesive fracture energy of adhesively bonded composite joints. The MSLJ was made by implanting two end pre-cracks within the middle of the bond line in a conventional SLJ. In addition tests were also conducted on SLJ and double cantilever beam (DCB) specimens made from the same composites and adhesives configuration. The SLJ joints made form Redux 322, 335K and 319A film adhesives gave mean values of adhesive fracture energy 434 J/m^2, 847 J/m^2 and 358 J/m^2 respectively; whereas the MSLJ geometry measured mean values of 252 J/m^2, 408 J/m^2 and 150 J/m^2 respectively. The adhesive fracture energy measured using MSLJ and DCB test geometry is in good agreement. The standard deviation data revealed that there was a reduction in scatter of the results by as much as 30-60% when the MSLJ specimens were used in place of the SLJ to estimate the fracture energy of the joints. Thus, the results from this investigation showed that the KO-model is a valid model for the estimation of the mode I fracture energy of the adhesive in a MSLJ. These results are especially useful in the critical design of structural components for aerospace and defense ap-

plications as a typical design engineer can use the value of G_a obtained from the model to design for how long an adhesively bonded joint will last when subjected to external stresses. In addition, by using the KO-model, industrial manufacturers of adhesives may, in future, be able to include details on the fracture properties of adhesives in their product specification.

4. The following conclusions are drawn from the investigation of moisture absorption effect on bulk adhesive, substrates and bonded joints:

   (i) Bulk adhesive

   (a) The weight gain in the bulk adhesive increased linearly with $\sqrt{t}$ in the beginning and reached a plateau (5.5 % weight gain) after about 2500 hr of exposure; (b) the dimensional changes in length and width of the bulk adhesive were about the same with a maximum of around 1.1 %; (c) In the thickness direction the dimensional change was approximately twice that in the width and the length directions; (d) an initial increase followed by a drop was observed in the tensile strength and the tensile modulus of bulk adhesive; (e) the Poisson's ratio was more or less insensitive to the exposure time.

   (ii) Composite substrate/adherend

   (a) The weight gain experiment on the substrate material showed that the gain in weight increased linearly with $\sqrt{t}$ throughout the experiment and the time of exposure was not sufficient to reach the plateau; (b) the composite laminate tested in water immersion experiment showed a maximum of 1.3% weight gain and a highest expansion of around 2.4 % was observed in thickness direction after some 4000 h of exposure; (c) the longitudinal tensile strength of aged composite reduced by about 28% as compared to the dry composite; (d) the transverse tensile strength reported a marginal decrease with exposure time and all other properties were almost insensitive within the experimental scatter for the exposure period considered in this investigation; (e) the Poisson's ratio of the composite laminate was also more or less insensitive to the

exposure time.

(iii) Bonded joints

(a) In the adhesive sandwiched between two substrates, most of the water weight gain occurred in the first few weeks of the exposure time; (b) sandwiched adhesive absorbed more moisture (6.5% by weight) as compared to bulk adhesive (around 5.5% by weight); (c) in case of adhesive layer sandwiched between the two substrates the plateau was reached much earlier (only after about 625 hr of exposure) than that of the bulk adhesive; (d) the adhesive fracture energy increased to twice that of dry conditions in the beginning of the exposure period and after around 84 days of exposure some degradation occurred in the properties and fracture energy decreased. Both DCB as well as MSLJ results showed a similar trend. Thus, it can be concluded that the modification is effective and useful for accurately predicting the mechanical properties of the bonded systems; (e) the shear strength and the shear modulus of bonded joints showed a decreasing pattern throughout the exposure period.

5. Fatigue tests (i.e., tension-tension cyclic loading tests) were performed on modified single lap joint (MSLJ), conventional single lap joint and double cantilever beam (DCB) test specimens. The fatigue life of MSLJ and SLJ were recorded by performing cyclic tests for a range of maximum nominal stress ranging from 30 to 90% of the average initial value, obtained from the constant displacement rate tests. In addition, the fatigue life of MSLJs was calculated analytically using a crack growth rate model. In this method the fracture mechanics parameters obtained from cyclic tests on DCB test specimens were used. The experimental and analytical results were analyzed by plotting maximum load per unit width, T_{max} against the Number of cycles to failure, N_f. A remarkable difference in the fatigue life measurements of SLJ and MSLJ was noticed. This difference in experimental measurements may be attributed to the spew fillets, which form during the curing process at the end of the overlap. The MSLJ test specimens survived less number of fatigue cycles

because the starter pre-crack at both ends of the overlap circumvented the effect of spew fillets and the crack propagated without any hindrance from the tip of the starter pre-crack. The experimental results were also compared with analytical results obtained on the basis of a fracture mechanics approach (i.e., crack growth rate model). A good agreement between the MSLJ experimental results and the analytical solution was observed. Thus, it was concluded that the MSLJ test geometry is effective and superior to that of the conventional SLJ test geometry in many respect for varieties of studies related to the bonded joints/components.

8.2 Recommendations for Future Research Scope

1. In Chapter 3, an attempt was made to understand the uniaxial compressive and tensile behavior of bonded scarf joint comprising unidirectional carbon fibre reinforced polymer (CFRP) laminate and aerospace grade "AF-163-2" structural film adhesive. It has enhanced the current understanding of compressive failure mechanisms of scarf joints made from unidirectional composites. Having developed a good understanding of the subject matter it was felt that the effect of bondline thickness and surface pretreatment on the joint performance would provide information for design of bonded joints. Thus, a study of the compressive behavior of adhesively-bonded scarf joints with various adhesive layer thickness and surface pretreatment methods is recommended. The effect of interface debond length in the bonded region on compressive and tensile failure is recommended. For a scarf joint under tensile loading conditions, a mode-II toughness expression can be derived and its value be measured experimentally. The mode toughness may be compared with shear lap joint, which gives a pure mode-II toughness.

2. Adhesive fracture energy, G_a can be calculated using numerical simulations of MSLJ with material properties of substrate and adhesive in the present research work and compared with the experimental measurements. The effect of surface

pretreatment (surface roughness variation) and bondline thickness variation on joint strength and adhesive fracture energy can be studied with MSLJ as it may be a good research direction. The effect of substrate thickness on stress distribution in the overlap region of MSLJ will also be a good research area.

3. Effort was put to demonstrate the capability of the new test geometry in studying the effect of moisture absorption on the fracture mechanics parameter (mode-I adhesive fracture energy) as described in Chapter 6. Good correlations was observed between the results of the new test geometry (MSLJ) and the existing test geometry (DCB). On the basis of the test results obtained in Chapter 6, it is recommended that the MSLJ be used instead of SLJ to evaluate the effect of moisture on the mechanical behavior of the bonded joints. The study of the effect of moisture by changing the bonded parameters such adhesives, surface pre-treatment process, adhesive layer thickness is also recommended.

4. In Chapter 7, with limited tests an attempt was made to illustrate the usefulness of the MSLJ test geometry by measuring the fatigue life of adhesively bonded joints made from unidirectional carbon fiber reinforced polymer (CFRP) and an aerospace grade Redux 322 film adhesive at ambient conditions. It is recommended that this MSLJ test geometry be used to obtain endurance limit curves for bonded joints with different substrate and adhesive systems. The effect of fatigue cycle parameters (e.g., load ratio, frequency, mean stress, etc.) on fatigue life can be accurately evaluated by employing this test geometry. It is also recommended that the new test geometry be employed to study the fatigue life of bonded joints in hostile environments such as water, high temperature, etc.

Publications

Journal papers

[1] S. B. Kumar, S. Sivashanker, Asim Bag, and I. Sridhar "Failure of Aerospace Composite Scarf Joints under Uniaxial Compression" *Materials Science & Engineering A*, 412:117-122, 2005.

[2] S. B. Kumar, I. Sridhar, S. Sivashanker, S. O. Osiyemi and Asim Bag "Tensile Failure of Adhesively Bonded CFRP Composite Scarf-Joints" *Materials Science & Engineering B* (online available from March 30, 2006).

[3] S. B. Kumar, I. Sridhar, S. Sivashanker and S. O. Osiyemi "The Determination of Adhesive Fracture Energy with a Novel Modification to the SLJ Test Geometry" *Journal of Adhesion Science & Technology* (accepted for publication).

[4] S. B. Kumar, I. Sridhar and S. Sivashanker "Predicting Fatigue Life of Bonded Composite Joints with Modified Single Lap Joint (MSLJ) " *International Journal of Adhesion and Adhesives* (under review).

Appendix A

A.1 Constitutive failure model

This appendix summarizes Hashin and Lee's [171, 172] failure criteria for a composite laminate. Hashin [171] identified four lamina failure modes, namely fiber tension, fiber compression, matrix tension and matrix compression in composite laminates (see equations (A.1) - (A.4) as described below in terms of σ_{11}, σ_{22}, σ_{33}, σ_{12}, σ_{13} and σ_{23}, where σ_{ij} represents stress in tensor notation). Later on Lee [172] extended Hashin's argument to include delamination effects in unidirectional composites (see equation (A.5)).

Fiber tension failure (for $\sigma_{11} > 0$):

$$(\frac{\sigma_{11}}{{\sigma_f}^+})^2 + \frac{1}{\tau_f^2}({\sigma_{12}}^2 + {\sigma_{13}}^2) = 1 \tag{A.1}$$

Fiber compression failure (for $\sigma_{11} < 0$):

$$(\frac{\sigma_{11}}{\sigma_f^-}) = 1 \tag{A.2}$$

Matrix tension failure (for $\sigma_{22} > 0$):

$$\frac{1}{{\sigma_m}^{+2}}(\sigma_{22} + \sigma_{33})^2 + \frac{1}{{\tau_m}^2}({\sigma_{23}}^2 + \sigma_{22}\sigma_{33}) + \frac{1}{{\tau_m}^2}(\sigma_{12}^2 + \sigma_{13}^2) = 1 \tag{A.3}$$

Matrix compression failure (for $\sigma_{22} < 0$):

$$\frac{1}{{\sigma_m}^{-2}}((\frac{{\sigma_m}^{-2}}{2\tau_m})^2 - 1)(\sigma_{22}+\sigma_{33}) + \frac{1}{4{\tau_m}^2}(\sigma_{22}+\sigma_{33})^2 + \frac{1}{{\tau_m}^2}({\sigma_{23}}^2 + \sigma_{22}\sigma_{33}) + \frac{1}{{\tau_f}^2}(\sigma_{12}^2+\sigma_{13}^2) = 1 \tag{A.4}$$

Delamination:

$$(\frac{\sigma_{33}}{\sigma_m^+}) + \frac{(\sigma_{12}^2 + \sigma_{13}^2)}{{\sigma_m^+}^2} = 1 \tag{A.5}$$

where ${\sigma_m}^+$ is the matrix tensile failure strength, ${\sigma_m}^-$ is the matrix compressive failure strength, τ_m is the matrix shear failure strength, ${\sigma_f}^+$ is the fiber tensile failure stress, ${\sigma_f}^-$ is the fiber compressive failure stress, τ_f is the fiber shear failure stress.

Appendix B

B.1 Material Properties Data

This appendix summarizes material properties data for bonded joints, composite substrate and adhesive material for complete moisture aging experiments. Table B.1 summaries mode I adhesive fracture energy of MSLJ and DCB joints. The mechanical properties of base composites such as longitudinal tensile strength (LTS), σ^t_{11}, transverse tensile strength (TTS), σ^t_{22}, in-plane shear strength (IPSS), σ_{12}, longitudinal tensile modulus (LTM), E^t_{11}, transverse tensile modulus (TTM), E^t_{22}, in-plane shear modulus (IPSM), G_{12}, and Poisson's ratio (PR), ν_{12} of the composite material are summarized in Table B.2 with its standard deviation.

The mechanical properties of the cured adhesive were obtained by testing the specimens extracted from cured adhesive panel and exposing to the distilled water medium in the identical conditions as substrate/MSLJ/DCB specimens. Tensile strength (TS), shear strength (SS), tensile modulus (TM), shear modulus (SM) and Poisson's ratio (PR) of the cured adhesive material were evaluated. Summary of all these properties is given in Table B.3.

Table B.1: Summary of test results for MSLJ and DCB with for the three adhesives (i.e. Redux 322, 335K and 319A) tested

Exposure time (days)	MSLJ		DCB	
	Adhesive fracture energy $G_a(J/m^2)$	Standard deviation (J/m^2)	Adhesive fracture energy $G_a(J/m^2)$	Standard deviation (J/m^2)
0	252	25	250	21
28	461	57	459	26
56	481	48	478	33
84	482	58	479	33
112	452	30	436	27
140	339	24	330	25
168	240	31	221	24

Table B.2: Summary of mechanical properties of composites under dry and aged conditions

Exposure time (days)	LTS, S_{11} (MPa)	TTS, S_{22} (MPa)	IPSS, S_{12} (MPa)	LTM, E_{11} (GPa)	TTM, E_{22} (GPa)	SM, G_{12}	PR,ν_{12}
0	1800 ± 188	48 ± 4	186 ± 20	140 ± 8	8.0 ± 0.75	12.0 ± 1.5	0.35 ± 0.002
28	1308 ± 101	45 ± 3	181 ± 30	130 ± 7	7.8 ± 0.75	11.0 ± 1.2	0.24 ± 0.005
56	1326 ± 64	45 ± 2.5	250 ± 25	120 ± 10	7.7 ± 0.64	13.8 ± 1.5	0.34 ± 0.001
84	1356 ± 280	43 ± 6	200 ± 50	123 ± 8	7.5 ± 0.50	12.0 ± 1.3	0.35 ± 0.005
112	1357 ± 182	43 ± 10	160 ± 35	125 ± 6	7.5 ± 0.55	11.6 ± 1.3	0.36 ± 0.007
140	1380 ± 88	42.5 ± 3	140 ± 60	130 ± 6	7.0 ± 0.20	10.0 ± 2.0	0.36 ± 0.008
168	1472 ± 178	40 ± 4	150 ± 50	126 ± 5	7.6 ± 0.30	13.0 ± 3.0	0.36 ± 0.007

Table B.3: Summary of mechanical properties of adhesive under dry and aged conditions

Exposure time (days)	TS, S (MPa)	SS, S_{12} (MPa)	TM, E (GPa)	SM, G (GPa)	PR, ν
0	41 ± 1.53	18 ± 3.0	4.08 ± 0.4	1.3 ± 0.03	0.44 ± 0.009
28	55 ± 2.5	14 ± 4.0	4.8 ± 0.5	1.3 ± 0.09	0.42 ± 0.005
56	62 ± 3.6	13 ± 2.0	5.0 ± 0.8	1.3 ± 0.04	0.43 ± 0.008
84	65 ± 3.0	12 ± 1.2	5.1 ± 0.6	1.2 ± 0.049	0.44 ± 0.006
112	49 ± 4.0	13 ± 1.5	4.2 ± 0.6	1.1 ± 0.06	0.43 ± 0.005
140	39 ± 2.0	12 ± 1.6	3.9 ± 0.3	1.1 ± 0.057	0.42 ± 0.003
168	30 ± 4.5	12 ± 1.2	3.5 ± 0.5	1.0 ± 0.05	0.43 ± 0.002

References

[1] http://engineers.ihs.com/pdf/litcenter/444.pdf. Composites in aerospace applications, 2005.

[2] S.K. Mazumdar. *Composites Manufacturing, Materials, Product, and Process Engineering*. CRC Press LLC, Florida, 2002.

[3] http://www.msm.cam.ac.uk/phase trans/2001/stef/img11.htm. Composites for aerospace applications by stefanie feih, 2005.

[4] O. Volkerson. Die nietkraftverteilung in zugbeanspruchten mit konstanten laschenquerschritten mit konstanten laschenquerschritten. *Lufrfahrtforschung*, 15:41–47, 1938.

[5] A.J. Kinloch and A.C. Taylor. The use of fracture mechanics techniques to predict the service life of adhesive joints. In D.R. Moore, editor, *The Application of Fracture Mechanics to Polymers, Adhesives and Composites*, ESIS Publication 33, pages 187–192. Elsevier Ltd, UK, 2004.

[6] R.W. Messler Jr. *Joining of materials and structures from pragmatic process to enabling technology*. Elsevier Butterworth-Heinemann, Burlington, MA 01803, USA, 2004.

[7] http://www.astm.org/. American society for testing and materials, 2004.

[8] http://www.bsi global.com. British standards institute, 2004.

[9] http://www.cenorm.be/catweb. European standards, 2004.

[10] http://www.iso.ch/iso/ISOOnline. International standards organisation, 2004.

[11] K.L. DeVries and P.R. Borgmeier. *Handbook of adhesive technology*. Marcel Dekker, Inc., second edition, 2003.

[12] E.W. Petrie. *Handbook of adhesives and sealants*. McGraw-Hill, USA, 2000.

[13] A.J. Kinloch. *Adhesion and adhesives: science and technology*. Chapman and Hall Ltd, London, 1987.

[14] R.D. Adams, J. Comyn, and W.C. Wake. *Structural adhesive joints in engineering*. Marcel Dekker, Inc., second edition, 1997.

[15] ASTM D1002. *Standard test method for apparent shear strength of single lap joint adhesively bonded metal specimens by tension loading (metal-to-metal)*, 2001.

[16] A.J. Kinloch and S.O. Osiyemi. Predicting the fatigue life of adhesively-bonded joints. *Journal of Adhesion*, 43:79–90, 1993.

[17] H. Hadavinia, A.J. Kinloch, M.S.G. Little, and A.C. Taylor. The prediction of crack growth in bonded joints under cyclic-fatigue loading ii. analytical and finite element studies. *International Journal of Adhesion and Adhesives*, 23(6):463–471, 2004.

[18] H. Hadavinia, A.J. Kinloch, M.S.G. Little, and A.C. Taylor. The prediction of crack growth in bonded joints under cyclic-fatigue loading I. experimental studies. *International Journal of Adhesion and Adhesives*, 23(6):449–461, 2003.

[19] A.J. Curley, H. Hadavinia, A.J. Kinloch, and A.C. Taylor. Predicting the service-life of adhesively-bonded joints. *International Journal of Fracture*, 103(1):41–69, 2000.

[20] L. Tong and G.P. Steven. *Analysis and design of structural bonded joints*. Kulwer Academic Publishers, 1999.

[21] G.B. Portelli. *Structural adhesives: chemistry and technology*, chapter 9. Plenum Press, New York, USA, 1986.

[22] Y. Frostig, O.T. Thomsen, and F. Mortensen. Analysis of adhesive-bonded joints, square-end, and spew-fillet - high-order theory approach. *Journal of Engineering Mechanics*, 125(11):1298–1307, 1999.

[23] T.P. Lang and P.K. Mallick. Effect of spew geometry on stresses in single lap adhesive joints. *International Journal of Adhesion and Adhesives*, 18(3):167–177, 1998.

[24] M.Y. Tsai and J. Morton. Effect of a spew fillet on adhesive stress distributions in laminated composite single-lap joints. *Composite Structures*, 32(1-4):123–131, 1995.

[25] http://composite.about.com/Airbus A3XX Makes Extensive Use of Composites.htm. Airbus A3XX makes extensive use of composites, 2006.

[26] http://www.airbus.com/en/aircraftfamilies/a350/advanced materials.html. Airbus aircraft families-the all-new A350-advanced materials, 2006.

[27] H.F. Brinson. *Engineered Materials Handbook*, volume 3. ASM International, 1990.

[28] D.A. Dillard and A.V. Pocius, editors. *The mechanics of adhesion*. Adhesion Science and Engineering-1. Elsevier Science B.V., Amsterdam, Netherlands, 2002.

[29] N. Tsuji and K. Kubomura. Non-linear compression stress-strain curve of pitch-based high modulus carbon fibre composites and structural responses. *Journal of Materials Science*, 27:3782–3788, 1992.

[30] S.W. Yurgartis and S.S. Sternstein. Micrographic study of bending failure in five thermoplastic-carbon fibre composite laminates. *Journal of Materials Science*, 23(9):1861–1870, 1988.

[31] C.R. Sculthesiz and A.M. Waas. Compressive failure of composites, part i: Testing and micromechanical theories. *Progress in Aerospace Science*, 32:1–42, 1996.

[32] A.M. Waas and C.R. Sculthesiz. Compressive failure of composites, part ii: Experimental studies. *Progress in Aerospace Science*, 32:43–78, 1996.

[33] B. Budiansky and N.A. Fleck. Compressive failure of fibre composites. *Journal of Mechanics and Physics of Solids*, 41(1):183–211, 1993.

[34] B. Budiansky and N.A. Fleck. Compressive kinking of fibre composites: A tropical review. *Applied Mechanics Reviews*, 47(6):S246–S250, 1994.

[35] P.M. Jelf. *Compressive failure of aligned fibre composites*. PhD thesis, Cambridge University Engineering Department, England, 1992.

[36] C. Soutis. *Compressive failure of notched carbon fibre-epoxy panels*. PhD thesis, Cambridge University Engineering Department, England, 1989.

[37] C. Soutis and F.Z. Hu. Failure analysis of scarf-patch-repaired carbon fiber/epoxy laminates under compression. *AIAA Journal*, 38(4):737–740, 2000.

[38] C. Soutis and F.Z. Hu. 3-d failure analysis of scarf patch repaired cfrp plates. In *Collection of Technical Papers - AIAA/ASME/ASCE/AHS/ASC Structures, Structural Dynamics & Materials Conference*, volume 3 of *AIAA-98-1943*, pages 1971–1977. 1998.

[39] H. Hamada, N. Oya, K. Yamashita, and Z. Maekawa. Tensile strength and its scatter of unidirectional carbon fibre reinforced composites. *Journal of Reinforced Plastics and Composites*, 16(2):119–130, 1997.

[40] M. Fuwa, A.R. Bunsell, and B. Harris. Tensile failure mechanisms in carbon fibre reinforced plastics. *Journal of Materials Science*, 10:2062–2070, 1975.

[41] Z. Qian and A.R. Akisanyna. An experimental investigation of failure initiation in bonded joints. *Acta Materialia*, 46(14):4895–4904, 1998.

[42] H. Sasaki and A. McArthur. Improving scarf joint strength. *Forest Products Journals*, 23(5):37–39, 1973.

[43] D. Liu and N.A. Fleck. Scale effects in the initiation of cracking of a scarf joint. *International Journal of Fracture*, 95(1-4):67–88, 1999.

[44] D.D. Brink, C.G. Levi, A.C.F. Cocks, and F.A. Leckie. The role of scarf angle in the performance of aluminum matrix composite joints. *Acta Materialia*, 45(7):2765–2775, 1997.

[45] S.C. Pradhan, N.G.R. Iyengar, and N.N. Kishore. Elasto-plastic analysis of adhesively bonded joints. *Mechanics Research Communications*, 20(2):155–163, 1993.

[46] D.M. Gleich, M.J.L. Van Tooren, and P.A.J. De Haan. Shear and peel stress analysis of an adhesively bonded scarf joint. *Journal of Adhesion Science and Technology*, 14(6):879–893, 2000.

[47] D.M. Gleich, M.J.L. van Tooren, and P.A.J. de Haan. Shear and peel stress analysis of an adhesively bonded scarf joint. *Journal of Adhesion Science and Technology*, 14(6):879–893, 2000.

[48] A.B. Macander and D.R. Mulville. Failure analysis of an adhesively bonded graphite composite/steel scarf joint. *Journal of Engineering Materials and Technology, Transactions of the ASME*, 100(1):64–69, 1978.

[49] S. Marcolefas, V. Kostopoulos, and S.A. Paipetis. Non-linear analysis of a metal-to-composite scarf joint. *International Journal of Mechanical Sciences*, 33(12):961–973, 1991.

[50] D.W. Adkins and R.B. Pipes. End effects in scarf joints. *Composites Science and Technology*, 22:209–221, 1985.

[51] D.W. Adkins and R.B. Pipes. Tensile behavior of bonded scarf joints between composite adherends. In *Proceedings of the Fourth Japan-U.S. Conference on Composite Materials*, pages 845–854, Washington, D.C., USA, 27-29 June 1988 1989.

[52] M.N. Charalambides, R. Hardouin, A.J. Kinloch, and F.L. Matthews. Adhesively-bonded repairs to fibre-composite materials I: Experimental. *Composites Part A*, 29A:1371–1381, 1998.

[53] M.N. Charalambides, A.J. Kinloch, and F.L. Matthews. Adhesively-bonded repairs to fibre-composite materials II: Finite element modelling. *Composites Part A*, 29A:1383–1396, 1998.

[54] A.A. Baker, R.J. Chester, and G.R. Hugo. Scarf repairs to graphite/epoxy aircraft components. In *National Conference Publication - Institution of Engineers, Australia*, volume 1 of *93 pt 6*, pages 193–197, 1993.

[55] J.L. Lubkin. Theory of adhesive scarf joints. *ASME Transactions Journal of Applied Mechanics*, 24:255–260, 1957.

[56] J.M. Emerson and A.J. Fawcett. Scarf repair of heavily loaded cfrp-to-metal joints. In *International SAMPE Technical Conference, SAMPE 2004*, pages 3307–3321, 2004.

[57] R.A. Odi and C.M. Friend. An improved 2d model for bonded composite joints. *International Journal of Adhesion and Adhesives*, 24(5):389–405, 2004.

[58] A. Objois, Y. Gilibert, and Y. Delmas. Influence of the scarf angle value upon the micro-mechanical behavior of the scarf-joint bonded structure. *Transactions of the Canadian Society for Mechanical Engineering*, 25(2):209–225, 2001.

[59] A. Objois, Y. Gilibert, and B. Fargette. Theoretical and experimental analysis of the scarf joint bonded structure: Influence of the adhesive thickness on the micro-mechanical behavior. *Journal of Adhesion*, 70(1):13–32, 1999.

[60] L.J. Hart-Smith. Analysis and design of advanced composite bonded joints. 43p, NASA Contractor Reports, April 1974.

[61] R.D. Adams, N.A. Peppiatt, and J. Coppendale. Prediction of strength of joints between composite materials. *IEEE Transactions on Nuclear Science*, pages 64–78, 1978.

[62] C.L. Johnson. Effect of ply stacking sequence on stress in a scarf joint. *American Institute of Aeronautics and Astronautics*, 27(1):79–86, 1989.

[63] A.A. Baker, R.J. Chester, G.R. Hugo, and T.C. Radtke. Non-linear analysis of a metal-to-composite scarf joint. *International Journal of Adhesion and Adhesives*, 19(2-3):161–171, 1999.

[64] K. Ishii, M. Imanaka, H. Nakayama, and H. Kodama. Evaluation of the fatigue strength of adhesively bonded cfrp/metal single and single-step double-lap joints. *Composites Science and Technology*, 59(11):1675–1683, 1999.

[65] F. Mortensen and O.T. Thomsen. Simplified linear and non-linear analysis of stepped and scarfed adhesive-bonded lap-joints between composite laminates. *Composite Structures*, 38(1-4):281–294, 1997.

[66] J. Du, F.T. Salmon, and A.V. Pocius. Modelling of cohesive failure processes in structural adhesive bonded joints. *Journal of Adhesion Science and Technology*, 18(3):287–299, 2004.

[67] Y.H. Chui. Strength of osb scarf joints in tension. *Wood and Fiber Science*, 32(1):7–10, 2000.

[68] J. Schon and T. Nyman. Spectrum fatigue of composite bonded joints. *International Journal of Fatigue*, 24:273–279, 2002.

[69] A. Higgins. Adhesive bonding of aircraft structures. *International Journal of Adhesion and Adhesives*, 20:367–376, 2000.

[70] T.P. Lang and P.K. Mallick. Effect of recessing on the stresses in adhesively bonded single-lap joint. *International Journal of Adhesion and Adhesives*, 19(4):257–271, 1999.

[71] M. Goland and E. Reissner. The stresses in cemented joints. *Journal of Applied Mechanics*, 66:A 18–27, 1944.

[72] L.J. Hart-Smith. Adhesive bonding of composite structures - progress to date and some remaining challenges. *Journal of Composites Technology and Research*, 24(3):133–151, 2002.

[73] D. Kustcha. Mechanics of adhesive bonded lap-type joints: survey and review. *Technical Report AFML-TDR-64-298*, 1964.

[74] D. Kutcha and K.E. Hofer Jr. Feasibility of joining advanced composite flight vehicles. *Technical Report AFML-TDR-68-391*, 1969.

[75] F.L. Matthews, P.F. Kitty, and E.W. Godwin. A review of the strength of joints in fiber-reinforced plastics-part 2 adhesively bonded joints. *Composites*, pages 29–37, 1982.

[76] J.R. Vinson. Adhesive bonding of polymer composites. *Polymer Engineering and Science*, 29(19):1325–1331, 1989.

[77] L.J. Hart-Smith. *Developments in Adhesives-2*, chapter 1, pages 1–44. Applied Science Publishers, 1981.

[78] R.D. Adams and W.C. Wake, editors. *Structural adhesive joints in engineering*. Elsevier Applied Science Publishers, London & New York, 1984.

[79] A. Baldan. Adhesively-bonded joints in metallic alloys, polymers and composite materials: Mechanical and environmental durability performance. *Journal of Materials Science*, 39(15):4729–4797, 2004.

[80] A. Baldan. Adhesively-bonded joints and repairs in metallic alloys, polymers and composite materials: Adhesives, adhesion theories and surface pretreatment. *Journal of Materials Science*, 39(1):1–49, 2004.

[81] J. Mackerle. Finite element analysis and simulation of adhesive bonding, soldering and brazing: A bibliography (1976 - 1996). *Modelling and Simulations in Materials Science and Engineering*, 5:159–185, 1997.

[82] P.N.B. Reis, F.J.V. Antunes, and J.A.M. Ferreira. Influence of superposition length on mechanical resistance of single-lap adhesive joints. *Composite Structures*, 67(1):125–133, 2005.

[83] L.F.M. Da Silva, R.D. Adams, and M. Gibbs. Manufacture of adhesive joints and bulk specimens with high-temperature adhesives. *International Journal of Adhesion and Adhesives*, 24(1):69–83, 2004.

[84] A. Francesco. Effect of stitching on the static and fatigue performance of co-cured composite single-lap joints. *Journal of Composite Materials*, 38(3):243–257, 2004.

[85] C. Yang, H. Huang, J.S. Tomblin, and W. Sun. Elastic-plastic model of adhesive-bonded single-lap composite joints. *Journal of Composite Materials*, 38(4):293–309, 2004.

[86] J.K. Kim and D.G. Lee. Effects of applied pressure and temperature during curing operation on the strength of tubular single-lap adhesive joints. *Journal of Adhesion Science and Technology*, 18(1):87–107, 2004.

[87] J.M. Lees and G. Mrkarov. Mechanical/bonded joints for advanced composite structures. In *Proceedings of the Institution of Civil Engineers: Structures and Buildings*, volume 157, pages 91–97, 2004.

[88] J.D. Melograna and J.L. Grenestedt. Revisiting a wavy bonded single lap joint. *American Institute of Aeronautics and Astronautics*, 42(2):395–402, 2004.

[89] G.P. Zou, K. Shahin, and F. Taheri. An analytical solution for the analysis of symmetric composite adhesively bonded joints. *Composite Structures*, 65(3-4):499–510, 2004.

[90] A. Ozel, M.D. Aydin, and S. Temiz. The effects of overlap length and adherend thickness on the strength of adhesively bonded joints subjected to bending moment. *Journal of Adhesion Science and Technology*, 18(3):313–325, 2004.

[91] M.J.L. Van Tooren, D.M. Gleich, and A. Beukers. Experimental verification of a stress singularity model to predict the effect of bondline thickness on joint strength. *Journal of Adhesion Science and Technology*, 18(4):395–412, 2004.

[92] S. Narasimhan and P.C. Pandey. Three-dimensional material and geometrical nonlinear analysis of adhesively bonded single lap joint. *Defence Science Journal*, 53(2):175–188, 2003.

[93] C. Dartevelle, E. McAlpine, G.E. Thompson, and R. Morgan. Low pressure plasma treatment for improving the strength and durability of adhesively bonded aluminium joints. *Surface and Coatings Technology*, 173(2-3):249–258, 2003.

[94] E. Sancaktar and P. Nirantar. Increasing strength of single lap joints of metal adherends by taper minimization. *International Journal of Adhesion and Adhesives*, 17(5):655–675, 2003.

[95] K.T. Hsiao, J. Alms, and S.G. Advani. Use of epoxy/multiwalled carbon nanotubes as adhesives to join graphite fibre reinforced polymer composites. *Nanotechnology*, 14(7):791–793, 2003.

[96] J.N. Boss, V.K. Ganesh, and C.T. Lim. Modulus grading versus geometrical grading of composite adherends in single-lap bonded joints. *Composite Structures*, 62(1):113–121, 2003.

[97] V.K. Ganesh and T.S. Choo. Modulus graded composite adherends for single-lap bonded joints. *Journal of Composite Materials*, 36(14):1757–1767, 2002.

[98] I. Pires, L. Quintino, J.F. Durodola, and A. Beevers. Performance of bi-adhesive bonded aluminium lap joints. *International Journal of Adhesion and Adhesives*, 23(3):215–223, 2003.

[99] A.F. Avila and P.De.O. Bueno. An experimental and numerical study on adhesive joints for composites. *Composite Structures*, 64(3-4):531–537, 2004.

[100] A.F. Avila and P.De.O. Bueno. Stress analysis on a wavy-lap bonded joint for composites. *International Journal of Adhesion and Adhesives*, 24(5):407–414, 2004.

[101] S. Mahdi, H.J. Kim, B.A. Gama, S. Yarlagadda, and J.W. Gillespie Jr. A comparison of oven-cured and induction-cured adhesively bonded composite joints. *International Journal of Adhesion and Adhesives*, 37(6):519–542, 2003.

[102] Q. Zeng and C.T. Sun. Fatigue performance of a bonded wavy composite lap joint. 27(5):413–422, 2004.

[103] S. Feih and H.R. Shercliff. Composite failure prediction of single-L joint structures under bending. *Composites Part A*, 36:381–395, 2005.

[104] M.S. Kafkalidis and M.D. Thouless. The effects of geometry and material properties on the fracture of single lap-shear joints. *International Journal of Solids and Structures*, 39(17):4367–4383, 2002.

[105] M.K. Apalak and A. Engin. Effect of adhesive free-end geometry on the initiation and propagation of damaged zones in adhesively bonded lap joints. *Journal of Adhesion Science and Technology*, 18(5):529–559, 2004.

[106] R.D. Adams and N.A. Peppiatt. Stress analysis of adhesive-bonded lap joints. *Journal of Strain Analysis*, 9(3):185–196, 1974.

[107] A.D. Crocombe and R.D. Adams. Influence of the spew fillet and other parameters on the stress distribution in the single lap joint. *Journal of Adhesion*, 13(2):141–155, 1981.

[108] E.J. Ripling, S. Mostovoy, and R.L. Patrick. Measuring fracture toughness of adhesive joints. *Materials Research and Standards*, 4(3):129–134, 1964.

[109] S. Mostovoy and E.J. Ripling. Fracture toughness of epoxy system. *Journal of Applied Polymer Science*, 10(9):1351–1371, 1966.

[110] E.J. Ripling, S. Mostovoy, and R.L. Patrick. Application of fracture mechanics to adhesive joints. *American Society for Testing and Materials - Special Technical Publications*, 360:5–19, 1964.

[111] S.O. Osiyemi. *The fatigue performance of adhesively bonded fibre composite joints*. PhD thesis, Department of Mechanical Engineering, Imperial College of Science Technology and Medicine, London, 1992.

[112] W. Sun and C. Yang. Fracture analysis of adhesive-bonded single-lap composite joints. In *International SAMPE Technical Conference*, pages 3931–3942. SAMPE 2004, 2004.

[113] M. Qin and Y.A. Dzenis. Analysis of single lap adhesive composite joints with delaminated adherends. *Composites Part B*, 34(2):167–173, 2003.

[114] R.S. Court, M.P.F. Sutcliffe, and S.M. Tavakoli. Ageing of adhesively bonded joints - fracture and failure analysis using video imaging techniques. *IJAA*, 21:455–463, 2001.

[115] B. Blackman, J.P. Dear, A.J. Kinloch, and S. Osiyemi. The calculation of adhesive fracture energies from double-cantilever beam test specimens. *Journal of Materials Science Letters*, 10:253–256, 1991.

[116] B.R.K. Blackman, A.J. Kinloch, M. Paraschi, and W.S. Teo. Measuring the mode i adhesive fracture energy, g_{IC}, of structural adhesive joints: The results of an international round-robin. *International Journal of Adhesion and Adhesives*, 23(4):293–305, 2003.

[117] A.J. Bell and A.J. Kinloch. Effect of the substrate material on the value of the adhesive fracture energy, gc. *Journal of Materials Science Letters*, 16(17):1450–1453, 1997.

[118] S. Ravi, N.G.R. Iyengar, and B.D. Agarwal. Influence of moisture absorption on fracture toughness of kevlar fabric/epoxy composite. *Journal of the Institution of Engineers (India): Aerospace Engineering Journal*, 76:23–28, 1995.

[119] J.P. Lucas and J. Zhou. The effects of sorbed moisture on resin-matrix composites. *Journal of Metals*, 45(12):37–40, 1993.

[120] R.A. Gledhill, S.J. Shaw, and D.A. Tod. Durability of adhesive-bonded joints employing organosilane coupling agents. *International Journal of Adhesion and Adhesives*, 10(3):192–198, 1990.

[121] B.M. Parker. Durability of adhesive bonded epoxy carbon fibre composite. *ASTM Special Technical Publication*, (1227):68–81, 1994.

[122] J.F. Watts, R.A. Blunder, and T.J. Hall. Failure mode of adhesively bonded aluminium following aqueous exposure. *Surface and Interface Analysis*, 16(1-12):227–235, 1990.

[123] M. Ouddane and R. Boukhill. Moisture absorption effect on adhesive filled bonded joints. *Polymer Composites*, 19(6):680–688, 1998.

[124] S.J. John, A.J. Kinloch, and F.L. Matthews. Measuring and predicting the durability of bonded carbon fiber/epoxy composite joints. *Composites*, 22(2):121–127, 1991.

[125] Y. Nakanishi. Decrease in strength of adhesive bonded joint of cfrp in acidic water and salt water. *Zairyo/Journal of the Society of Materials Science, Japan*, 44(499):407–411, 1995.

[126] S.K. Mazumdar. Static and fatigue behavior of adhesive joints in smc-smc composites. *Polymer Composites*, 19(2):139–146, 1998.

[127] B.M. Parker. The strength of bonded carbon fiber composite joints exposed to high humidity. *International Journal of Adhesion and Adhesives*, 10(3):187–191, 1990.

[128] J.C. McMillian. *Developments in Adhesives-2*, chapter 7, pages 243–278. Applied Science Publishers, 1981.

[129] J. Comyn. *The Role of Water Diffusion in the durability of Adhesive Joints*, volume 6, chapter 12, pages 159–171. Applied Science Publishers, 1982.

[130] B.M. Parker. Some effects of moisture on adhesive-bonded cfrp-cfrp joints. *Composite Structures*, 6(1-3):123–139, 1986.

[131] D.G. Lee, J.W. Kwon, and D.H. Cho. Hygrothermal effects on the strength of adhesively bonded joints. *Journal of Adhesion Science and Technology*, 12(11):1253–1275, 1998.

[132] H.M. Hand, C.O. Arah, D.K. McNamara, and M.F. Mecklenburg. Effects of environmental exposure on adhesively bonded joints. *International Journal of Adhesion and Adhesives*, 11(1):15–23, 1991.

[133] A.J. Curley, J.K. Jethwa, A.J. Kinloch, and A.C. Taylor. Fatigue and durability behaviour of automotive adhesives part iii: Predicting the service life. *Journal of Adhesion*, 66(1-4):39–59, 1998.

[134] M.M. Abdel Wahab, I.A. Ashcroft, A.D. Crocombe, and P.A. Smith. Finite element prediction of fatigue crack propagation lifetime in composite bonded joints. *CA*, 35(2):213–222, 2004.

[135] B.R.K. Blackman, A.J. Kinloch, and M. Paraschi. The effect of the substrate material on the value of the adhesive fracture energy, gc: Further considerations. *Journal of Materials Science Letters*, 20(3):265–267, 2001.

[136] A.B. Pereira and A.B. De Morais. Strength of adhesively bonded stainless steel joints. *International Journal of Adhesion and Adhesives*, 23(4):315–322, 2003.

[137] Y. Hosaka, K. Miyazaki, T. Fujii, H.O. Kubo, K. Nejigaki, and K. Kurosawa. Static and fatigue fracture characteristics of rubber modified epoxy adhesives. In *Proceedings of the International Conference on Advanced Composite Materials*, pages 561–567. Minerals, Metals & Materials Soc. (TMS), Warrendale, PA, USA, 1993.

[138] S. Erpolat, I.A. Ashcroft, A.D. Crocombe, and M.M. Abdel-Wahab. Fatigue crack growth acceleration due to intermittent over stressing in adhesively bonded cfrp joints. *Composites Part A: Applied Science and Manufacturing*, 35(10):1175–1183, 2004.

[139] D. Tzetzis, P.J. Hogg, and M. Jogia. Double cantilever beam mode-i testing for vacuum infused repairs of gfrp. *Journal of Adhesion Science and Technology*, 17(3):309–328, 2003.

[140] J.D. Bardis and K.T Kedward. Surface preparation effects on mode i testing of adhesively bonded composite joints. *Journal of Composites Technology and Research*, 24(1):30–37, 2002.

[141] B.R.K. Blackman, H. Hadavinia, A.J. Kinloch, M. Paraschi, and J.G. Williams. The calculation of adhesive fracture energies in mode i: Revisiting the tapered double cantilever beam (tdcb) test. *Engineering Fracture Mechanics*, 70(2):233–248, 2003.

[142] R.Y. Ting and R.L. Cottington. Adhesive fracture energies of some high performance polymers. *Journal of Adhesion*, 12(4):243–255, 1981.

[143] J.F. Davalos, P. Qiao, P. Madabhusi-Raman, and E.M. Lang. Mode i fracture toughness of fiber reinforced composite-wood bonded interface. *Journal of Composite Materials*, 32(10):987–1013, 1998.

[144] C.F. Korenberg, A.J. Kinloch, and J.F. Watts. Crack growth of structural adhesive joints in humid environments. *Journal of Adhesion*, 80(3):169–201, 2004.

[145] S.T. Halliday, W.M. Banks, and R.A. Pethrick. Dielectric studies of adhesively bonded cfrp/epoxy/cfrp structures - design for ageing. *Composites Science and Technology*, 60(2):197–207, 2000.

[146] J.W. Wylde and J.K Spelt. Measurement of adhesive joint fracture properties as a function of environmental degradation. *International Journal of Adhesion and Adhesives*, 18(4):237–246, 1998.

[147] P. Frantzis. Environmental attack on adhesive joints (part i: Test equipment). *ASME International Journal, Series A*, 41(2):231–242, 1998.

[148] M.M. Abdel Wahab, I.A. Ashcroft, A.D. Crocombe, and P.A. Smith. Fatigue crack propagation in adhesively bonded joints. *Key Engineering Materials*, 251-252(1-4):229–233, 2003.

[149] M.M. Abou-Hamda, M.M. Megahed, and M.M.I. Hammouda. Fatigue crack growth in double cantilever beam specimen with an adhesive layer. *Engineering Fracture Mechanics*, 60(5-6):605–614, 1998.

[150] S. Mall and G. Ramamurthy. Effect of bond thickness on fracture and fatigue strength of adhesively bonded composite joints. *International Journal of Adhesion and Adhesives*, 9(1):33–37, 1989.

[151] E.F. Rybicki and M.F. Kanninen. Finite element calculation of stress intensity factors by a modified crack closure integral. *Engineering Fracture Mechanics*, 9(4):931–938, 1977.

[152] D.M. Parks. Stiffness derivative finite element technique for determination of crack tip stress intensity factors. *International Journal of Fracture*, 10(4):487–502, 1974.

[153] T.K. Hellen. On the method of virtual crack extensions. *International Journal for Numerical Methods in Engineering*, 9(1):187–207, 1975.

[154] I.S. Raju. Calculation of strain-energy release rates with higher order and singular finite elements. *Engineering Fracture Mechanics*, 28(3):251–274, 1987.

[155] R. Sethuraman and S.K. Maiti. Finite element based computation of strain energy release rate by modified crack closure integral. *Engineering Fracture Mechanics*, 30(2):227–231, 1988.

[156] Scotch Weld. Manufacturer's data sheet for structural film adhesive af-163. Technical report, 3M Singapore, 1999.

[157] S. Sivashanker. *Compressive failure of composites*. PhD thesis, Cambridge University Engineering Department, England, 1997.

[158] M.S. Madhukar, R.P. Kosuri, and K.J. Bowels. Monitoring fibre stress during curing of single fibre glass and graphite/epoxy composites. Technical report, NASA TECHNICAL MEMORANDUM 4568, November 1994.

[159] S.W. Yurgartis. Measurement of small angle fibre misalignment in continuous fibre composites. *Composites Science and Technology*, 30:279–293, 1987.

[160] S. Kyriakides, R. Arseculeratine, E.J. Perry, and K.M. Liechti. On the compressive kinking of fibre reinforced composites. *International Journal of Solids and Structures*, 32(6/7):689–738, 1995.

[161] M.R. Wisnom. The effect of fibre misalignment on the compressive strength of unidirectional carbon fibre/epoxy. *Composites*, 21(5):403–407, 1990.

[162] C. Soutis and F.Z. Hu. Failure analysis of scarf-patch-repaired carbon fiber/epoxy laminates under compression. *AIAA Journal*, 38(4):737–740, 2000.

[163] C.R. Chaplin. Compressive fracture in unidirectional glass-reinforced plastics. *Journal of Materials Science*, 12(2):347–352, 1977.

[164] A.G. Evans and W.F. Adler. Kinking as a mode of structural degradation in carbon fiber composites. *Acta Metallurgica*, 26(5):725–738, 1978.

[165] N.A. Fleck, L. Deng, and B. Budiansky. Prediction of kink width in compressed fiber composites. *Journal of Applied Mechanics, Transactions ASME*, 62(2):329–337, 1995.

[166] S. Sivashanker and S.O. Osiyemi. Uniaxial compressive failure of unidirectional composites with small imperfections. *Metallurgical and Materials Transactions A: Physical Metallurgy and Materials Science*, 30A(7):1867–1876, 1999.

[167] V.V. Kozey. Splitting-related kinking failure mode in unidirectional composites under compressive loading. *Journal of Materials Science Letters*, 12(1):43–47, 1993.

[168] N.L. Hancox. Compression strength of unidirectional carbon fibre reinforced plastic. *Journal of Materials Science Letters*, 10(2):234–242, 1975.

[169] A.R. Khamesh and A.M. Waas. Failure mechanisms of uni-ply composite plates with a circular hole under static compressive loading. *Journal of Engineering Materials and Technology, Transactions of the ASME*, 114(3):304–310, 1992.

[170] *Abaqus/cae with standard solver, Hibbitt, Karlsson & Sorensen, Inc.* 2002.

[171] Z. Hashin. Failure criteria for unidirectional fibre composites. *Journal of Applied Mechanics*, 47:329–334, 1980.

[172] J.D. Lee. Three dimensional analysis of damage accumulation in composite laminates. *Computer Structures*, 15(3):335–350, 1982.

[173] ASTM D3039/D3039M. Standard test methods for tensile properties of polymer matrix composite materials. Technical report, ASTM, 2001.

[174] L.J. Hart-Smith. Adhesive-bonded scarf and stepped-lap joints. Nasa contractor report no. n7413197, Mcdonnell-Douglas Corporation, Long Beach, California, January 1973.

[175] L.J. Hart-Smith. Analysis and design of advanced composite bounded joints. Nasa contractor report no. n7420564, Mcdonnell-Douglas Corporation, Long Beach, California, January 1974.

[176] L.J. Hart-Smith. Designing to minimize peel stresses in adhesively bonded joints. In *Delamination and Debonding of Materials, ASTM STP 876*, pages 238–266. American Society for Testing Materials, Philadelphia, W. S. Johnson Edition, 1985.

[177] J.G. Williams. On the calculation of energy release rates for cracked laminates. *International Journal of Fracture*, 36(2):101–119, 1988.

[178] http://www.me.ic.ac.uk/AACgroup/index.html. Adhesive fracture energy analysis sheet, 2004.

[179] I. Sridhar and Z.W. Zuwei. Effect of friction and adhesion on the loaddisplacement of a spherical probe in contact with a compliant incompressible elastic coating. *Tribology International*, (In Press), 2005.

[180] ASTM D 570-98. Standard test method for water absorption of plastics. *ASTM Annual Book*, 1998.

[181] R.F. Gibson. *Principles of composite material mechanics*. McGraw-Hill, Inc., New York, 1994.

[182] T.K.O. O'Brien and R.H. Martin. In *4th Tech. Conf.: Composite Materials and Systems*, pages 275–267, 1989.

[183] A.C. Taylor. *The impact durability behaviour of adhesively-bonded metal joints*. PhD thesis, Department of Mechanical Engineering, University of London, London, 1997.